การศึกษาการแพร่ของเกสท์โมเลกุลเคลื่อนผ่านโพรงซีโอไลท์โดยวิธีเคมีควอนตัมการจำลองแบบโดยคอมพิวเตอร์
และการทดลองพัลส์ฟิลด์เกรเดียนท์-นิวเคลียร์แมกเนติกเรโซแนนซ์สเปกโทรสโกปี

นางสาวชื่นจิต บุษสาย

STUDY OF DIFFUSION OF GUEST MOLECULES THROUGH ZEOLITE PORES USING
METHODS OF QUANTUM CHEMISTRY, COMPUTER SIMULATIONS, AND PULSE
FIELD GRADIENT-NUCLEAR MAGNETIC RESONANCE EXPERIMENTS

MISS CHUENCHIT BUSSAI

Thesis Title   Study of Diffusion of Guest Molecules through Zeolite Pores Using Methods of Quantum Chemistry, Computer Simulations and Pulse Field Gradient-Nuclear Magnetic Resonance Experiments

By   Miss Chuenchit Bussai

Field of Study   Chemistry

Thesis Advisor   Associate Professor Supot Hannongbua, Ph. D.

Thesis Co-advisor   Professor habilitatus Reinhold Haberlandt, Dr. rer. nat.

         Accepted by the Faculty of Science, Chulalongkorn University in Partial Fulfillment of the Requirements for the Doctor's Degree

………………………………… Dean of Faculty of Science

(Associate Professor Wanchai Phothipichitr, Ph. D.)

THESIS COMMITTEE

………………………………… Chairman

(Professor Udom Kokpol, Ph. D.)

………………………………… Thesis Advisor

(Associate Professor Supot Hannongbua, Ph. D.)

………………………………… Thesis Co-advisor

(Professor habilitatus Reinhold Haberlandt, Dr. rer. nat.)

………………………………… Member

(Associate Professor Sirirat Kokpol, Ph. D.)

………………………………… Member

(Associate Professor Kritsana Sagarik, Ph. D.)

………………………………… Member

(Aticha Chaisuwan, Ph. D.)

ชื่นจิต บุษสาย: การศึกษาการแพร่ของเกสท์โมเลกุลเคลื่อนผ่านโพรงซีโอไลท์โดยวิธีเคมีควอนตัมการจำลองแบบโดยคอมพิวเตอร์และการทดลองพัลส์ฟิลด์เกรเดียนท์-นิวเคลียร์แมกเนติกเรโซแนนซ์สเปกโทรสโกปี. (STUDY OF DIFFUSION OF GUEST MOLECULES THROUGH ZEOLITE PORES USING METHODS OF QUANTUM CHEMISTRY, COMPUTER SIMULATIONS, AND PULSE FIELD GRADIENT-NUCLEAR MAGNETIC RESONANCE EXPERIMENTS) อาจารย์ที่ปรึกษา: รศ. ดร. สุพจน์ หารหนองบัว, อาจารย์ที่ปรึกษาร่วม: ศ. ดร. เรนโฮล ฮาเบอร์ลานท์, 189 หน้า. ISBN 974-17-1403-3.

การคำนวณทางเคมีควอนตัมที่ระดับการคำนวณความถูกต้องที่ฮาร์ทรี ฟอคก์และโมลเลอร์-เพลสเสทอันดับที่สองโดยใช้เบซิสเซทขยายชนิด 6-31G* ถูกนำมาใช้ในการศึกษาอันตรกิริยาระหว่างน้ำกับซิลิคาไลท์-1 และมีเทนกับซิลิคาไลท์-1 โครงสร้างผลึกของซิลิคาไลท์-1 แทนด้วยส่วนย่อย 3 ส่วนซึ่งมีส่วนประกอบทางเคมีของซิลิคาไลท์-1 คือ O[10]Si[10]H[20], O[30]Si[22]H[44] และ O[35]Si[29]H[58] ผลการคำนวณบ่งชี้ว่า ลักษณะการเคลื่อนที่ของโมเลกุลน้ำในระหว่างการแพร่เป็นการเคลื่อนที่แบบม้วน โดยโมเลกุลจะหมุนและเคลื่อนเพื่อค้นหาเส้นทางที่ดีที่สุด โดยแพร่ผ่านศูนย์กลางของโพรงซิลิคาไลท์-1 รวมทั้งได้วิเคราะห์อย่างละเอียดเพื่อหาตำแหน่งที่เกิดการยึดเหนี่ยวที่ชอบของโมเลกุลน้ำ แต่ไม่ได้พิจารณาในกรณีของมีเทนหลังจากนั้นได้พัฒนาฟังก์ชันพลังงานศักย์ของระบบน้ำกับซิลิคาไลท์-1และมีเทนกับซิลิคาไลท์-1 โดยใช้ค่าพลังงานที่ได้จากอันตรกิริยาระหว่างน้ำกับส่วนย่อยและมีเทนกับส่วนย่อยของซิลิคาไลท์-1 จำนวน 1,032 และ 150 ค่าตามลำดับ นำฟังก์ชันที่พัฒนาขึ้นใหม่นี้ได้ไปใช้ในการศึกษาสมบัติเชิงโครงสร้างและเชิงพลวัตของน้ำและมีเทนในซิลิคาไลท์-1โดยวิธีโมเลกุลาไดนามิกซ์ ผลการทดลองแสดงโครงสร้างและค่าสัมประสิทธ์ของการแพร่ของเกสท์ในโพรงซิลิคาไลท์-1 ที่ความเข้มข้นและอุณหภูมิที่ต่างๆ นอกจากนั้นยังได้พบ "กลุ่มก้อนของน้ำความหนาแน่นต่ำ" การวัดค่าสัมประสิทธ์ของการแพร่ของโมเลกุลน้ำในซิลิคาไลท์-1 โดยวิธีการทดลองพัลส์ฟิลด์เกรเดียนท์-นิวเคลียร์แมกเนติกเรโซแนนซ์สเปกโทรสโกปีให้ผลที่สอดคล้องกับค่าสัมประสิทธ์ของการแพร่ของโมเลกุลด้วยวิธีการจำลองแบบโดยคอมพิวเตอร์

ภาควิชา.......เคมี.........................ลายมือชื่อนิสิต……………………………..…………..

สาขาวิชา......เคมี.…......................ลายมือชื่ออาจารย์ที่ปรึกษา……………..….........

ปีการศึกษา...2545.........................ลายมือชื่ออาจารย์ที่ปรึกษาร่วม………..………..

4173807423: MAJOR CHEMISTRY

KEY WORD: *ab initio* fitted potential / simulation / PFG NMR / diffusion / silicalite-1

CHUENCHIT BUSSAI: STUDY OF DIFFUSION OF GUEST MOLECULES THROUGH ZEOLITE PORES USING METHODS OF QUANTUM CHEMISTRY, COMPUTER SIMULATIONS, AND PULSE FIELD GRADIENT-NUCLEAR MAGNETIC RESONANCE EXPERIMENTS. THESIS ADVISOR: ASSOC. PROF. DR. SUPOT HANNONGBUA, THESIS CO-ADVISOR: PROF. DR. RER. NAT. HABIL. REINHOLD HABERLANDT, 189 pp. ISBN 974-17-1403-3.

Quantum chemical calculations at Hartree Fock and the second order Møller-Plesset perturbation levels with a basis set of 6-31G* have been performed to investigate water/silicalite-1 and methane/silicalite-1 interactions. The silicalite crystal structure has been represented by three fragments, in which the chemical compositions are O[10]Si[10]H[20], O[30]Si[22]H[44] and O[35]Si[29]H[58]. The results indicate how the water molecule moves and turns, "rolling movement", in order to search for the optimal route via diffusion through the center of the silicalite pore. Preferential binding sites with the corresponding binding energies have been intensively evaluated for water molecules but not for methane. Subsequently, water/silicalite-1 and methane/silicalite-1 potential functions have been developed from 1,032 fragment-water and 150 fragment-methane interactions, respectively. The newly developed pair potentials have been applied for series of molecular dynamics simulations in order to evaluate structural and dynamics properties of water and methane molecules in silicalite-1. The results show that structures and diffusion coefficients of guest molecules in silicalite-1 channels change dramatically as a function of loading and temperature. In addition, a formation of 'low density water cluster' has been detected. The PFG NMR diffusion measurements of water in silicalite-1 samples have been also performed and the results are in satisfactory agreement with those obtained from the simulations.

Department……Chemistry………………… Student's signature……………………...

Field of study….Chemistry………………Advisor's signature……………………..

Academic year....2002……………………... Co-advisor's signature…………………..

ACKNOWLEDGEMENTS

First of all, I express my deep gratitude to my beloved parents, Major Vatcharapan-Phoranee Bussai, for a complete understanding, and supports. These keep my life always going. My sister, Ms. Chuthathip Bussai, she is the most beautiful part of me, no word would have been instead.

I am truly grateful to Assoc. Prof. Dr. Supot Hannongbua, Prof. Dr. rer. nat. habil Reinhold Haberlandt, Privatdozent Dr. rer. nat. habil. Siegfried Fritzsche for their multifarious understanding, functional hints and encouragements through the study. I pass my sincerely thanks to Prof. Dr. rer. nat. habil Jörg Käger, Dr. Sergey Vasenkov and the colleagues for the kindly experimental assistances. Dr. Aticha Chaisuwan who gives me first impression of 'zeolite' is obliged, as well as Assoc. Prof. Dr. Vuchichai Parasuk, who always assists in intensive quantum details. I am expressed my special thanks to Assoc. Prof. Dr. Sirirat Kokpol, Assoc. Prof. Dr. Kritsana Sagarik for the thesis advices as the committee, whom make the dissertation properly done. Dipl. Phys. Steffen Jost, Dipl. Phys. Andreas Schüring, and Mr. Arthorn Loisruangsin are pleased for the stimulating discussions.

CONTENTS

CONTENTS (cont.)

CONTENTS (cont.)

CONTENTS (cont.)

LIST OF FIGURES

LIST OF FIGURES (cont.)

LIST OF FIGURES (cont.)

LIST OF FIGURES (cont.)

LIST OF FIGURES (cont.)

LIST OF TABLES

NOTATIONS

Sections

INTRODUCTION

MD	Molecular dynamics simulation	1.1
PFG NMR	Pulse field gradient nuclear magnetic resonance	1.1
ZLC	Zero-length column technique	1.2.1
QENS	Quasielastic neutron scattering technique	1.2.1
D	Diffusion coefficient	1.2.2
AIMD	*Ab initio* molecular dynamic simulation	1.3
HF	Hartree Fock	1.3
MP2	Møller-Plesset Perturbation at second order	1.3

FUNDAMENTAL DIFFUSION

J	Net rate of a flow particle	2.1
c	Concentration	2.1
t	Time	2.1
r^2	Mean square displacement	2.1.1
P	Propagator	2.1.1
$\mathbf{r}$	Position at time t	2.1.2
l	Mean displacement on x, y or z directions	2.1.2

QUANTUM MECHANICS

SCF	Self-Consistent Field	2.2.1
Ψ	Wave function	2.2.2
m	Mass	2.2.2
V	Potential energy	2.2.2
$\hat{H}$	Hamiltonian operator	2.2.2
Z	Atomic number	2.2.3
LCAO-MO	Linear combination of atomic orbitals to molecular orbital	2.2.4.1
φ	Molecular orbitals	2.2.4.1

NOTATIONS (cont.)

Sections

χ	Atomic orbital	2.2.4.1
c_{ij}	Molecular orbital expansion coefficient	2.2.4.1
$\hat{F}$	Fock operator	2.2.4.1
J	Columbic potential	2.2.4.1
K	Exchange potential	2.2.4.1
STO	Slater-type orbital	2.2.4.1
s	Slater-type orbital	2.2.4.1
ζ	Slater orbital exponential coefficient	2.2.4.1
n	principle number	2.2.4.1
l	angular number	2.2.4.1
α	Gaussian orbital exponential coefficient	2.2.4.1
m	number of basis functions	2.2.4.1
GTF	Gaussian type functions	2.2.4.1
CGTF	Contracted Gaussian-type functions	2.2.4.1
MB	Minimal basis sets	2.2.4.1
STO-3G	minimal basis function	2.2.4.1
3.21G, 4-31G	Split valence basis functions	2.2.4.1
6-31G*, 6-31G**	Split-valence plus polarization basis functions	2.2.4.1
$E_{corr}^{(2)}$	MP2 energy	2.2.4.2
DFT	Density functional theory	2.2.4.3
ρ	Density	2.2.4.3
v_{xc}	Exchange-correlation potential	2.2.4.3
J	Columbic potential	2.2.4.3

Subscripts and superscripts

r_0	denotes position at time zero	2.1.2
D_x, D_y, D_z	denote diffusion coefficient along x, y, z-axes	2.1.2
α, β	denote nuclei	2.2.3
i, j	denote electrons	2.2.3

NOTATIONS (cont.)

STATISTICAL MECHANICS

NOTATIONS (cont.)

Sections

A	Helmholtz free energy	2.3.2.1
C_v	Heat capacity at constant volume	2.3.2.1
h	Plank constant	2.3.2.1

Subscripts and superscripts

$^-$	denotes average	2.3.2.1

MOLECULAR DYNAMICS SIMULATION

MC	Monte Carlo simulation	2.4
F	Force	2.4.3
a	Acceleration	2.4.3
t	Time	2.4.4
N	Number of particle	2.4.5.1
r_c	Cut-off distance	2.4.5.3
v'	Shifted-force potential	2.4.53
Δt	Time step	2.4.5.4
r	A position	2.4.5.4
RDF	Radial distribution function	2.4.5.5
ρ_r	Average density number	2.4.5.5
$g(r)$	Pair distribution function	2.4.5.5
V	A volume	2.4.5.5
∇c	Concentration gradient	2.4.5.6
j	Flux	2.4.5.6
D	Diffusion coefficient	2.4.5.6
c	Concentration	2.4.5.6
τ	$t-t''$	2.4.5.6
VACF	Velocity autocorrelation function	2.4.5.6

Subscripts and superscripts

i	denotes a particle i	2.4.3
x	denotes x-direction	2.4.3

NOTATIONS (cont.)

PULSE FIELD GRADIENT NUCLEAR MAGNETIC RESONANCE

METHODOLOGY AND CALCULATIONS

NOTATIONS (cont.)

Sections

ΔE	Interaction energy	3.2
q	Charge	3.2
w	atoms in water molecule	3.2.1
m	atoms in methane molecule	3.2.2
s	silicalite-1 atoms	3.2
r	distance between i and j	3.2
a, b, c	lattice parameters of silicalite-1 unit	3.3
NVT	Constant N, V, and T	3.3
BJH	Bopp, Jancso and Heinzinger water model	3.3.1
CF	Central force water model	3.3.1
V	Potential function	3.3

Subscripts and superscripts

O1,O6	denote oxygen number 1, 6	3.1.2.1
Ow	denotes oxygen atom of water molecule	3.1.2.1
x, y, z	denote x, y, and z axes	3.1.2.2
i, j	denote particle	3.2
a, b	denote different silicalite atom types	3.2
O, H, C	denote oxygen, hydrogen and carbon atoms	3.3.1, 3.3.2

RESULTS AND DISCUSSIONS

ΔE_{out}^{min}	The most stable energy of water inside pores	4.2.31
ΔE_{in}^{min}	The most stable energy of water outside pores	4.2.3.1
ΔE^{max}	The maximum energy lied on the bottle neck	4.2.3.1
ΔE_{net}	The energy change ΔE_{in}^{min} - ΔE_{out}^{min}	4.2.3.1
$\Delta E_{barrier}$	The energy barrier ΔE^{max} - ΔE_{in}^{min}	4.2.3.1
1H, 2H, 3H	Methane orientations	4.2.4
$\vec{r}$	Vector distance perpendicular to wall(for water)	4.3.1.2

NOTATIONS (cont.)

Sections

T	Si atoms referred to TO_4 tetrahedral bridging	4.3.1.3
$\vec{s}$	Vector distance for methane	4.3.2.2
n_{ld}	Loading number	4.4
n	Average coordination number (RDF)	4.4
β	Correlated parameter	4.4

Subscripts and superscripts

1, 2	denote path along and perpendicular to walls	4.3.2.2
S, W, C	denote silicalite-1, water and methane	4.4
It, St, Sd	denote intersection, straight and sinusoidal channel	4.4
R_{M1}	denote first maximum distance of RDF	4.4
R_{m1}	denote first minimum distance of RDF	4.4

CHAPTER 1

INTRODUCTION

This dissertation attempts to apply three approaches of scientific methods, quantum calculations, molecular dynamics (MD) simulations and pulse field gradient nuclear magnetic resonance (PFG NMR) measurements to elucidate diffusion processes of guest molecules in zeolite micropores. Such microscopic understanding would be highly requisite for predicting microscopic zeolite-behaviors and leads directly to long-termed development, and hence, application of zeolites in industries.

1.1. Zeolite: Supposititious Material

1.1.1. What a zeolite is.

A zeolite was first discovered in 1756 by a Swedish Mineralogist, named Cronstedt.[1] Zeolites,[2-4] groups of hydrated aluminosilicates of the alkali or alkaline earth metals (principally sodium, potassium, magnesium and calcium), are natural volcanic minerals with a number of unique characteristics, which are discovered in many parts of the world. Zeolites were formed
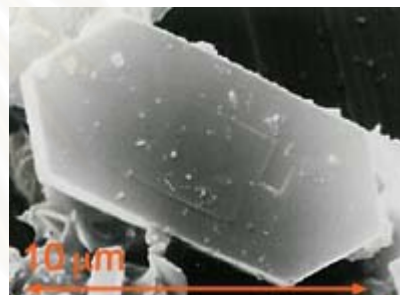
Figure 1.1 Electron micrograph of the MFI-type zeolite.

when volcanic ash was deposited in ancient alkaline lakes. The interaction of the volcanic ash with the salts in the lake water alters the ash into various zeolite materials. However, most zeolites used commercially are produced synthetically. Figure 1.1 shows an electron micrograph of the MFI type zeolite.

1.1.2. Structures of zeolites

The building blocks for the framework of zeolites usually consist of silicon or aluminium and oxygen. The silicon or aluminium tetrahedron is a central atom surrounded with other shared oxygen atoms. These elements are arranged within the mineral in a manner that gives the crystal a framework of channels and cavities, three-dimensional crystalline structures containing (-Si-O-Al-) linkages. These (-Si-O-Al-) linkages form pores of uniform diameter and enclose regular internal cavities and channels of different sizes and shapes, depending on the chemical composition

and the crystal structure of the specific zeolite involved. These cavities can host cations, water or other molecules.

One gram of zeolite provides up to several hundred square meters of surface area for chemical reactions to take place.[5] This characteristic of zeolites leads to great adsorptive power.

1.1.3. Expansive applications

The zeolitic channels (or pores) are microscopically small, and have molecular size dimensions such that they are often termed "molecular sieves". The size and shape of the channels have extraordinary effects on the properties of this material for adsorption processes and these properties lead to their use in separation processes (Figure 1.2) in petroleum refining and syn-fuels production.[6-8]

Molecules can be separated via shape and size effects related to their possible orientation in the pore, or by differences in strength of adsorption. They can be used also in other applications; e. g. to exchange the ion in a treatment of waste water.[9-11] The latest application is to store the heat,[12] without requirement of the insulation. The idea is when heated, zeolites release water vapor. As long as they stay dry, they can store large amounts of heat for months. When zeolites are allowed to absorb moisture, they release their stored heat. Additionally, it can be used as a molecular nanodevice to design of precise functionalities.[13,14] However, the zeolite heat storage is not yet available for residential use because of the relatively high cost.
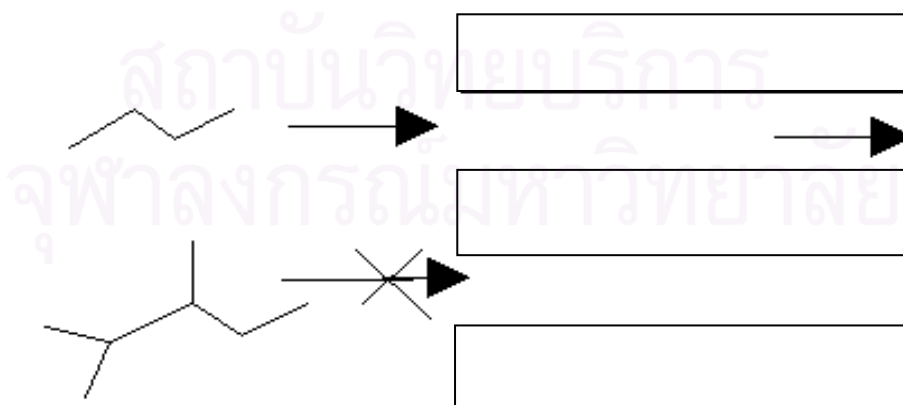
Figure 1.2 A picture of the sieve principle.

1.2. Recent Situation on the Diffusion Processes in Zeolite:

Diffusion of adsorbed molecules in zeolites is the known common phenomenon which plays an important role in the use of zeolites. The dynamical behaviors of molecules in zeolites and other microporous solids have become attractive to both fundamental investigations and applied researches. The regular structures and numerous technical applications as catalysts, ion exchangers, adsorbents and host materials for advance technologies have made zeolites to a particularly important candidates of research.[2,3,15] At present, computational chemistry can provide moderate data even for the complicated multicomponent diffusion.

1.2.1. Water/zeolites

It is well-known for all types of zeolites that they remain rigid in the presence of water.[2,16] Also it is common knowledge that the water presence has large impact on the arrangement of the cations in zeolites.[17-20] Water molecules in zeolites, even at small amount, can significantly influence properties of zeolite-like materials and lead to difficulties during some technological processes, i.e., separation processes. The understanding of such phenomena cannot be obtained purely by experimental techniques due to the complex interplay between many physical and chemical processes taking place in the zeolites.[21] As a complementary technique in obtaining insight into the microscopic details, many MD studies on the interaction of water to various zeolites have been performed.[22-33]

To our best knowledge, first MD simulations for water in zeolites have been reported by Demontis et al.,[34-36] the vibrations of water in natrolite and by Leherte et al.,[37-42] the structural properties and the self-diffusion coefficient of water in ferrierite in quantitative agreement with experiments.[43-45] In the late 1990s, the sodium ions in hydrated zeolite A have been examined for the ranges of hydrations. The self-diffusion coefficients obtained from this simulation agrees within a factor of 3 with those obtained from experiments. More recently, the conformation of the triple helix of water in VPI-5, aluminophosphate-type material formation has been investigated by Fois et al. through Car-Parrinello molecular

dynamics simulations. It was found that the helice lies close to the channel walls and avoids the channel center. Empirical potential functions including electronic-field-dependent terms have been developed and applied by Cicu *et al.*[46] to simulate classically water in natrolite. It was found that the electric-field-dependent terms in the intramolecular potential of water can improve the results in comparison to experimental one. Interestingly, quantum or at least a semiclassical treatment is required in order to reasonable simulate particularly systems containing water and other polar molecules. Consequently, *ab initio* molecular dynamics (AIMD) has been performed for H_2O and H_3O^+ in HSAPO-34 by Termath *et. al.*[47] and it has been found also that an acid-base reaction in HSAPO-34 requires at least three water molecules per two nearby acidic sites, leading to a protonated water cluster, $H_3O^+(H_2O)_2$. More recently, the AIMD simulations of water-HSAPO-34, that have been studied by Jeanvoine *et al.*[48] in order to elucidate the water behavior to Bronsted acidic sites, stated the demand on a water dimer for the occurrence of proton transfer in the cage, hence the basicity of a hydrogen-bonded water dimer is required. However, such AIMD simulation is indeed still computer time consuming. This requires the restriction on few 100 atoms systems, and the typical run length of some picoseconds.

For the silicalite, the only available data on the water-silicalite interactions are the experimental measurements by Flanigen *et al.*[49] and Vigné-Maeder *et al.*,[50] who reported the initial isostatic heat of adsorption of 6 kcal.mol^{-1} and the mean heat of adsorption of the first four water molecules of 9.6 kcal.mol^{-1}, respectively. Vigné-Maeder *et al.* have also calculated the water-silicalite potential map in which the average energy is expressed as a sum of electrostatic, polarization, dispersion and repulsion interactions between the atom pairs. The various atomic parameters for the first term are the *ab initio* results while those of other terms are empirical. The calculations yield an average water-silicalite interaction at 300 K of -12.5 kcal.mol^{-1} and the approximate energy barrier via diffusion through the intersection between the straight and the zigzag channels of the silicalite of 8 kcal.mol^{-1}. However, it has been mentioned that the calculated results are very sensitive to the experimental geometry of the silicalite used. Recently, Turov *et al.*[51-54] have measured water adsorption in silicalite by H^1 NMR and

thermogravitric methods and observed a high chemical shift. This corresponds to the formation of more than three hydrogen bonds of the attributed water in the pores. More recently, this issue has been investigated using quantum chemical calculations[23] and found that water can enter the silicalite channel. Activation energy of approximately 1.9 kcal.mol^{-1} is required to diffuse through the linked domain to or from the intersection channel. In addition, experimental results by Kärger *et al.*[20] using PFG-NMR measurements indicate that diffusion of water in silicalite takes place even at room temperature.

1.2.2. Methane/zeolites

The understanding the diffusion of hydrocarbons in zeolites is a requisite for optimizing catalytic processes using these materials.[40] Nowadays, these topics have attached attention of either theoretical or experimental research groups,[55-57] in particular methane, as it is commonly associated with petroleum deposits, and occurs naturally as the principal component of natural gas. Numbers of different experimental techniques are applied to measure the diffusivity in zeolites, for instance, the frequency response Zero-Length Column (ZLC) technique,[58,59] an isotope exchange method,[60] Quasielastic Neutron Scattering (QENS),[61] or Pulsed-Field Gradient Nuclear Magnetic Resonance (PFG-NMR).[2] However, the methane diffusivities depend on methods used.

D /x10^{-9} m^2.s^{-1}
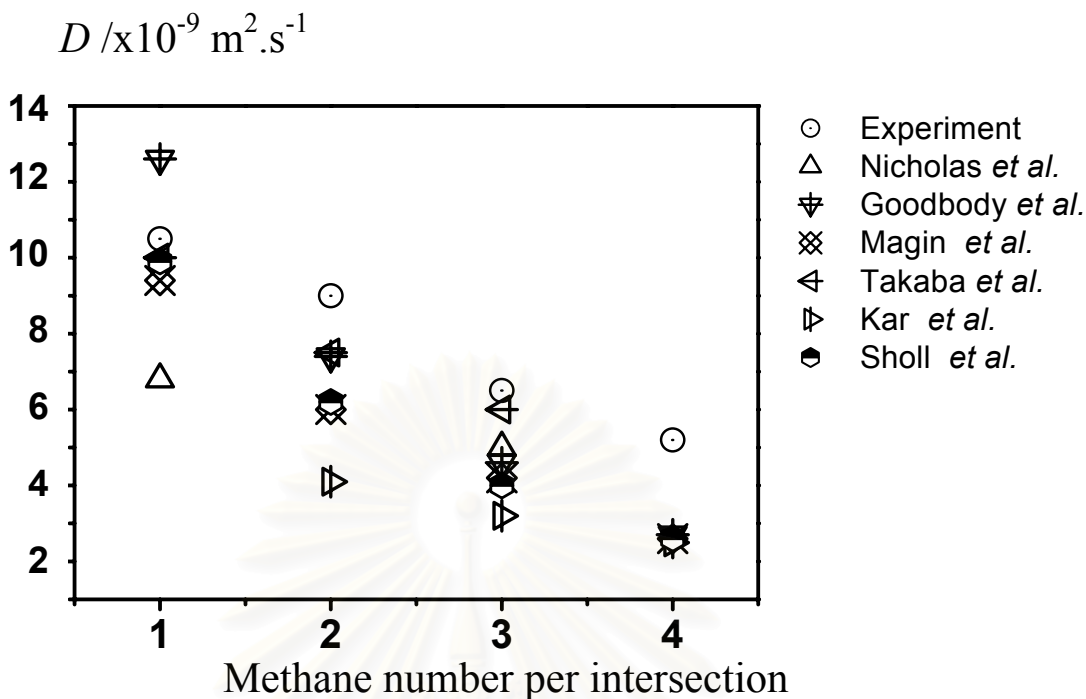
Figure 1.3 Comparison of diffusion coefficients (D) of methane molecules at various loadings in silicalite-1.

Ergo, computational simulations have become an increasingly important tool for studying guest molecules in zeolite.[62,63] With the molecular dynamics simulation (MD), both structural as well as the dynamical properties of a system can be carried out. Methane is one of the most frequently considered molecules. Although, the simulated self-diffusion coefficients are in good agreement with those of experimental results (Figure 1.3).[64-70] However, only some of them have investigated structural properties of the system.[71,72]

The methane diffusivities in Silicalite-1 have been investigated using MD simulations with spherical methane model, '*united atom model*' by Demontis *et. al.*[71,73,74] and by Goodbody *et al.*[75] in which the framework has been treated either rigid[66,67,72] or flexible.[76-78] However, five center methane models, based on the force field parametization by Ruthven *et. al.*[79] and Bezus *et. al.*[80] are also available. Recently, Engel *et. al.*[81] have developed the new methane/silicalite

model as a sum of electrostatic, inductive, dispersive and repulsive interactions. These parameters include every kind of interaction particles, i.e., the van der Waals radius, the ionic charge, the polarizability, and the number of valence electrons. Remark, it is empirical force field type. More recently, the new simulation, the so-called Dual Control Volume- Grand Canonical Molecular Dynamics simulation[82] has been applied in order to understand the dynamics dictating the diffusion of methane molecule through the single crystal membrane.[83,84]

More recently, Fritzsche *et al.*[85] present new simulations of 10 ns length using the parameters taken from ref. [78,86,87]. The framework flexibility as well as the internal methane vibration have also been taken into consideration. It turns out that the approximation of a rigid lattice gives the same results as a full flexibility treatment. Nevertheless, the authors suggest a flexible treatment of methane molecules.

1.3. Scope of this Work

Although, several attempts have been made to study the adsorption and diffusion of hydrocarbons in silicalite-1 by means of both theoretical.[88-90] and experimental[91-94] investigations. However, very little information is available for the water/silicalite-1 system because one believes that water is not able to enter and diffuse in hydrophobic silicalite-1 channels. In order to demonstrate the statement of the presence of water molecules, the PFG NMR measurements have been proposed to be performed and water diffusion in silicalite-1 samples have been, in addition, evaluated.

Furthermore, *ab initio* calculations for the optimal water configurations before and after entering channels have been examined and discussed, in terms of movement, encapsulation and energy barriers. The silicalite-1 crystal structure has been represented by three fragments, in which the chemical compositions are $O_{10}Si_{10}H_{20}$, $O_{30}Si_{22}H_{44}$ and $O_{35}Si_{29}H_{58}$. Preferential binding sites with the corresponding binding energies have also been intensively evaluated.

The main part of this work is centered on molecular dynamics simulations of water and methane molecules in silicalite-1 using *ab initio* fitted potentials. As a

matter of fact, most previous classical simulations[63-67,69-94] of water and methane as well as all other guest molecules in zeolites used intermolecular potentials based on empirical force field parameterization. Some doubts arise when the force field potential was used to represent the interaction between guests and zeolites, in which hydrogen bonding is very important as this is better represented by *ab initio* derived potentials. In addition, it is known that unbalance of the pair potentials, guest-zeolite and guest-guest, can easily lead to artificial results. To avoid this discrepancy, an *ab initio* fitted potential for guest/silicalite-1 and guest-guest at the equivalent level have been developed. Such potentials are, therefore, newly developed and used in the present work. To derive potential function parameters based on quantum chemical calculations, numerous silicalite-1/water and silicalite-1/methane energy points have been generated using the Hartree-Fock (HF) and secondary Møller Plesset (MP2) levels, respectively. The energy points have been, then, fitted to an analytical function form, while, the water/water,[95] and methane/methane[96] potentials are taken from literatures as they are already developed using *ab initio* data.

Molecular dynamics simulations have been performed using the novel developed *ab initio* potential and diffusion coefficients for a water and methane molecule as a function of loading and temperature in the silicalite-1. Changes of structural and dynamics properties of water and methane molecules in silicalite-1 have cautiously been examined.

The content of this dissertation starts with theoretical background in which fundamental diffusion principles, quantum mechanics, statistical mechanics, and also molecular dynamics have been briefly summarized. Next, the calculation and methodological details how to develop the guest/zeolite potential functions, as well as to perform MD simulations, and PFG NMR measurements, have been presented. All results are, then, reported, and debated in comparison to the previous works, in the next chapter. Last, new and significant enumerate have been concluded.

CHAPTER 2

THEORY

2.1. Fundamental Diffusion Principles

The spontaneous decrease of the concentration gradient is so-called 'diffusion'. The well-known definition of the diffusion (D) is formulated for the case of transport through thin membranes by Adolf Fick, which is named Fick's First Law:

$$J = -D\frac{\partial c}{\partial z},$$

(2.1)

in which J is the net rate of flow of a particle, D is called the transport diffusion coefficient. Or, a more general formula is

$$J = -D \; grad \; c.$$

(2.2)

This will lead to the conservation equation

$$\frac{\partial c}{\partial t} = D\frac{\partial^2 c}{\partial t^2},$$

(2.3)

which is commonly known as Fick's Second Law of Diffusion. Before Fick's Laws in 1850s,[97,98] in the late 1820s Robert Brown gave the expression of another phenomenon, which is closely related to diffusion. It is about the behavior results from the continuously changing interaction between small particles and the molecules of the surrounding fluid. Analogy, the individual particles undergo a sequence and apparently random movements. This phenomenon is generally referred to as Brownian motion.[99,100]

2.1.1. Random walk

The closed relationship between Brownian motion and diffusion was first elaborated by Einstein.[101] An experimentally accessible quantity that describes Brownian motion is the time dependence of the concentration distribution, starting from the assumptions that the random walkers (systematic particles) do not interfere with each other and may step with equal probability in any direction. By a complex

mathematical work,[3] the quantity, called the 'propagator', P, in which the mean square displacement has been shown:

$$\left\langle r^2(t) \right\rangle = \int r^2 \frac{e^{-r^2/4Dt}}{(4\pi Dt)^{3/2}} \, dz = 6Dt \,. \tag{2.4}$$

This equation is generally known as Einstein's relation, and dispenses a direct correlation between diffusivity and the time dependence of the mean square displacement.

2.1.2. Self-diffusion

There are two different diffusion phenomena: transport diffusion and self-diffusion. In this section, the self-diffusion will be introduced mainly. The self-diffusion or Brownian molecular motion may be observed following the trajectories of a large number of individual diffusants and determining their mean square displacement, which is what simulators normally do. Although, transport diffusion and self-diffusion generally occur by essentially the same microscopic mechanism, the coefficients of both are in general not the same.

The self-diffusion coefficients are calculated from the particle displacements. The process of self-diffusion was generally related to the moments of the propagator.[102-104] The propagator $P(r,r_0,t)$ represents the probability density to find a particle at position r at time t when it was at r_0 at time $t = 0$.

The nth moment of the propagator is defined by the relation,[104]

$$\left\langle |r - r_0|^n \right\rangle = \int |r - r_0|^n P(r,r_0,t) \, dr, \tag{2.5}$$

$P(r,r_0,t)$ is the solution of the diffusion equation for the initial concentration $C(r,t=0) = \delta(r - r_0)$. In the case of isotropic diffusion and of a homogeneous system the propagator is

$$P(r,r_0,t) = (4\pi Dt)^{-3/2} \exp\left\{ \frac{-(r - r_0)^2}{4Dt} \right\}. \tag{2.6}$$

Although zeolites are not homogeneous the propagator can be represented in this way if the displacements exceed the size of the inhomogeneities.[103] Then $P\left(r, r_0, t\right)$ depends only on the difference $|r - r_0|$. For shorter times this is not true. As the transition time to the Gaussian behavior and the final D values were the quantities of main interest in the present paper an averaging over r_0 has been carried out. For all times the resulting propagator P depends upon $|r - r_0|$ only.

The first four moments can be calculated from eqs. (2.6) and (2.7) in the case of normal diffusion as:[104]

$$\left\langle |r - r_o| \right\rangle = 4\sqrt{\frac{Dt}{\pi}} \qquad (2.7)$$

$$\left\langle |r - r_o|^2 \right\rangle = 6Dt \qquad (2.8)$$

$$\left\langle |r - r_o|^3 \right\rangle = \frac{32}{\sqrt{\pi}}(Dt)^{\frac{3}{2}} \qquad (2.9)$$

$$\left\langle |r - r_o|^4 \right\rangle = 60(Dt)^2. \qquad (2.10)$$

In the anisotropic system, the corresponding equations for each direction are[85]

$$\left\langle |l - l_o| \right\rangle = 2\sqrt{\frac{D_l t}{\pi}} \qquad (2.11)$$

$$\left\langle |l - l_o|^2 \right\rangle = 2D_l t \qquad (2.12)$$

$$\left\langle |l - l_o|^3 \right\rangle = \frac{8}{\sqrt{\pi}}(D_l t)^{\frac{3}{2}} \qquad (2.13)$$

$$\left\langle |l - l_o|^4 \right\rangle = 12(D_l t)^2, \qquad (2.14)$$

where l is x, y or z, respectively. The D values estimated from these four moments must synchronize each other in the case of normal diffusion for t values larger than the decay time of the velocity auto-correlation function. The elements of the diffusion tensor, corresponding to the x-, y- and z-axes, are calculated from eqs. (2.11)-(2.14). In this case, the diffusivity D can be assumed to be one third of the trace of the diffusion tensor:

$$D = \frac{1}{3}\left(D_x + D_y + D_z\right).$$
(2.15)

The good agreement (within the range of fluctuations) of the final D values will indicate that the diffusion time used in the evaluation procedure exceeds the correlation time.

2.2. Quantum Mechanics

2.2.1. Introduction

By classical physics, which obeys the laws of classical mechanics, which developed in the late nineteenth century, various experimental results could not be explained. Those phenomena, for instance black-body radiation, heat capacity of solids at low temperature, atomic spectra, and the structure of the hydrogen atom, were able to solve by treating new physics schemes. Since the electrons and other microscopic 'particle' show wavelike as well as particle like behavior, which implies that electrons do presently obey classical mechanics, the fusion of the apparently complementary concepts of waves and particles was started by de Broglie and carried to fruition in the quantum mechanics[105-109] of Heisenberg and Schrödinger. However, the uncertainty principle of Heisenberg, which is authentically the limitation of the obtained microscopic information of a system, seems to be essential as the consequences of the wave-particle duality.

In the first part of this chapter, a brief concept of the Schrödinger equation was given. Then, the Born-Oppenheimer approximation has been introduced. The second part introduces the molecular quantum-mechanics methods, including Self-Consistent Field (SCF), and Møller-Plesset perturbation theory. Moreover, the density functional theory will be discussed in this chapter.

2.2.2. The Schrödinger equation

The state of a system defined by a mathematical function Ψ or the state function, which is a mathematical description of all the possibilities for a particle, where $\Psi^*\Psi$ equals the probability of finding the particle at that position. As in general, the state changes as well with time, thus, a time dependent Ψ will be then introduced. For a single particle of mass m, one-dimension system, the equation is postulated to be

$$-\frac{\bar{h}}{i}\frac{\partial \Psi(x,t)}{\partial t} = -\frac{\bar{h}^2}{2m}\frac{\partial^2 \Psi(x,t)}{\partial x^2} + V(x,t)\Psi(x,t), \qquad (2.16)$$

where $\bar{h} \equiv \dfrac{h}{2\pi}$, and $V(x,t)$ is the potential energy function of a system. The eq. (2.16) is introduced by Schrödinger in 1926. It is known as the time-dependent Schrödinger equation, which contains the first derivative of the wave function with respect to time and enable us to calculate the future state at any time, if one knows the wave function at time t.

As the solution of Schrödinger equation is an eigenvalue problem, the energy E are the eigenvalues, eigenfunctions are the wave function Ψ. Their eigenvalues and eigenfunctions are desired. One calls, $\hat{H}$ the Hamiltonian operator which is

$$\hat{H} = -\left(\frac{\bar{h}^2}{2m}\right)\frac{d^2}{dx^2} + V(x). \qquad (2.17)$$

Hence, a measurement of any properties must give a result as one of the eigenvalues of the corresponding operator. However, only the single-electron atom is exactly solvable, others are analytically unsolvable. The main problem is to solve the inter-electronic repulsion terms in the Hamiltonian. Therefore, one must make an approximation. The fundamental one based on the molecular orbital theory is the Born-Oppenheimer approximation.

2.2.3. Born-Oppenheimer approximation

One recognizes that the mass of electron is much less than the mass of the atomic nuclei as well as the instantaneously motion responding of an electron. Therefore, instead of solving an equation for several nuclei and electrons, one solves the equations for electrons in the potential, which is provided, be static nuclei. The molecular Hamiltonian is then

$$\hat{H} = -\frac{\bar{h}^2}{2}\sum_\alpha \frac{1}{m_\alpha}\nabla_\alpha^2 - \frac{\bar{h}^2}{2m_e}\sum_i \nabla_i^2 + \sum_\alpha\sum_{\beta>\alpha}\frac{z_\alpha z_\beta e'^2}{r_{\alpha\beta}} - \sum_\alpha\sum_i \frac{z_\alpha e'^2}{r_{i\alpha}} + \sum_j\sum_{i>j}\frac{e'^2}{r_{ij}}, \quad (2.18)$$

where α and β describe nuclei while i and j describe electrons. The first term assigns to the kinetic energy operator of the nuclei. The second term assigns to the kinetic operator of the electrons. The third term is the repulsions potential energy between the nuclei, where $r_{\alpha\beta}$ is the distance between nuclei α and β with atomic number Z_α and Z_β. The forth term assigns the attraction potential energy between the electrons and the nuclei, where $r_{i\alpha}$ is the distance between electron i and nuclei α. Last, the fifth term assigns to repulsions potential energy between the electrons, where r_{ij} is the distance between electron i and electron j. The hard core then would be the so called electronic Hamiltonian, which includes the second, forth and fifth terms. This separating electronic and nuclear motions approximation is expressly, Born-Oppenheimer approximation. The electronic Hamiltonian in atomic units can be written as

$$\hat{H} = -\frac{1}{2}\nabla_i^2 - \sum_\alpha\sum_i Z_\alpha e^2 + \sum_i\sum_{i<j}\left(\frac{1}{r_{ij}}\right) \qquad (2.19)$$

2.2.4. Quantum mechanics methods
2.2.4.1. Hartree Fock method

The principle of this method is to assume any single electron moves in a potential that is a spherical average of all the other electrons potentials. One solves numerically the Schrödinger equation for such a potential. By this approximation, the wave function of an atom or a molecule is the Slater determinant. For an n-electron system, one gets the wave function as

$$\Psi(r_1,r_2,r_3,...,r_n) = \frac{1}{\sqrt{n!}} \begin{vmatrix} \varphi_1(r_1) & \varphi_2(r_1) & ... & ... & ... & \varphi_n(r_1) \\ \varphi_1(r_2) & ... & ... & ... & ... & \\ ... & ... & ... & ... & ... & \\ ... & ... & ... & ... & ... & \\ \varphi_1(r_n) & ... & ... & ... & ... & \varphi_n(r_n) \end{vmatrix}. \qquad (2.20)$$

In deed, the molecular orbital function is built up by a linear combination of atomic orbitals, LCAO-MO. A set which is used to prescribe the one-electron functions is namely basis functions. For instant, the molecular orbital φ_i is able to build by a linear combination of m atomic orbitals $\chi(r)$, where c_{ij} is a molecular orbital expansion coefficient.

$$\varphi_i(r_1) = c_{1i}\chi_1(r_1) + c_{2i}\chi_2(r_1) + c_{3i}\chi_3(r_1) + ...c_{mi}\chi_m(r_1) \qquad (2.21)$$

or

$$\varphi_i(r_i) = \sum_{j=1}^{m} c_{ij}\chi_j(r_1). \qquad (2.22)$$

Since, the amount of these coefficients is unknown, except this value must not be less than a half of total electrons of a system. Presently, one knows how to build the wave function for a system. What this method does, is to guess reasonable unknown coefficients for all the orbitals and calculate a mean potential. The equation of a particular electron must be solved subsequently. The calculated wave equation from this equation is then used to polish the potential, which another electron experiences in the atom. The equation for this other electron is then solved and used to refine the original potential felt by eventually another electron. These steps are repeated, and recalculated on the basis of new functions until the solutions for all electrons are unchanged, which is an origin of the word, self-consistent field.

If one looks for the set of n orbitals yielding the lowest energy of a molecular system in the sense of the variational principle, one finds that they are determined by the equations

$$\hat{F}(r_1)\psi_i(r_1) = E_i\psi_i(r_1), \qquad (2.23)$$

called Hartree Fock (HF) equations. The orbitals $\psi_i(r_1)$ are named molecular orbitals, and the Fock operator, $\hat{F}$, is given by

$$\hat{F}(r_1) = \hat{H}^{core}(r_1) + \sum_k^n \left(2J_k(r_1) - K_k(r_1)\right), \tag{2.24}$$

where $\hat{H}^{core}(r_1) = -\frac{1}{2}\nabla_1^2 - \sum_i \sum_A \frac{Z_A}{r_{iA}}$. The first part represents the one-electron part comprising the differential operator of the kinetic energy and the potential of the nuclei i. Interesting is the second term, which is the electron-electron interaction, and describes the whole electron mean potential. Those consisting two terms are respectively Coulomb and Exchange potential with

$$J(r_1) = \sum_{k=1}^n \int \frac{|\psi_k(r_1)|^2}{r_2 - r_1} dr_2 \tag{2.25}$$

and

$$K(r_1)\psi(r_1) = \delta_{s_k s} \sum_{k=1}^n \psi_k(r_1) \int \frac{\psi_k(r_2)\psi(r_2)}{|r_2 - r_1|} dr_2 \tag{2.26}$$

where the $\delta_{s_k s}$ equals 0 if the spin functions belong to the different orbital ψ and ψ_k and equals 1 if the same spin functions are assigned. Hence, the HF equations are integrodifferential equations, which must be solved iteratively until the second-term potential of eq. (2.24) is 'self-consistent'. The further approximations are virtually necessary for all solutions for molecules based on the so-called *algebraic approximation*. The HF equations are able to transformed into matrices equations (Roothaan equations)[110] and become

FC=SCE $\tag{2.27}$

With the Fock and overlap matrices

$$F \equiv \langle \chi | F_\chi \rangle \tag{2.28}$$

and

$$S \equiv \langle \chi | \chi \rangle \tag{2.29}$$

The bracket $\langle|\rangle$ is used as a short-hand notation for integration over the coordinates of an electron i. The C would finally be the HF solutions given as m column vectors c_j of coefficients referring to a chosen basis set.

Basis set

There are two exiting basis functions, in which the first type is so-called Slater-type orbital (STO) and defined as

$$s(\varsigma, A, l) = N_{\varsigma,l} r_A^{(n-1)} e^{-\varsigma\, r_A}, \tag{2.30}$$

where ς, r_A, n, and l are respectively the Slater orbital exponent coefficient, orbital radius in Å, the principle and angular number. Another analytical form of the basis functions, which was suggested by Boys;[111] is

$$g(\alpha, A, l) = N_{\alpha,l} x_A^i y_A^j z_A^k e^{-\alpha r_A^2}, \tag{2.31}$$

where α is the Gaussian orbital exponent. Obviously, the Gaussian type $e^{-\alpha r_A^2}$ decays much more rapidly and hence integrate easier than the Slater type $e^{-\varsigma\, r_A}$.

In the past, the two-electron integral term is solved by their number grown as m^4, where m means the number of basis function. Hence, one should keep m as small as possible. The way to achieve this is the use of fixed linear combinations of several Gaussian type orbitals (GTF) as a basis functions in the molecular calculations,

$$\chi_\mu = \sum_j c_{j\mu} g_j. \tag{2.32}$$

The coefficients of the 'primitives' in these 'contracted' GTF (CGTF) as transferred from calculations on atoms. Since the selection of an appropriate basis set is critical for an *ab initio* study to be successful, a short account of the classification and performance of basis sets will be given.

Minimal Basis Sets

A basis set is called 'minimal' (MB) if the single CGTF is employed for each type of atomic orbital occupied in the ground state of the respective atom. For example,

C: 1s, 2s, $2p_x$, $2p_y$, $2p_z$.

The STO-3G basis set is the use of three Gaussian primitives per basis function, where STO stands for a Slater-type-orbitals having the radial dependence $e^{-\xi r}$ as basis set.

Split Valence Basis Sets

The increasing the number of the basis functions per atom is a way to make a larger basis set and so-called split valence basis sets, for example 6-31G, which has two sizes of basis function for each valence orbital. The core consists of 6 GTOs which are not split, while the valence orbitals are described by one orbital constructed from 3 primitive GTOs and one single GTO. In case of C, it is represented as:

C: 1s, 2s, $2p_x$, $2p_y$, $2p_z$, 2s', $2p_x'$, $2p_y'$, $2p_z'$.

Here, primed and unprimed enormities have the different orbit size.

Polarized Basis Sets

Polarized basis sets allow some small contributions from the unfilled orbital, what is required for the ground state for atom description by adding orbitals with angular momentum beyond. For example, the d functions are added to the C atom. The first star in 6-31G** will stand for the polarized function (particular d orbitals) on non-hydrogen atom. The second one will add the p orbitals to the hydrogen atom. The other notation is 6-31(d,p).

Particularly widespread are the basis sets suggested by the Pople group:[109] STO-3G (minimal), 3-21G and 4-31G (split valence), 6-31G* and 6-31G** (split-valence augmented by polarized functions). For another survey and specific comments for a particular problem can be found in reviews.[112,113]

Mulliken Population Analysis

A Mulliken population analysis,[114] which is actually the total charge among the atoms in the molecule, computes charges by dividing orbital overlap evenly between the two atoms involved.

2.2.4.2. Møller-Plesset perturbation theory

One could see that the HF determinant is a good zero-order approximation. Hence, this type of correlation makes minor corrections to the HF results of molecular geometries, force constants, or molecular properties. However, a typical dynamical correlation effect is the dispersion energy, which is not contributed to the intermolecular bonding and not obtained at the HF level. This is responsible for the van der Waals bond between rare gas atoms and non-polar molecules, also significantly to other types of intermolecular bonding, e.g. hydrogen bonds. In spite of the fact that going beyond the HF approximation and taking electron correlation into account, even in an approximating way, is computational demanding. The simplest approximation to the electron correlation energy, $E_{\text{corr}}^{(2)}$ is provided by the Møller-Plesset Perturbation Theory up to the second order (MP2)[115]

$$E_{\text{corr}}^{(2)} = \sum_{ijab} \frac{\langle ia \mid jb \rangle [2\langle ia \mid jb \rangle - \langle ib \mid ja \rangle]}{E_i + E_j - E_a - E_b}. \qquad (2.33)$$

This expression refers to a closed-shell ground state, i and j being doubly occupied orbitals. The most time consuming step is the transformation from the integrals over basis function, $\langle \mu \upsilon \mid \lambda \sigma \rangle$, to the integrals over molecular orbitals, $\langle ia \mid jb \rangle$:

$$\langle ia \mid jb \rangle = \sum_{\mu \upsilon \lambda \sigma} c_{i\mu} c_{a\upsilon} c_{j\lambda} c_{b\sigma} \langle \mu \upsilon \mid \lambda \sigma \rangle. \qquad (2.34)$$

However, in case it fails, one could take into account the doubly substitutions to higher orders, including higher substitutions (MP3, MP4, …) or switch to multireference treatment.

2.2.4.3. Density functional approach

The computational demanding in the most frustratingly problem in an including of include electron-correlation energy, Hohenberg and Köhn[116] have presented the energy of a many-electron system which is a unique functional of electron density, $\rho(r)$. Hence, to get the energy instead of knowing the many particles wave function, one needs only the one particle density $\rho(r)$. Köhn and Sham[117] have

shown further that the density yields the minimum energy by solving a single-particle equation with an effective 'exchange-correlation' potential $v_{xc}[\rho(r)]$

$$\{h(r_1) + j(r_1) + v_{xc}[\rho(r)]\}\psi_i(r_1) = E_i\psi_i(r_1),\qquad\qquad(2.35)$$

where

$$\rho(r) = \sum_i \psi_i(r)\psi_i^*(r).\qquad\qquad(2.36)$$

Note, $v_{xc}[\rho(r)]$ is non-exact, depending on method uses. This equation is closely related to the HF eq. (2.23) with the Coulomb potential $J(r_1)$, but instead of the HF exchange potential, $K(r_1)$ is replaced by $v_{xc}[\rho(r)]$.

2.3. Statistical Mechanics

2.3.1. Introduction

If one considers 1 mole of any typical amount of material, it contains about 6×10^{23} molecules. In the macroscopic system of these 10^{23} molecules, it is impossible to follow a detailed history of what has happened to each molecule. One expects that the average macroscopic behavior of some molecules do not depend on all of the microscopic detail.

Statistical mechanics[118] gives macroscopic properties from microscopic principles (for example, quantum mechanics, etc.) by an assumption of a random distribution. It now becomes a question, how one can calculate the macroscopic thermodynamic properties of matter, i. e., *E* (energy), *S* (entropy), *H* (enthalpy), *G* (Gibbs free energy), etc., from the microscopic quantum or classical mechanical properties of the molecules. Although these quantities are possible to solve out, however, this is impractical to compute them for 10^{23} molecules, and provides all details than needed. What one wants is a long termed average for large system. One can defined the state of the system by the wave function $\Psi(r,t)$, time dependent, or $\Psi(r)$, time independent or definite energy associated. Statistical mechanics is another way to treat a very complicated quantum mechanics problem of many particles.

As interests are focused on a few macroscopic properties of the system, what one considers is not only a single system, but infinite copies of the same system.

These are known as 'ensemble'. A density function $\rho(p,q,t)$, is the probability density of finding any particle with momenta p and coordinate q at time t, characterizes a distribution point in Γ-space, defined as

$$\rho(p,q,t)\mathrm{d}^{3N}p\,\mathrm{d}^{3N}q = \text{Number of representative containing points in the}$$

volume element $\mathrm{d}^{3N}p\mathrm{d}^{3N}q$ located at (p, q) in Γ \hfill (2.37)

The fundamental postulate of statistical mechanics is that all quantum states Ψ of a system consisting of the macroscopic description are equally likely, in other words the system consisting of number of particles, each of which can have different energy or can distribute differently among their energy levels, is often quantized. On one side, one can not measure the individual energy levels of each particle in the laboratory. Instead one can measure only macroscopic quantities, such as N (particle number), V (volume), T (temperature), or P (pressure), respectively. On another side, a basic tool in statistical mechanics is an ensemble of systems, all alike in natures, but in different states. Then, the identification of the type of ensemble by macroscopic variables, which is able to be measured, is necessary. For instance, in a canonical ensemble, the conserved quantities are N, V and T. Positions and momenta, as coordinates in a multidimensional space or phase space $6N$ dimensions for a system of N atoms, define the instantaneous mechanical state.

If the long time average over an arbitrary function of the phase space coordinates is equal to the average of the same function taken over all possible, and equally probable, states that the system can go through, this important hypothesis is the ergodicity problem. However, the functions that describe the macroscopic state of the system have to become independent of the time interval used in the averaging process, hence, the system has reached equilibrium. Consequently, the experimental observable macroscopic property B_{obs} is equivalently assumed to the time average $B(\Gamma)$, taken over a large finite time interval and the abbreviation Γ is used for a particular position in phase space (p, q). Thus one can compute any quantity by time averaging or by ensemble averaging. The relation for B is finalized as

$$B_{\mathrm{obs}} = \langle B \rangle_{\mathrm{time}} = \langle B \rangle_{\mathrm{ens}} = \frac{1}{\Gamma_{\mathrm{obs}}}\sum_{\tau=1}^{\tau_{\mathrm{obs}}} B(\Gamma(\tau)), \hfill (2.38)$$

while $\langle B \rangle_{\text{time}}$ and $\langle B \rangle_{\text{ens}}$ are a time and ensemble average of the observable properties, respectively. Γ_{obs} is a total observable time, and $B(\Gamma(\tau))$ is the observable property at each small time interval, τ.

2.3.2. Ensembles in common use
2.3.2.1. Microcanonical ensemble

The above postulate actually implies the microcanonical ensemble, in thermodynamics equilibrium, with the density function

$$\rho(p,q) = \begin{cases} 1 & \text{if } E < H(p,q) < E + \Delta E \\ 0 & \text{otherwise} \end{cases} . \tag{2.39}$$

$H(p,q)$ is a Hamiltonian to find an energy (E) of this ensemble system. In equilibrium, the system in this ensemble has N particles, in the volume V, and the energy lying between E and $E + \Delta E$.

The fundamental quantity, entropy, furnishes a connection between the microcanonical ensemble and thermodynamics and its determination is a main task. The volume in the Γ-space is expressed by $\Gamma(E)$ as

$$\Gamma(E) \equiv \int_{E<H(p,q)<E+\Delta} d^{3N}p \, d^{3N}q \, \rho(p,q). \tag{2.40}$$

It is noticed that $\Gamma(E)$ depend on N, V, and ΔE and if ΔE is much smaller than E, then $\Gamma(E) = \omega(E) \Delta E$. Where $\omega(E)$, the density of states, of the system at the energy E is defined by

$$\omega(E) = \frac{\partial \Sigma(E)}{\partial E}, \tag{2.41}$$

and the entropy is defined by

$$S(E,V) \equiv k \log \Gamma(E), \tag{2.42}$$

where k is Boltzmann 's constant.[119] All the entropy properties are possessed by this equation in thermodynamics. S satisfied the property as required by the second law of the thermodynamics has to be an extensive quantity. If $\Sigma(E)$, enclosed by the energy surface of energy E, denotes the volume in Γ-space, one gets

$$\Sigma(E) = \int\limits_{H(p,q)<E} d^{3N}p\, d^{3N}q \ . \tag{2.43}$$

If one considers two subsystems isolated from each other which molecular systems consist of N_1 and N_2 particles and $N_2 \gg N_1$, then the system entropy is finally derived as

$$S(E,V) = S_1(\overline{E_1},V_1) + S_2(\overline{E_2},V_2). \tag{2.44}$$

This proves the extensive property of the entropy, also implies that the subsystems energies have their definite values under the restriction $E_1 + E_2 = E$. Thus the proof also reveals the meaning of the isolated system temperature or in other words, the temperature of an isolated system is a parameter controlling the equilibrium between one part of the system and another. The fact, the number of particles becomes very large (almost all members of the ensemble have the values $(\overline{E_1},\overline{E_2})$, is fundamental to the success of statistical mechanics as a theory of matter. Three equivalent possibilities of deriving the entropy has been shown

$$S = k \log \Gamma(E) = k \log \omega(E) = k \log \Sigma(E) . \tag{2.45}$$

Thus the success in deriving the first and second laws of thermodynamics is done. One summarizes some practical thermodynamics functions, which are possible to calculate as the following:

$$T = \left(\frac{\partial U}{\partial S}\right)_V , \tag{2.46}$$

$$P = -\left(\frac{\partial A}{\partial V}\right)_T , \tag{2.47}$$

$$A = U - TS, \tag{2.48}$$

$$G = U + PV - TS, \tag{2.49}$$

$$C_v = \left(\frac{\partial U}{\partial T} \right)_V , \qquad\qquad (2.50)$$

where *P, A, U,* are pressure, Helmholtz free energy, and intrinsic energy, respectively, while C_v is heat capacity at constant volume.

2.3.2.2. Canonical ensemble

If one is interested in the thermal equilibrium with a large system, which ensemble is appropriated for this non-isolated system becomes diagnostic. The answer is to find the probability, proportional to the density in Γ-space for this ensemble, that the system has energy *E*.

Consider an isolated system, included two subsystems with macroscopic number of particles N_1 and N_2, respectively, and assume $N_2 \gg N_1$. The probability density of finding any particle in this phase space for the small subsystem is finally derived as

$$\rho(p,q) = e^{-H(p,q)/kT} . \qquad\qquad (2.51)$$

This ρ vanishes only in the case that E_1 (energy of subsystem 1) $> E$ (E_1+E_2). In reality the larger subsystem behaves like a heat reservoir in thermodynamics. The small subsystem, determining the temperature through the contact with a heat reservoir, is the so-called *canonical* ensemble. Then, the partition function in its semi-classical version is defined as:

$$Q_N(V,T) \equiv \int \frac{d^{3N}p\, d^{3N}q}{N!h^{3N}} e^{-\beta H(p,q)} , \qquad\qquad (2.52)$$

where $\beta = 1/kT$, and where *h,* the Plank constant, has the power $3N$ of the dimensional of momentum and distance. The factor $1/N!$ is a corrected factor for Boltzmann counting. To obtain the thermodynamics of the system, the formula is performed as

$$Q_N(V,T) = e^{-\beta A(V,T)} , \qquad\qquad (2.53)$$

where A(V,T) is the Helmholtz free energy. By the thermodynamical Maxwell relations one gets

$$P = -\left(\frac{\partial A}{\partial V}\right)_T , \tag{2.54}$$

$$S = -\left(\frac{\partial A}{\partial T}\right)_V , \tag{2.55}$$

$$G = A + PV, \tag{2.56}$$

$$U = <H> = A + TS. \tag{2.57}$$

In canonical ensembles, due to the exponential density function, the densities of particles go away from the origin of Γ-space exponentially. By counting the number of particles on the energy surface, the energy distribution can be easily evaluated. The energy and the area of the energy surface increase when those particles are far from the origin. For a macro system of N atoms, the area increases as e^E, $E \propto N$. This is an explanation that thermodynamics properties are insensitive to methods of derivation.

2.4. Molecular Dynamics

2.4.1. Introduction

The earliest computer simulations of liquids were deliberated already for about 50 years ago.[120] It was to investigate structural properties of a system laid on the 'Monte Carlo' (MC) simulation, in which the role of the random numbers play. Nevertheless, a different technique required for providing the dynamics properties of well-defined systems of particles, so-called Molecular Dynamics (MD)[121,122] simulation, has been introduced. This method lies on the solution of classical equations of motion. Newton, Hamilton, or Lagrange equations are normally used, depending on the characteristics of the system and the computer code optimization. In particular, the MD technique was first proficiently developed by Alder and Wainwright[123,124] in the late 1950's. In these papers, the system was simulated using hard sphere molecules. Then in 1964, Rahman[125] has made a successful attempt to solve the equations of motion for Lennard-Jones particle systems. Since then, the feasible Lennard-Jones model's properties have been thoroughly investigated. Subsequently, the computer simulations become more feasible.

MD is virtually used for any atomic or molecular system. A set of N classical particles characterized by coordinates, velocities, and masses is selected. The forces acting on the particles are evaluated from the derivatives of the potentials, usually interacting through the sum of suitable pairs in most investigations. The equations of motion are solved numerically by standard methods. The statistical averages of interest are figured out by the positions and the velocities of the particles as time averages over the trajectories of the system in its phase space.

2.4.2. Motivation and applications

The results from the simulations might be able to compare with those obtained from the real experiments. In spite of this, the initial step is to test the inherent potential model used in simulations. While, at the end one expects to visualize microscopic insights to the macroscopic experimental results and assists to analyze new results. The role of simulations is on one hand to be a bridge between models and the theoretical prediction and on the other hand to be a bridge between models and the experimental results and often called as 'computer experiment'. The schematic connection (Figure 2.1) is illustrated in the way that simulation is conducted and analyzed.
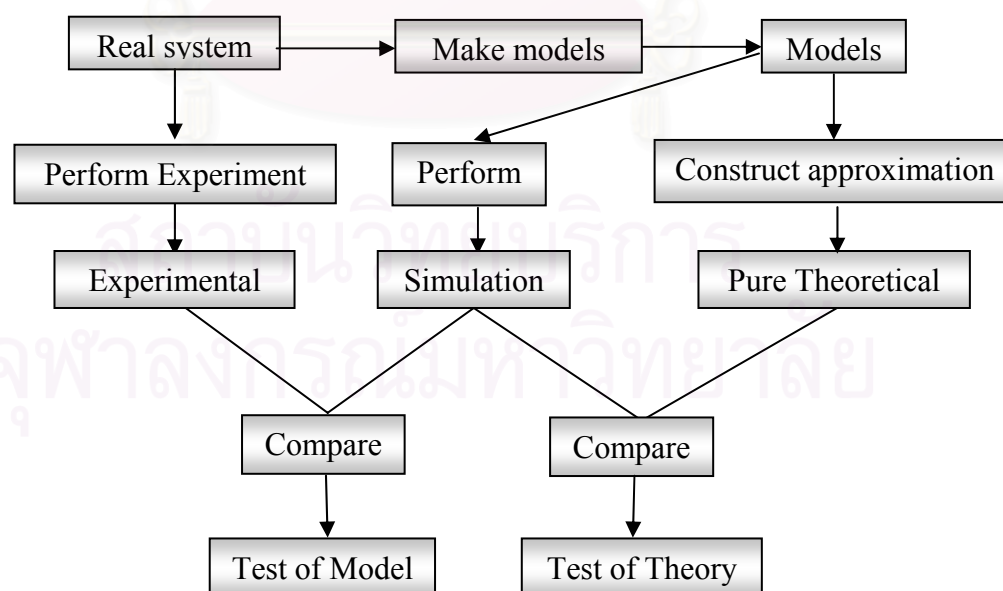
Figure 2.1 The connection between experiment, theory and computer simulation.[126]

2.4.3. Equation of motion

The main idea in molecular dynamics simulation is the integration of Newton's laws of motion. But, the choice of algorithm is important. The successive system configurations will generate the trajectory, which illustrates how positions and velocities of the particles changed with time.

Herein, the Newton's laws of mechanics are:

1. A particle moves continuously at a constant velocity, unless, a force acts and causes the velocity change.
2. The rate of momentum change is equal to force (Equation of motion).
3. An equivalent force of action and reaction is conserved.
4. The forces are vectors.

In another form, the Newton's second law ($F = ma$), which demonstrates how the trajectory of the particle can be generated where a is an acceleration, can be written as a differential equation by,

$$\frac{\mathrm{d}^2 x_i}{\mathrm{d}t^2} = \frac{F_{x_i}}{m_i}.$$ (2.58)

This equation describes the motion of a particle i, with the mass m_i, along one coordinate x_i. The total force F_{x_i} can be assumed to be a sum of all atom pair forces in the system in x-axis.

2.4.4. A basic algorithm

To carry out the MD simulation, the program is constructed in the rule, as following:

1. The parameters specifying the conditions of the system, e. g., initial temperature, particles number, time step, total time, are read in.
2. The system is initialized.
3. The forces for each pair of particles in the system have been computed.
4. The Newton's equation has been integrated. This step and the previous steps of force calculations, the core of MD simulation, will be repeated until the total or evaluation time is reached.

5. After the core loop is completed, either dynamics or structural quantities could be carried out now.

The above algorithm is illustrated in Figure 2.2.
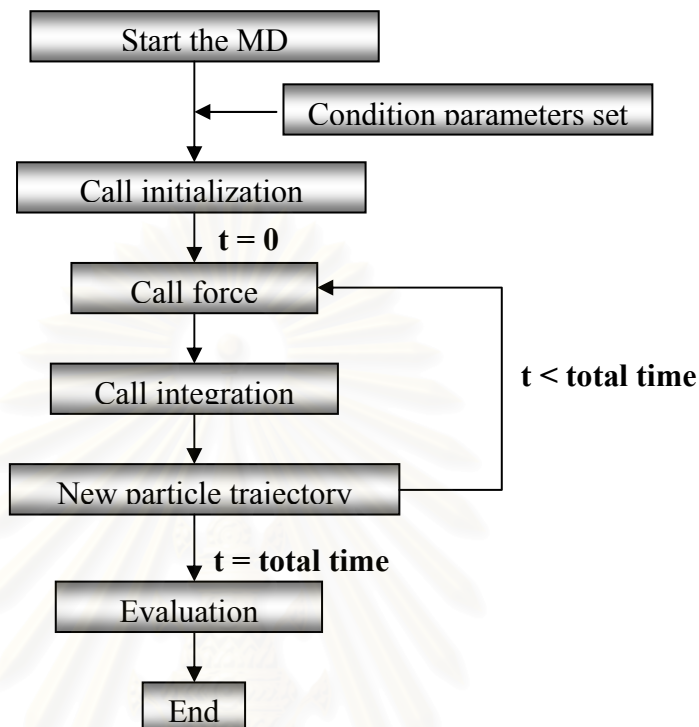
Figure 2.2 The schematic representation of the simple subroutines in the MD program.

2.4.5. Technical details

In this section, the great practical importance of computational tricks will be discussed. One must compromise between computational time and accuracy of the results. Those useful tricks have in deed no deeply physical significance.

2.4.5.1. Boundary conditions

One advantage of the simulation is that macroscopic properties are achievable by using a small numbers of particles, utilizing by the treatment of boundaries. Boundary condition[127] is a mimic of the presence of an infinite bulk surrounding of the N-particle system in order to avoid surface effects, whilst explicitly treating the simulation cell, replicated through space to produce an infinite periodic system. In Figure 2.3, the volume containing the marked N particles, which enables to interact with all others in this infinite periodic system, is treated as the primitive box of infinite identical cells. The utility of this mimic is to perform a simulation

condition in such a way that the particles experience forces like they were in bulk fluid. Additionally, the number of particles in the central box, thus, remains constant.
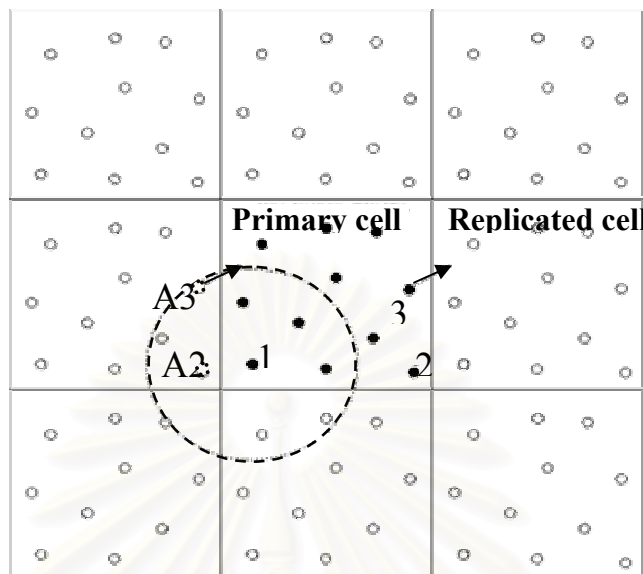
Figure 2.3 Schematic representation of the periodic boundary condition

As a particle leaves the simulation cell, its image in the replicated cell on the opposite side re-enters the simulation cell. As particle 3 in Figure 2.3 leaves the cell as depicted by the arrow, its image in the cell to the left of the simulation cell, A3, re-enters the simulation cell. It can be seen in Figure 2.3 that the separation between particles 1 and 2 is large but the image of particle 2, labeled A2, is much closer to particle 1. An important artifact of this technique, which is known as the minimum image convention, is that when the cell is too large and the interactions between particles become significant by half of the length of the simulation cell as shown as a circle of that radius about particle 1 in Figure 2.3. Consequently, an energy summation over the particles in the primary simulation cell will miss some significant interactions.

2.4.5.2. Truncation of interactions

Calculations of the non-bonded energies or forces are the most time consuming step in the simulation. To solve this dilemma, one of the most common and smart ways is to employ a non-bonded cut-off and to apply the minimum image convention. The further apart than cut-off values of all pair interactions are set to be zero. However, the cut-off radius ought to be not so large that the particles see their own mimics when periodic condition applied.

2.4.5.3. Shifted–force potential

A discontinuity in both potential energy and force at a cut-off radius is virtually appeared and caused the energy conservation problem in the simulation. The most common technique using for this discontinuity is to apply a shifted force. The energy and the force before (solid line) and after (dashed line) shifted have been visualized in Figure 2.4. The approach of this kind of force is to subtract from all potential energy values a constant term:

$$v'(r) = v(r) - v(r_c) \qquad\qquad r \leq r_c, \qquad\qquad (2.59a)$$
$$v'(r) = 0 \qquad\qquad\qquad\qquad r > r_c, \qquad\qquad (2.59b)$$

where r_c is the cut-off distance, $v(r)$, and $v(r_c)$ are the potentials at the distance r and r_c, respectively. Although, the term $v(r_c)$ would not affect in the process of the force calculation as it is constant, but to avoid instability in the equation of motion, a linear function, making derivative zero at cut-off, has been applied. Then, eqs. (2.59a) and (2.59b) become

$$v(r) = v(r) - v(r_c) - \left(\frac{\mathrm{d}v(r)}{\mathrm{d}r}\right)_{r=r_c} (r - r_c) \qquad r \leq r_c, \qquad\qquad (2.60a)$$

$$v'(r) = 0 \qquad\qquad\qquad\qquad\qquad\qquad r > r_c, \qquad\qquad (2.60b)$$

However, a drawback of this is directly connected to any thermodynamics property calculation since it is relatively straightforward to the unshifted potential.
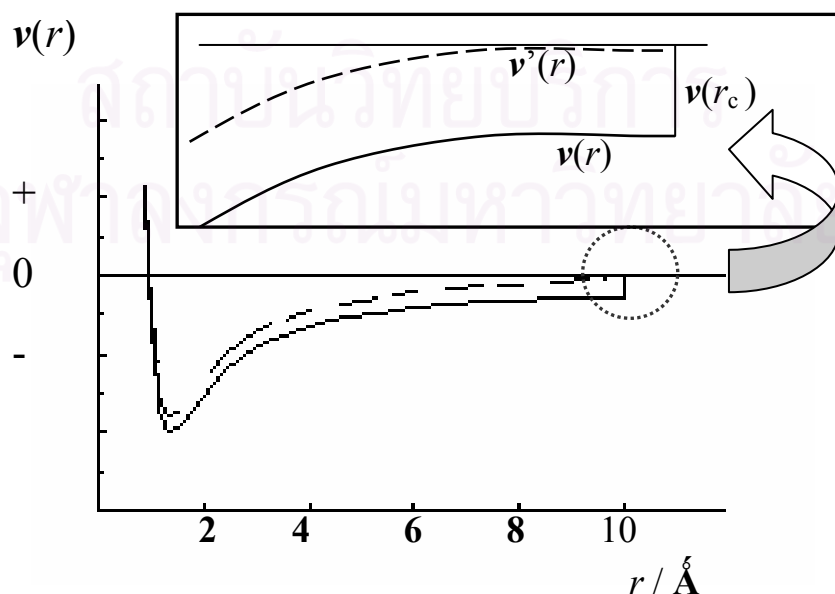
Figure 2.4 Schematic representation of an applying shifted-force potential

2.4.5.4. Verlet algorithm

Despite the fact, that several possible algorithms are available in order to solve the equation of motion. Still, the Verlet algorithm[128] is not only one of the simplest but usually one of the best. This algorithm is straightforward. Therefore, the obvious benefit is to handle a very large systematic study. To derive the Verlet algorithm, a position r is expanded by a Taylor expansion of a particle coordinate around time t,

$$r(t + \Delta t) = r(t) + v(t)\Delta t + \frac{f(t)}{2m}\Delta t^2 + \frac{\Delta t^3}{3!}\dddot{r} + O(\Delta t^4),$$ (2.61)

as well as,

$$r(t - \Delta t) = r(t) - v(t)\Delta t + \frac{f(t)}{2m}\Delta t^2 - \frac{\Delta t^3}{3!}\dddot{r} + O(\Delta t^4).$$ (2.62)

where $O(\Delta t^4)$ is an expanded Taylor function, and Δt is the time step. Note, that the Verlet algorithm does not take up the velocity in connecting with the new position calculation. By summation of both eqs. (2.61) and (2.62), one obtains

$$r(t + \Delta t) + r(t - \Delta t) = 2r(t) + \frac{f(t)}{m}\Delta t^2 + 2O(\Delta t^4),$$ (2.63)

or

$$r(t + \Delta t) \approx 2r(t) - r(t - \Delta t) + \frac{f(t)}{m}\Delta t^2.$$ (2.64)

The errors in eq. (2.64) are of order Δt^4. Nevertheless, a simple approach to carry out the velocity is to divide the difference in positions at time $t + \Delta t$ and $t - \Delta t$ by $2\Delta t$:

$$v(t) = \frac{r(t + \Delta t) - r(t - \Delta t)}{2\Delta t},$$ (2.65)

which are subject to errors of order Δt^2. By integrating Newton's equations, the acceleration is just the force divided by the mass,

$$a(t) = f(t)/m,$$ (2.66)

and using eq. (2.64), r($t+\Delta t$) is calculated. Last, the velocity is calculated each time step. However, neither Verlet nor any other algorithms, e. g., predictor-corrector algorithm,[129] would be expected to reproduce the exact trajectory.

2.4.5.5. Radial distribution function

The radial distribution function (RDF) allows a straightforward theoretical measurement in a simulation to the real laboratory experiment measurements, e. g., neutron or X-ray scattering. It is basically defined as the ratio between the average number density $\rho(r)$ at a distance r from any determined atom (assuming all atoms are identical) and the number density at a distance r from an atom at the same overall density. By the definition,[130,131] the RDF, displayed in Figure 2.5, is calculated as

$$g(r)_{ab} = \frac{N_b(r)}{\rho_{ab} \Delta V(r)}, \qquad (2.67)$$

where $\Delta V(r)$, a volume in between the spheres of radials r and $r + dr$, is equal to $\frac{4}{3}\pi\{(r+dr)^3 - r^3\}$, and ρ_{ab} is a number density of unrepeated pair between atom 'a' and atom 'b' found in the volume shell, $\Delta V(r)$. A number of particles of type 'b' around a particle 'a' in the volume ΔV are collected as $N_b(r)$.

Figure 2.5 To evaluate $g(r)$ as shown in eq. (2.67), number of particles of type 'b' around a particle of type 'a' in the volume ΔV are collected.

2.4.5.6. Diffusion

The tendency of matter to migrate in such a way to eliminate spatial variations in composition, thereby approaching a uniform equilibrium state, is well-known called diffusion.[132] Fick's law, as recognized as a macroscopic law to describe diffusion, states that the flux j of the diffusing species is proportional to the negative gradient in the concentration (c) of that species as shown,

$$j = -D \cdot c, \tag{2.68}$$

where D is a constant of proportionality and referred as the transport diffusion coefficient. To compute the time evaluation of the concentration profile, the Fick's law must be combined with the expressing conservation of the total amount of the labeled material,

$$\frac{\partial c(r,t)}{\partial t} + \nabla \cdot j(r,t) = 0. \tag{2.69}$$

Combining eqs. (2.68) and (2.69), one gets

$$\frac{\partial^2 c(r,t)}{\partial t^2} - D\nabla^2 c(r,t) = 0. \tag{2.70}$$

To solve eq. (2.69), one has to introduce the boundary condition

$$c(r,0) = \delta(r), \tag{2.71}$$

where δ(r) is the Dirac delta function. This yields

$$c(r,t) = \frac{1}{(2\pi Dt)^{d/2}} \exp(-\frac{r^2}{2Dt}), \tag{2.72}$$

where d denotes the dimension of the system. In practice, one does not need $c(r,t)$ itself, but instead the time dependence of its second moment $<r^2(t)>$:

$$\langle r^2(t) \rangle = \int dr c(r,t) r^2, \tag{2.73}$$

as well as it is obligatory that

$$\int dr c(r,t) = 1 \tag{2.74}$$

Multiplying eq. (2.70) by r^2 and integrating over all space, the time evaluation of $<r^2(t)>$ is straight carried out:

$$\frac{\partial}{\partial t} \int dr r^2 c(r,t) = D \int dr r^2 \nabla^2 c(r,t). \tag{2.75}$$

Simply, one can derive the left-hand side as $\dfrac{\partial \langle r^2(t) \rangle}{\partial t}$. After all, the eq. (2.75), becomes

$$\frac{\partial \langle r^2(t) \rangle}{\partial t} = 2dD. \tag{2.76}$$

This relation is derived by Einstein, where D is a transport diffusion coefficient. Where $<r^2(t)>$ is a mean square displacement during time interval (t) and representing the microscopic interpretation. This $<r^2(t)>$ can be simply written as,

$$\partial \langle r^2(t) \rangle = \frac{1}{N} \sum_{i=1}^{N} \Delta r_i(t)^2, \tag{2.77}$$

where N is the total particle numbers of the system. To be more particular, the displacement is simply derived as the time integral of the marked particle's velocity, and this type of diffusion is the so-called 'self-diffusion'.

For example, if only one Cartesian component of the mean squared displacement is considered in this case,

$$2D = \lim_{t \to \infty} \frac{\partial \langle x^2(t) \rangle}{\partial t}, \tag{2.78}$$

and if one writes $x(t)$ as the time integral of the x component of the marked particle velocity, one conclusively gets

$$\langle x^2(t) \rangle = 2 \int_0^t \int_0^{t'} dt' \, dt'' \langle v_x(t') v_x(t'') \rangle. \tag{2.79}$$

The quantity, $\langle v_x(t') v_x(t'') \rangle$, called the velocity autocorrelation function (VACF), measures the correlation between the velocity of a particle at time t' and t'', by determined along an equilibrium trajectory. Under a change of time origin, the VACF will depend only on the difference of time t' and t'', as the invariant equilibrium properties as defined,

$$\langle v_x(t') v_x(t'') \rangle = \langle v_x(t' - t'') v_x(0) \rangle. \tag{2.80}$$

By inserting eq. (2.79) into eq. (2.76), one finally gets

$$D = \int_0^\infty d\tau \langle v_x(\tau) v_x(0) \rangle \tag{2.81}$$

by $\tau \equiv t - t''$ was introduced. It is obvious that this equation, D is derived by an integral of the velocity autocorrelation function as known as Green-Kubo relation. Note, both the Green-Kubo relation and the Einstein relation must be strictly equivalent in calculating the diffusion values.

2.5. Pulse Field Gradient Nuclear Magnetic Resonance

There are distinct with respect to the study of diffusion: the elementary process at the molecular level investigation, the tracer or self-diffusion studies, and the transport diffusion measurement. The NMR pulse field gradient (PFG) method,[21,133-136] which has the great advantage in providing a direct determination of the mean square displacement in a given time interval and regarding as a direct measurement of the self-diffusivity, allows measurements made over the distance in the micrometer range. It is applicable to both intracrystalline and long-range diffusion measurements, except the relaxation time of the nuclear spins is sufficiently long.

Considering the principle of NMR self-diffusion measurement, as schematically shown in Figure 2.6, the inhomogeneous field (the field gradient) is superimposed on the homogeneous field (Figure 2.6b) over two short time interval. Under the influence of the field gradient pulse, the procession of the transverse magnetization $M_\perp(z)$ depends on the spatial coordinate (z). A de-phasing of the vector of the transverse magnetization at the different positions is risen by the first gradient pulse (Figure 2.6c), and gives a result as the vector sum decay (Figure 2.6d). The broken lines in Figure 2.6c and d show the incompletely re-focusing of the molecules (spin) moving during the time interval between the gradient pulses and indicate the behavior with molecular migration. Hence, the decrease in the NMR signal becomes larger as the mean square displacement increase.
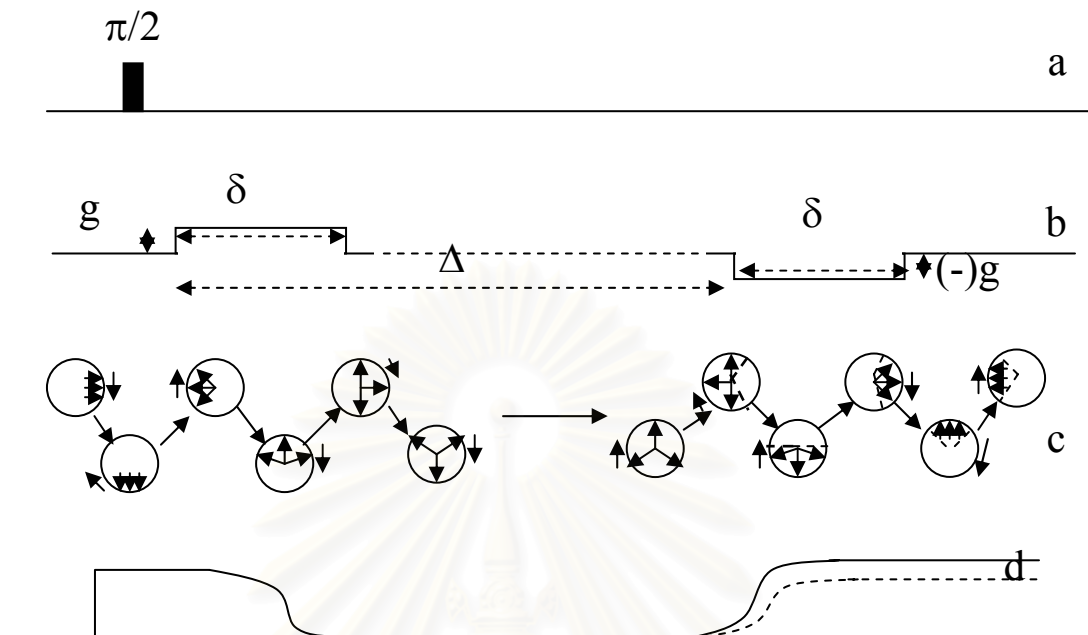
Figure 2.6 Schematic representations of the fundamentals of NMR self-diffusion measurements (a) radio frequency (r. f.) pulses, (b) gradient pulses, (c) transverse magnetization $M_\perp(z)$ of different regions, and (d) total transverse magnetization $M_\perp(z)$.[137]

The pulse field gradient, which yields a gentle treatment of the signal attenuation by diffusion under the pulse sequence, is one of the field gradient techniques. In order to visualize all procedures, the time program of the pulse field gradient technique is shown in Figure 2.7. Rigorous treatment of the signal attenuation by diffusion under these sequences yields[138,139]

$$\psi(t=2\pi)=\exp\left\{-\gamma^2 D\left[\frac{2}{3}\tau^3 g_0^2 + \delta^2(\Delta-\delta/3)g^2 - \delta\left(t_1^2 + t_2^2 + \delta(t_1+t_2)+2\delta^2/3-2\tau^2\right)gg_0\right]\right\}$$

(2.82)

where the meaning of the parameters t_1 and t_2 is explained in Figure 2.7.
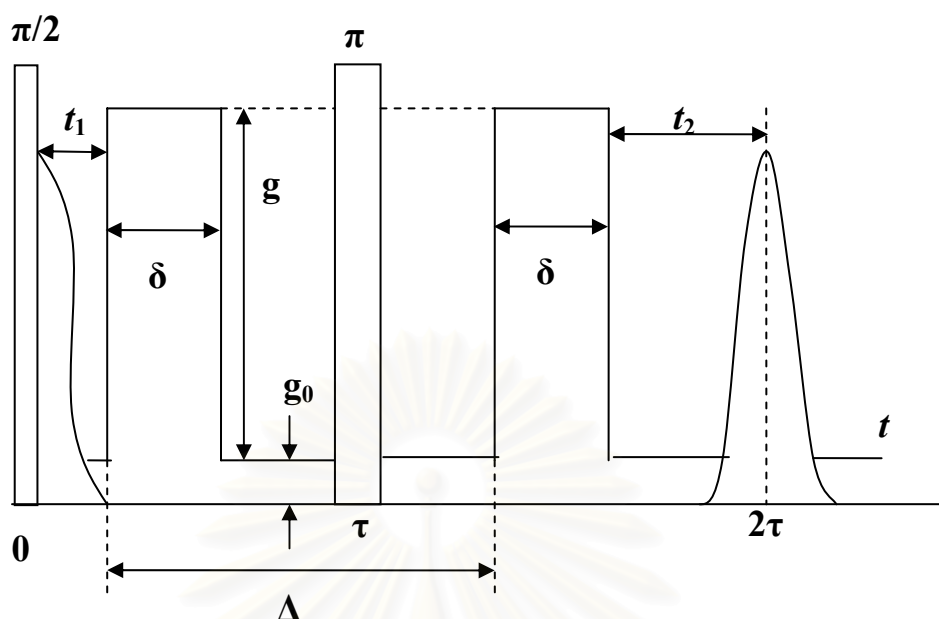
Figure 2.7 Diagram of time program of the pulse field gradient technique using primary echo[102]

For simplicity, under condition $\delta g \geq \tau g_0$, which means for sufficiently intense field gradient pulses, eq. (2.82) obviously coincides to be

$$\psi = \exp\left[-\gamma^2 D \delta^2 g^2 (\Delta - \delta/3)\right], \tag{2.83}$$

where γ and D denote the gyromagnetic ratio and the diffusion coefficient. The duration of the applied field gradient pulses, the duration of the 'dephasing' and the 'read' intervals, and the value of the time interval between the two echo sequence pulses are δ, τ and Δ, respectively.

CHAPTER 3

METHODOLOGY DETAILS AND CALCULATIONS

In order to get the drift of sections including in this chapter, the schematic representative methodology details and calculations are demonstrated in Figure 3.1.

CALCULATIONS AND METHODOLOGY DETAILS

3.1 Quantum Chemical Calculations

3.1.1 Silicalite-1 Representation

3.1.2 Selected Guest-Host Configurations

3.1.2.1 For the Investigations of preferential Binding Sites

3.1.2.2 For the Development of Guest-Host Potential Functions

3.1.3 Perform the Calculations

3.1.3.1 Water/silicalite-1

3.1.3.2 Methane/silicalite-1

3.2 Development of Guest-Host Intermolecular Potential Function

3.2.1 Water/silicalite-1

3.2.2 Methane/silicalite-1

3.3.1 Water in Silicalite-1

3.3 Molecular Dynamics Simulations

3.3.2 Methane in Silicalite-1

3.3.3 Water-Methane Mixtures in Silicalite-1

3.4 Pulse Field Gradient NMR Measurements

Figure 3.1 Schematic representation of the content of this chapter.

3.1. Quantum Chemical Calculations

3.1.1. Silicalite-1 representation
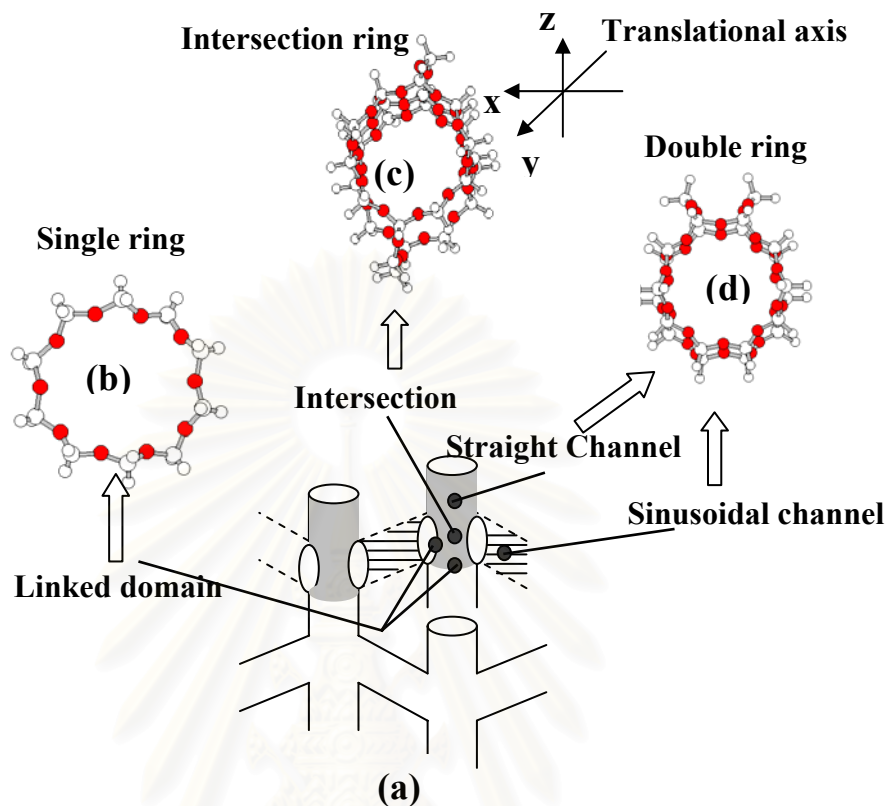
Figure 3.2 Schematic representations of the (a) silicalite-1 crystal structure, (b) linked domain, (c) straight and sinusoidal channels and (d) intersection channel

The silicalite-1 structure is characterized by the straight and sinusoidal channels, whose symmetry group is *Pnma*. The crystallographic cell[140] contains 288 atoms, namely 96 Si and 192 O, with cell parameters a = 20.07 Å, b = 19.92 Å and c = 13.42 Å. It is clear that the system consisting of all atoms in the unit cell does not allow the use of quantum chemical calculation even with a small basis set because of the unreasonable computation time that would be required. Therefore, the silicalite-1 crystal structure was represented by the three fragments (Figures 3.2b-3.2d), namely single, intersection and double rings. The sinusoidal and main parts of the straight channels of the crystal (Figure 3.2a), in which the inner surfaces are almost identical, were represented by the double 10-oxygen membered ring (Figure 3.2d). This fragment (mentioned later, for simplicity as the double ring) consists of 30 O and 22 Si atoms. The bigger fragment (35 O and 29 Si atoms), containing parts of the sinusoidal and straight channels, was used to represent the intersection and so-called

intersection ring (Figure 3.2c).[23,24] Note that the remaining valence orbitals of the silicon atoms of both fragments are then filled up by the hydrogen atoms. The chemical compositions of the single, double rings, and intersection, after filling up the remaining valence orbitals of the silicon atoms with hydrogen atoms, are $O_{10}Si_{10}H_{20}$, $O_{30}Si_{22}H_{44}$ and $O_{35}Si_{29}H_{58}$, respectively.

3.1.2. Selected guest-host configurations
3.1.2.1. For the investigations of preferential binding sites

Determining the water-silicalite-1 interactions based on *ab initio* calculations in order to understand the water orientation, preferable binding sites and energy barrier during the movement into and in the silicalite-1 pores are part of the main aims. Investigations have been made only for water molecules in which its intersections with silicalite-1 is more attractive due to its higher-polarity and lower-symmetry in comparison to those of methane molecule.

To follow the movement of water molecule in the silicalite-1 pore, quantum chemical calculations have been performed when water were located at various positions along the vector distance L, varying between the oxygen atom of water and the referred center of the coordinate system over the range of –5.0 Å to 5.0 Å, the translation step (ΔL) is 1 Å. The translational- or y-axis (see Figure 3.3) is defined as a vector pointing through the origin and perpendicular to the plane defined by the window of each channel. Then, the z-axis is parallel to the vector pointing from O6 to O1 (labeled on the rings shown in Figure 3.3).

Positive or negative distance vectors are determined from the origin to the oxygen atom of the water molecule along the positive or negative translation axis, respectively. In order to search for the optimal binding sites both outside and inside the windows, interactions between water and silicalite-1 for each fragment in the four configurations shown in Figure 3.3 have been calculated. The out-of-plane (Figures 3.3a-3.3b) and in-plane (Figures 3.3c-3.3d) configurations are assumed to represent the binding of water to the silicalite-1 framework before and after entering the channels, respectively.
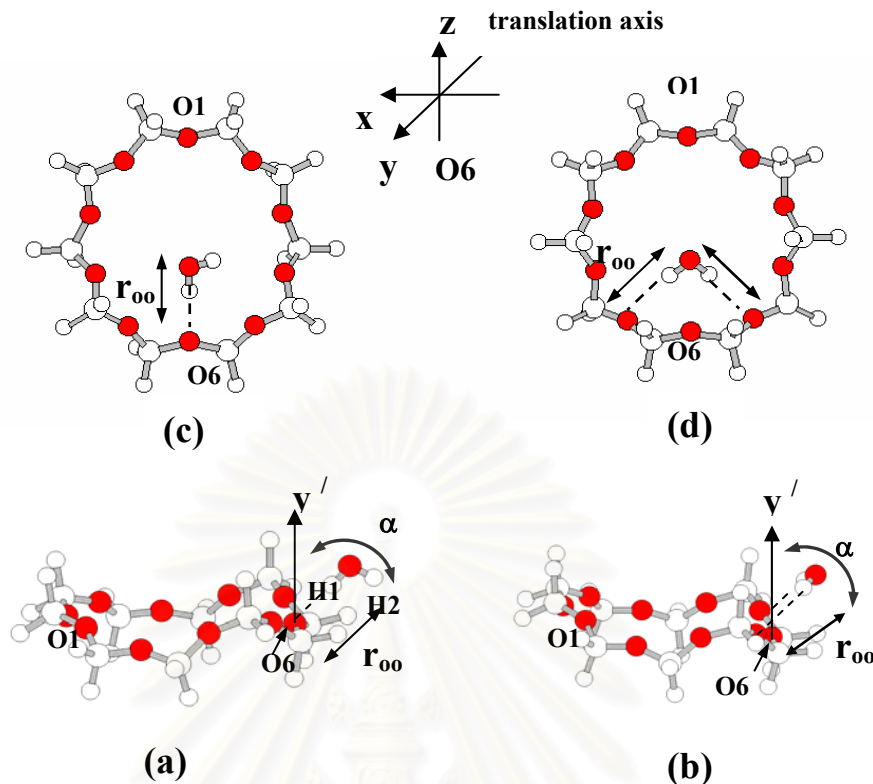
Figure 3.3 Schematic representations of the binding of water molecule (a) - (b) outside and (c) – (d) inside the silicalite-1 channels.

For the double hydrogen-bond (2HB) configurations (Figures 3.2b and 3.2d), the two O-O distances (r_{OO}) were simultaneously optimized. Inside the pore (Figures 3.3c and 3.3d), the molecular plane of the water molecule was kept parallel to the plane of the 10-oxygen membered ring (the window plane). For the out-of-plane configurations (Figures 3.3a-3.3b), we additionally optimized angles y'-O6-Ow (α) as well as rotation around the H_1-Ow bond of water for the single-hydrogen-bond (1HB) system (Figure 3.3a), where vector y' is perpendicular to the window plane at O6, Ow denotes the oxygen atom of water and the H_1-Ow vector points to O6, and α is the angle between vectors y' and r_{OO}.

3.1.2.2. For the development of guest-host potential function

In order to develop intermolecular potential functions representing the interaction between two molecules in all configurations, numerous coordinations of the second molecule around the first one have to be generated. Subsequently, the interaction energies of configurations will be calculated using quantum chemical calculations. Those obtained data points must then be fitted to an

analytical form. For the water/silicalite-1 and methane/silicalite-1 systems, numerous coordinates have been generated inside the three fragments defined in Figure 3.2, varying over $0^o \leq \phi_x \leq 360^o$ and $0^o \leq \phi_y, \phi_z \leq 180^o$, where ϕ_x, ϕ_y and ϕ_z denote rotational angles around x, y and z-axes, respectively. The origin of the coordinate system for each fragment is the average of the positions of all oxygen atoms lying on the 10-oxygen membered rings, which later is defined as the referred center. The translation or y-axis (see Figure 3.2) is defined as a vector pointing through the origin and perpendicular to the plane defined by the window of each channel. Then, the z-axis is parallel to the vector pointing from O6 to O1. The rotational steps are $\Delta\phi_x = \Delta\phi_y = \Delta\phi_z = 15^o$ while the translation step is 0.1 Å.

In addition to the above definition, the generating configurations for methane molecule are restricted only to the three main orientations clarified by the pointing 1, 2, and 3 hydrogen atoms to the fragment (Figure 3.4). This is possible for methane because of its highly symmetry.
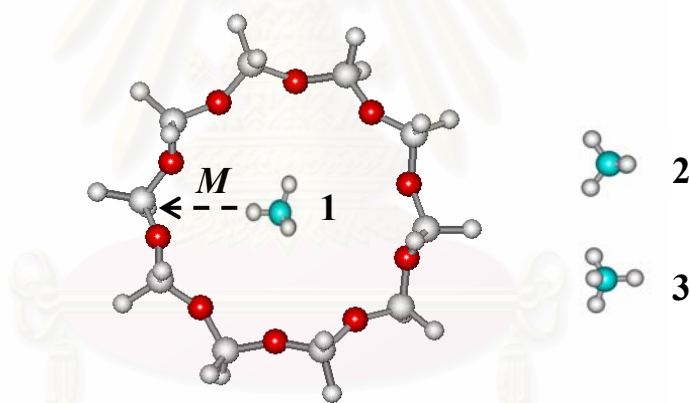
Figure 3.4 Three main proposed orientations for methane molecule as an example of a linkage domain, where the dash line shown the path *M*.

The configurations have been generated along vector distance (M), which counts from referred center of the coordinate system to any oxygen or silicon atom on the surface (Figure 3.4) where the translation step (ΔM) is kept equal 0.3 Å.

3.1.3. Perform the calculations

3.1.3.1. Water/silicalite-1

Ab initio or first principle calculations at the Hartree Fock (HF) and the second order Møller-Plesset perturbation (MP2) levels have been performed for the water/silicalite-1 system using extended 6-31G and 6-31G* basis sets. [141,142] Experimental geometries of water[143] and silicalite-1[140] have been used and kept constant throughout. An error due to the unbalance of the basis set, basis set superposition error (BSSE), has also been examined and taken into consideration. All calculations are performed using the G98 program.[144] All optimizations have been done using the HF method with the 6-31G* basis set with BSSE corrections.

3.1.3.2. Methane/silicalite-1

As known the main interaction for non-polar molecule is due to the dispersion force. Therefore, the Møller-Plesset perturbation (MP) as well as density functional theory[145] (DFT) based Becke's three parameter hybrids functional of Lee, Yang, and Parr (B3LYP) method[146] has been applied for the methane/silicalite-1 system. All calculations have been performed using 6-31G* basis set. Experimental geometries of methane[147] as well as silicalite-1 geometries have been kept constant.

3.2. Development of Guest-Host Intermolecular Potential Function

3.2.1. Water/silicalite-1

More than 1,000 *ab initio* data points were consequently fitted to an analytical function of the form:

$$\Delta E(\text{w, s}) = \sum_i^3 \sum_j^{288} \left\{ \frac{A_{ij}^{\text{ab}}}{r_{ij}^6} + \frac{B_{ij}^{\text{ab}}}{r_{ij}^{12}} + \frac{C_{ij}^{\text{ab}}}{r_{ij}^3} + \frac{q_i q_j}{r_{ij}} \right\} \tag{3.1},$$

where 3 and 288 denote the numbers of atoms in a water molecule (w) and the silicalite-1 (s) unit cell, respectively. The constants A_{ij}, B_{ij} and C_{ij} are fitting constants and r_{ij} is the distance between atom i of water and atom j of silicalite-1. Here, q_i and q_j are the atomic net charges of atoms i and j in atomic units, as obtained from the population analysis[114] of the isolated molecules in the quantum chemical

calculations. Superscripts *a* and *b* on the fitting parameters have been used to classify atoms of equal atomic number but different environmental conditions, for example, oxygen and silicon atoms of silicalite-1 in the different channels. The third polynomial term $\left(C_{ij}/r_{ij}^3\right)$ was added in order to obtain better numerical fitting. Concerning an assignment of a negative or positive value to the fitting parameters, it is generally not possible in all cases to force A/r^6 to be negative and B/r^{12} to be positive, in order to represent attractive and repulsive interactions of the pair, respectively.[148-150]

3.2.2. Methane/silicalite-1

About 150 selected data points yielded from the MP2 calculations using the extended 6-31G* basis sets have been used. Due to a requirement of numerous computational time, because of the use of highly accurate MP2 method, therefore, those data points has been carefully selected. By considering shape of the water/silicalite-1 potential energy surface, the methane/silicalite-1 force-field potentials which are available in the literature[66,67,74,75,79,80,151,152] and the specific character of the methane molecule which is highly symmetric, numbers of unnecessary energy data points can be easily removed.

The optimal analytical function form for the methane/silicalite-1 system is:

$$\Delta E(\mathrm{m,s}) \quad = \quad \sum_{i}^{5}\sum_{j}^{288}\left\{\frac{A_{ij}^{\mathrm{ab}}}{r_{ij}^{8}}+\frac{B_{ij}^{\mathrm{ab}}}{r_{ij}^{12}}+\frac{C_{ij}^{\mathrm{ab}}}{r_{ij}^{5}}+\frac{q_{i}q_{j}}{r_{ij}}\right\} \tag{3.2},$$

where 5 (in the sum) denotes the numbers of atoms in a methane molecule (m). All other parameters are identical to those of the water/silicalite-1 system.

3.3. Molecular Dynamics Simulations

The silicalite-1 crystal structure used in this study is characterized by two types of channels, sinusoidal and straight channels whose symmetry group is *Pnma*. The crystallographic cell contains 288 atoms ($Si_{96}O_{192}$), with the lattice parameters a = 20.07 Å, b = 19.92 Å and c = 13.42 Å.[140] Simulations have been carried out for the consisting system of 2 silicalite-1 unit cells. The statistical mechanics ensemble employed is the canonical (NVT) ensemble. The thermalization

during which the total energy is adjusted to a value that leads to the wished average kinetic energy, implying the temperature constant. The Newton equation of motion solved through Verlet algorithm.[128] Periodic boundary conditions have been applied; all simulations carried out at 298 K and 393 K, respectively. According to ref. [153] the use of Ewald summations can be avoided in systems with total charge zero if shifted force potentials are applied instead.

3.3.1. Water/silicalite-1

Simulations have been carried out with the time step of 0.5 fs. The occupancies were varied from 1 to 8 water molecules per intersection of the silicalite-1 corresponding to 8 to 64 molecules per MD box, respectively.

The potential proposed by Bopp, Jancso and Heinzinger[95] was employed to describe the water-water interactions. The oxygen-oxygen ($V_{OO}(r)$), oxygen-hydrogen, ($V_{OH}(r)$) and hydrogen-hydrogen ($V_{HH}(r)$) potentials are shown in eqs. (3.3)–(3.5). These BJH functions are developed from CF model by Lemberg and Stillinger:[154]

$$V_{OO}(r) = \frac{144.538}{r} + \frac{26758.2}{r^{8.8591}} - 0.25 * \exp\left[-4(r-3.4)^2\right] - 0.25 * \exp\left[-1.5(r-4.5)\right]^2, \quad (3.3)$$

$$V_{OH}(r) = -\frac{72.269}{r} + \frac{6.23403}{r^{9.18812}} - \frac{10}{1+\exp[40(r-1.05)]} - \frac{4}{1+\exp[5.49305(r-2.2)]}, \quad (3.4)$$

$$V_{HH}(r) = \frac{36.1345}{r} + \frac{100.04}{1+\exp[29.9(r-1.968)]}. \quad (3.5)$$

The energy is given in kcal·mol^{-1}, and r in Å. For each evaluation, the trajectory is corresponding to length of 10 ns; while 0.5 ps is the thermalizing length.

3.3.2. Methane/silicalite-1

Simulations have been carried out at 298 K for various loadings of methane, 1 to 8 molecules per intersection, in silicalite-1 using the newly methane/silicalite-1 and methane/methane potential (shown below). The classical equations of motion are integrated in time steps of 1 fs. The trajectories are collected from 10 ns after 0.5 ps thermalization.

The methane/methane interaction potential function[96] is developed at the MP2 level. The data points have been used and fit to represent interactions between each atomic pair, carbon-carbon, carbon-hydrogen, and hydrogen-hydrogen. The obtained methane/methane formula and the corresponding parameters are:

$$V_{CC}(r) = \frac{-3959}{r^6} + 12505 * \exp(-2.5829r),$$ (3.6)

$$V_{CH}(r) = \frac{815.9}{r^6} + 2742 * \exp(-3.5955r),$$ (3.7)

$$V_{HH}(r) = \frac{-87.32}{r^6} + 849.2 * \exp(-3.4782r).$$ (3.8)

Here again, the energy is given in kcal·mol^{-1}, and r in Å.

3.4. Pulse Field Gradient (PFG) NMR measurements

In order to manifest the presence of water molecules in silicalite channels, the measurements of self-diffusion of guest molecules including water, ethane, propane, butane and their mixtures, in silicalite-1 samples have been carried out using the home-built PFG NMR spectrometer FEGRIS 400 operating at a ^{1}H resonance frequency of 400 MHz.[155] The idea is to ratify the presence of water, diffusivities of alkanes in the presence and absence of deuterium water formula (D_2O).

For diffusion measurements, the standard stimulated echo and Hahn echo PFG NMR pulse sequences[3] were used. To obtain the diffusivity, the attenuation of the PFG NMR spin echo signal (Ψ) was measured as a function of the amplitude of the applied field gradient (g). For the PFG NMR diffusion measurements using both sequences, the duration of the applied field gradient pulses (δ) was set to 0.26 ms and the duration of the 'dephasing' and the 'read' intervals (τ) were set to 0.8 ms. The other measurements using the stimulated echo sequence the value of the time interval between the two gradient pulses (Δ) was in the range between 1.2 ms and 2 ms. The intensity of the applied gradients was varied between 0 and 24 T/m.

The average size of silicalite-1 crystals is 100x30x20 µm^3. The zeolite was used in the calcined form. The sample of silicalite-1, applied in the PFG NMR

studies, was synthesized as described in ref. [156]. The samples for the PFG NMR measurements were prepared as follows. Around 300 mg of silicalite-1 were introduced into the NMR tube. Then the tube was connected to the vacuum system and the zeolite sample was activated by keeping the sample under high vacuum at 473 K for 20 hours. Subsequently, the zeolite sample was loaded with water by freezing it from a fixed volume of the vacuum system. When preparing the samples with D_2O/alkane mixtures, upon loading with D_2O, the samples were additionally loaded with alkane by freezing it from another fixed volume of the vacuum system. Upon loading, the NMR tube was sealed and separated from the vacuum system. The total amount adsorbed of water in the alkane-free and of D_2O in the samples with the D_2O/alkane mixtures sample are corresponded to 24 mg.g^{-1} and to 28 mg.g^{-1}, respectively. To be comparable to MD results, the measurements of the sample concentrations are prepared to be identical to those of MD simulations. The amounts of ethane, propane and n-butane adsorbed in the samples with the D_2O/alkane mixtures as well as in the samples loaded only with alkane were 42, 61 and 81 mg.g^{-1}, respectively.

CHAPTER 4

RESULTS AND DISCUSSIONS

In this chapter, results which are obtained from pulse field gradient nuclear magnetic resonance or PFG NMR of water molecules in silicalite-1 have been first deliberated in order to manifest the presence of water molecules. Subsequently, the results analyzed from first principle calculations have been given and debated for water and methane molecules inside silicalite. Besides, the new *ab initio* fitted potential functions for these guest-systems have been argued. Further, results of molecular dynamic simulations have been discussed in both terms of dynamics and structural properties. All sections are roughly organized as the following schematic representation (Figure 4.1) as similarly to those in chapter 3, except the PFG NMR results has been given first.
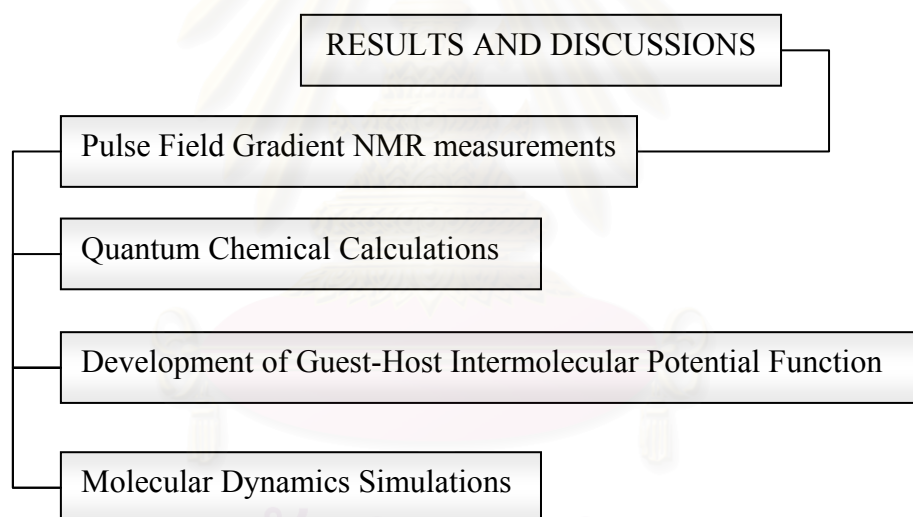
Figure 4.1 Schematic representative four main sections contained in this chapter.

4.1. PFG NMR Measurement: Presence of Water

The measurements of single and binary guests' self-diffusion in silicalite-1 samples have been carried out using a home-built PFG NMR spectrometer for water, alkane including ethane, propane and butane with and without D_2O.

The attenuation curves were recorded using the stimulated echo and the Hahn echo PFG NMR sequences.[3] For both sequences the spin echo attenuation can be written as[102]

$$\Psi(g,\Delta) = \exp\left(-\gamma^2 D \, \delta^2 g^2 \left(\Delta - \tfrac{1}{3}\delta\right)\right), \tag{4.1}$$

where γ and D denote the gyromagnetic ratio and the diffusion coefficient. In deriving eq. (4.1) it was assumed, that the diffusion can be described by a normal Gaussian propagator,[102,157] which represents the probability density for the diffusing molecules to be displaced over a distance $|r-r_0|$ during a time interval t. This diffusivity can be obtained from the initial slope of the $\ln(\Psi)$-vs-g^2 representation using eq. (4.1). It was shown in ref. [158] that for sufficiently small PFG NMR attenuations measured in powder samples, eq. (4.1) is a good approximation even for anisotropic diffusion like diffusion in silicalite-1.

4.1.1. Water in silicalite-1 samples

Figure 4.2 shows examples of the attenuation of the NMR signal $\left(\Psi(g,\Delta) \equiv \left(\dfrac{M(g,\Delta)}{M(0,\Delta)}\right)\right)$ of water molecules in the sample of silicalite-1 at 298 K and at 393 K. It is seen in Figure 4.2 that the attenuation curve measured at 298 K shows a pronounced non-linear behavior. Probably PFG NMR attenuations diffusion anisotropy leads to such deviations from the linear dependence of $\ln(\Psi)$ on g^2 as predicted by eq. (4.1). On the other hand, the curve measured at 393 K exhibits only minor deviations from a linear behavior except for the very rapid decay in the initial part of the curve. The deviations of the attenuation curves in Figure 4.2 from straight lines can be attributed to the diffusion anisotropy of water molecules in silicalite-1 and/or to the existence of the distribution of the diffusivities of water molecules in silicalite-1 samples. Note that the root mean square displacements of water molecules were always sufficiently small in comparison to the size of the crystals so that the effect of diffusion restriction of water molecules in the crystals by the outer surface of the crystals was negligible. Hence, it is unlikely that the diffusion restriction is the reason of the deviations of the measured attenuation curves from the linear dependencies predicted by eq. (4.1).

Figure 4.2 ^{1}H PFG NMR spin echo attenuation curves for water in the sample of silicalite-1 recorded by using the stimulated echo PFG NMR sequence at 298 K (Δ = 2 ms) and by using the Hahn echo PFG NMR sequence at 393 K (Δ = 0.8 ms). The lines show the fit curves used to calculate the diffusion coefficients.

An existence of a distribution of the diffusivities of the water molecules in the silicalite-1 samples, on the other hand, is feasible. It can be assumed that a part of the water molecules in the sample forms monolayers on the external surfaces of the zeolite crystals or even exists in the form of the liquid. The difference between the diffusion coefficient of this type of water and that of water molecules residing in silicalite-1 crystals can lead to the non-linear attenuation curves at 298 K. The diffusion results are given in Table 4.1 in comparison to those calculated diffusion tensors from molecular dynamics simulations, using the recent fitting *ab initio* fitted model of water sorbate.

Table 4.1 The diffusion coefficients D_x, D_y, and D_z, of water molecules in x, y, and z direction as well as the average value D (one third of the trace of the diffusion tensor) obtained from the simulations and comparison with the mean diffusivity obtained in the PFG NMR studies at 298 K and 393 K.[21]

Temp (K)	MD Simulation				PFG NMR
	D_x $(m^2.s^{-1})$	D_y $(m^2.s^{-1})$	D_z $(m^2.s^{-1})$	D $(m^2.s^{-1})$	D $(m^2.s^{-1})$
298	2.6×10^{-9}	6.5×10^{-9}	7.9×10^{-10}	3.3×10^{-9}	1.7×10^{-9}
393	5.7×10^{-9}	1.3×10^{-8}	1.4×10^{-9}	6.7×10^{-9}	1.5×10^{-9}

The diffusivity obtained from the initial slope of the attenuation curve measured at 298 K (Figure 4.2) is equal to 1.7×10^{-9} $m^2.s^{-1}$. This diffusivity can be attributed to the characteristic mean diffusivity of all the types of water in the sample. A heating of the sample up to 393 K will reduce or completely eliminate the liquid phase and the monolayers of water in the sample. At this temperature the water molecules can be expected either to be primarily in the gas phase of the NMR sample or to reside in silicalite-1 crystals. This is in agreement with the experimental observation of the very fast initial signal decay followed by the almost linear signal decay at 393 K (Figure 4.2). The fast initial decay can be attributed primarily to the water in the gas phase while the slower portion of the attenuation curve can be assigned to the water in silicalite-1 crystals. The diffusion coefficient of water obtained from the slower portion of the attenuation curve (Figure 4.2) using eq. (4.1) is equal to 1.5×10^{-9} $m^2.s^{-1}$. This diffusivity is significantly lower than the diffusivity of water in the liquid phase even at 373 K (8.7×10^{-9} $m^2.s^{-1}$ from ref. [159]). Hence, the diffusivity measured at 393 K may definitely not be assigned to the diffusion coefficient of water in a liquid or a quasi-liquid phase. We tentatively assign this diffusivity to the diffusion of water in silicalite-1 crystals. The small deviations of the slower part of the attenuation curve from a straight line (Figure 4.2, 393 K) may be attributed primarily to the diffusion anisotropy in silicalite-1 crystals.

According to the experimental values by PFG NMR measurements, it can be seen that the simulation values overestimate the experimentally observed self-diffusivities of water by PFG NMR by approximately a factor of 2 at 298 K and of 4 at 393 K.[21] Possibly experimental explanations for these discrepancies are discussed in terms of the contributions of extra-crystalline and intra-crystalline water to the measured signals by PFG NMR. Note that the model employed in this study yields practically a one-to-one correspondence between the predicted (by the potential function) and the observed (by the ab initio calculation) interaction energies.

4.1.2. Alkanes with/without D₂O in silicalite-1 samples

The study of the diffusion of one component in zeolite under the influence of other diffusants was recently a point of interest for both theoreticians and experimentalists.[160-163] It was generally observed that the diffusivity of one component kept at constant loading decreases as the loading level of another, usually less mobile component increases. Here, we report the preliminary results of the PFG NMR diffusion measurements of ethane, propane and n-butane in samples of silicalite-1 with and without pre-adsorbed D_2O. The loadings of alkanes in both types of the samples were kept at the same level. In all cases the initial part of the PFG NMR attenuation curves ($-1.0 < \ln(\Psi) < 0.0$) of alkane diffusion in silicalite-1 shows the linear behavior as predicted by eq. (4.1). The diffusion coefficients of the alkanes in the samples with and without water are presented in Table 4.2.

Table 4.2 The diffusion coefficients D of ethane, propane and n-butane obtained from the PFG NMR measurements at 298 K in the samples of silicalite-1 with and without pre-adsorbed D_2O.

Alkane	D without pre-adsorbed D_2O ($m^2 \cdot s^{-1}$)	D with pre-adsorbed D_2O ($m^2 \cdot s^{-1}$)
Ethane	1.3×10^{-9}	4.0×10^{-10}
Propane	4.4×10^{-10}	2.2×10^{-10}
n-Butane	1.9×10^{-10}	1.4×10^{-10}

The diffusivities were obtained from the initial slope of the attenuation curves. Diffusion studies of small alkanes in water-free MFI-type zeolites by the PFG NMR technique are reported.[68,164,165] The comparison of the present data obtained for the water-free samples with those previously reported shows general agreement between the absolute values of the diffusion coefficients. The data presented in Table 4.2 show that the diffusivities of all three alkanes are lower in the samples with pre-adsorbed water than in the water-free samples. It can be seen in Table 4.2 that for smaller, more mobile alkanes, the influence of water on the self-diffusion of alkane molecules is larger. This observation is in qualitative agreement with the results previously reported for other two-component systems.[162-166] The data presented in Table 4.2 provide, in our opinion, evidence that under our experimental conditions significant loadings of water molecules in silicalite-1 crystals are achieved.

4.1.3. Difficulty and problems in experiments

As in most experimental setting, zeolites are used in the form of powders; thus, those powders do not fill all the available space. The absorbed substances, which occupy in the interstitial volume, possibly entrench in the solvent, not absorbed in the zeolite channels.[167] Thereupon, the at least five limitations of diffusive guest molecule can be taken place:

1. A molecule moves along Zeolite channels and cavities without traveling along the crystal defects, 'unrestricted intracrystalline diffusion'.

2. The particle move along the extended or localized crystal defects, hindering or enhancing a diffusant motion, 'modified intracrystalline diffusion'.

3. The diffusant is reflected at the crystal environs, owing to a very low probability of desorption, 'restricted intracrystalline diffusion'.

4. The molecule migrates between difference crystals, 'intercrystalline diffusion'.

5. The particle, which remains in the gas or liquid phase, is delaminated only by the walls of a sample tube, 'fluid phase diffusivity'.

Furthermore, the values of the diffusion coefficient measurement depend upon the size and the time scale at each experimental technique operates.

Being based on the perpetual transformation of matter, molecular migration *i.e.*, diffusion phenomena, plays such important role. PFG NMR[168] has been demonstrated as a tool provided the new insights for less mobile systems, including the zeolitic system.[169-171]

Nevertheless, computer simulations using different technique have become feasible in the last decade – achievable to study the details of the diffusive processes in order to assist the experiment framing precious upshots.

4.2. Quantum Chemical Calculations

As mentioned in section 3.1.2.1, only water in silicalite-1 has been considered for the favorable binding sites. Yet, Optimal Basis Set, Optimal Method, and Optimal size of the fragment would be discussed for both water and methane/silicalite-1 calculations.

4.2.1. Optimal basis set, optimal method, and optimal size of the fragment

4.2.1.1. Water/silicalite-1

To examine discrepancies due to the method of calculation and the size of the basis set as well as BSSE corrections,[172,173] the water-silicalite interactions have been calculated for the frameworks of single and double rings using HF and MP2 methods and 6-31G and 6-31G* basis sets with and without BSSE corrections. The calculated results are plotted in Figures 4.3 and 4.4.
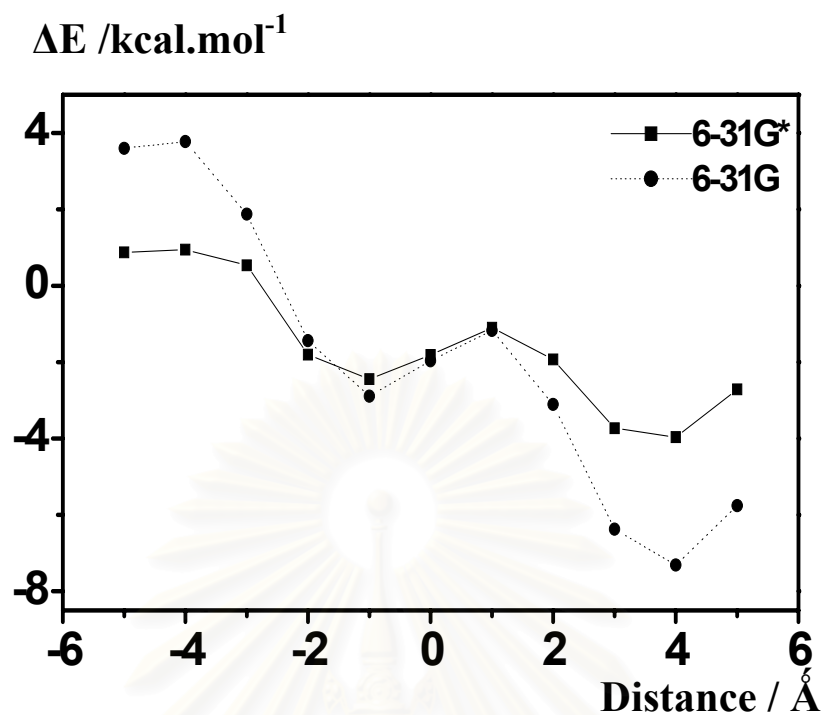
Figure 4.3 Interaction energy versus water-silicalite distance, calculated using HF method with the 6-31G and 6-31G* basis sets without BSSE corrections for the double ring framework and a water molecule lying on the translation axis as shown in Figure 3.3.

Figure 4.4 Interaction energy versus water-silicalite distance, calculated using HF/ 6-31G* basis set with and without BSSE corrections for the frameworks of (a) single, as well as the given MP calculations and (b) double rings and a water molecule lying on the same translation axis as shown in Figure 3.3.

According to Figure 4.3, the HF interaction energies between water and silicalite in the double-ring framework have been calculated using the 6-31G and 6-31G* basis sets. Both plots exhibit a local minima at L = -1.0 Å. (L was defined in section 3.1.2.1) and the most attractive minimum at L = 4.0 Å. The interaction energies obtained from the two basis sets are significantly different, especially in the repulsive and attractive regions where $|L| \geq 2$ Å, as the difference in the interaction energy in both regions is around 100%. Though it is known that a smaller basis set could be less accurate than a larger one, evidently one could conclude the 6-31G* basis set is substantially more reliable than 6-31G for the investigated system.

Figure 4.4a and 4.4b display calculated results for both frameworks, single and double rings, using HF calculations and the 6-31G* basis set with and without BSSE corrections. For the MP2 method the requirement of computational time for the double ring is not affordable. Therefore, the calculations have been performed only for the framework of the single ring, with and without BSSE corrections. These results are also shown in Figure 4.4a. It is seen in both Figures that there is a rather high error due to the BSSE for both HF and MP2 methods in terms of the interaction energy. For instance, HF and MP2 give the values at the most attractive region for both single and double ring systems amount to an error of about 40% and 100%, respectively. Dependence of the calculated results on the method used can be understood from Figure 4.4a. The interaction energies including correlation effects based on the MP2 approximation are more stable than those from the HF method. After the correction for BSSE, the effect of the electron correlation is almost negligible, *i.e.*, no significant differences were found between the interaction energies obtained from the two methods for any distance. Another conclusion is that although interaction energies from both HF and correlated MP2 methods for single and double ring systems suffer from BSSE errors, but the two methods are in good agreement in predicting the geometry of the complex. Note that the difference in the distance to the energy minimum for the frameworks of single (L = 2.0 Å) and double (L = 4.0 Å) rings are due to different definitions of the origins of the two systems.

The above observations suggest that correlation methods and BSSE corrections do not play a role regarding the predicted geometry of the system.

However, in order to increase the reliability of the derived interaction energies, all data points reported in the next sections, including encapsulation, barrier, and the diffusion energies in quantum parts are the results of HF calculations with BSSE corrections.

In addition to the above results, Figure 4.4a and 4.4b also contain information on the optimal size of the fragment, which is used to represent the silicalite. Taking into account the definition of the origin, the difference in the optimal interaction energies take place at 2.0 Å and 4.0 Å for the frameworks of single and double rings, respectively, are almost negligible. This fact is valid for the results obtained both before and after BSSE corrections. For instance, the interaction energy after the BSSE correction at $L = -3.0$ Å for the framework of single ring and at $L = -5.0$ Å for that of the double ring are almost identical (about 1.5 kcal.mol^{-1}). The corresponding values before the BSSE correction for the single and the double rings are 1.0 and 0.7 kcal.mol^{-1}, respectively. Therefore, a one useful state one could be made is that the framework of single 10-oxygen membered ring is already large enough to represent the silicalite crystal structure in the investigation of the water-silicalite interaction energy. However, a guest molecule is needed to travel along the inner pores in terms of the diffusion process. Nevertheless, the double ring and intersection are necessary.

4.2.1.2. Methane/silicalite-1

In contrast to the water/silicalite-1 system, interaction between the non-polar CH$_4$ molecule and silicalite-1 are mainly due to the dispersion forces. It is known that the Hartree Fock method fails to describe such kind of interactions. Therefore, it is not taken into consideration for the methane/silicalite-1 calculations. The stabilization energies calculated at DFT and MP2 levels for all three framework types with the 6-31G* basis set have been calculated. The results for the single ring, double ring, and intersection, in the configuration where one of the hydrogen atom of methane points toward to the ring along the central line (see Figure 3.4) have been displayed in Figure 4.5a-4.5c, respectively. Note that the selected basis set is the upper limit, which we are able to effort. The CPU times require are approximately, 100000, 2500000 and 7000000 sec for the complexes of one methane molecule with the single, double, and intersection rings using the MP2 calculations, *i.e.*, on the HP Workstation Series 700 and 800,[174] respectively.
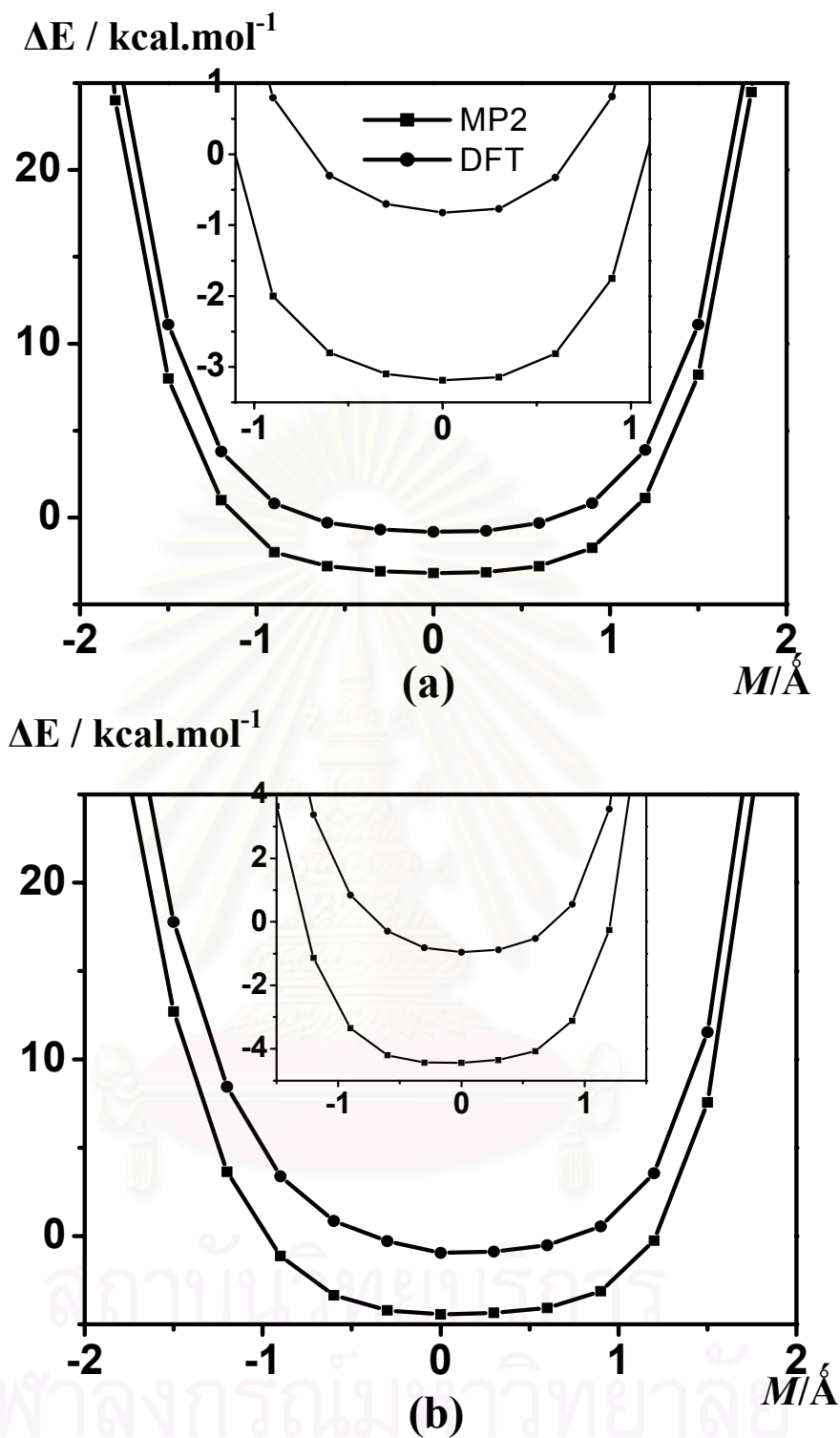
Figure 4.5 Methane-silicalite interaction energy, calculated using MP2 and B3LYP methods with 6-31G* basis set for the frameworks of (a) single ring, (b) double ring, and (c) intersection, respectively where a methane molecule lies on the same translation axis as shown in Figure 3.4 and distance *M* defines as that from C atom of methane to center of the ring (more details see text). For single and double rings, the plots with an enlarged scale in an area around the minimum have been also displayed.

ΔE / kcal.mol^{-1}

(c)
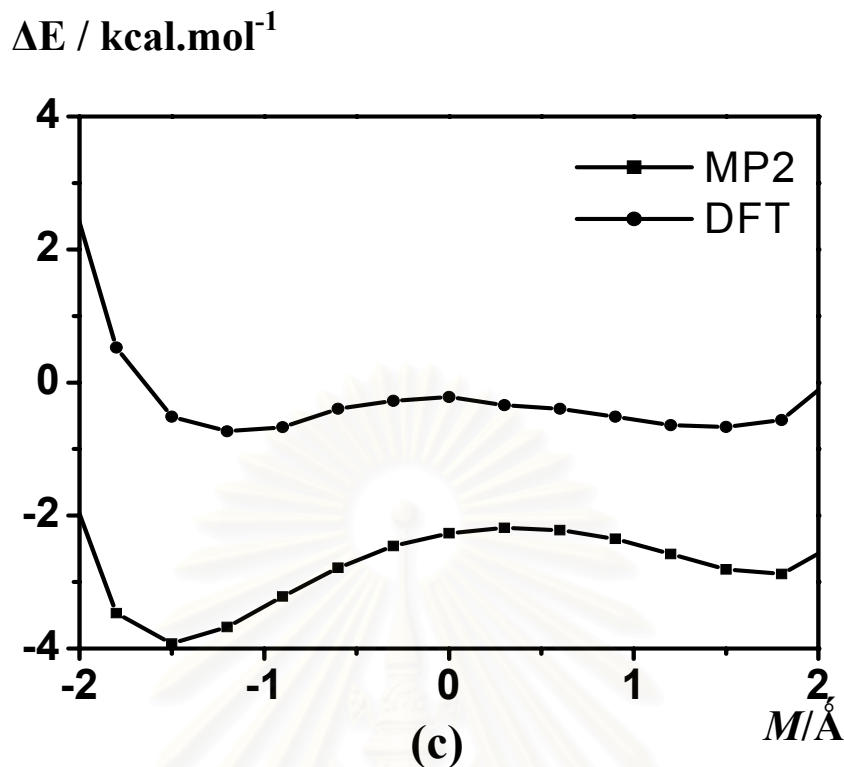
Figure 4.5 (cont.)

The plots for both single and double rings (Figures 4.5a and 4.5b), show the minima, while that of the intersection (Figure 4.5c), displays two local minima at -1.5 Å and 1.8 Å. This could be explained as the geometry of the intersection, in which one side of the window is the 10-oxygen membered ring connecting to the zigzag-channels, and the other side is the 5-oxygen membered ring. The attractive energy at -1.5 Å for the intersection is the position where the molecule is on the opposite side of the zigzag channels. The local interaction energy of -4 kcal.mol^{-1} in the intersection channel is slightly higher than that of -4.7 kcal.mol^{-1} in the double ring. This evidence agrees with that reported in ref. [72,163] which found that preferential sites for methane molecule are the zigzag channels. The plots in Figure 4.5a-4.5c show also that in relative scale, energies obtained from both DFT and MP2 calculations are in good agreement. However, the MP2 energies are significantly lower than those of DFT ones for all configurations.

As it is known, that simulation results depend directly on the relative interaction energy among the particles in the system as well as on an unbalance of the pair potential due to the use of energy points derived from different

level of accuracy. As the MP2 fitted potential for CH_4-CH_4 is available in the literature.[96] This function has been applied to represent CH_4-CH_4 interactions in the silicalite-1 system. Therefore, the MP2 has been used to calculate the CH_4/silicalite-1 interaction energy.

4.2.2. Optimal diffusing route: Water/silicalite-1 system
4.2.2.1. Diffusion through the center of the window

Based on the above conclusions for water/silicalite-1, HF calculations with the 6-31G* basis set and BSSE correction have been carried out for the three fragments. For each system, numerous water-framework configurations have been generated by varying L, ϕ_x, ϕ_y and ϕ_z as described in section 3.1.2.1. Results for four main routes defined by the $\{\Delta\phi_x, \Delta\phi_y, \Delta\phi_z\}$ coordinates of $\{0, 0, 0\}$, $\{0, 90, 0\}$, $\{180, 0, 0\}$ and $\{180, 90, 0\}$ have been displayed in Figure 4.6. The optimal route, in which the energy minimum for each distance takes place, has been given for all plots too. An area inside the pores for the three fragments have been estimated and labeled as the regions between the two vertical-dot lines (Figures 4.6a-4.6c). These ranges for the single, double and intersection rings are -0.5 Å $\leq L \leq 0.5$ Å, -1.5 Å $\leq L \leq 1.5$ Å and -2.5 Å $\leq L \leq 2.5$ Å, respectively.

The plots for all fragments indicate how the water molecule, moves and turns via diffusion along the translation axis (Figure 3.3) through the center of the channel. The water molecule starts to interact with the window of the silicalite at a long distance, far from the molecular center. The preferred configuration at this distance is to point its dipole vector towards the center of the pore (graphs 3 and 4 for all plots of Figure 4.6). Then the water molecule leaves the pore by pointing its dipole vector towards the center of the channel (graphs 1 and 2). In addition, the interaction energy in the region around center of the pore of the intersection ring (Figure 4.6c), -1.0 Å $\leq L \leq 3.0$ Å, is strongly orientation dependent. It is interesting to note here, that the energy gap (ΔE_{gap}) between two plots of parallel dipole moments, graphs 1 and 2 ($\Delta E_{gap} \approx 2$ kcal.mol^{-1}) or graphs 3 and 4 ($\Delta E_{gap} \approx 2$ kcal.mol^{-1}), as shown in Figure 4.6b is higher than that seen in Figures 4.6a ($\Delta E_{gap} \leq 1$ kcal.mol^{-1})and 4.6c ($\Delta E_{gap} \leq 1$ kcal.mol^{-1}). This leads us to conclude that the energy barriers for the rotation around the dipole axis of the water molecule in the straight and the sinusoidal

channels (represented by double ring) are higher than those of the intersection channel and the linked domain.
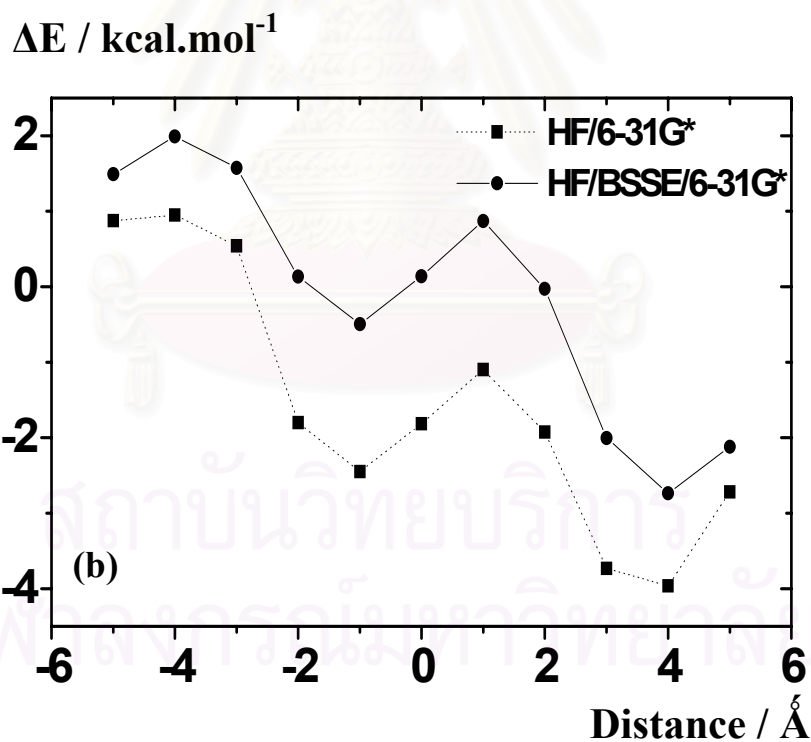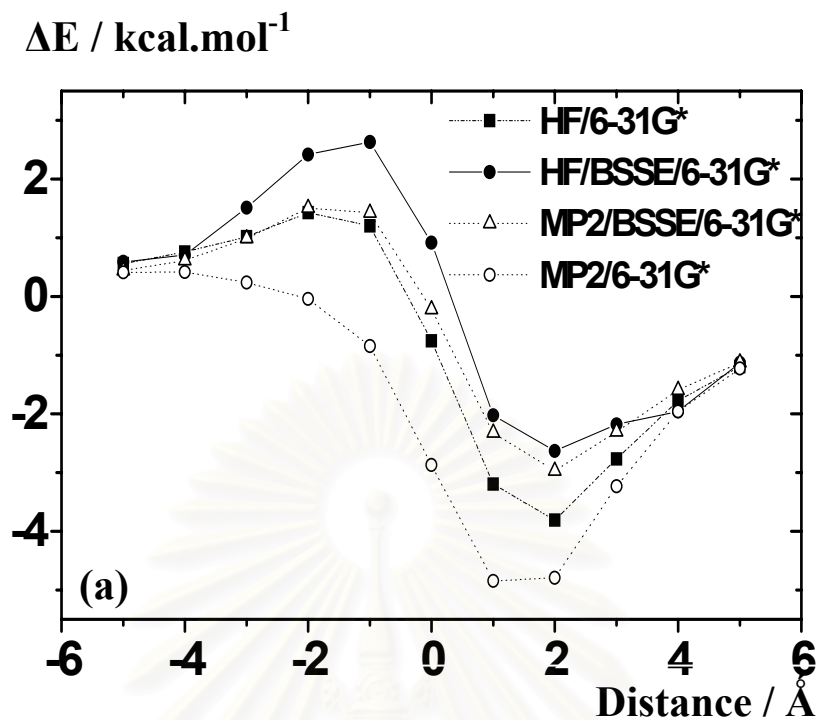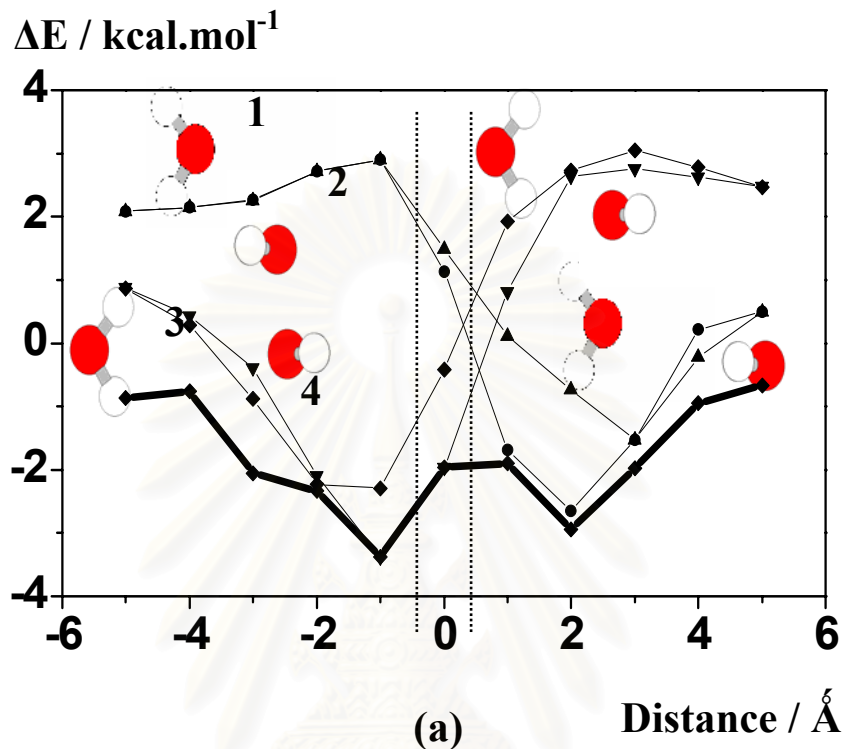

Figure 4.6 Interaction energy versus water-silicalite distance, calculated using HF method with the 6-31G* basis set and BSSE corrections for the frameworks of   (a) single, (b) double ring, and (c) interaction where a water molecule lying on the translation axis in the configurations given in the insert; ●={0,90,0}; ◆={0,0,0}; ▲={180,0,0}; ▼={180,90,0}. The bold solid-lines represent the optimal route (Calculation details in 3.1.2.1). An area between the two vertical dot-lines is estimated to be inside the pore (more details see text).

(b)
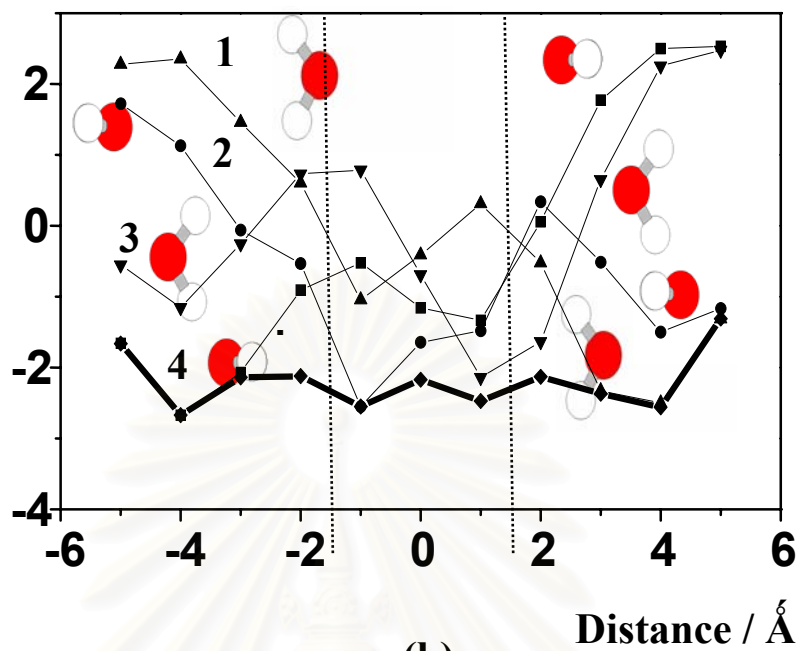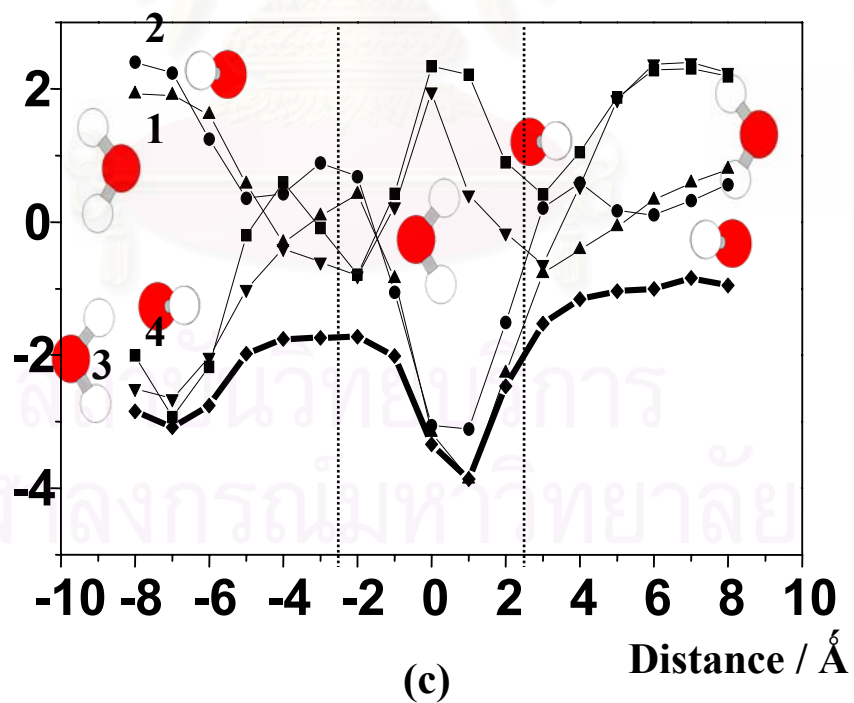
(c)

Figure 4.6 (cont.)

It can be also seen from Figure 4.6a-4.6c that the diffusion of a water molecule along the translation axis through the center of a window of the silicalite is a kind of rolling movement. The molecule must move and turn in order to find the optimal route (bold-solid lines in Figures 4.6a–4.6c). As the energy fluctuations on the optimal route for the double ring (Figure 4.6b) is much lower than those of the other fragments. The change of the interaction energies during the diffusion into and in the channel along the optimal route is within thermal fluctuations at room temperature, which amounts to about 0.6 kcal.mol^{-1}. This leads to a conclusion that the motion of a water molecule in the straight and the sinusoidal channels is rather smooth compared to that in the linked domain and the intersection channel.

4.2.2.2. Diffusion along the inner wall

Another possible pathway for the water molecule to diffuse in the silicalite channel is to attach to a specific binding site on the window, then enter the pore, find the next binding site and move from one site to another along the inner wall of the channel. Such information can be calculated using the supramolecular approach as described in detail in section 3.1.2.1 and as schematically displayed in Figure 3.3. The obtained optimization energies and corresponding distances are summarized in Table 4.3.

The following information can be extracted from the interaction data given in Table 4.3: (*i*) The most stable binding site for the water molecule before entering into the silicalite channel is to coordinate to the oxygen atom of the linked domain to form a single hydrogen bond outside the pore (Figure 3.3a). The corresponding interaction energy of –2.61 kcal.mol^{-1} is comparable to the energy obtained from the optimal route, -3.58 kcal.mol^{-1} (Figure 4.6a). Therefore, the water molecule can enter the pore via the linked domain either by using the optimal route at the center of other pore or by binding to the window as a single hydrogen bond. The situations are different for the double and the intersection fragments. Enter the pore through the optimal route is much more favorable than when the molecule binds to the framework. (*ii*) To bind to the inner wall, the interaction energies obtained from the three fragments fluctuate within a thermal limit at room temperature. This implies no any preferential binding site for water molecule in the inner wall of the silicalite pores. The observed result supports the fact that the silicalite channel is hydrophobic.

(*iii*) The interaction energy between the water molecule and the inner wall as mentioned above is less attractive compared to that when the water molecule moves along the optimal route through center of the pore (Figure 4.6). These data indicate that the diffusion in the silicalite pore takes place via the optimal route (Figure 4.6).

Table 4.3 Optimal binding distance (r_{oo} in Å), angle (α in degree), and interaction energy (ΔE in kcal.mol^{-1}) obtained from the geometry optimization using 6-31G* basis set with BSSE corrections for the water-silicalite complexes in the four configurations (a), (b), (c) and (d) which correspond to those shown in Figures 3.3a-3.3d, respectively.

Configuration \ Fragment		Single ring	Double ring	Intersection ring
(a)	r_{oo}	3.93	3.91	3.48
	α	79.9	47.5	101.3
	ΔE	-2.61	3.67	-0.35
(b)	r_{oo}	3.64	3.66	3.52
	α	60.3	52.8	96.4
	ΔE	-1.32	-1.02	0.84
(c)	r_{oo}	3.42	3.51	3.59
	ΔE	0.34	-0.95	-0.4
(d)	r_{oo}	3.69	3.60	3.83
	ΔE	-0.81	-0.98	-1.04

4.2.3. *Ab initio* based energy barriers: Water/silicalite-1 system
4.2.3.1. Diffusing into the channels

The energy change (ΔE_{net}) for a water molecule to enter the silicalite channel is simply defined as the difference between the most stable water-silicalite interaction energies inside (ΔE_{in}^{min}) and outside (ΔE_{out}^{min}) the pores. According to our model, the possible pathway for entering the single fragment is either to bind to the framework first or to move along the optimal route via the central line, while only the second pathway is preferable for the double and the intersection fragments. However, the most stable interaction energy to bind a water molecule to the single

ring outside the pore (Figure 3.3a) of -2.61 kcal.mol^{-1} is higher than in the case that the molecule moves along the optimal route of –3.58 kcal.mol^{-1} taken place at L = -1 Å (Figure 4.6a). Therefore, the energy change and the energy barrier for all fragments have been calculated only when a water molecule moves along the optimal route. The results are summarized in Table 4.4.

The maximum of the interaction energy (ΔE^{max}) which lies between the $\Delta E_{\mathrm{in}}^{\mathrm{min}}$ and $\Delta E_{\mathrm{out}}^{\mathrm{min}}$ on the optimal route suggests how easily water can enter the pore via this pathway. The energy barrier ($\Delta E_{\mathrm{barrier}}$) for the water molecule to enter the pore can then be expressed as ΔE^{max} - $\Delta E_{\mathrm{out}}^{\mathrm{min}}$, resulting in the values of 1.62, 0.67 and 1.28 kcal.mol^{-1} for the single, double and intersection rings, respectively.

Table 4.4 The water-silicalite interaction energies (kcal.mol^{-1}) along the optimal route taken from the corresponding L distance: $\Delta E_{\mathrm{out}}^{\mathrm{min}}$, $\Delta E_{\mathrm{in}}^{\mathrm{min}}$, and ΔE^{max} are the minimum outside the pore, the minimum inside the pore, and the maximum which lies between the $\Delta E_{\mathrm{out}}^{\mathrm{min}}$ and $\Delta E_{\mathrm{in}}^{\mathrm{min}}$, respectively (more details see text).

Fragment	$\Delta E_{\mathrm{out}}^{\mathrm{min}}$	ΔE^{max}	$\Delta E_{\mathrm{in}}^{\mathrm{min}}$	$\Delta E_{\mathrm{barrier}}$	ΔE_{net}
Single ring	-3.58 (L=-1 Å)	-1.96 (L=0 Å)	-1.96 (L=0 Å)	1.62	1.62
Double ring	-2.79 (L=-4 Å)	-2.12 (L=-2 Å)	-2.55 (L=-1 Å)	0.67.	0.24
Intersection ring	-3.14 (L=-7 Å)	-1.86 (L=-2 Å)	-3.86 (L=1 Å)	1.28	-0.72

The energy data in Table 4.4 indicate that the energy barrier of 1.28 and 1.62 kcal.mol^{-1} is required to drive the water molecule to enter the pore of the silicalite, the linked domain (represented by the single ring) and the intersection channel (represented by the intersection ring). The situation is different for entering the straight and the sinusoidal channels (represented by the double ring), *i.e.*, a water molecule enters these channels via the optimal route without energy barrier (0.6 kcal.mol^{-1} is within a thermal fluctuation of room temperature).

In terms of the energy change, the ΔE_{net}, which defines as $\Delta E_{\text{in}}^{\text{min}}$ - $\Delta E_{\text{out}}^{\text{min}}$ (Table 4.4) indicates that entering the linked domain and the intersection channel are endothermic and exothermic processes, respectively. On the other hand, the energy changes for diffusing process to enter the straight or the zigzag channels are almost zero.

4.2.3.2. Diffusing across the channels

To investigate the energy barrier for a water molecule to diffuse from one to another channel inside the silicalite, the most stable interaction energies (shown in Table 4.4) for encapsulation of water molecules in the three channels, represented by the three fragments are considered and the diffusion process is schematically drawn in Figure 4.7. The small barrier takes place only when a water molecule crosses the linked domain, which is represented by the single ring (Figures 3.3b) to and from the intersection channels (Figures 3.3d). The energy requirement of 1.96 kcal.mol^{-1} is equivalent to a temperature of about 973 K. This value is much less than that of 8 kcal.mol^{-1} obtained from the development of the water-silicalite potential map using an empirical method.[50]
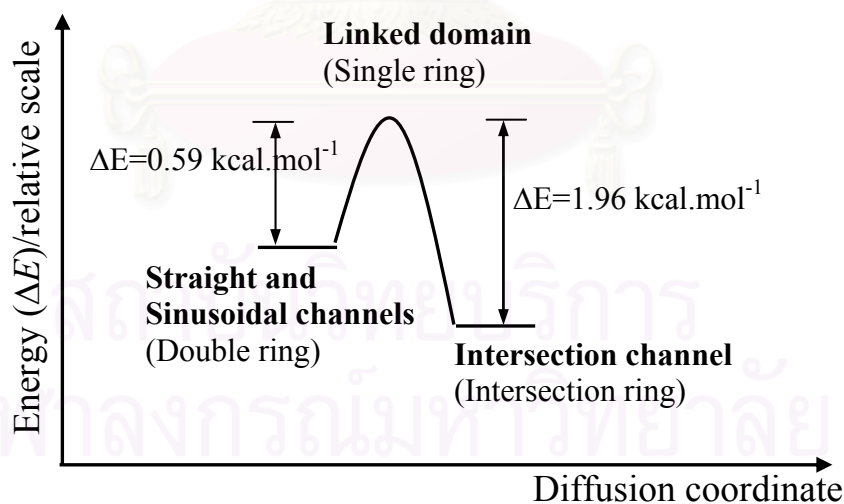
Figure 4.7 Changes of the water-silicalite interaction energy via diffusion in the silicalite channels.

Some comments can be made concerning the encapsulation energy shown in Table 4.4 in which the most stable position takes place in the intersection channel. This observation is different from that reported theoretically for

the light alkane molecules, which stated that they bind more strongly in the straight or sinusoidal than in the intersection channels.[72,90,175-177] Therefore, it is suggested by these results that the degree of hydrophobicity, typical character of the silicalite, of the intersection channel is less than those of the other channels. In addition, our value for the encapsulation energy (Figure 4.6c, thick line, at $L = 1$ Å) of the water molecule in the silicalite pore of -3.9 kcal.mol^{-1} is much higher than the experimental value of -9.6 kcal.mol^{-1} and the calculated one of -12.5 kcal.mol^{-1} reported by Vigné-Maeder et al..[50] However, it would be noted here, therefore, that the two values given in ref. [50] are too strong to represent the interaction energy between a polar molecule such as water and the hydrophobic channels of the silicalite. This statement was supported by the simulation results published recently by Takabe et al..[33] The simulated results for the water-methanol mixture in the silicalite membranes show that no water molecule diffuses into the silicalite pore. Adsorption takes place only with the silanol groups on the external surface. Therefore, a heat of adsorption obtained from the experiment is a consequence of the adsorption on the surface but not in the hydrophobic micropores of the silicalite. However, a preliminary result by Kärger et al.[21] using PFG-NMR measurement indicates the diffusion of water molecule in the silicalite micropores at high temperatures.

4.2.4. Orientation dependences: Methane/silicalite-1

Three main different orientations of methane molecules (Figure 3.4) coordinated on the center of the single ring have been computed on the basis of MP2 calculations where the translating axis is parallel to the wall with a step (ΔM), defined in section 3.1.2.2, of 0.3 Å. Figure 4.8 shows stabilized energy of those three major orientations of methane at various vector distances (M) terminating to target wall atoms, Si and O. Notations 1H-x, 2H-x and 3H-x denote methane orientations where 1, 2 and 3 hydrogen atoms of methane point toward x (Si or O) atoms of surface. As expected, no any preferential sites have been found for methane/silicalite-1 system.
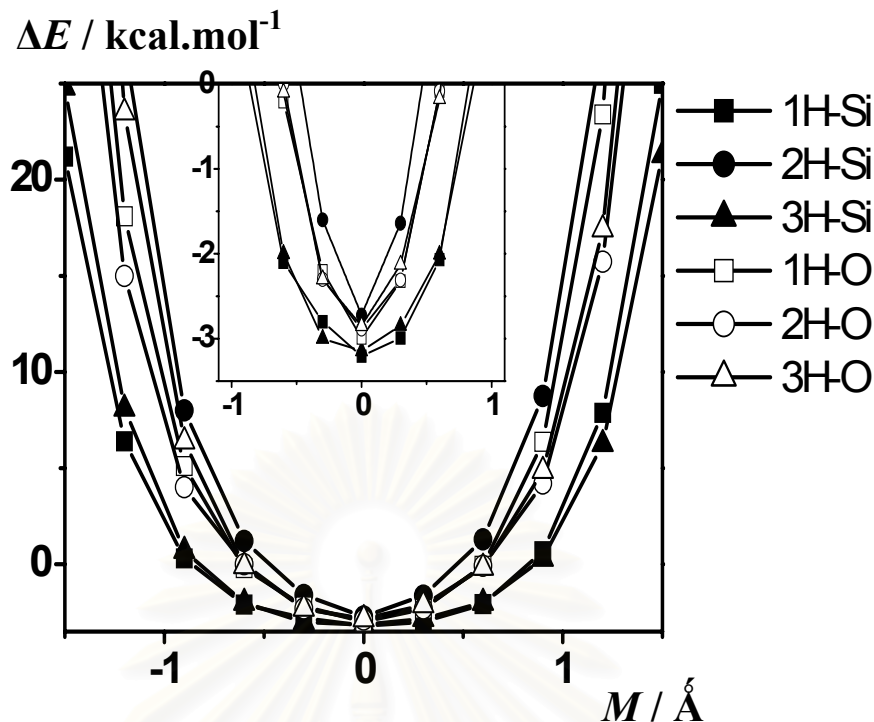
Figure 4.8 Interaction energy versus methane-silicalite distance, calculated in three different major orientations terminating to Si and O atoms carried out by MP2 method using a 6-31G* basis set where the inserted picture zooms to the minimum. (See text for more details)

The MP2 based interaction energies for three main different orientations show typical repulsive interactions when different orientations of methane molecule approach the wall at different positions, Si or O atom. The plots display that the interactions at the center of the channel are orientation dependent. The differences are emerged when methane molecule move closely to the wall. It is interesting to note that the most repulsive orientation is to point 2 hydrogen atoms of methane to Si atom of silicalite-1 (2H-Si). In addition, a methane molecule can approach closest to the wall by pointing 1 to 3 hydrogen atoms to Si (1H-Si and 3H-Si)

4.3. Development of Guest-Host Intermolecular Potential Functions

The reason to develop such a function is as known that the simulation results depend strongly on the quality of the potential function used, which one could directly parameterize from the data, yielded from quantum mechanical calculations. However, in practice it is not possible, especially for large molecular systems, to generate such data even with a small basis set, because of the unreasonable computation time that would be required. Several attempts have been made with substantial success by

Demontis *et al.*,[178] Catlow *et al.*,[179-181] Sauer *et al.*,[182-185] and some others.[186-191] The potential parameters were derived from the results of *ab initio* calculations.[181,185,186,188-191] The molecular models, which represent typical structural elements of zeolites, consist of SiO_4 and protonated AlO_4 tetrahedral connected to chain rings and cages.

4.3.1. Water/silicalite-1

In this study, an alternative choice in deriving potential function parameters is proposed. Several numerous silicalite-1/water energy points have been generated using quantum chemical calculations at the HF level.

4.3.1.1. Functional feature and set of parameters

More than 1,000 *ab initio* data points at the HF level with the extended 6-31G* basis sets were fitted to an analytical function of the form:

$$\Delta E(\text{w,s}) = \sum_i^3 \sum_j^{288} \left\{ \frac{A_{ij}^{ab}}{r_{ij}^6} + \frac{B_{ij}^{ab}}{r_{ij}^{12}} + \frac{C_{ij}^{ab}}{r_{ij}^3} + \frac{q_i q_j}{r_{ij}} \right\}, \qquad (4.2)$$

where 3 and 288 denote the numbers of atoms in a water molecule (w) and the silicalite-1 (s) unit cell, respectively. The constants A_{ij}, B_{ij} and C_{ij} are fitting constants and r_{ij} is the distance between atom i of water and atom j of silicalite-1. Also, q_i and q_j are the atomic net charges of atoms i and j in atomic units, as obtained from the population analysis of the isolated molecules in the quantum chemical calculations. Superscripts a and b on the fitting parameters have been used to classify atoms of equal atomic number but different environmental conditions, for example, oxygen and silicon atoms of silicalite-1 in the different channels. The third polynomial term (C_{ij}/r^3_{ij}) with the arbitrary exponent 3 was added in order to obtain better numerical fitting. The silicalite-1/water fitting parameters were summarized in Table 4.5.

Table 4.5 Final optimization parameters for atom i of water interacting with atom j in each channel of the silicalite-1 lattice. Subscripts sd and st denote sinusoidal (zig-zag) and straight channels, respectively. Energies in kcal.mol^{-1}, distances (r_{ij}) in Å and atomic net charges (q) in atomic units.

i	j	q_i	q_j	A ($Å^6$kcal.mol^{-1})	B ($Å^{12}$kcal.mol^{-1})	C ($Å^3$kcal.mol^{-1})
O	Si$_{sd}$	-0.87	1.57	- 9044	1161168	1419
O	Si$_{st}$	-0.87	1.67	- 4160	989964	617
O	O$_{sd}$	-0.87	-0.78	1371	-21046	-352
O	O$_{st}$	-0.87	-0.84	- 111	51208	-111

i	j	q_i	q_j	A ($Å^6$kcal.mol^{-1})	B ($Å^{12}$kcal.mol^{-1})	C ($Å^3$kcal.mol^{-1})
H	Si$_{sd}$	0.43	1.57	3725	-4315	-792
H	Si$_{st}$	0.43	1.67	2077	-8925	-416
H	O$_{sd}$	0.43	-0.78	-406	689	222
H	O$_{st}$	0.43	-0.87	35	33	103

Concerning an assignment of a negative or positive value to the fitting parameters, it is generally not possible in all cases to force A/r^6 to be negative and B/r^{12} to be positive, in order to represent attractive and repulsive interactions of the pair, respectively. Some examples are those in references.[150,156,192,193] In these cases, the physical meaning of the atomic-based pair potentials, 864 pairs running over i = 1-3 and j = 1-288 for eq. (4.2), is not achieved. However, the physical meaning, as well as quality, of the molecular-based water-silicalite-1 function is its ability in representing *ab initio* data. An advantage of this approach is that it is a one-to-one correspondence between the predicted (by the potential function) and the observed (by the *ab initio* calculation) interaction energies. With the same reason, as well as for a better numerical fitting, the third polynomial term (C_{ij}/r^3_{ij}) was added and its sign was not able to be controlled.

4.3.1.2. Quality of the function

Here, the oxygen atom of the water molecule moves from one surface to the opposite surface along the vector r (see Figure 4.9); its dipole moment point is parallel to vector r and its molecular plane is parallel to the window of the lattice.
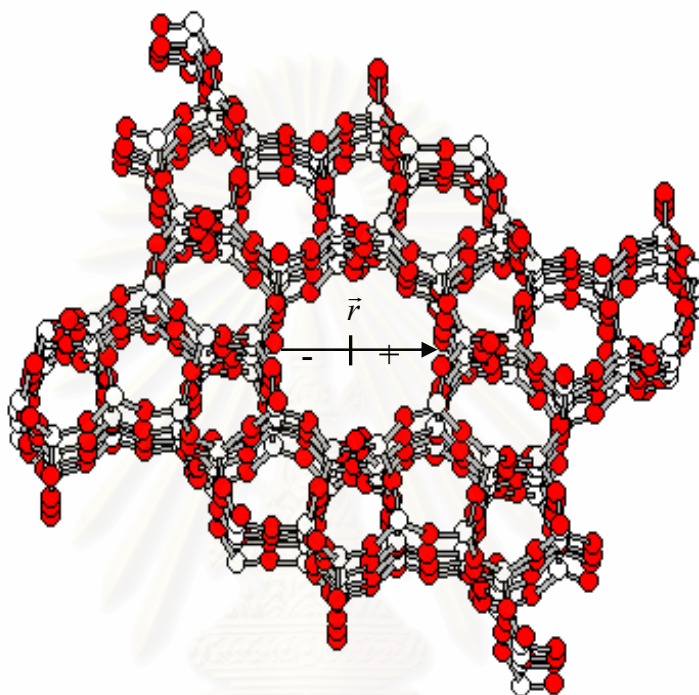
Figure 4.9 Schematic representations of the path perpendicular to wall of the silicalite-1 channels.

With the analytical potential shown in eq. (4.2), the lattice-water interactions in the straight channel have been calculated and plotted in Figure 4.10. The *ab initio* interaction energies at the same lattice-water configurations have been calculated and given also for comparison. The good agreement between the two curves in Figure 4.10 illustrates the reliability and quality of the fit. This conclusion was, again, confirmed by the plot shown in the Figure 4.11, where all 1,050 *ab initio* and fitted energies have been compared.
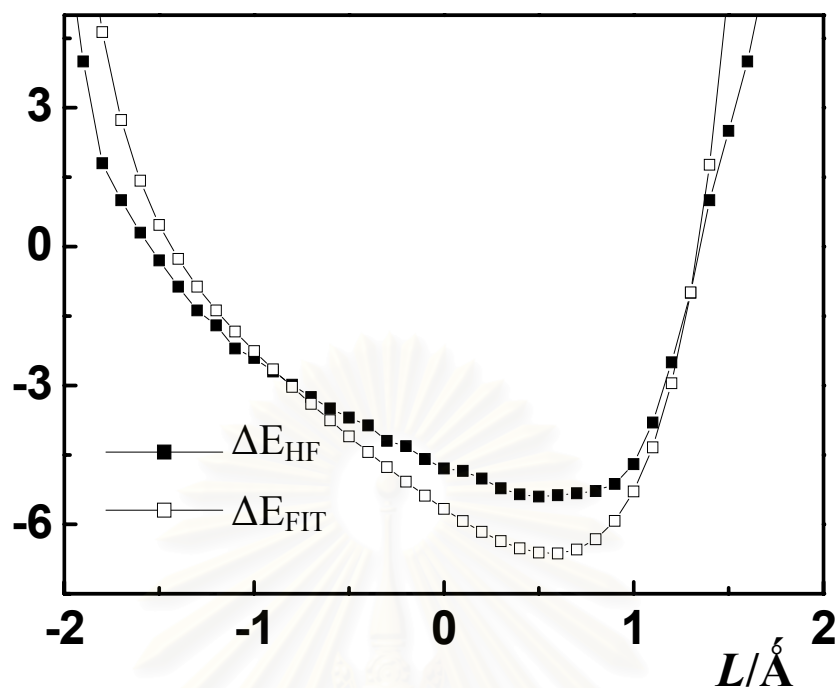
Figure 4.10 Silicalite-1/water interaction energies (ΔE) obtained from the *ab initio* calculations (ΔE_{HF}) with the extended 6-31G* basis sets and from the potential function (ΔE_{FIT}) according to eq. (4.2), where the oxygen atom of the water molecule lies along the vector *r* (see Figure 4.9), its dipole moment point is parallel to *r* and its molecular plane is parallel to the window of the lattice.
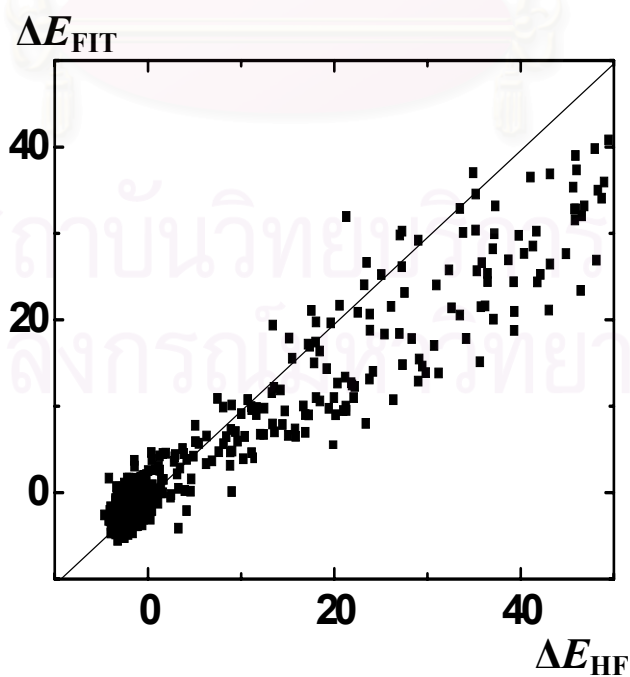
Figure 4.11 A comparison of *ab initio* and fitted data points on the unit of kcal.mol^{-1}.

Some comments could be made concerning the quality of the *ab initio* interaction energies given in this dissertation. The energies calculated from the *ab initio* fitting potential function, E_{FIT}, and the actual energies calculated from *ab initio* method, E_{HF}, have been given in comparison. The E_{FIT}'s are in excellent agreement to those E_{HF}, if the energies are lower than zero. Vise versa, the E_{FIT}'s have been shown the less repulsion than those E_{HF}. Discrepancies and reliabilities of the data points due to the size of the fragments, the calculated methods and the basis sets used as well as an error due to the unbalance of the basis set, basis set superposition error, have been intensively examined and discussed in the beyond section 4.2.1.

4.3.1.3. Specific character to different channel

To visualize the characteristics of the silicalite-1/water potential function, the interaction energies for different orientations of the water molecule in the straight channel have been computed according to eq. (4.2). The changes of the energies as functions of the distances along *r* were plotted in Figure 4.9.
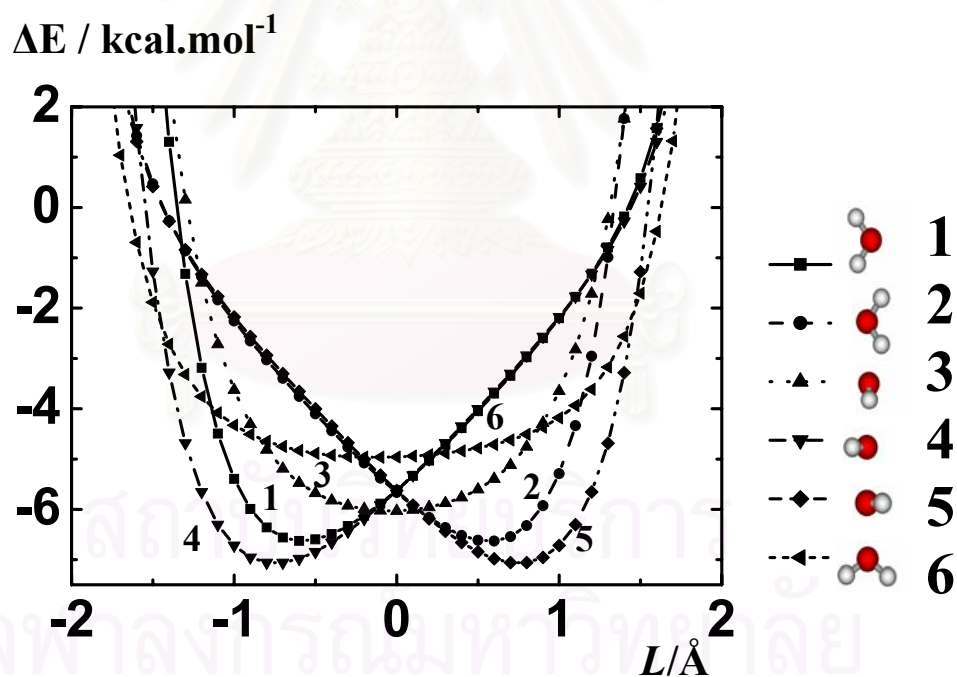
Figure 4.12 Silicalite-1/water interaction energies (ΔE, kcal.mol^{-1}) obtained from the potential function according to eq. (4.2) for different orientations of a water molecule, where its oxygen atom lies along *r* (see Figure 4.9) in the straight channel.

The curves 1 and 4 in Figure 4.12 show the minima at *L* < 0, and the interaction energies for *L* > 0 increase more slowly than those for *L* < 0. This

occurrence can be understood as water molecules in these configurations (at the right of this Figure) approach the surface at $L > 0$ by pointing hydrogen atoms toward the oxygen atoms of the lattice, *i.e.*, attractive Coulomb interactions between the hydrogen atoms of water and the oxygen atoms of the surface compensate the water-surface repulsion. This leads to a slow increase of the interaction energy and hence to an asymmetry of the lattice-water potential. The difference between the shapes of the two curves indicates how sensitive the obtained function is. That means it is able to classify the two orientations of the water molecule which differ only by rotating the molecule by 90° around its dipole vector. The situation is very similar for the curves 2 and 5, in which the minima take place at $L > 0$ and the interaction energies for $L < 0$ increase faster than those for $L > 0$. For the curves 3 and 6, the shapes are much more symmetric than the other curves. The reason is that the water molecule in these configurations approaches the lattice, both for $L > 0$ and $L < 0$, by pointing its dipole vector parallel to the surface. The curve 6 is broader than the curve 3 because in the curve 3 water moves toward the surface in configurations for which distances from the surface to the two hydrogen atoms are identical. For the curve 6, at the same position of water as in the curve 3, one hydrogen atom is closer to the surface than the other (see legend of Figure 4.12). This fact confirms the *ab initio* interaction energies reported in ref. [22].

As can be seen from eq. (4.2), different fitting data sets have been used to represent the interaction between the lattice and a water molecule lying in the sinusoidal (zig-zag) or in the straight channel. To visualize this effect, the interaction energies have been calculated separately for a water molecule in the two channels. In this example, the water molecule was in the same configurations as that of Figure 4.10. The results are displayed in Figure 4.13. The sensitivity of the silicalite-1/water potential to different environments has been monitored, in addition to that due to the water orientation as shown in Figure 4.12.
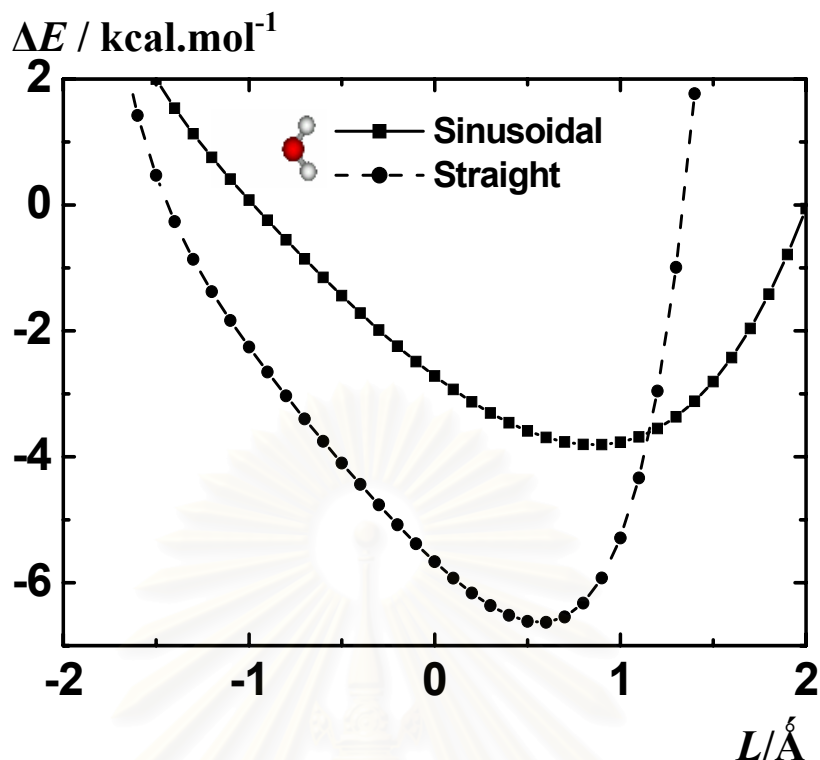
Figure 4.13 Silicalite-1/water interaction energies obtained from the potential function according to eq. (4.2), where the water molecule lies in the same configuration as that of Figure 4.10 in the sinusoidal and the straight channels.

The difference between the interactions in the straight and the sinusoidal channels is consistent with the energy data analyzed intensively in section 4.2.1.1 where the optimal diffusion route has been considered. Note, it is the first time to use fairly large fragments of 10 T, 20T, and 27 T of zeolite in quantum chemical calculations with high quantity basis sets, where T denotes the silicon of corner sharing TO_4 tetrahedral in zeolite crystalline.[23]

4.3.2. Methane/silicalite-1

Similarly to the water-guest system, numerous silicalite-1/methane energy points have been generated using quantum chemical calculations at the MP2 level and subsequently fitted.

4.3.2.1. Functional feature and set of parameters

About 150 *ab initio* carefully selected data points at the MP2 level with the extended 6-31G* basis sets have been fitted to an analytical function as stated below,

$$\Delta E(\text{m,s}) \quad = \quad \sum_i^5 \sum_j^{288} \left\{ \frac{A_{ij}^{\text{ab}}}{r_{ij}^{10}} + \frac{B_{ij}^{\text{ab}}}{r_{ij}^{12}} + \frac{C_{ij}^{\text{ab}}}{r_{ij}^8} + \frac{q_i q_j}{r_{ij}} \right\} \tag{4.3},$$

where 5 and 288 denote the numbers of atoms in a methane molecule (m) and the silicalite-1 (s) unit cell, respectively. The other parameters have referred to those clarified parameters in water/silicalite-1 potential function. The fitting parameters were summarized in Table 4.6. Analogy to water/silicalite function, an assignment of a negative or positive value to the fitting parameters is generally not possible to control.

Table 4.6 Final optimization parameters for atom i of methane interacting with atom j in each channel of the silicalite-1 lattice; subscripts sd and st denote sinusoidal (zig-zag) and straight channels, respectively; energies in kcal.mol^{-1}, distances (r_{ij}) in Å and atomic net charges (q) in atomic units.

i	j	q_i	q_j	A (Å^{10}kcal.mol^{-1})	B (Å^{12}kcal.mol^{-1})	C (Å^{8}kcal.mol^{-1})
C	Si$_{sd}$	-0.87	-0.66	-7349979	35791283	484120
C	Si$_{st}$	-0.87	-0.66	-47973904	283370791	2316815
C	O$_{sd}$	-0.87	-0.66	1157607	-3234971	-113445
C	O$_{st}$	-0.87	-0.66	2281723	-7914489	-185328

i	j	q_i	q_j	A (Å^{10}kcal.mol^{-1})	B (Å^{12}kcal.mol^{-1})	C (Å^{8}kcal.mol^{-1})
H	Si$_{sd}$	0.43	0.165	652722	-1199457	-67753
H	Si$_{st}$	0.43	0.165	1386542	-2765365	-141278
H	O$_{sd}$	0.43	0.165	-13594	7620	5704
H	O$_{st}$	0.43	0.165	94594	-291945	-3738

4.3.2.2. Quality of the function

To visualize the quantity of the function, therefore, changes of interaction energies have to be plotted as a function of methane/silicalit-1 distance. Here, moving paths with respect to the channels of silicalite-1 have been defined. Figure 4.14 shows two paths along vector s_1 (Figure 4.14a) and vector s_2 (Figure 4.14b), in which a methane molecule moves parallel, and the perpendicular to the surface, respectively. Note s_1 parallels to y-axis while s_2 is in the xz-plan and tilts 45° from the z-axis.

(a)

(b)
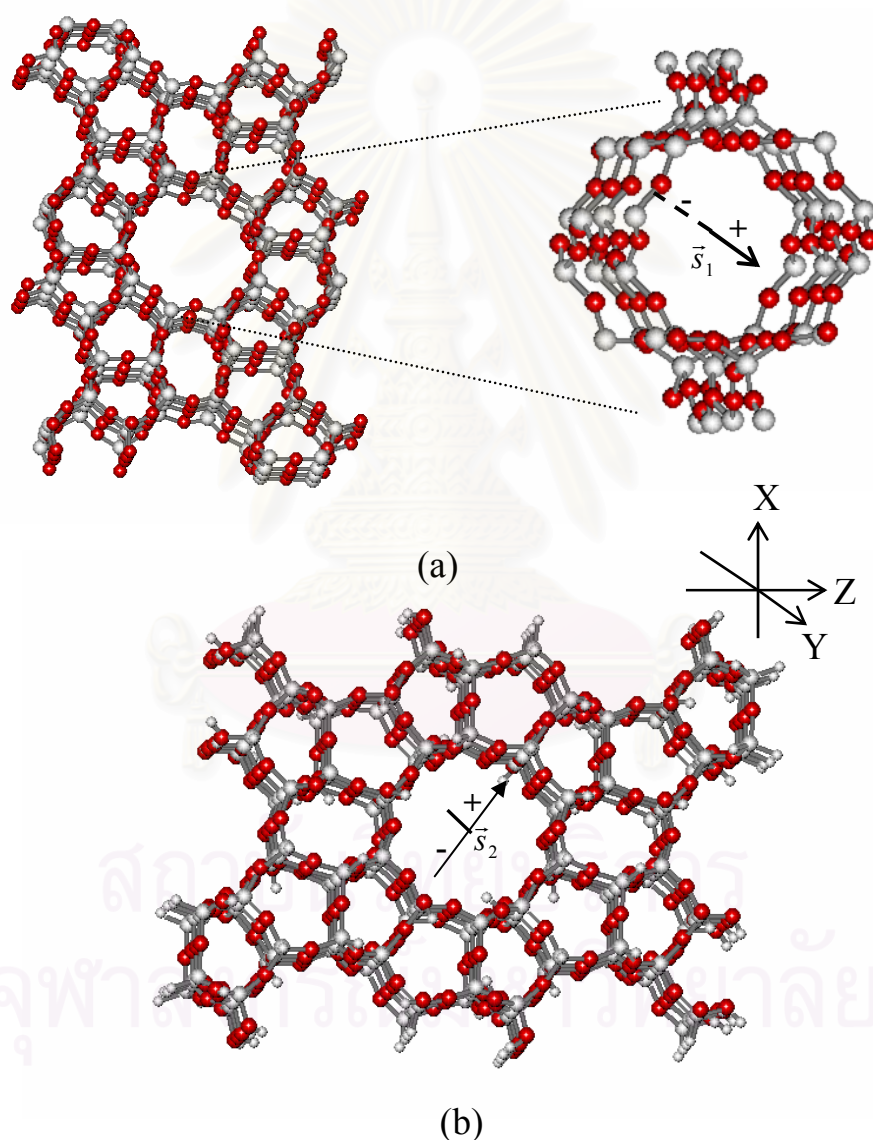
Figure 4.14 Schematic representations of the moving paths (a) along and (b) perpendicular to the straight channel; the methane molecule points one hydrogen atom toward vectors s_1 and s_2.

The reliability of the methane/silicalite function has first been displayed in Figure 4.15 in which the fitted and *ab initio* data for all configurations are compared. By using the analytical potential shown in eq. (4.3), the lattice-methane interactions for both parallel and perpendicular paths in the straight channel have been plotted in Figures 4.16a and 4.16b, respectively. The *ab initio* interaction energies at the same lattice-methane configurations have additionally been calculated and given in comparison. The two curves in each Figure, 4.16a or 4.16b, illustrate the reliability and quality of the fit. The two minima of the curves in Figure 4.16a indicate the specific character of the junction in the intersection channels in which the two channels, straight and sinusoidal, jam together.
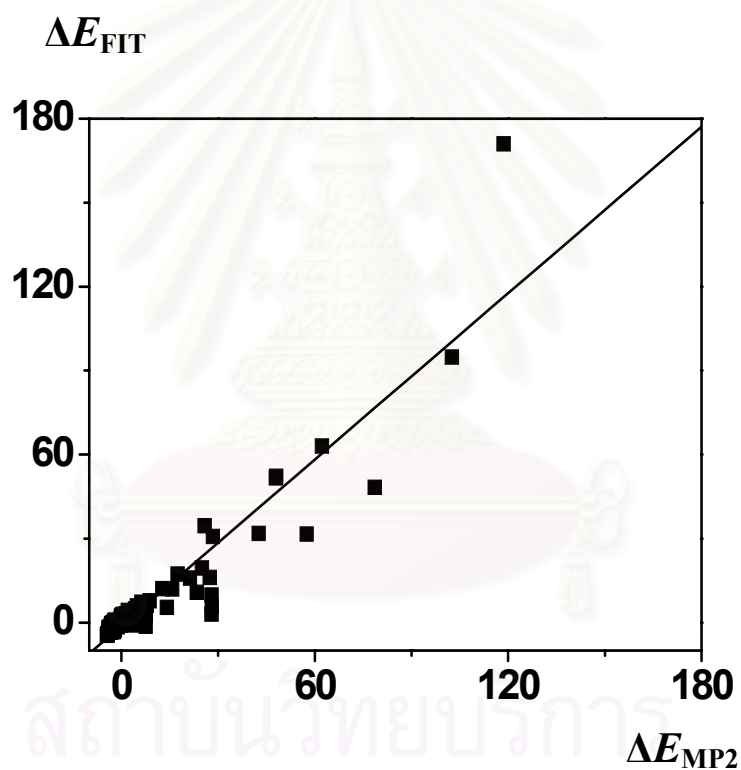
Figure 4.15 A comparison of *ab initio* and fitted data on the unit of kcal.mol^{-1}.
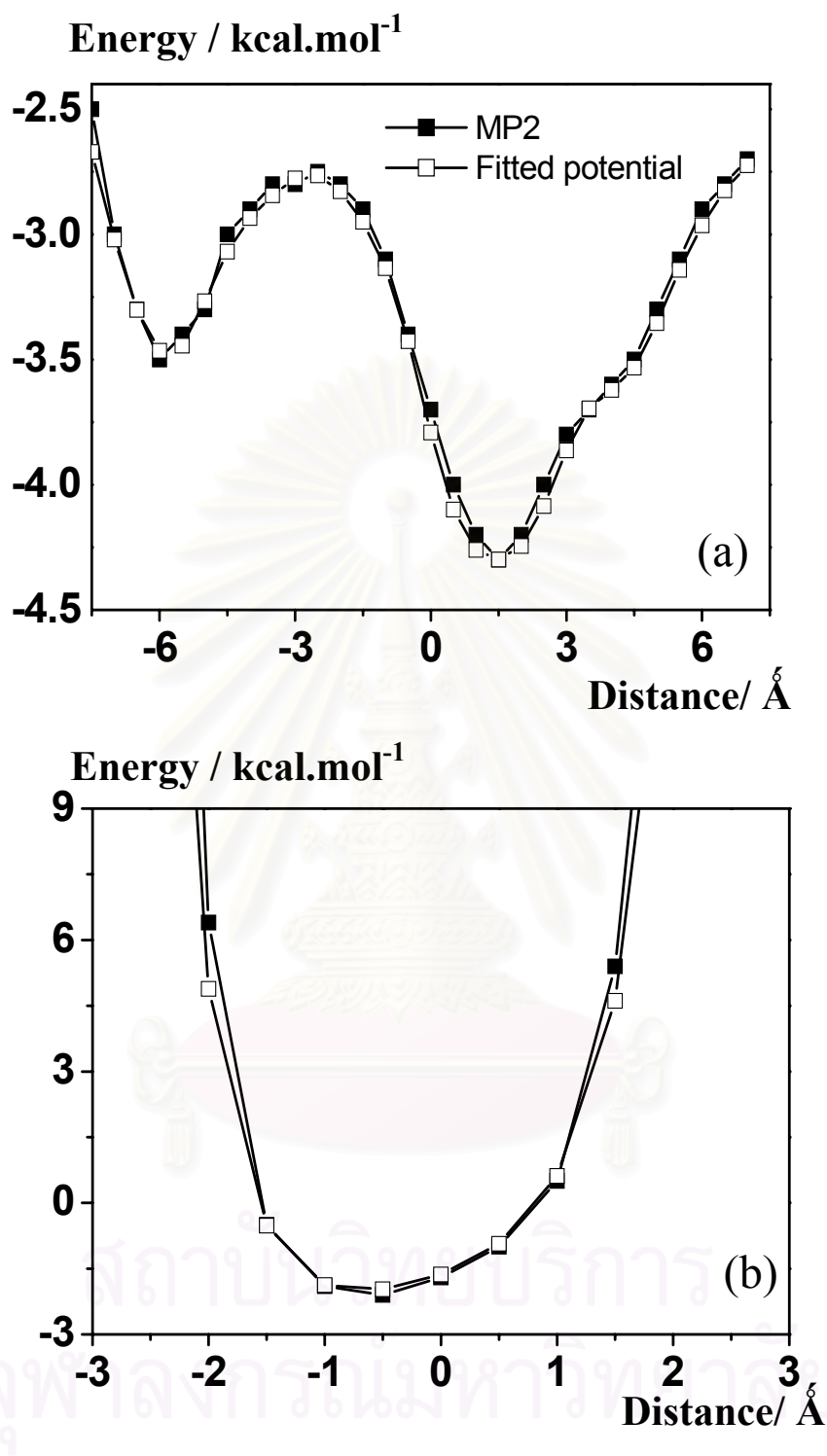
Figure 4.16 Silicalite-1/methane interaction energies (ΔE) obtained from the *ab initio* calculations (ΔE_{MP2}) with the extended 6-31G* basis sets at MP2 level and from the potential function (ΔE_{FIT}) according to eq. (4.3), where methane molecule move (a) along and (b) perpendicular to the straight channel as defined in Figure 4.14.

4.3.2.3. Specific character to different channel

Similar to the water/silicalite-1 potential function, the different fitting data sets as well as function formula have been used to represent the interaction between the lattice and a methane molecule lying in the sinusoidal (zigzag) or in the intersection channel.
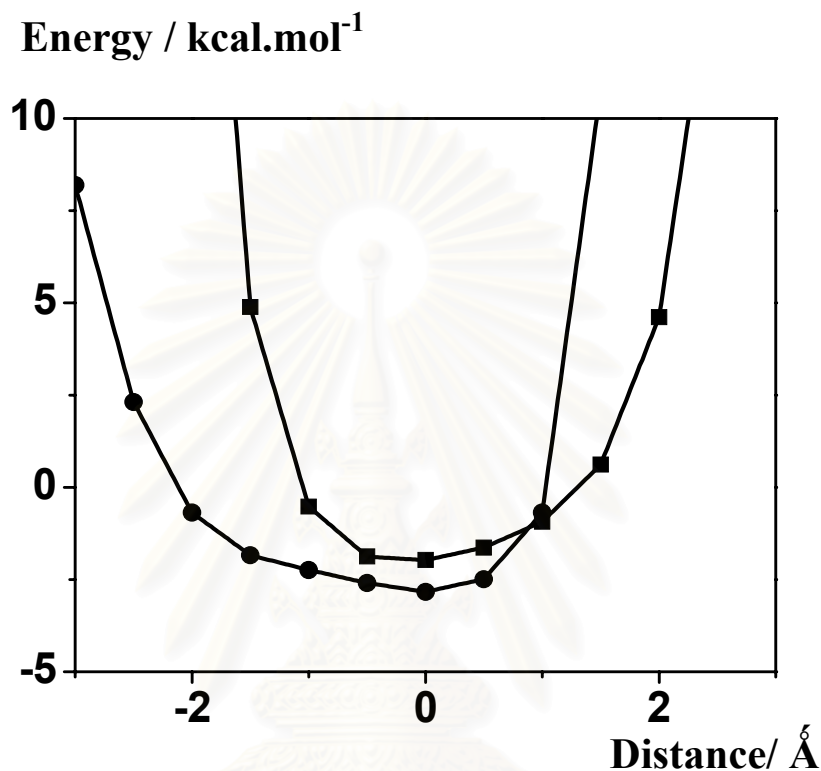
Figure 4.17 Silicalite-1/methane interaction energies obtained from the potential function according to eq. (4.3), where the CH_4 molecule pointing one hydrogen atom, perpendicular to the intersection (filled squared symbols) and sinusoidal (filled circled symbols) channels.

To visualize the functional characteristic, the interaction energies have been calculated separately for a CH_4 molecule in the two channels. In this example, the methane molecule was in the same configurations as that of Figure 4.16. The results are displayed in Figure 4.17. Sensitivity of the silicalite-1/methane potential to different channel environments has been monitored. The methane-lattice interactions in sinusoidal are more attractive than those in the intersection channels. The asymmetry of the potential surface is due to methane orientation. Thus, the recent methane/silicalite-1 function could classify not only the diversity of the channels but also of its orientations.

4.4. Theoretical Dynamics and Structural Properties

The results, which contain in these parts, are carried out by series molecular dynamics simulations at various concentrations, at some ambitious temperatures. Both dynamics and structural properties could be elucidated via the trajectories of the guest molecules.

4.4.1. Water/silicalite-1

With a time step of 0.5 fs at 298 K and 393 K, the simulations have been performed for systems containing 1 - 8 water molecules per intersection, equivalent to 8 – 64 molecules per simulation cube, which contains 2 silicalite-1 unit cells. The BJH water-water potential[95] and the new fitted *ab initio* water/silicalite-1 potential model have been applied.[22,24,25]

4.4.1.1. Structural properties:

- **Silicalite-water radial distribution functions**
  - **Average RDF for all channels**

In order to investigate structural data of water molecules via diffusion in zeolite silicalite-1 at various loadings (n_{1d}), the radial distribution functions (RDFs) from surface oxygen atom (O_S) to water oxygen (O_W) and hydrogen (H_W) atoms of water have been evaluated and plotted in Figure 4.18. The change of the water behavior has been exhibited by the O_S- O_W RDFs in which the transition takes place between the loadings of 6 and 7 water molecules per intersection.

The O_S-O_W RDFs for $n_{1d} \leq 6$ display firstly broad maxima around 4.2 Å, followed by a pronounced shoulder at around 5.8 Å and second broad peaks centered at 8.4 Å. Due to the cylinder-like structure with the diameter of 8.2 Å of the silicalite channels, the water molecules lied under the first maximum and the established shoulder of the O_S-O_W RDFs can be assigned to molecules moving along the center of the tube. The distances from O_W to O_S of the nearest 10-oxygen membered-ring and their adjacent rings are between 4 to 6 Å. This is in good agreement with those predicted by *ab initio* calculations which state that central line is the optimal path for water molecule to travel along the silicalite channels.[23]

A transition takes place for the $n_{ld} > 6$, in which the first broad O_S-O_W peak splits into two sharp peaks centered at 3.45 Å and 5.25 Å. This feature indicates dramatic changes of the water behavior in silicalite-1 channels. With concentrations higher than 6 water molecules per intersection, the water molecules are forced by their repulsion to stay out of the central line region. This information cannot be obtained from *ab initio* calculations because only the interaction of a pair or only a few molecules can be taken into consideration. It is interesting to note here, therefore, that these two peaks are contributed from the same set of water because the sum of O_S-O_W distances for O_W centered at 3.45 Å far from O_S on one side and 5.25 Å from the opposite side of the 10-oxygen membered ring are, somehow, equivalent to the diameter of 8.2 Å of the tube.

Figure 4.18 Radial distribution functions (RDFs) of (a) O_S-O_W and (b) O_S-H_W at various loadings n_{ld} from 1 to 8.

Some comments could be made concerning an appearance of the O_S-O_W peak at 3.45 Å for $n_{1d} > 6$. The sharp, pronounced and discrete characters of the peaks are usually due to the tight binding between the two molecules. This is surely not true for the water/silicalite-1 system in which the interaction energies derived from *ab initio* calculations or the *ab initio* fitted potential for any configurations where the O_S-O_W distance = 3.45 Å of about -4 kcal.mol^{-1} is almost equal to that at the optimal configuration of the water dimer of -5.6 kcal.mol^{-1}, *i.e.*, the water-water binding is superior to the surface-water one. Therefore, the formation of this peak can only be assigned to a cluster formation of water molecules. The repulsion among molecules in the cluster in a limited space inside the silicalite-1 channels, leads not only to a shift of water positions out of the central line but also to a lower flexibility of their positions. As a consequence of the cluster formation and the repulsion of the water molecule in a limited space, the O_S-O_W RDF starts to be detected at a shorter distance, when the concentration increases. The investigation and the discussion on the cluster formation are given in more details in the water-water radial distribution function part.

Considering the O_S-H_W RDFs in Figure 4.18b, the plots for all loadings show corresponding RDFs with established shoulders around 3.2 Å, and first maxima around 5.2 Å. As a function of the water loading, the following conclusions can be made (*i*). An appearance of the first pronounced O_S-H_W shoulder at a shorter distance than that of the O_S-O_W first peak implies that the water molecules point their hydrogen atoms toward the inner surface of silicalite-1.; (*ii*) With the distances to the first peak of the O_S-O_W RDFs of 3.4 Å and the O_S-H_W shoulder of distances of both peaks mentioned earlier, it can be concluded that hydrogen bonding between water molecules and the inner surface of silicalite-1 cannot be formed. (*iii*) Broadening of these peaks and their shoulders indicate a flexibility of the water molecules in terms of both their positions and orientations. This finding confirms the *ab initio* results which suggest the changes of water orientations via the diffusion in the silicalite-1 channels;[23] (*iv*) For the same reasons as that of the O_S-O_W RDFs, the O_S-H_W RDF for low loadings start to be detected after those of high loadings. This is also true for the distance to the first shoulder of the O_S-H_W RDFs while their first peaks appear at the same position.

o   **Separated RDF for each channel**

To understand more details of the water behavior in the different channels, the RDFs from oxygen surface of each channel to all oxygen and hydrogen atoms of water molecules have been evaluated. The results are given as examples in Figures 4.19a and 4.19b for n_{ld} = 1 and 8, respectively. Here, the notations O_s representing oxygen atoms of the silicalite-1 surface were replaced by O_{It}, O_{St} and O_{Sd} for the intersection, straight and sinusoidal oxygens, respectively. Average O_S-O_W and O_s-H_w RDFs for both loadings are also given for comparison. The following conclusions can be extracted from the plots.
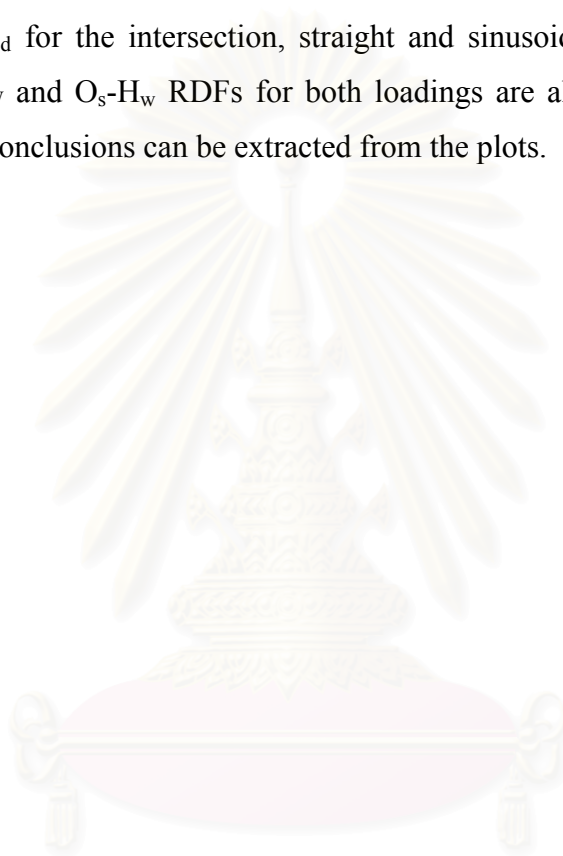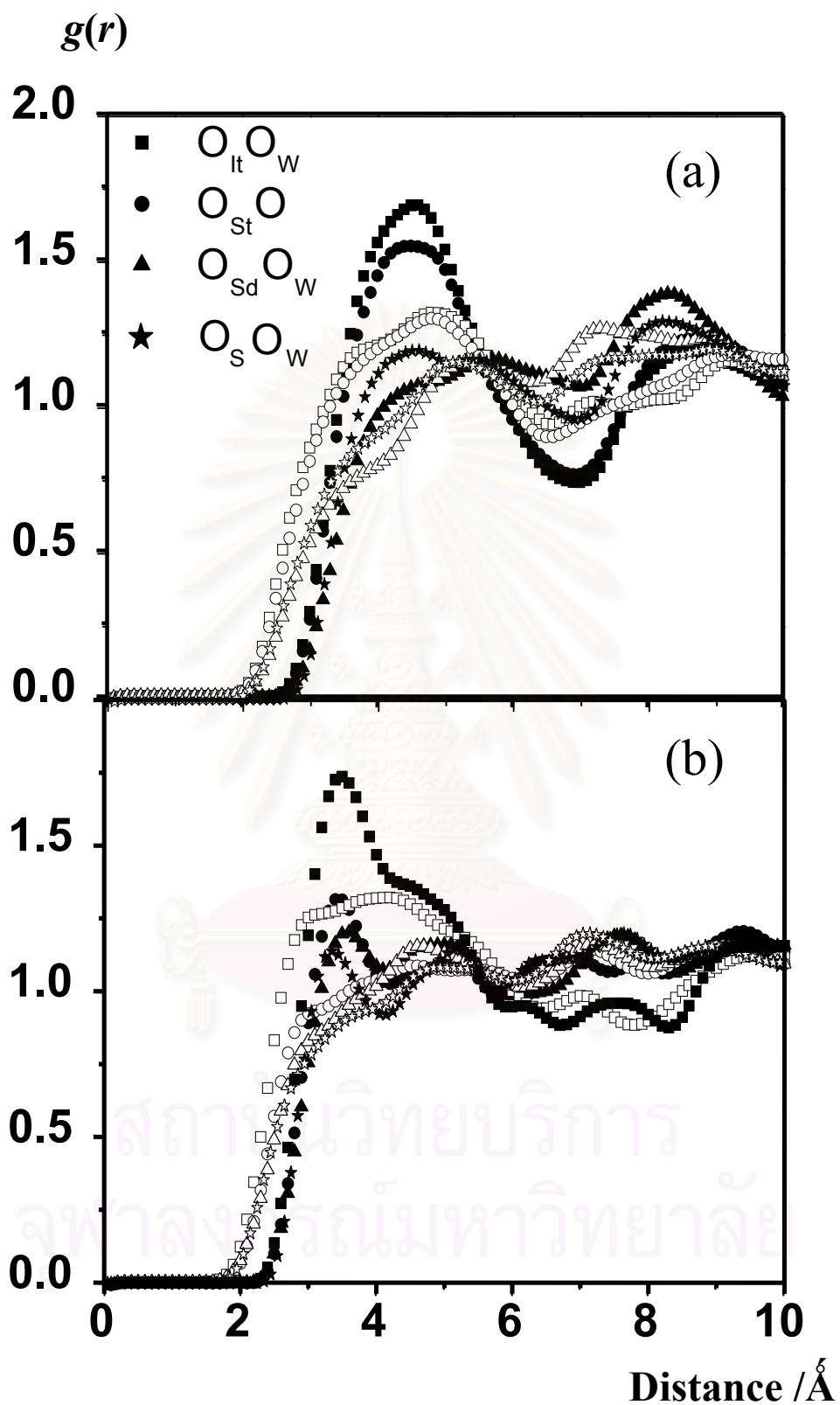
Figure 4.19 RDFs of O_{It}, O_{St}, O_{Sd} to water molecule, where filled and unfilled symbols referred to O_W and H_W, respectively, (a) for $n_{ld} = 1$, and (b) for $n_{ld} = 8$.

In terms of the peak height, which give informations on the probability of finding water molecules residence in the investigated channel, the detected order is intersection > straight > sinusoidal. This conclusion is valid for the RDFs from silicalite-1 surface to both oxygen and hydrogen atoms of water and both n_{ld} = 1 and 8. Note that, the averaged O_S-O_W and O_S-H_w RDFs are not able to compare with those of the separated channels because the number density, ρ ($\rho = n/V$ where n is number of water molecules moving in each channel and V denotes the volume of the simulation cube), for each channel is not known. Therefore, the separated RDFs are not possible to properly normalized and the total number of water molecules in the simulation cube, N, was used instead. In other words, the y-axis for the separated RDFs is in arbitrary units. However, the peak position doesn't depend on the number density. In addition, the height of the O_{St}-O_W RDFs is similar to those of the O_{It}-O_W for n_{ld} = 1 (Figure 4.19a) and of O_{Sd}-O_W for n_{ld} = 8 (Figure 4.19b). What we learn from these facts is, that at low loadings, the probabilities to detect water molecules in the intersection and the straight channels are considerably higher than those in the sinusoidal one, *i.e.*, the diffusion along the straight channel is superior. In contrary, no significant difference has been found for n_{ld} = 8 in the diffusion of water molecules along straight and sinusoidal channels. The trajectory density plot shown in Figure 4.20 confirms this statement.
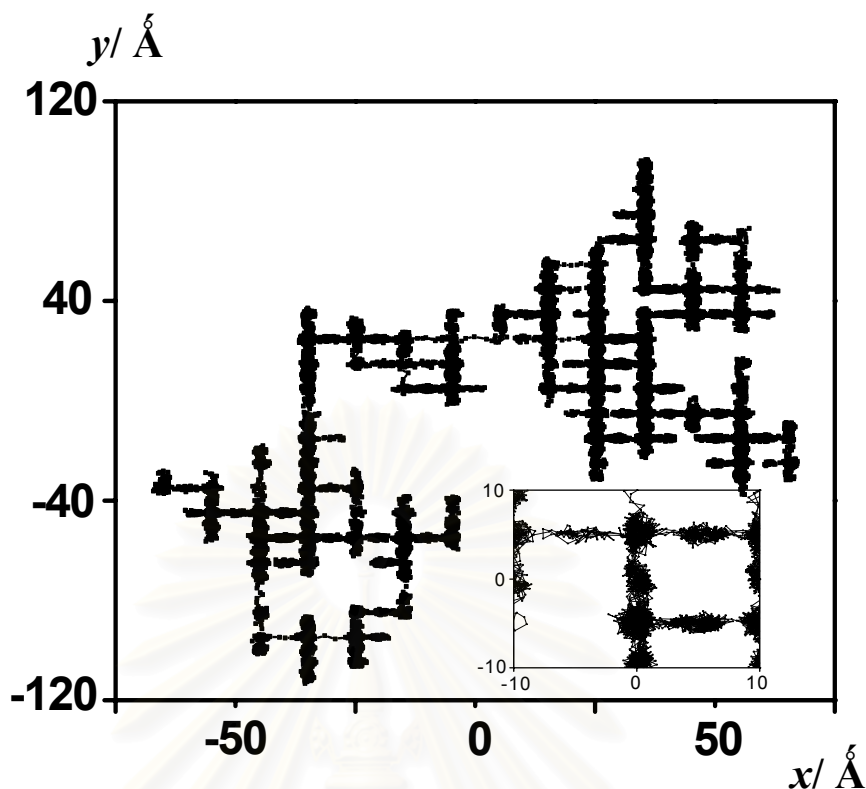
Figure 4.20 The trajectory of one water molecule at n_{ld} = 1 after 10 ns (Å) coordinated on x- v. s. y-axis at 298 K; inserted picture for the zoom out.

Considering the RDFs in Figure 4.19 in terms of the peak position and their shapes, all plots for separated RDFs are almost identical with those of averaged ones (for both concentrations and RDF to both oxygen and hydrogen atoms of water). The only separated RDF, which has a different shape from the others, is the O_{Sd}-O_W one. In addition to the first peak at 4.2 Å of the averaged O_S-O_W RDF, the separated O_{Sd}-O_W RDF shows also a second peak at 5.6 Å. An appearance of this peak can be assigned to a contribution from the water molecules lying in the other channels. It can be seen from the trajectory density plot (Figure 4.20), that high density regions in the intersection and sinusoidal channels lay within a spherical shell with a radius of 5.3 Å with respect to the oxygen atoms of the sinusoidal channel. On the other hand, the contributions to the O_{It}-O_W and O_{St}-O_W RDFs are not visible because the water density in the sinusoidal channel is significantly lower than those in the other channels (Figure 4.19a).

- **Water-water radial distribution functions**

In order to get insights how water molecules formulate inside the channels, the RDFs from oxygen atom (O_W) to oxygen (O_W) and to hydrogen (H_W) atoms of water at 8 loadings have been calculated and illustrated in Figure 4.21a and 4.21b respectively. The O_W-O_W RDF for pure water has been also given for comparison. Characteristics of the pronounced peaks of the RDFs are summarized in Table 4.7.

o **The Oxygen-Oxygen radial distribution function**

Significant changes in the water structure can be observed, in comparison between that of pure water and water in the silicalite-1 cage. The O_W-O_W RDF for pure water shows a typical first peak at 2.80 Å, a second peak at 4.50 Å and a first shell coordination number (*n*) of 4.5 water molecules.[194]

Inside the cage, the O_W-O_W RDF changes dramatically as a function of loading. With the concentration of 8 water molecules per intersection, the plot shows a first sharp peak at 3.35 Å, an apparent minimum at 5.25 Å and *n* = 3.9 water molecules. The distances to the first maxima (R_{M1}) and the first minima (r_{m1}) increase steadily if the concentration decreases. In addition, peak splitting starts to be detected if n_{ld} = 4 and separates at n_{ld} = 1. This indicates the changes of the water structure in the cage of silicalite-1. An appearance of the first sharp peak (for high loading) is assigned to the formation of water clusters in the cage of silicalite-1 (details in the next paragraph) while the splitting peak (for low loading, especially for n_{ld} = 1) at 4.5 Å is interpreted as the water molecules lying separately in different channels.

In terms of the first shell coordination numbers, a linear relation with the water concentrations has been detected and plotted in Figure 4.22. The coordination number of 3.9 for the loading of 8 water molecules per intersection is close to that of 4.5 for pure water.[194]

Table 4.7 Characteristics of the radial distribution functions for water loadings (n_{1d}) of 1 to 8 molecules per intersection in silicalite-1 where R_{M1} and r_{m1} are the distances in Å for the first maxima and minima of RDFs, respectively, and n is the average coordination number integration up to r_{m1}.

RDF $O_W O_W$	n_{1d}								Bulk[**]
	1	2	3	4	5	6	7	8	
R_{M1}	3.65, 4.3[***]	3.55, 4.3[***]	3.45, 4.2[***]	3.45, 4.2[***]	3.35	3.35	3.35	3.35	2.80
r_{m1}	8.05	6.45	5.95	5.85	5.65	5.45	5.35	5.25	3.2
n	0.1	0.7	1.2	1.9	2.5	2.9	3.4	3.9	4.5
RDF $O_W H_W$	n_{1d}								Bulk[**]
	1	2	3	4	5	6	7	8	
R_{M1}	4.05	4.05	3.95	3.95	3.85	3.85	3.75	3.75	1.85
r_{m1}	8.45[*]	9.05[*]	8.95[*]	8.75[*]	8.55[*]	5.65	5.45	5.35	2.4
n	1.3	5.7	9.6	11.9	15.8	7.5	8.3	9.2	4.4

Some comments could be made concerning the O_W-O_W RDFs of pure water and of the high concentration of water in the silicalite-1 cage, especially for n_{ld} = 8, in which the shapes of the RDFs are totally similar and their first shell coordination numbers are about the same. It is known that bulk water forms a hydrogen bond network with the O-O distance, indicated by the first peak of the O_W-O_W RDF, of 2.80 Å. Therefore, it is evident from the O_W-O_W RDF of water molecules in the cage of silicalite-1, at least for n_{ld} = 8, that clusters are formed.

* the RDFs show flat minima

** values taken from ref. [194] where the simulation was performed using the CF2 water model.

*** the RDFs show broad splitting peak

Characteristics of the cluster can be figured out from the RDF and summarized as the following: (*i*) Water molecules in the cluster in the cage of silicalite-1 do not bind together via hydrogen bond because the O-O distance of 3.35 Å (R_{M1} of the O_W-O_W RDF for n_{ld} = 8) which is about 0.5 Å longer than the typical hydrogen bond distance in bulk water, does not fit to the geometrical, and hence the energetic, criteria[195-197] of the hydrogen bond formation; (*ii*) The height of the O_W-O_W RDF indicates that the water clusters in the cage of silicalite-1 are less flexible than that of pure water. This observation can be understood in terms of their interactions with water molecules in the second solvation shell and with the silicalite-1 wall. Due to the limited space in the channel, the second solvation shell of water doesn't allow to be formed (the second peak at about 6.5 Å of the O_W-O_W RDF is shown in Figure 4.21a for other loadings is due, surely, to the water molecules lying in different channels). This fact leads to a destruction of the hydrogen bond networks and, hence, a lower stability of the water clusters in the cage of silicaite-1 in comparison to those of pure water. Destructive contributions can be compensated by the interaction with the silicalite-1 wall in which the first shell molecules can be weakly held in place by the water-silicalite-1 potential. A conclusion is that, in spite of interactions among water molecules in the cluster, its stability which leads consequently to the sharp and pronounced O_W-O_W first peak at 3.35 Å, can be described in terms of destructive and constructive contributions from the second solvation shell and the silicalite-1 wall, respectively.; (*iii*) Based on the detailed description given in (*ii*), the size of the "low density water clusters", in terms of spherical radius, r_{sphere}, (equivalent to R_{M1} of the O_W-O_W RDF), is expected to depend strongly on Δr, the difference between the radius of the pure water cluster and of the silicalite-1 channels *i.e.*, r_{sphere} increases as a function of Δr. In contrary, "high density water clusters" (R_{M1} of the O_W-O_W RDF > 2.80 Å) would be also possible to be formed for the high loading of water molecules in small-channel zeolite.

Figure 4.21 RDFs of (a) $O_W O_W$ and (b) $O_W H_W$ for n_{ld} = 1 to 8; RDFs for bulk water inserted for comparison, * marked at the first maximum.
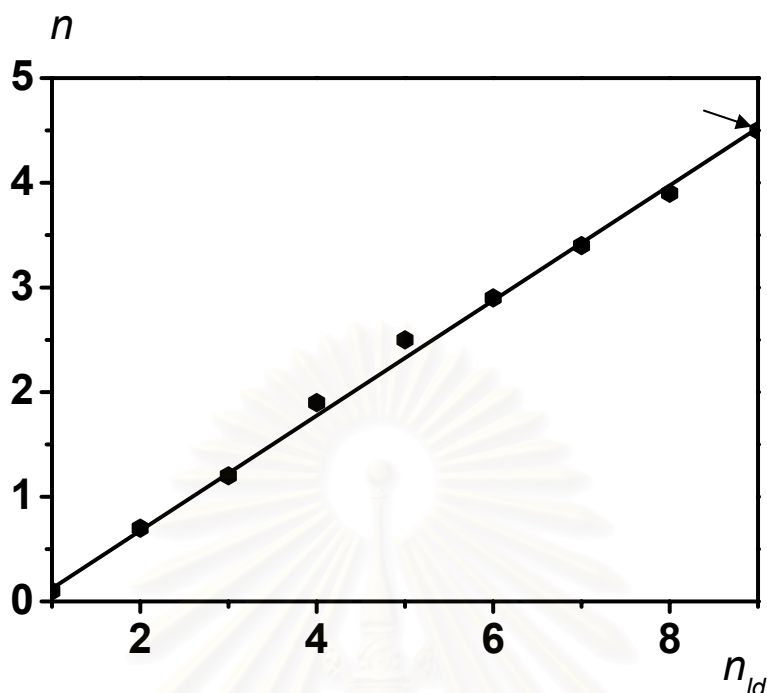
Figure 4.22 The average coordination number integration up to r_{m1} as a function of the loading.

○ **Oxygen-Hydrogen radial distribution function**

Additional characteristics of the low density cluster of water molecules in the silicalite-1 cage can be extracted from the O_W-H_W RDFs, shown in Figure 4.21b. In good agreement with those of O_W-O_W RDF, the plots for high loadings show a pronounced shoulder centered at about 2.8 Å. This shoulder is less pronounced when the concentration decreases and it disappears for n_{ld} = 1. An appearance of the clear shoulder at longer distances than that of the first O_W-H_W main peak implies that H_2O....H-OH is superior. This hydrogen-bond like configuration confirms the formation of low density clusters of water. Note, as already mentioned, that, the distances to the established shoulder of about 2.8 Å and to the first main peak of the O_W-H_W RDFs ranging from 3.75 Å to 4.05 Å for n_{ld} = 1-8, are surely not fit to any criteria of hydrogen bond formation.[196-198]

4.4.1.2. Dynamical properties

- **Self-diffusion coefficients**

The self-diffusion coefficients are calculated from the particle displacements. The process of self-diffusion was quite generally related to the moments of the propagator.[102,103,104] The propagator $P(r,r_0,t)$ represents the probability density to find a particle at position r at time t if it was at r_0 at time $t = 0$. The nth moment of the propagator is defined by the relation[103]

$$\langle |r-r_0|^n \rangle = \int |r-r_0|^n P(r,r_0,t)\,dr \,.$$ (4.4)

Here, $P(r,r_0,t)$ is the solution of the diffusion equation for the initial concentration $C(r,t=0) = \delta(r-r_0)$. The elements of the diffusion tensor, corresponding to the x-, y- and z-axes, are calculated. The overall diffusivity D is assumed to be one third of the trace of the diffusion tensor.
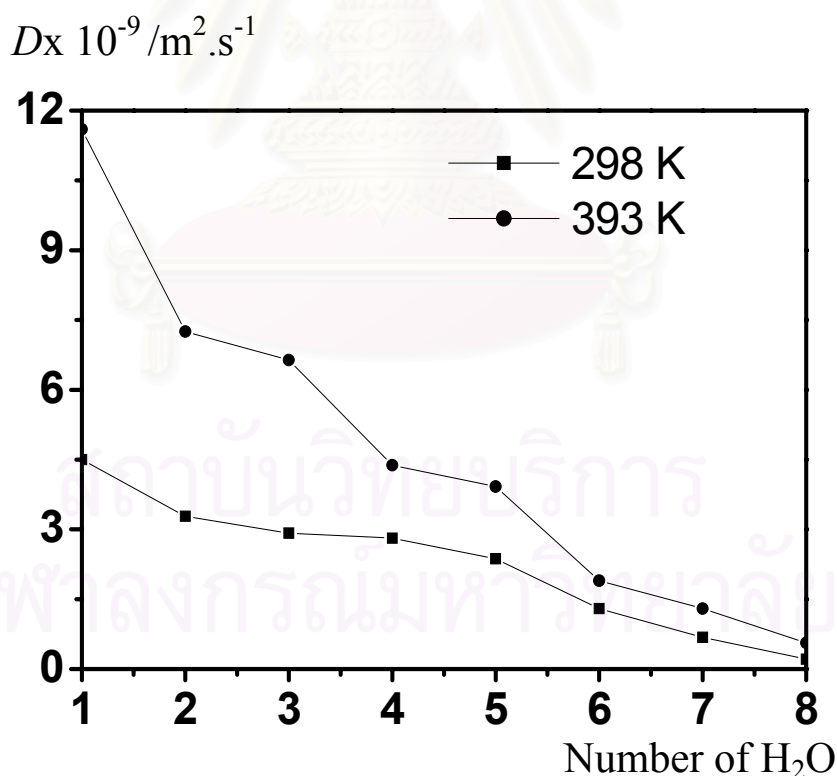
Figure 4.23 The self-diffusion coefficients ($m^2.s^{-1}$) v. s. the loading (molecules per intersection) at 298 and 393 K.

The self-diffusion coefficients of the water molecules as a function of the loading, varying from 1 to 8 water molecules per intersection, at 298 K and 393 K are shown in Figure 4.23. Changes of the water self-diffusion coefficients as a function of the loading can be seen from the plots. Similar to the case of other small guest molecules such as, CH_4, CF_4, He, Ne, Ar, Xe and SF_6 in silicalite-1,[64] the diffusion of water decreases if the concentration increases. As expected, the diffusivities for all concentrations at 393 K are higher than those of 298 K. The temperature dependence is stronger at low concentrations, *i.e.*, the difference of the diffusion coefficients obtained from the two temperatures disappeared almost at the loading of 8 water molecules per interaction.

- **Anisotropic effect**

It has been observed experimentally and theoretically that the diffusion of alkanes and light gases in silicalite-1 is anisotropic.[66,164,198-200] To visualize this effect, a formula for the relation between the components of the diffusivity tensor (*D*) proposed by Kärger *et al.*[200] eq. (4.5) has been applied,

$$\frac{c^2}{D_z} = \frac{a^2}{D_x} + \frac{b^2}{D_y},$$
(4.5)

where *a, b* and *c* are the unit cell lengths. The deviation from eq. (4.5) can be accounted by introducing an parameter,[66,158,201]

$$\beta = \frac{c^2 / D_z}{\left(a^2 / D_x + b^2 / D_y \right)}$$
(4.6)

where, $\beta = 1$ denotes random processing, e.g., a water molecule passing an intersection continues the diffusion path independent of how it gets to the intersection. A hint on preferentially continuative diffusion path either along in one or the same channel type is when $\beta > 1$. Vice versa, a higher diffusivity in z-direction, that is only possible by changes between straight and sinusoidal channels, occurs if $\beta < 1$. The interchange between the two channel types is more probable in this case.
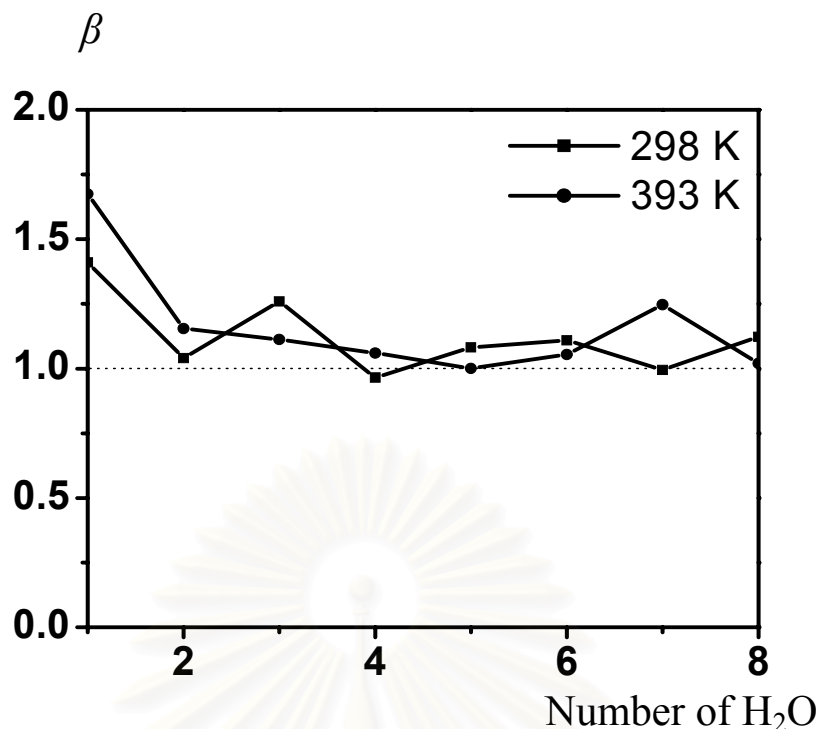
Figure 4.24 The correlated movement parameter calculated from eq. (4.6) vs. the loading.

Figure 4.24 visualizes the computed β as a function of the loading at the two temperatures. The β's for almost all concentrations and temperatures are higher than 1, indicating preferential continuation-diffusivity of the water molecule in the same silicalite-1 channels. This is in good agreement with examinations for xenon and alkane molecules in silicalite-1 in which $\beta = 1.2$ and 1.3 have been detected.[160] However, as the changes of the β's as functions of loading and temperature observed in the present paper are within the fluctuation limit, relations between these variables cannot be concluded.

The fact, the continuation-diffusivity preferred by non-polar molecules in comparison to polar molecules in silicalite-1, can be due to the diffusion of a polar molecule is stronger influenced by its interaction with the silicalite-1 inner surface. Polar molecules are expected to approach closer to the channel wall as non-polar ones. Therefore, when a molecule gets into an intersection from a channel of type A, it expects to take the closest pore - which belongs to the other type of channel, B (pores to the same type of channel are almost on the opposite side of the intersection) for continuation diffusion. This leads directly to decrease probability of

taking the same channel type for the polar molecule, *i.e.*, β for polar molecules is lower than that of non-polar molecules.

4.4.2. Methane/silicalite-1

Similar to the water system, the simulations were conducted in the canonical statistical ensemble (NVT), at 298 K and various concentrations, n_{ld} ranged from 1 to 4 molecules per intersection, equivalent to 4 – 32 molecules per simulation cube, respectively. Newton's equations of motion were integrated with the Verlet algorithm, with a time step of 1 fs. To stabilize the system, thermalization has been applied within the first 10 ps. Another 10 ns were conducted in which the trajectories were collected and self-diffusion coefficients as well as radial distribution functions were evaluated. The methane-methane interaction model recently developed by Rowley and Pakkanen[96] at the MP2 level, has been used while the methane/silicalite-1 model was newly developed, (section 3.2.2) by fitting 150 MP2 methane/silicalite-1 interaction energies into an analytical form.

4.4.2.1. Structural properties:

- **Silicalite-methane radial distribution functions**
  - **Average RDF for all channels**

To investigate structural data of methane molecules via diffusion in zeolite silicalite-1, the radial distribution functions (RDFs) from surface oxygen atom (O_S) to methane carbon atom (C) have been calculated. The RDFs as a function of loadings, n_{ld} at 298 K have been plotted in Figure 4.25.

The RDFs at all loadings display first sharp maxima around 4.2 Å, and second broad peaks centered at 5.8 Å. This could also be explained as in the water cases, due to the cylinder-like structure with the diameter of 8.2 Å of silicalite-1 channels, methane molecules lied under this first maximum can be assigned to those moving along central line at the center of the tube. Hence, it can be concluded that central line is the optimal path for both methane and water ($n_{ld} \leq 5$) molecules to travel along the silicalite-1 channels.

In consistence with other works,[74,72] the plots show the other 2 peaks at approximately 6 Å and 8 Å. The first one corresponds to the distance from O_{It} to the methane molecule lying in the sinusoidal channels, and vice versa where O_{It} denote oxygen atoms in the intersection channel. For the other peaks

at 8.3 Å, they represent the distance from oxygen surface of sinusoidal channels to methane molecule in the straight channels, and vice versa.
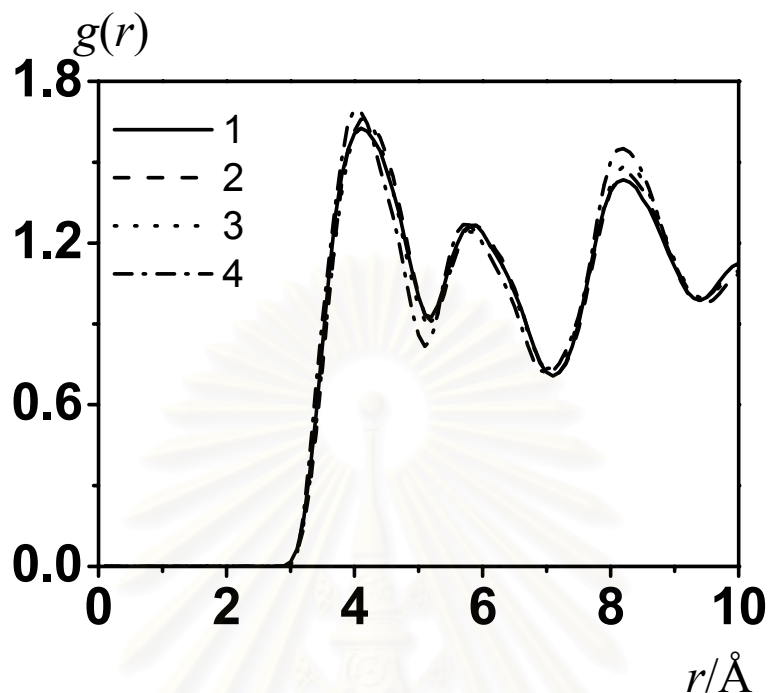
Figure 4.25 O_SC Radial distribution functions (RDFs) at various loadings of the methane molecule in silicalite-1, n_{ld} from 1 to 4.

o   **Separated RDF for each channel**

To understand more details of the methane behavior in different channels, the RDFs from the oxygen surface of each channel to all carbon atoms of methane molecules have been evaluated. The results are given, as examples only for $n_{ld} = 1$ and 4, in Figures 4.26 where the notation the O_{lt}, O_{St} and O_{Sd} were defined as those in Figure 4.19. The following conclusions can be extracted from the plots.
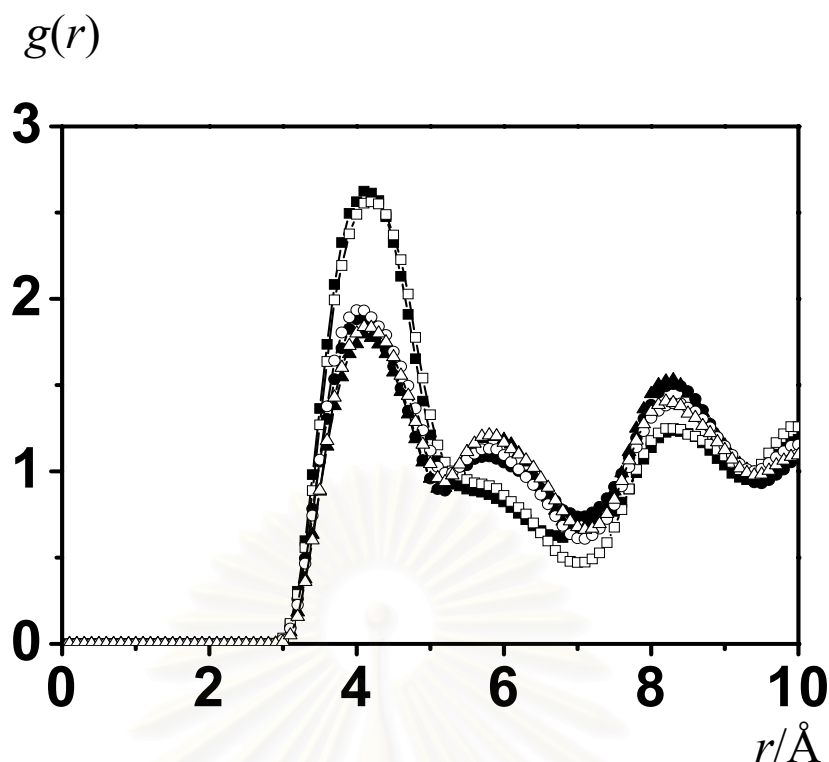
Figure 4.26 RDFs of O_{It}, O_{St}, O_{Sd} to the methane molecule where filled and unfilled symbols referred to n_{ld} =1 and 4; the symbols defined as those in Figure 4.19.

The plots are concentration independent. The three main peaks, which are found for the average RDFs, still remained in the separated ones. The sharp first peaks at 4.2 Å for all separated RDFs confirm preferential movement along the central axis of each channel. In terms of the peak height, which give the information about the probability of finding methane molecules residence in the investigated channel, the detected order is that the methane molecule spends more times in the intersection than those in the two channels of sinusoidal and straight. It is interesting to be noted that sinusoidal channels are as preferable as straight channels for methane molecule occupation. This corresponds to the energy data derived from both *ab initio* calculations, and, the potential energy surface in which interactions between methane and the sinusoidal or straight channels are no significant difference. (See detail section 4.3.2).

- **Methane-methane radial distribution functions**

To get some insights into structured data of methane molecules inside the channels, the RDFs from carbon to other carbon atoms of methane molecules at various loadings have been calculated and illustrated in Figure 4.27.
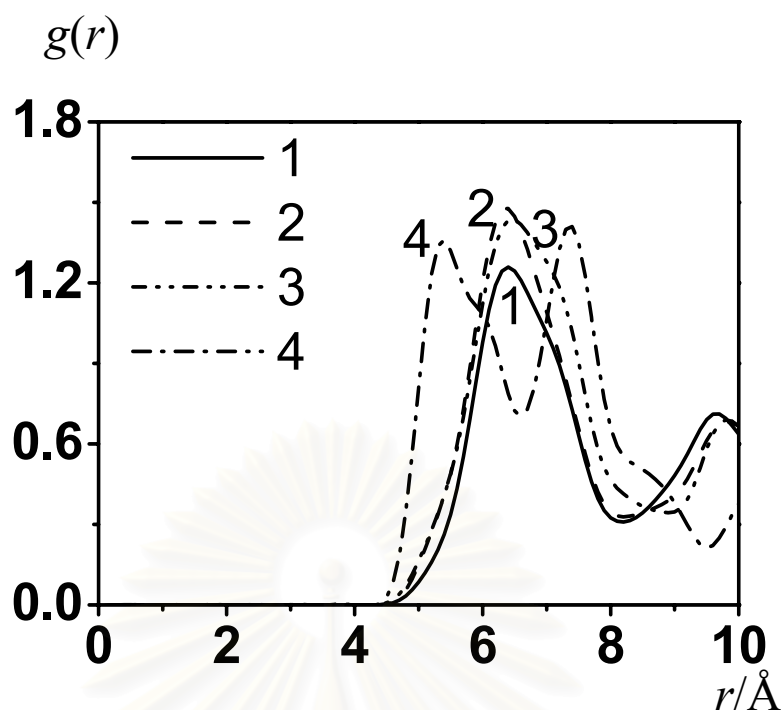
Figure 4.27 Carbon-carbon radial distribution functions (RDF), $g(r)$ for methane molecules in silicalite-1 at $n_{ld} = 1 - 4$.

Before going into detailed structural properties of methane, the distances between the channels have been visualized in Figure 4.28.[72] The distance from any intersection to center of the adjacent straight, sinusoidal, and intersection channels are around 4 Å, 6 Å, and 10 Å, respectively, while that from center of any straight channel to center of another adjacent sinusoidal channel is approximately 8 Å. The radial distribution functions of the centers of mass of methane at various loading according to ref. [72] have been in addition given in Figure 4.29 for discussing.
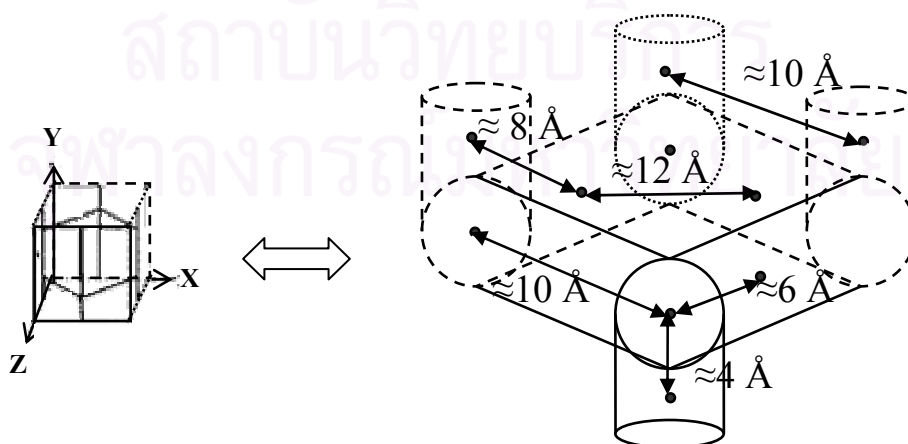
Figure 4.28 Schematic representations of distances at various channels in silicalite-1

As a function of loading, the distinct changes of the methane-methane structure have been observed. At adequate high loading the methane molecule (n_{ld} = 4), the plot shows a first sharp peak (R_{M1}) at 5.4 Å with a first minimum (r_{m1}) at 6.6 Å, as well as a second sharp peak at 7.4 Å, followed by the shoulder at 8.6 Å. However, there is no particular tendency detected, for the decrease of the concentration. At a loading of 2, the apparent R_{M1} at 6.4 Å as well as r_{M1} at 8.2 Å is established. In striking to these distinct peaks, the broaden peaks have been found at n_{ld} = 1 and 3, the established shoulder at 5.1 Å with R_{M1} at 6.3 Å and the ensuing boarded peak at 6.4-6.5 Å have respectively been demonstrated. The detected distances agree, somehow, with those exhibited peaks in Figure 4.28. Note that the distances in Figure 4.28 are from center to center of channels. In practice, the guest molecules are able to move covered broad regions in the channel with changes of its potential energy within thermal fluctuation, $kT \approx$ 0.6 kcal.mol^{-1} at room temperature (k denotes the Boltzmann constant).
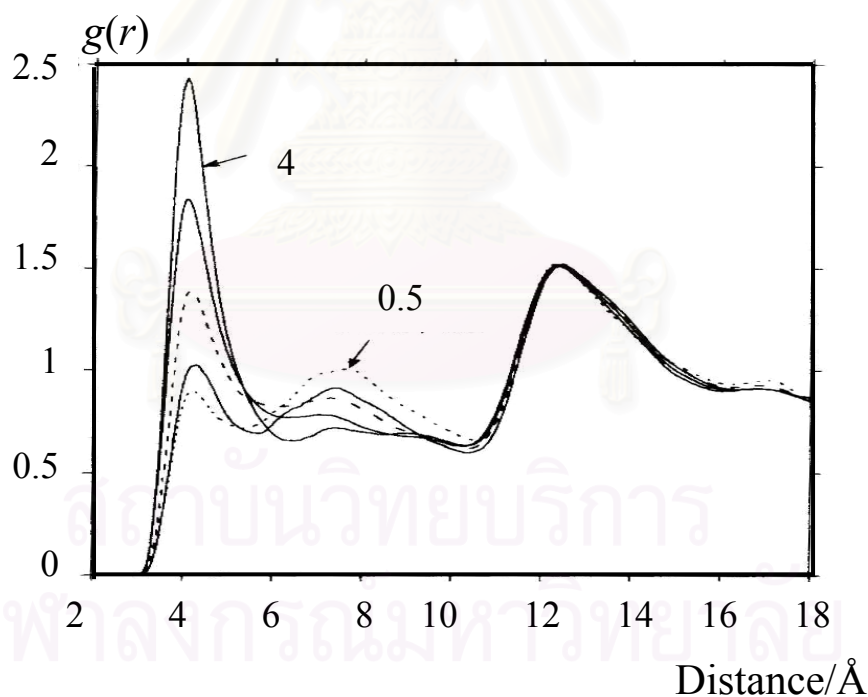
Figure 4.29 Radial distribution function (RDF) of the centers of mass of the methane molecules at various loadings taken from ref. [72].

The plots show pronounced increasing peaks at about 4 Å as a function of loading. In contrary to the peaks at 12 Å, the denoting distances between the zigzag channels are concentration independent. Intensive discussions have been

performed in ref. [72] concerning an appearance of the first C-C peak at 4 Å for low concentration, for example $n_{ld} = 1$ and 0.5. As it is comprehended that sinusoidal channels of silicalite-1 is preferential for sitting residence[72] for methane. Therefore, at the concentration lower than 1 methane per intersection, methane molecule should not available in the intersection and straight channels at the same time, *i.e.*, the C-C peak at 4 Å is expected to disappear. This is the reason why the authors[72] perform simulations at $n_{ld} = 0.5$. This matter is not yet understood. The only possibility, which leads to this discrepancy, is an artifact due to the methane/methane and methane/silicalite-1 pair potential functions. Note that all available methane/silicalit-1 data are based on the force-field parametizations. The methane/methane potentials used in all previous simulations are also the force field ones, although the *ab initio* fitted models are also available.

Considering the recent structural results using the MP2 interactions for both methane/methane and methane/silicalite-1 shown in Figure 4.27, the characteristic of the plot for $n_{ld} = 4$ is comparable to that obtained from the simulations using force field potential,[72,74] except the second peak of the present study is much pronounced. The decrease of the methane concentration, the first peak is shifted to about 6.5 Å while that at 5.4 Å is disappeared for $n_{ld} = 3$ and $n_{ld} = 2$. However, a decrease of the first peak at 6.5 Å, in comparison to those of $n_{ld} = 2$ and 3, are not yet understood.

4.4.2.2. Dynamical properties

- **Self-diffusion coefficients**

Similarly to water/silicalite-1 system, the self-diffusion coefficients have been calculated from the particle displacements related to the moments of the propagator.[102,103,104]
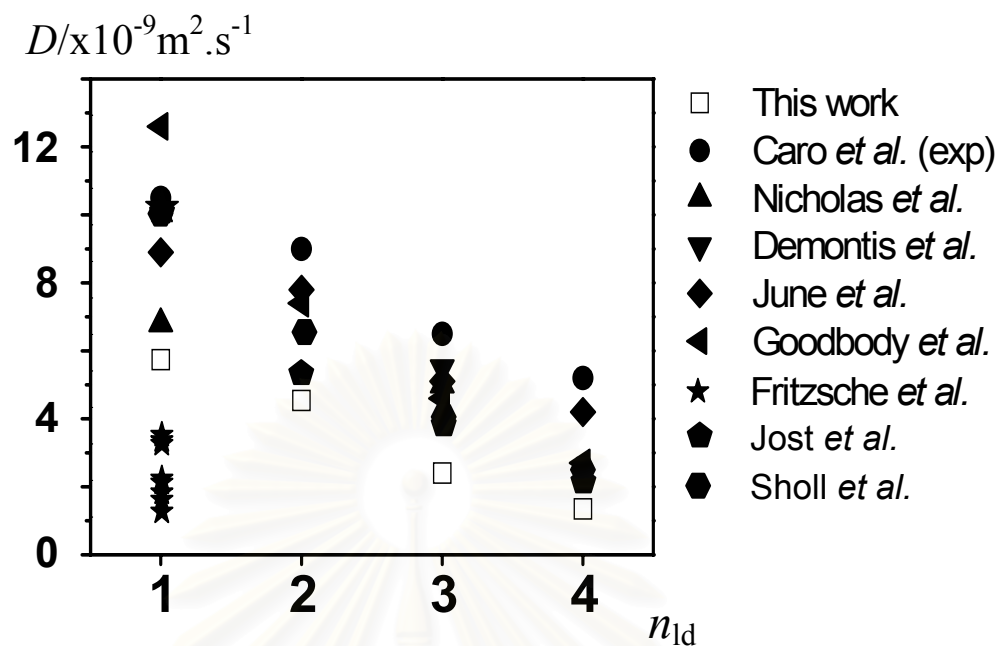
Figure 4.30 The self-diffusion coefficients as a function of loading, n_{ld} at 298 K (Fritzsche *et al.* simulates using various available models).

The self-diffusion coefficients of the methane molecules as a function of the loading, varying from 1 to 4 molecules per intersection, at 298 K are shown in Figure 4.30. Experimental values by PFG NMR measurements since 1985 at the same concentrations have been also given for comparison. The other diverse simulated self-diffusion coefficients[64,66,68,72,74,75,162] carried out by various groups have also been given. However, the recent work using various available methane/silicalite-1 models with 10 ns evaluation length, by Fritzsche *et al.*[85] shows the outmost values from the experiment in a fluctuation range, closed to the values carried out from this work, while MM2 diffusion coefficients are in excellent agreement that of experimental values. However, the explanations for those discrepancies could be due to the intermolecular potential functions used, as well as the lengths of the production time. Although, the results for all loading from this study are slightly lower than other works. However, all data shown in Figure 4.30 are in satisfactory agreement to each others. As a function of loading, the results from all works are almost linearly decreasing.

- **Anisotropic effect**

Due to such three-dimensional channels in silicalite-1, the diffusion is anisotropic as discussed first for water system in section 4.4.1.2. However, in order to get a prompt idea the β values have again defined; $\beta = 1$, if a correlation role is valid; $\beta > 1$, preferential continuation of diffusion path; $\beta < 1$, interchanging between straight and sinusoidal channels.
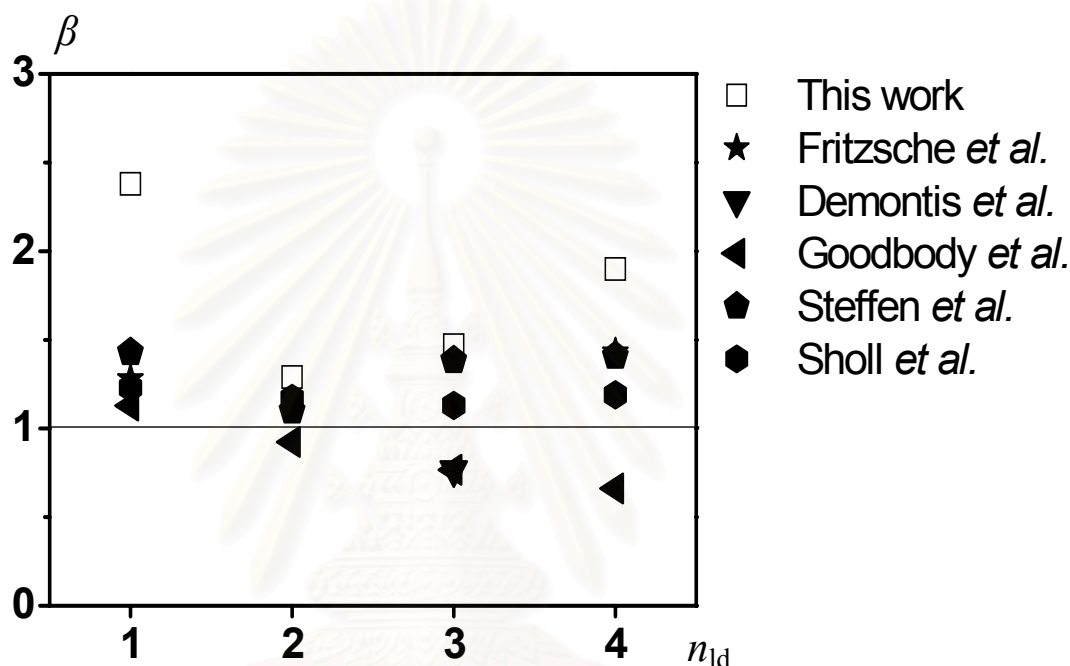
Figure 4.31 The correlated movement parameter (β) calculated from eq. (4.6) as a function of loading n_{ld}.

Figure 4.31 visualizes the computed β as a function of the loading. In good agreement with other works,[66,68,72,74,75,162] most of the β values are higher than 1, indicating a preferential continuation-diffusivity of the methane molecule. However, at $n_{ld} = 1$ and 4, the βs are considerably larger than others. As discussed in section 4.4.1.2 in comparison with those of water molecule, the βs for methane as well as other hydrocarbons are larger that those from water. This confirms that dipole molecule prefer more to switch the diffusivity paths but not for non-polar molecule.[202]

CHAPTER 5

CONCLUSION

The three scheme investigations, quantum chemical calculations, molecular dynamics simulations and pulse field gradient nuclear magnetic resonance measurements have successfully been used in order to evaluate the diffusion phenomena of water and methane molecules in silicalite-1. The results are summarized below.

5.1. Binding and Encapsulation of Water

Changes of water/silicalite-1 interactions, when water molecule moves along the translation axis through the center of a window of the silicalite-1, have been proposed.

The energy barrier for the water molecule to enter the pores via the single, double and intersection rings are respectively 1.62, 0.67 and 1.28 kcal.mol^{-1}. The barrier of about 1.9 kcal.mol^{-1} is required to cross from zigzag or straight channels to intersection channels. The encapsulation or stabilization for water molecule in the silicalite-1 pore is -3.9 kcal.mol^{-1}, and the preferential location is in the intersection part. Additionally, it was also found that a water molecule enters and leaves the pores by pointing its dipole vector towards the center of the cavity.

5.2. Ab initio Fitted Potentials

The novel water/silicalite-1 and methane/silicalite-1 interaction models have been formulated on the basis of quantum calculations at the Hartree-Fock and secondary order Møller Plesset levels. The rather large fragments of silicalite-1 fragments consisting of 20, 52 and 64 heavy atoms (oxygen and silicon atoms), in which the chemical compositions are $O_{10}Si_{10}H_{20}$, $O_{30}Si_{22}H_{44}$ and $O_{35}Si_{29}H_{58}$ have been used to represent the bottle neck (single 10-oxygen-membered ring), the straight or zigzag channel (double 10-oxygen-membered ring), and the intersection channels, respectively. The intermolecular potential functions have been represented by fitting ab initio data of 1,032 water and 150 methane configurations. The outstanding features of these functions are their ability to classify guest-framework interactions in

different channels as well as the orientations of guest molecule which are not possible in the previous works.

5.3. Dynamical and Structural Properties of Water

Series of molecular dynamics simulations have been performed in order to examine changes of structural and dynamical properties of water molecules in silicalite-1 as a function of temperatures and loadings. The ab initio fitted silicalite-1/water potential which is newly developed and the BJH flexible water/water potential have been employed. The water loading was varied from 1 to 8 water molecules per intersection, equivalent to 8 to 64 molecules per simulation cube. The simulations have been carried out at 298 and 393 K. The results show that the water structure inside the silicalite-1 cages changes dramatically as a function of loading. The probability of water molecules to reside in the straight channel is always higher than that to find them in the sinusoidal channels. The formation of water clusters has been detected for high loading. The observed clusters display pure water like-structure. It is named "low density cluster" due to the following reasons: (i) The cluster consists of 5 water molecules (4 in the first hydration shell of the central one) which is consistent with that of pure water; (ii) Molecules in the cluster are not coordinated together via hydrogen bond. The radius of the first hydration shell of 3.35 Å is 0.5 Å longer than that of pure water; (iii) Molecules in the cluster are less flexible than those of pure water.

In terms of dynamical properties, for low loadings a preferential diffusion path for sufficiently low loadings is observed along center of the channel tube. The water molecules were detected to diffuse closer to the surface when the concentration is higher than 6 molecules per intersection. The diffusion coefficient (D) of water decreases when the concentration increases. The D values for all concentrations at 393 K are higher than those of 298 K. The temperature dependence almost disappears at a loading of 8 water molecules per intersection. In addition, the anisotropic diffusion is less pronounced for water in silicalite-1 in comparison to that of non-polar molecules

5.4. Dynamical and Structural Properties of Methane

In the same manner of water, series of molecular dynamics simulations of methane molecule in silicalite-1 have been performed in order to examine changes of structural and dynamical properties when the concentration increases. The MP2 ab initio fitted silicalite-1/methane potential, which is newly developed and the MP2 rigid methane/methane potential have been utilized. The methane loading was varied from 1 to 4 water molecules per intersection, equivalent to 8 to 32 molecules per simulation cube. The simulations have been carried out at 298 K. The results show that the methane structure inside the silicalite-1 cages changes dramatically as a function of loading, similar to water/silicalite-1 system. In addition, a probability of methane molecules to reside in the intersection at all loadings is always higher than that in the sinusoidal or straight channels. A transition of the methane-methane radial distribution function takes place when concentration increases. This event has never detected when the force-field model has been applied. The anisotropic diffusion parameter beta displays a fluctuation at $n_{ld} = 1$, and 4.

REFERENCES

1. Cronstedt, A. F. *Akad. Handl. Stockholm*, **1756**, *18*, 120.

2. Breck, D. W. *Zeolite Molecular Sieves: Structure, Chemistry, and Use*; Wiley: New York, 1974.

3. Kärger, J.; Ruthven, D. M. *Diffusion in Zeolites and Other Microporous Solids*; Wiley: New York, 1992.

4. Galarneau, A.; Di Renzo, F.; Fajula, A.; Vendrine, J. *Zeolites and Mesoporous Materials at the Dawn of the 21st Century*, 13th International Zeolite Conference Montpellier, France; Elsevier Science: Amsterdam, 2001.

5. Eder, F.; Stockenhuber, M.; Lercher, J. A. *J. Phys. Chem. B* **1997**, *101*, 5414.

6. Chen, N. Y. *Ind. Eng. Chem. Res.* **2001**, *40*, 4157.

7. Liu, X. M.; Yan, Z. F. *Catal. Today* **2001**, *68*, 145.

8. Degnan, T. F. *Top Catal.* **2000**, *13*, 349.

9. Poulton, S. W.; Krom, M. D.; Van Rijn, J.; Raiswell, R. *Water Res.* **2002**, *36*, 825.

10. Querol, X.; Moreno, N.; Umana, J. C.; Juan, R.; Hernandez, S.; Fernandez-Pereira, C.; Ayora, C.; Janssen, M.; Garcia-Martinez, J.; Linares-Solano, A.; Cazorla-Amoros, D. *J. Chem. Technol. Biot.* **2002**, *77*, 292.

11. Hall, C.; Wales, D. S.; Keane, M. A. *Separ. Sci. Technol.* **2001**, *36*, 223.

12. Kanamori, M.; Hiramatsu, M.; Shibata, T.; Watanabe, F.; Matsuda, H.; Hasatani, M. *Kagaku. Kagaku. Ronbon.*, **1998**, *24*, 243.

13. Hamlaouia, M. L.; Kherrata, R.; Marrakchib, M.; Jaffrezic-Renaultb, N.; Walcariusc, A. *Mat. Sci. Eng. C* **2002**, *21*, 25.

14. Wan, Y. S. S.; Chau J. L. H.; Gavriilidis, A.; Yeung, K. L. *Micropor. Mesopor. Mat.* **2001**, *42*, 157.

15. Ruthven, D. M. *Principles of Adsorption and Adsorption Processes*; Wiley: New York, 1984.

16. Kalipcilar, H.; Culfaz, A. *Micropor. Mesopor. Mat.* **2002**, *52*, 39.

17. Smith, J. V.; Bennett, J. M.; Flanigen, E. *Nature* **1967**, *215*, 241.

18. Dempsey, E. *J. Phys. Chem.* **1969**, *73*, 3660.

19. Dendooven, E.; Mortier, W. J.; Uytterhoeven, J. B. *J. Phys. Chem.* **1984**, *88*, 1916.

20. Van Dun, J. J.; Mortier, W. J. *J. Phys. Chem.* **1988**, *92*, 6740.

21. Bussai, C.; Vasenkov, S.; Liu, H.; Böhlmann, W.; Fritzsche, S.; Hannongbua, S.; Haberlandt, R.; Kärger, J. *Appl. Catal. A-Gen* **2002**, *232*, 59.

22. Bussai, C.; Fritzsche, S.; Hannongbua, S.; Haberlandt, R. *Chem. Phys. Lett.* **2002**, *354*, 310.

23. Bussai, C.; Hannongbua, S.; Haberlandt, R. *J. Phys. Chem. B* **2001**, *105*, 3409.

24. Bussai, C.; Haberlandt, R.; Hannongbua, S.; Jost, S. *Studies in Surf. Sci. Catal.* **2001**, *135*, 263.

25. Bussai, C.; Fritzsche, S.; Haberlandt, R.; Hannongbua, S. *Studies in Surf. Sci. Catal.* **2002**, *142B*, 1979.

26. Fois, E.; Gamba, A.; Tilocca, A. *J. Phys. Chem. B* **2002**, *106*, 4806.

27. Demontis, P.; Gulín González, J.; Suffritti, G. B.; Tilocca, A. *J. Amer. Chem. Soc.* **2001**, *123*, 5069.

28. Demontis, P.; Spanu, S.; Suffritti, G. B. *J. Chem. Phys.* **2001**, *114*, 7980.

29. Cicu, P.; Demontis, P.; Spanu, S.; Suffritti, G. B.; Tilocca, A. *J. Chem. Phys.* **2000**, *112*, 8267.

30. Demuth, T. H.; Benco, L.; Hafner, J.; Toulhoat, H. *Int. J. Quantum Chem.* **2001**, *84*, 110.

31. Pereira, J. C. G.; Catlow, C. R. A.; Price, G. D. *J Phys. Chem. A* **2001**, *105*, 1909.

32. Hill, J. R.; Minihan, A. R.; Wimmer, E.; Adams, C. J. *Phys. Chem. Chem. Phys.* **2000**, *2*, 4255.

33. Takaba, H.; Koyama, A.; Nakao, S-I. *J. Phys. Chem. B* **2000**, *104*, 6353.

34. Demontis, P.; Suffritti, G. B.; Quartieri, S.; Fois, E. S.; Gamba. A.; Morosi, G. *Mater. Chem. Phys.* **1991**, *29*, 357.

35. Demontis, P.; Suffritti, G. B. ; Quartieri, S.; Fois, E. S.; Gamba. A. *Zeolites* **1987**, *7*, 522.

36. Demontis, P.; Suffritti, G. B.; Alberti, A.; Quartieri, S.; Fois, E. S.; Gamba. A. *Gazz. Chim. Ital.* **1986**, *116*, 459.

37. Leherte. L.; André, J. M.; Derouane, E. G.; Vercauteren, D. P. *Int. J. Quantum Chem.* **1992**, *42*, 1291.

38. Leherte. L.; André, J. M.; Derouane, E. G.; Vercauteren, D. P. *Comput. Chem.* **1991**, *15*, 273.

39. Leherte. L.; André, J. M.; Derouane, E. G.; Vercauteren, D. P. *Catal. Today* **1991**, *10*, 177.

40. Leherte. L.; André, J. M.; Derouane, E. G.; Vercauteren, D. P. *J. Chem. Soc. Faraday Trans.* **1991**, *87*, 1959.

41. Leherte, L.; André, J. M.; Vercauteren, D. P.; Derouane, E. G. *J. Mol. Catal.* **1989**, *54*, 426.

42. Leherte, L.; Lie, G. C.; Swamy, K. N.; Clementi, E.; Derouane, E. G.; André, J. M. *Chem. Phys. Lett.* **1988**, *145*, 237.

43. Faux, D. A. *J. Phys. Chem. B* **1999**, *103*, 7803.

44. Faux, D. A. *J. Phys. Chem. B* **1998**, *102*, 10658.

45. Faux, D. A.; Smith, W.; Forester, T. R. *J. Phys. Chem. B* **1997**, *101*, 1762.

46. Cicu, P.; Demontis, P.; Spanu, S.; Suffritti, G. B.; Tilocca, A. *J. Chem. Phys.* **2000**, *112*, 8267.

47. Termath, V.; Haase, F.; Sauer, J.; Hutter, J.; Parrinello, M. *J. Amer. Chem. Soc.* **1998**, *120*, 8512.

48. Jeanvoine, Y.; Angyan, J. G.; Kresse, G.; Hafner, J. *J. Phys. Chem. B* **1998**, *102*, 7307.

49. Flanigen, E. M.; Bennett, J. M.; Grose, R. W. *Nature* **1978**, *271*, 512.

50. Vigné-Maeder, F.; Auroux, A. *J. Phys. Chem.* **1990**, *94*, 314.

51. Turov, V. V.; Mironyuk, I. F. *Colloid Surf. A* **1998**, *134*, 257.

52. Turov, V. V.; Brei, V. V.; Khomenko, K. N.; Leboda, R. *Micropor. Mesopor. Mater.* **1998**, *23*, 189.

53. Turov, V. V.; Leboda, R. *Advan. Colloid Interface Sci.* **1999**, *79*, 173.

54. Turov, V. V.; Chodorowski, S.; Leboda, R.; Skubiszewska-Zieba, J.; Brei, V. V. *Colloid Surf. A* **1999**, *158*, 363.

55. Krishna, R. *Chem. Eng. Res. Des.* **2001**, *79*, 182.

56. Sanborn, M. J.; Snurr, R. Q. *Sep. Purif. Technol.* **2000**, *20*, 1.

57. Jobic, H. *Micropor. Mesopor. Mat.* **2002**, *55*, 159.

58. Hufton, J. R.; Ruthven, D. M. *Ind. Eng. Chem. Res.* **1993**, *32*, 2379.

59. Van den Begin, N.; Rees, L. V. C.; Caro, J.; Bülow, M. *Zeolites*, **1989**, *9*, 287.

60. Saravannan, C.; Auerbach, S. M. *J. Chem. Phys.* **1997**, *107*, 8132.

61. Jobic, H.; Beé, M.; Kearley, G. J. *J. Phys. Chem.* **1994**, *98*, 4660.

62. Theodorou, D. N.; Snurr, R. Q.; Bell, A. T. *Molecular dynamics and diffusion in microporous materials in Comprehensive Supramolecular Chemistry*: edited by Bein T.; Pergamon Press; Oxford; **1996**, *7*, 507.

63. Demontis, P.; Suffritti, G. B. *Chem. Rev.* **1997**, *97*, 2845.

64. Skoulidas, A. I.; Sholl, D. S. *J. Phys Chem. B* **2002**, *106*, 5058.

65. Kar, S.; Chakravarty, C. *J. Phys. Chem. A* **2001**, *105*, 5785.

66. June, R. L.; Bell, A. T.; Theodorou, D. N. *J. Phys. Chem.* **1990**, *94*, 8232.

67. Nowak, A. K.; den Ouden, C. J. J.; Pickett, S. D.; Smit, B.; Cheethan, A. K.; Post, M. F. M.; Thomas, J. M. *J. Phys. Chem.* **1991**, *95*, 848.

68. Caro, J.; Bülow, M.; Schirmer, W.; Kärger, J.; Heink, W.; Pfeifer, H. *J. Chem. Soc. Faraday Trans. I.,* **1985,** *81,* 2541.

69. Takaba, H.; Koshita, R.; Muzkami, M. *J. Membr. Sci.* **1997**, *134*, 127.

70. Maginn, E. J.; Snurr, R. Q.; Bell, A. T.; Theodorou, D. N. *Stud. Surf. Sci. Catal.* **1997**, *105*, 1851.

71. Demontis, P.; Fois, E. S.; Suffritti, G. B.; Quartieri, S. *J. Phys. Chem.* **1992**, *96*, 1482.

72. Nicholas, J. B.; Trouw, F. R.; Mertz, J. E.; Iton, L. E.; Hopfinger, A. J. *J. Phys. Chem.* **1993**, *97*, 4149.

73. Demontis, P.; Fois, E. S.; Suffritti, G. B.; Quartieri, S. *J. Phys. Chem.* **1990**, *94*, 4329.

74. Demontis, P.; Suffritti, G. B.; Mura, P. *Chem. Phys. Lett.* **1992**, *191*, 553.

75. Goodbody, S. J.; Wanatabe, K.; MacGowan, D.; Walton, J. P. R. B.; Quirke, N. *J. Chem. Soc. Faraday. Trans.* **1991**, *87*, 1951.

76. Smirnov, K. S. *Chem. Phys. Lett.* **1994**, *229*, 250.

77. Catlow, C. R. A.; Freeman, C. M.; Vessal, B.; Tomlinson, S. M.; Leslie, M. *J. Chem. Soc. Faraday Trans.* **1991**, *87*, 1947.

78. Dumont, D.; Bougeard, D. *Zeolites* **1995**, *15*, 650.

79. Ruthven, D. M.; Derrah, R. I. *J. Chem. Soc. Faraday Trans. I* **1972**, *68,* 2332.

80. Bezus, A. G.; Kiselev, A. V.; Lupatkin, A. A.; Du, P. Q. *J. Chem. Soc. Faraday Trans. II* **1978**, *74*, 229.

81. Ermosshin, V. A.; Engel, V. *J. Phys. Chem. A* **1999**, *103*, 5116.

82. Ahunbay, M. G.; Elliott, Jr.; Talu, O. *J. Phys. Chem. B* **2002**, *106*, 5163.

83. Sun, M. S.; Talu, O.; Shah, D. B. *AIChE J.* **1996**, *42*, 3001.

84. Talu, O.; Sun, M. S.; Shah, D. B. *AIChE J.* **1998**, *44*, 681.

85. Fritzsche, S.; Wolfsberg, M.; Haberlandt, R. *Submitted for publication..*

86. Fritzsche, S.; Haberlandt, R.; Kärger, J.; Pfiefer, H.; heinzinger, K. *Chem. Phys.* **1993**, *174*, 229.

87. Smit, B. *J. Chem. Phys.* **1995**, *99*, 5597.

88. Krishna, R.; Paschek, D. *Sep. Purif. Technol.* **2000**, *21*, 111.

89. Macedonia, M. D.; Maginn, E. J. *Fluid Phase Equilib.* **1999**, *150,* 19.

90. Vlugt, T. J. H.; Krishna, R.; Smit, B. *J. Phys. Chem. B* **1999**, *103,* 1102.

91. Van de Graaf, J. M.; Kapteijn, F.; Moulijn, J. A. *Micropor. Mesopor. Mater.* **2000***, 35*, 267.

92. Zhu, W.; Kapteijn, F.; Moulijn, J. A. *Phys. Chem. Chem. Phys.,* **2000,** *2,* 1989.

93. Millot, B.; Methivier, A.; Jobic, H. *J. Phys. Chem. B* **1998**, *102*, 3210.

94. Sun, M. S.; Shah, D. B.; Xu, H. H.; Talu, O. *J. Phys. Chem.* **1998**, *102*, 1466.

95. Bopp, P.; Jancso, G.; Heinzinger, K. *Chem. Phys. Lett.* **1983**, *98*, 129.

96. Rowley, R. L. ; Pakken, T. *J. Chem. Phys.* **1999**, *110*, 3368.

97. Fick, A. E. *Ann. Phys.* **1855**, *94*, 59.

98. Fick, A. E. *Phil. Mag.* **1855**, *10*, 30.

99. Brown, R. *Phil. Mag.* **1828**, *4*, 161.

100. Brown, R. *Phil. Mag.* **1830**, *8*, 41.

101. Einstein, A. *Ann. Phys.* **1905**, *17*, 349.

102. Kärger, J.; Pfeifer, H.; Heink, W. *Principles and Applications of Self-diffusion Measurements by Nuclear Magnetic Resonance*: Advances in Magnetic Resonance, *Vol.12*; Academic Press: New York, 1988.

103. Haberlandt, R.; Kärger, J. *Chem. Eng. J.* **1999**, *74*, 15.

104. Fritzsche, S.; Haberlandt, R.; Kärger, J.; Pfeifer, H.; Heinzinger, K. *Chem. Phys. Lett.* **1992**, *198*, 283.

105. Schaefer, H. F. Methods of Electronic Structure Theory. *Modern Theoretical Chemistry Vol. 3*; Plenum: New York, 1977.

106. Schaefer, H. F. Methods of Electronic Structure Theory. *Modern Theoretical Chemistry Vol. 4*; Plenum: New York, 1977.

107. Hehre, W. J.; Random, L.; Schleyer, P. V. R.; Pople, J. A. *Ab Initio Molecular orbital Theory*; Wiley: New York, 1986.

108. Lawley, K. P. *Ab Initio Methods in Quantum Chemistry-I*; Wiley: New York, 1987.

109. Lawley, K. P. *Ab Initio Methods in Quantum Chemistry-II*; Wiley: New York, 1987.

110. Roothaan, C. C. J. *Rev. Mod. Phys.* **1951***, 23*, 69.

111. Boys, S. F. *Proc. R. Soc. London A* **1950**, *A200*, 542.

112. Huzinaga, S. *Comp. Phys. Rep.* **1985**, 2, 279.

113. Davidson, E. R.; Feller, D. *Chem. Rev.* **1986**, *86*, 691.

114. Mulliken, R. S. *J. Phys. Chem.* **1962**, *36*, 3428.

115. Pople, J. A.; Binkley, J. S.; Seeger, R. *Int. J. Quantum Chem., Symp.* **1976**, *S10*, 1.

116. Hohenberg, P.; Köhn, W. *Phys. Rev.* **1964**, *136B*, 864.

117. Köhn, W.; Sham, L. J. *Phys. Rev.* **1965**, *140A*, 1133.

118. Huang, K. *Statistical Mechanics*; Wiley: New York, 1987.

119. Boltzmann's constant: 1.38 x 10 -23 J/K

120. Metropolis, N.; Rosenbluth, A. W.; Rosenbluth, M.; Teller, A. H.; Teller, E. *J. Chem. Phys.* **1953**, *21*, 1087.

121. Alder, B. J.; Wainwright, T. E. *J. Chem. Phys.* **1957**, *27*, 1208.

122. Allen, M. P.; Tildesley, D. J. *Computer Simulation of Liquids*; Clarendon Press: Oxford, 1990.

123. Alder, B. J.; Wainwright, T. E. *J. Chem. Phys.* **1959**, *31*, 459.

124. Alder, B. J.; Wainwright, T. E. *J. Chem. Phys.* **1960**, *33*, 1439.

125. Rahman, A. *Phys. Rev.* **1964**, *136A*, 405.

126. Allen, M. P.; Tildesley, D. J. *Computer Simulation of Liquids*; Clarendon Press: Oxford, 1990, Page 5.

127. Born, M.; Von Karman, Th. *Physik. Z.* **1912**, *13*, 297.

128. Verlet, L. *Phys. Rev.* **1967**, *169*, 201.

129. Gear, C. W. *Numerical Initial Value Problems in Ordinary Differential Equations of Various Order*; Prentice-Hall: Englewood Cliffs: New Jersey, 1971.

130. McQuarrie, D. A. *Statistical Mechanics*; Harper and Row: New York. 1976.

131. Gray, C. G.; Gubbins, K. E. *The Theory of Molecular Fluids. I. Fundamentals*; Clarendon Press: Oxford, 1984.

132. Wilkinson, D. S. *Mass Transport in Solids and Fluids*; Cambridge, London, 2000.

133. Vasenkov, S.; Kärger, J.; Freude, D.; Rakoczy, R. A.; Weitkamp, J. *J. Mol. Catal. A-Gen.* **2000**, *158*, 373.

134. Kirmse, A.; Kärger, J.; Stallmach, F.; Hunger, B. *Appl. Catal. A-Gen.* **1999**, *188*, 241.

135. Hong, U.; Kärger, J.; Kramer, R.; Pfeifer, H.; Seiffert, T. G.; Müller, U.; Unger, K. K. Luck, H. B.; Ito, T. *Zeolites* **1991**, *11*, 816.

136. Kärger, J.; Spindler, H. *J. Am. Chem. Soc.* **1991**, *113*, 7571.

137. Kärger, J.; Pfeifer, H.; Heink, W. *Adv. Magn. Res.* **1988**, *12*, 1, P. x.

138. Stejskal, E. O.; Tanner, J. E. *J. Chem. Phys.* **1965**, *42*, 288.

139. Callaghan, P. T. *Aust. J. Phys.* **1984**, *37*, 359.

140. Olson, D. H.; Kokotailo, G. T.; Lawton, S. L.; Meier, W. M. *J. Phys. Chem.* **1981**, *85*, 2238.

141. Ditchfield, R.; Hehre W. J.; Pople, J. A. *J. Chem. Phys.* **1971**, *54,* 724; Hehre, W. J.; Ditchfield, R.; Pople, J. A. *J. Chem. Phys.* **1972**, *56,* 2257; Hariharan, P. C.; Pople, J. A. *Mol. Phys.* **1974,** *27,* 209; Gordon, M. S. *Chem. Phys. Lett.* **1980**, *76*, 163; Hariharan P. C.; Pople, J. A. *Theo. Chim. Acta.* **1973**, *28,* 213.

142. Petersson, G. A.; Al-Laham, M. A. *J. Chem. Phys.* **1991,** *94,* 6081; Petersson, G. A.; Bennett, A.; Tensfeldt, T. G.; Al-Laham, M. A.; Shirley, W. A.; Mantzaris, J. *J. Chem. Phys.* **1988**, *89*, 2193.

143. Benedict, W. S.; Gailar, N.; Plyler, E. K. *J. Chem. Phys.* **1956**, *24*, 1139.

144. Frisch, M. J.; Trucks, G. W.; Head-Gordon, M.; Gill, P. M. W.; Wong, M. W.; Foresman, J. B.; Johnson, B. G.; Schlegel, H. B.; Robb, M. A.; Replogle, E. S.; Gomperts, R.; Andres, J. L.; Raghavachari, K.; Binkley, J. S.; Gonzalez, C.; Martin, R. L.; Fox, D. J.; Defrees, D. J.; Baker, J.; Stewart, J. J. P.; Pople, J. A. *Gaussian 98*; Revision A: Gaussian, Inc.: Pittsburgh: P A, 1998.

145. Salahub D. R.; Zerner, M. C. Eds. *The Challenge of d and f Electrons*; ACS: Washington, D.C., 1989; Parr, R. G.; Yang, W. *Density-functional Theory of Atoms and Molecules*; Oxford Univ. Press: Oxford, 1989.

146. Becke, A. D. *J. Chem. Phys.* **1993**, *98*, 5648; Pople, J. A.; Head-Gordon, M.; Fox, D. J.; Raghavachari K.; Curtiss, L. A. *J. Chem. Phys.* **1989**; *90*, 5622; Curtiss, L. A.; Jones, C.; Trucks, G. W.; Raghavachari K.; Pople, J. A. *J. Chem. Phys.* **1990**, *93*, 2537.

147. Roder, P. M. *J. Phys. Chem.* **1990**, *94*, 6080.

148. Jorgensen, W. L.; Cournoyer, M. E. *J. Am. Chem. Soc.* **1978**, *101*, 4942.

149. Karlström, G.; Linse, P.; Wallqvist, A.; Jönsson, B. *J. Am. Chem. Soc.* **1983**, *105*, 3777.

150. Udomsub, S.; Hannongbua, S. *J. Chem. Soc. Faraday Trans*. **1997,** *93*, 3045.

151. Maginn, E. J.; Bell, A. T.; Theodorou, D. N.; *J. Phys. Chem.* **1993**, *97*, 4173.

152. Kiselev, A. V.; Lopatkin, A. A.; Shulga, A. A. *Zeolites* **1985**, *5*, 261.

153. Dufner, H.; Kast, S. M.; Brickmann, J.; Schlenkrich, M. *J. Comp. Chem.* **1997**, *18*, 660; Wolf, D.; Keblinski, P.; Phillpot, S. R.; Eggebrecht, J. *J. Chem. Phys.* **1999**, *110*, 17.

154. Lemberg, H. L.; Stillinger, F. H. *J. Chem. Phys.* **1975**, *62*, 1677; Stillinger, F. H.; Rahman, K. *J. Chem. Phys.* **1978**, *68*, 666.

155. Kärger, J.; Bär, N.-K.; Heink, W.; Pfeifer, H.; Seiffert, G. *Z. Naturforsch Teil A* **1996**, *50,* 186.

156. Staudte, B.; Gutsze, A.; Böhlmann, W.; Pfeifer, H.; Pietrewicz, B. *Micropor. Mesopor. Mat.* **2000**, *40*, 1.

157. Vasenkov, S.; Böhlmann, W.; Galvosas, P.; Geier, O.; Liu, H.; Kärger, J. *J. Phys. Chem. B* **2001**, *105*, 5922.

158. Hong, U.; Kärger, J.; Pfeifer, H.; Müller, U.; Unger, K. K. *Z. Phys. Chem. (Leipzig)* **1991**, *173*, 225.

159. Holz, K.; Heil, S. R.; Sacco, A. *Phys. Chem. Chem. Phys.* **2000**, *2*, 4740.

160. Jost, S.; Bär, N. K.; Fritzsche, S.; Haberlandt, R.; Kärger, J. *J. Phys. Chem. B* **1998**, *102*, 6375.

161. Snurr, R. Q.; Kärger, J. *J. Phys. Chem. B* **1997**, *101*, 6469.

162. Jost, S.; Fritzsche, S.; Haberlandt, R. *Chem. Phys. Lett.* **1997**, *219*, 385.

163. Gergidis, L. N.; Theodorou, D. N.; Jobic, H. *J. Phys. Chem. B* **2000**, *104*, 5541.

164. Heink, W.; Kärger, J.; Pfeifer, H.; Datema, K. P.; Nowak, A. K. *J. Chem. Soc. Faraday Trans.* **1992,** *88,* 3505.

165. Ylstra, W. D.; Kuipers, H. P. C. E.; Post, M. F. M.; Kärger, J. *J. Chem. Soc. Faraday Trans.* **1991,** *87,* 1935.

166. Paschek, D.; Krishna, R. *Langmuir* **2001**, *9*, 247.

167. Kärger, J.; Caro, J. *J. Chem. Soc. Faraday Trans.* **1977**, *173*, 1363.

168. Caro, J.; Hocevar, S.; Kärger, J.; Riekert, L. *Zeolites* **1986**, *6*, 213.

169. Stejskal, E. O.;Tanner, J. E. *J. Chem. Phys.* **1965**, *42*, 288.

170. Krüger, G. J. *Phys. Rep.* **1982**, *82*, 229.

171. Von Meerwall, E. D. *Adv. Polym. Sci.* **1983**, *54*, 1.

118

172. Frisch, M. J.; DelBene, J. E.; Binkley, J. S.; Schaefer, H. F. *J. Chem. Phys.* **1986**, *84*, 2279.

173. Schwenke, D. W.; Truhlar, D. G. *J. Chem. Phys.,* **1985**, *82*, 2418.

174. http://www.uni-leipzig.de/urz/

175. June, L. R.; Bell, A. T.; Theodorou, D. N. *J. Phys. Chem.* **1992**, *96*, 1051.

176. Zhu, W.; Van de Graaf, J. M.; Van den Broeke, L. P. J.; Kapteijn, F.; Moulijn, J. A. *Ind. Eng. Chem. Res.* **1998**, *37*, 1934.

177. Gergidis, L. N.; Theodorou, D. N. *J. Phys. Chem.* **1999**, *103*, 3380.

178. Demontis, P.; Suffritti, G. B.; Bordiga, S.; Buzzoni, R. *J. Chem. Soc. Faraday T.* **1995**, *91*, 525.

179. Jackson, R. A.; Catlow, C. R. A. *Mol. Simul.* **1988,** *1,* 207.

180. Aloisi, G.; Barnes, P.; Catlow, C. R. A.; Jackson, R. A.; Richards A. J. *J. Chem. Phys.* **1990,** *93,* 3573.

181. Sinclair P. E.; de Vries, A.; Sherwood, P.; Catlow, C. R. A.; van Santen, R. A. *J. Chem. Soc. Faraday T.* **1998,** *94*, 3401.

182. Hill, J. R.; Sauer, J. *J. Phys. Chem.* **1994,** *98*, 1238.

183. Hill, J. R.; Sauer, J. *J. Phys. Chem.* **1995,** 99, 9536.

184. Schröder, K. P.; Sauer, J. *J. Phys. Chem.* **1996,** *100,* 11043.

185. Eichler, U., Kolmel, CM., Sauer, J. J. *Comput. Chem.* **1997,** *18* ,463.

186. Nicholas, J. B.; Hopfinger, A. J., Trouw, F. R.; Iton, L. E. *J. Am. Chem. Soc.* **1991,** *113*, 4799.

187. Bartsch, M.; Bornhauser, P.; Calzaferri, G.; Imhof, R. *J. Phys. Chem.-US.* **1994,** *98,* 2817.

188. Ermoshin, V. A.; Smirnov, K. S.; Bougeard, D. *Chem. Phys.* **1996,** *202,* 53.

189. Ermoshin, V. A.; Smirnov, K. S.; Bougeard, D. *Chem. Phys.* **1996,** 209, 41.

190. Jaramillo, E.; Auerbach, S. M. *J. Phys. Chem. B* **1999,** *103*, 9589.

191. Mellot, C. F.; Cheetham, A. K. *J. Phys. Chem. B* **1999,** *103*, 3864.

192. Kroemer, R. T.; Michopoulos, Y.; Rode, B. M. *Z. Naturforsch. A* **1991**, *45,* 1303.

193. Michopoulos, Y.; Botschwina, P.; Rode, B. M. *Z. Naturforsch. A* **1991,** *46,* 32.

194. Rahman, A.; Stillinger, F. H.; Lemberg, H. L. *J. Chem. Phys.* **1975**, *63*, 5223.

195. Marti, J. *J. Chem. Phys.* **1999,** *110*, 6876.

196. Yoshii, N.; Yoshie, S.; Mira, S.; Okazaki, S. *J. Chem. Phys.* **1998**, *109*, 4873.

197. Kalinichev, A. G.; Bass, J. D. *J. Phys. Chem.* **1997**, *101*, 9720.

198. Runnebaum, R. C.; Maginn, E. J. *J. Phys. Chem. B* **1997**, *101*, 6374.

199. Maginn, E. J.; Bell, A. T.; Theodorou, D. *J. Phys. Chem.* **1996**, *100*, 7155.

200. Kärger, J. *J. Phys. Chem.* **1991**, *98*, 5558.

201. Kärger, J.; Demontis, P.; Suffritti, G. B.; Tilocca, A. *J. Chem. Phys.* **1999**, *110*, 2.

202. Bussai, C.; Fritzsche, S.; Haberlandt, R.; Hannongbua, S. *Submitted for publication*

APPENDICES

APPENDIX I

Understanding the Movement, Encapsulation, and
Energy Barrier of Water Molecule Diffusion into and in
Silicalites Using *Ab Initio* Calculation

Chuenchit Bussai, Supot Hannongbua, R. Haberlandt

Understanding the Movement, Encapsulation, and Energy Barrier of Water Molecule Diffusion into and in Silicalites Using Ab Initio Calculations

C. Bussai,[†,‡] S. Hannongbua,*,[†] and R. Haberlandt[‡]

Department of Chemistry, Faculty of Science, Chulalongkorn University, Bangkok 10330, Thailand, and Department of Molecular Dynamics and Computer Simulations, Institute for Theoretical Physics (ITP), Faculty of Physics and Geoscience, University of Leipzig, Augustusplaz 10-11, 4109, Leipzig, Germany

Quantum chemical calculations at the Hartree-Fock and MP2 levels have been performed to investigate water−silicalite interactions as well as the energy barrier and water orientations during diffusion into and in silicalite. Experimental geometries of water and silicalite have been used and kept constant throughout. The silicalite crystal structure has been represented by three fragments consisting of 20, 52, and 64 heavy atoms (oxygen and silicon atoms). Calculations have been performed using extended 6-31G and 6-31G* basis sets with BSSE (basis set superposition error) corrections. The results indicate obviously how the water molecule moves and turns via diffusion through the center of the silicalite pore in order to find the optimal route. The energy barriers for the water molecule to enter the pore and to diffuse from one channel to another have been clearly examined. The most stable binding site inside the pore is to be encapsulated in the intersection channel. It was also found that a water molecule enters and leaves the pores by pointing its dipole vector toward the center of the cavity.

1. Introduction

Zeolites[1,2] are outstanding among the interesting materials for chemical science and technology for their special characteristics and multifarious uses. Their active sites appear on the microporous inner wall positions. The size of the micropore or cavity plays an important role in the selectivity process. The widespread and diverse uses of zeolites are as catalysts and molecular sieves in the chemical industry and as ion exchangers, in particular as absorbents in detergents.[3−5] Diffusion phenomena,[6] which are the basis of those applications, lie in the adsorption and the transportation processes.[7,8] Interest in the water−zeolite interaction arises from the fact that water plays strong and essential roles for both absorption and catalytic properties of zeolite,[9,10] as it is known that all natural zeolites are hydrated. In addition, water molecules facilitate the exchange of the charge-compensating cations, which are essential for the industrial catalysts. Therefore, understanding the water−zeolite interactions as well as the behavior of water in zeolite, especially in relation with the zeolite structure, would lead to rapid development of the knowledge in this field, and hence of the application of the zeolites.

According to our best knowledge, the only available data on the water−silicalite interactions are the experimental measurements by Flanigen et al.[11] and Vigne-Maeder et al.,[12] who reported the initial isostatic heat of adsorption of 6 kcal mol^{-1} and the mean heat of adsorption of the first four water molecules of 9.6 kcal mol^{-1}, respectively. Vigne-Maeder et al. have also calculated the water−silicalite potential map in which the average energy is expressed as a sum of electrostatic, polarization, dispersion, and repulsion interactions between the atom pairs. The various atomic parameters for the first term are the

ab intio results, whereas those of the other terms are empirical. The calculations yield an average water−silicalite interaction at 300 K of −12.5 kcal mol^{-1} and the approximate energy barrier via diffusion through the intersection between the straight and the zigzag channels of the silicalite of 8 kcal mol^{-1}. However, it has been mentioned that the calculated results are very sensitive to the experimental geometry of the silicalite used.

The aim of this study is to use quantum chemical calculations at the Hartree−Fock (HF) and MP2 levels to determine the water−silicalite interactions in order to understand the water orientation, preferable binding sites and energy barrier during the movement into and in the silicalite pores. This framework is the dealuminated analogue of the zeolite type ZSM-5.

2. Calculation Details

2.1. Representation of the Silicalite. The silicalite structure is characterized by two types of channels whose symmetry group is *Pnma*. The crystallographic cell[13] contains 288 atoms, namely 96 Si and 192 O, with cell parameters $a = 20.07$ Å, $b = 19.92$ Å and $c = 13.42$ Å. It is clear that the system consisting of all atoms in the unit cell does not allow the use of quantum chemical calculation, even with a small basis set because of the unreasonable computation time that would be required. Therefore, the silicalite crystal structure was represented by the three fragments (Figure 1b−d), namely single, intersection, and double rings. The sinusoidal and main parts of the straight channels of the crystal (Figure 1a), in which the inner surfaces are almost identical, were represented by the double 10-oxygen-membered ring (Figure 1d). This fragment (mentioned later, for simplicity, as the double ring) consists of 30 O and 22 Si atoms. The larger fragment (35 O and 29 Si atoms) containing both parts of the sinusoidal and straight channels was used to represent the intersection and so-called intersection ring (Figure 1c). Note that the remaining valence orbitals of the silicon atoms of both fragments are then filled up by the hydrogen atoms.

* Corresponding author.
† Chulalongkorn University.
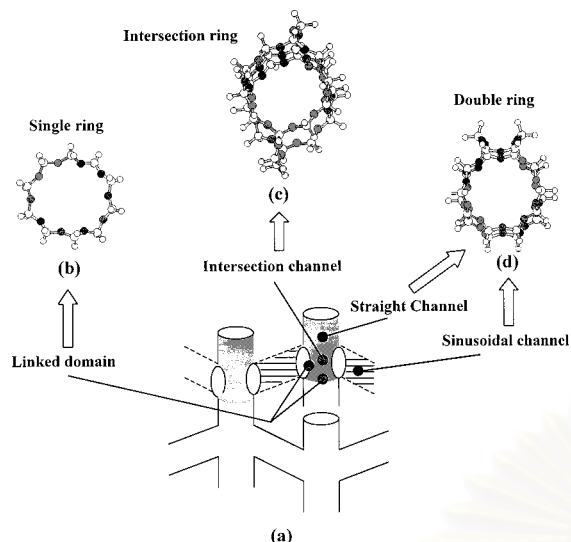‡ University of Leipzig.

Figure 1. Schematic representations of the (a) silicalite crystal structure, (b) linked domain, (c) straight and sinusoidal channels and (d) intersection channel (for more details see text).

Figure 2. Schematic representations of the binding of water molecule (a)−(b) outside and (c)−(d) inside the silicalite channels (for more details see text).

To investigate the energy barrier for diffusion from the intersection to the straight or to the sinusoidal channels, the water−silicalite interaction in the linked domain has been also calculated. The selected fragment is the 10-oxygen-membered ring (Figure 1b). This fragment, called the single ring, contains 10 O, 10 Si and 20 H atoms.

2.2. Configurations of the Water Molecule. Numerous configurations of water molecules have been generated, varying over -5.0 Å $\leq L \leq 5.0$ Å, $0° \leq \phi_x \leq 360°$ and $0° \leq \phi_y, \phi_z \leq 180°$ owing to its symmetry, where L is the distance between the oxygen atom of water and the origin of the coordinate system and ϕ_x, ϕ_y, and ϕ_z denote rotational angles around the x, y, and z axes, respectively. The rotational steps are $\Delta\phi_x = \Delta\phi_y = \Delta\phi_z = 15°$ while the translation step is $\Delta L = 1$ Å. The origin of the coordinate system for each fragment is the average of the positions of all oxygen atoms lying on the 10-oxygen-membered rings. The translation or y axis is defined as a vector pointing through the origin and perpendicular to the plane defined by the window of each channel. Then, the z axis is parallel to the vector pointing from O6 to O1 (labeled on the rings shown in Figure 2). Positive or negative distances are determined from the origin to the oxygen atom of the water molecule along the positive or negative translation axis, respectively.

To search for the optimal binding sites both outside and inside the windows, interactions between water and silicalite for each fragment in the four configurations shown in Figure 2 have been calculated. The out-of-plane (Figure 2a−b) and in-plane (Figure 2c−d) configurations are assumed to represent the binding of water to the silicalite framework before and after entering the channels, respectively. For the double hydrogen bond (2HB) configurations (Figure 2b,d), the two O−O distances (r_{OO}) were simultaneously optimized. Inside the pore (Figure 2c,d), the molecular plane of the water molecule was kept parallel to the plane of the 10-oxygen-membered ring (the window plane). For the out-of-plane configurations (Figure 2a,b), we additionally optimized angles y'−O6−Ow (α) as well as rotation around the H_1−Ow bond of water for the single hydrogen bond (1HB) system (Figure 2a), where vector y' is perpendicular to the window plane at O6, Ow denotes the oxygen atom of water, and the H_1−Ow vector points to O6.

2.3. Quantum Chemical Calculations. Ab initio calculations at the HF and the MP2 levels have been performed for the

Energy / kcal/mol
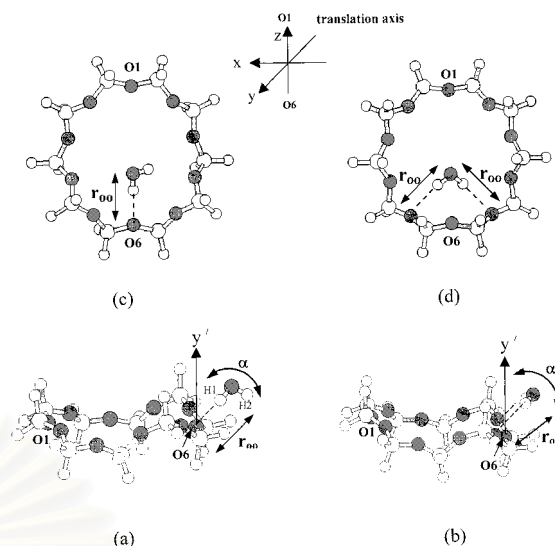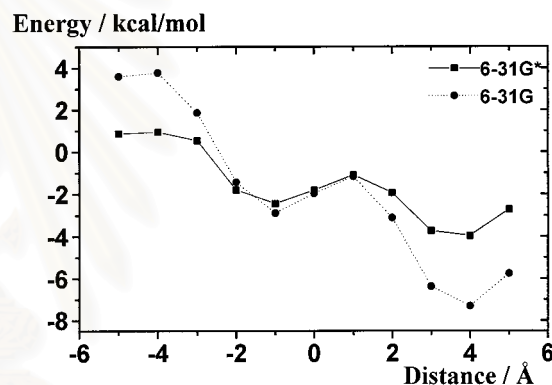
Figure 3. Interaction energy versus water−silicalite distance, calculated using HF method with the 6-31G and 6-31G* basis sets without BSSE corrections for the double-ring framework and a water molecule lying on the translation axis as shown in Figure 2 (for more details see text).

water−silicalite system using extended 6-31G and 6-31G* basis sets.[14,15] Experimental geometries of water[16] and silicalite[13] have been used and kept constant throughout. An error due to the imbalance of the basis set, basis set superposition error (BSSE), has also been examined and taken into consideration. All calculations were performed using the G98 program.[17] All optimizations have been done using the HF method with the 6-31G* basis set with BSSE corrections.

3. Results and Discussion

3.1. Optimal Basis Set, Optimal Method, and Optimal Size of the Fragment. To examine discrepancies due to the method of calculation and the size of the basis set as well as BSSE, the water−silicalite interactions have been calculated for the frameworks of single and double rings using HF and MP2 methods and 6-31G and 6-31G* basis sets with and without BSSE corrections. The calculated results are plotted in Figures 3 and 4.

Figure 3 shows the HF interaction energies between water and silicalite in the double-ring framework, calculated using the 6-31G and 6-31G* basis sets. Both plots exhibit a local minima at $L = -1.0$ Å (L was defined in section 2.2) and the most attractive minimum at $L = 4.0$ Å. The interaction energies obtained from the two basis sets are significantly different,

Water−Silicalite Interactions

J. Phys. Chem. B, Vol. 105, No. 17, 2001 **3411**
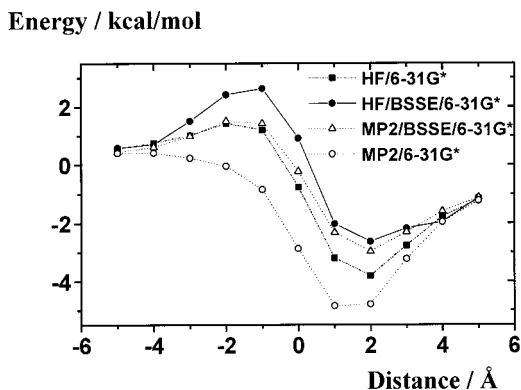
(a)
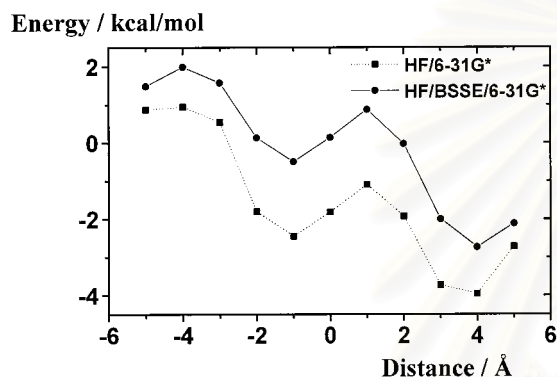
Figure 4. Interaction energy versus water−silicalite distance, calculated using the HF method with the 6-31G* basis set with and without BSSE corrections for the frameworks of (a) single and (b) double rings and a water molecule lying on the translation axis as shown in Figure 2. Results obtained from the MP2 calculations for the framework of a single ring with and without BSSE corrections are also given for comparison (more details see text).

especially in the repulsive and attractive regions where $|L| \geq 2$ Å. As the difference in the interaction energy in both regions is around 100%, it is known that a smaller basis set could be less accurate than a larger one. We therefore conclude that the 6-31G* basis set is substantially more reliable than 6-31G for the investigated system.

Figure 4 displays calculated results for both frameworks, single and double rings, using HF calculations and the 6-31G* basis set with and without BSSE corrections. For the MP2 method, the requirement of computational time for the double ring is not affordable; therefore, the calculations have been performed only for the framework of the single ring, with and without BSSE corrections, and these results are also shown in Figure 4a. It is seen in both figures that there is a rather high error due to the BSSE for both HF and MP2 methods in terms of the interaction energy. For instance, HF and MP2 values at the most attractive region for both single- and double-ring systems amount to an error of about 40% and 100%, respectively. Dependence of the calculated results on the method used can be understood from Figure 4a. The interaction energies including correlation effects based on the MP2 approximation are more stable than those from the HF method. After the correction for BSSE, the effect of the electron correlation is almost negligible, i.e., no significant differences were found between the interaction energies obtained from the two methods for any distance. Another clear conclusion is that although interaction energies from both HF and correlated MP2 methods for single- and double-ring systems suffer from BSSE errors,

the two methods are in very good agreement in predicting the geometry of the complex. Note that the difference in the distance to the energy minimum for the frameworks of single ($L = 2.0$ Å) and double ($L = 4.0$ Å) rings are due to different definitions of the origins of the two systems (see section 2.2).

The above observations suggest that correlation methods and BSSE corrections do not play a role regarding the predicted geometry of the system. However, to increase the reliability of the derived interaction energies, all data points reported in this study are the results of HF calculations with BSSE corrections.

In addition to the above results, Figure 4 also contains information on the optimal size of the fragment, which is used to represent the silicalite. Taking into account the definition of the origin, the difference in the optimal interaction energies taking place at 2.0 and 4.0 Å for the frameworks of single and double rings, respectively, is almost negligible. This fact is valid for the results obtained both before and after BSSE corrections. For instance, the interaction energy after the BSSE correction at $L = −3.0$ Å for the framework of single ring and at $L = −5.0$ Å for that of the double ring are almost identical (about 1.5 kcal mol^{-1}). The corresponding values before the BSSE correction for the single and the double rings are 1.0 and 0.7 kcal mol^{-1}, respectively. Therefore, a clear and useful conclusion is that the framework of a single 10-oxygen-membered ring is already large enough to represent the silicalite crystal structure in the investigation of the water−silicalite interaction energy.

3.2. Optimal Diffusion Route. *(i) Diffusion through the center of the window*. On the basis of the conclusions of section 3.1, HF calculations with the 6-31G* basis set and BSSE correction have been carried out for the three fragments. For each system, numerous water−framework configurations have been generated by varying L, ϕ_x, ϕ_y, and ϕ_z as described in section 2.2. Results for four main routes defined by the $\{\Delta\phi_x, \Delta\phi_y, \Delta\phi_z\}$ coordinates of $\{0, 0, 0\}$, $\{0, 90, 0\}$, $\{180, 0, 0\}$, and $\{180, 90, 0\}$ have been displayed in Figure 5. The optimal route, in which the energy minimum for each distance takes place, has been also given for all plots. The areas inside the pores for the three fragments have been estimated and labeled as the regions between the two vertical-dot lines (Figure 5a,c). These ranges for the single, double, and intersection rings are $−0.5$ Å $\leq L \leq 0.5$ Å, $−1.5$ Å $\leq L \leq 1.5$ Å, and $−2.5$ Å $\leq L \leq 2.5$ Å, respectively.

The plots for all fragments indicate clearly how the water molecule moves and turns via diffusion along the translation axis (Figure 2) through the center of the channel. The water molecule starts to interact with the window of the silicalite at a long distance, far from the molecular center. The preferred configuration at this distance is to point its dipole vector toward the center of the pore (graphs 3 and 4 for all plots of Figure 5). Then the water molecule leaves the pore by pointing its dipole vector toward the center of the channel (graphs 1 and 2). In addition, the interaction energy in the region around center of the pore of the intersection ring (Figure 5c), $−1.0$ Å $\leq L \leq 3.0$ Å, is strongly orientation dependent. It is interesting to note here that the energy gap between two plots of parallel dipole moments, graphs 1 and 2 or graphs 3 and 4 as shown in Figure 5b, is higher than that seen in Figures 5a and 5c. This leads us to conclude that the energy barriers for the rotation around the dipole axis of the water molecule in the straight and the sinusoidal channels (represented by a double ring) are higher than those of the intersection channel and the linked domain.

It can be also seen from Figure 5 that the diffusion of a water molecule along the translation axis through the center of a
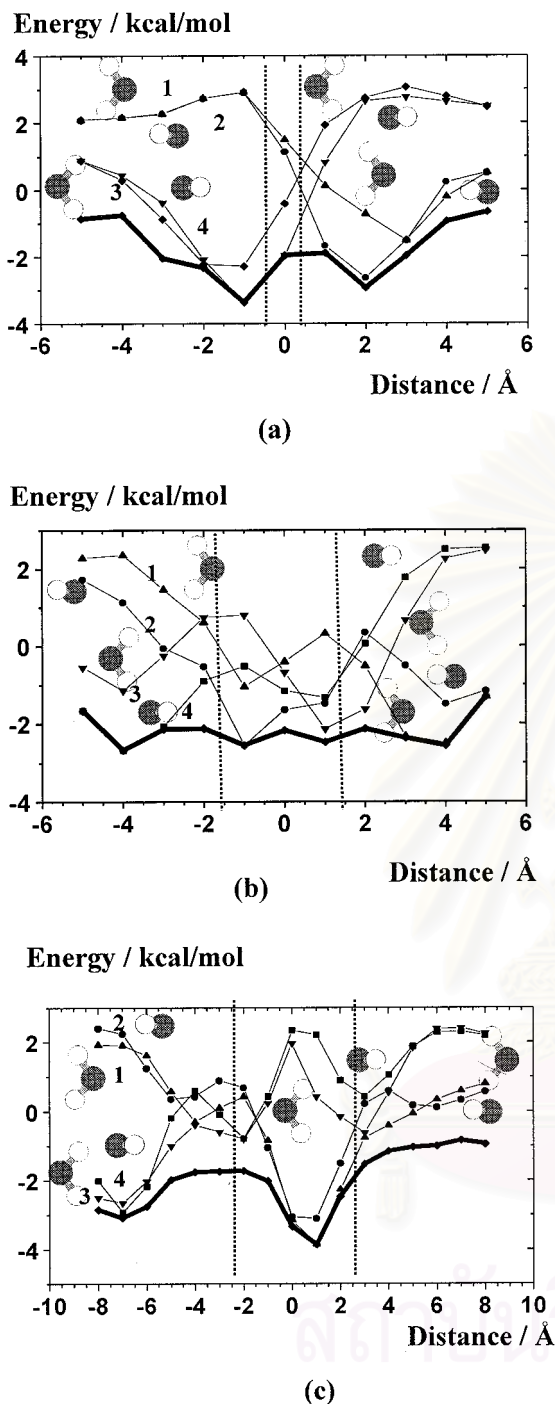
Energy / kcal/mol

(a)

Energy / kcal/mol

(b)

Energy / kcal/mol

(c)

Figure 5. Interaction energy versus water−silicalite distance, calculated using the HF method with the 6-31G* basis set and BSSE corrections for the frameworks of (a) single, (b) double, and (c) intersection rings and a water molecule lying on the translation axis in the configurations given in the insert; $l = \{0,90,0\}$; $n = \{0,0,0\}$; $s = \{180,0,0\}$; $t = \{180,90,0\}$. The bold solid-lines represent the optimal route. An area between the two vertical dot-lines is estimated to be inside the pore (more details see text).

window of the silicalite is a kind of rolling movement. The molecule must move and turn in order to find the optimal route (bold-solid lines in Figure 5a,c). As the energy fluctuation on the optimal route for the double ring (Figure 5b) is much lower than those of the other fragments. Change of the interaction energies during the diffusion into and in the channel along the optimal route is within thermal fluctuations at room temperature, which amounts to about 0.6 kcal mol^{-1}. This led to a clear conclusion that the motion of a water molecule in the straight

TABLE 1: Optimal Binding Distance (r_{OO} in Å), Angle (α in Degree), and Interaction Energy (ΔE in kcal mol^{-1}) Obtained from the Geometry Optimization Using 6-31G* Basis Set with BSSE Corrections for the Water−Silicalite Complexes in the Four Configurations (a), (b), (c), and (d), which Corresponds to Those Shown in Figures 2a−d, Respectively

configuration	fragment	single ring	double ring	intersection ring
(a)	r_{OO}	3.93	3.91	3.48
	α	79.9	47.5	101.3
	ΔE	−2.61	3.67	−0.35
(b)	r_{OO}	3.64	3.66	3.52
	α	60.3	52.8	96.4
	ΔE	−1.32	−1.02	0.84
(c)	r_{OO}	3.42	3.51	3.59
	ΔE	0.34	−0.95	−0.4
(d)	r_{OO}	3.69	3.60	3.83
	ΔE	−0.81	−0.98	−1.04

and the sinusoidal channels is rather smooth compared to that in the linked domain and the intersection channel.

(ii) Diffusion along the Inner Wall. Another possible pathway for the water molecule to diffuse in the silicalite channel is to attach to a specific binding site on the window, then enter the pore, find the next binding site, and move from one site to another along the inner wall of the channel. Such information can be calculated using the supramolecular approach as described in detail in section 2.3 and as schematically displayed in Figure 2. The obtained optimization energies and corresponding distances are summarized in Table 1.

The following information can be extracted from the interaction data given in Table 1: (I) The most stable binding site for the water molecule before entering into the silicalite channel is to coordinate to the oxygen atom of the linked domain to form a single hydrogen bond outside the pore (Figure 2a). The corresponding interaction energy of −2.61 kcal mol^{-1} is comparable to those when a water molecule moves along the optimal route (Figure 5a). Therefore, the water molecule can enter the pore via the linked domain either by using the optimal route at the center of other pore or by binding to the window as a single hydrogen bond. The situations are different for the double and the intersection fragments. To enter the pore through the optimal route is much more favorable than when the molecule binds to the framework. (ii) To bind to the inner wall, the interaction energies obtained from the three fragments fluctuate within a thermal limit at room temperature. This implies no preferential binding site for water molecule in the inner wall of the silicalite pores. The observed result supports the fact that the silicalite channel is hydrophobic. (iii) The interaction energy between the water molecule and the inner wall as mentioned above is less attractive compared to that when the water molecule moves along the optimal route through center of the pore (Figure 5). These data indicate clearly that the diffusion in the silicalite pore takes place via the optimal route (Figure 5).

3.3. Energy Barrier to Enter the Channel. The energy change (ΔE_{net}) for a water molecule to enter the silicalite channel is simply defined as the difference between the most stable water−silicalite interaction energies inside (ΔE_{in}^{min}) and outside (ΔE_{out}^{min}) the pores. According to our model, the possible pathways for entering the single fragment are either to bind to the framework first or to move along the optimal route via the central line; only the second pathway is preferable for the double and the intersection fragments. However, the most stable interaction energy to bind a water molecule to the single ring outside the pore (Figure 2a) of −2.61 kcal mol^{-1} is higher than
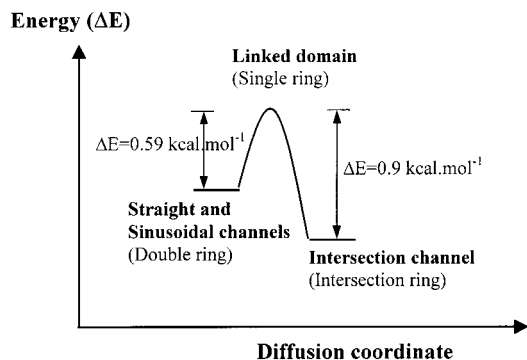
Figure 6. Changes of the water−silicalite interaction energy via diffusion in the silicalite channels.

TABLE 2: The Water−Silicalite Interaction Energies (kcal mol^{-1}) along the Optimal Route Taken from the Corresponding L Distance: ΔE_{out}^{min}, ΔE_{in}^{min}, and ΔE_{max} Are the Minimum Outside the Pore, the Minimum Inside the Pore, and the Maximum that Lies between the ΔE_{out}^{min} and ΔE_{in}^{min}, Respectively (more details see text)

fragment	ΔE_{out}^{min}	ΔE_{max}	ΔE_{in}^{min}	$\Delta E_{barrier}$	ΔE_{net}
single ring	−3.58 ($L = -1$ Å)	−1.96 ($L = 0$ Å)	−1.96 ($L = 0$ Å)	1.62	1.62
double ring	−2.79 ($L = -4$ Å)	−2.12 ($L = -2$ Å)	−2.55 ($L = -1$ Å)	0.67.	0.24
intersection ring	−3.14 ($L = -7$ Å)	−1.86 ($L = -2$ Å)	−3.86 ($L = 1$ Å)	1.28	−0.72

that to move the molecule along the optimal route of −3.58 kcal mol^{-1} taking place at $L = -1$ Å (Figure 5a). Therefore, the energy change and the energy barrier for all fragments have been calculated only when a water molecule moves along the optimal route. The results are summarized in Table 2.

The maximum of the interaction energy (ΔE_{max}), which lies between the ΔE_{in}^{min} and ΔE_{out}^{min} on the optimal route, suggests how easily a water can enter the pore via this pathway. The energy barrier ($\Delta E_{barrier}$) for the water molecule to enter the pore can then be expressed as $\Delta E_{max} - \Delta E_{out}^{min}$, resulting in the values of 1.62, 0.67, and 1.28 kcal mol^{-1} for the single, double, and intersection rings, respectively.

The energy data in Table 1 indicate clearly that the energy barrier of about 1.5 kcal mol^{-1} is required to drive the water molecule to enter the pore of the silicalite, the linked domain (represented by the single ring) and the intersection channel (represented by the intersection ring). The situation is different for entering the straight and the sinusoidal channels (represented by the double ring), i.e., a water molecule enters these channels via the optimal route without energy barrier (0.6 kcal mol^{-1} is within a thermal fluctuation of room temperature).

In terms of energy change, the ΔE_{net}, which defines as $\Delta E_{in}^{min} - \Delta E_{out}^{min}$ (Table 2) indicates clearly that entering the linked domain and the intersection channel are endothermic and exothermic processes, respectively. On the other hand, the energy change for this process is almost zero for the straight and the sinusoidal channels.

3.4. Energy Barrier to Diffuse across the Channels. To investigate the energy barrier for a water molecule to diffuse from one to another channel inside the silicalite, the most stable interaction energies for encapsulation of water molecules in the three channels, shown in Table 1, are considered and the diffusion process is schematically drawn in Figure 6. The small barrier takes place only when a water molecule crosses the linked domain, which is represented by the single ring (Figures 1a and 1b) to and from the intersection channels. The energy

requirement of 0.96 kcal mol^{-1} is equivalent to a temperature of about 450 K. This value is much less than that of 8 kcal mol^{-1} obtained from the development of the water−silicalite potential map using an empirical method.[12]

Some comments can be made concerning the encapsulation energy shown in Table 1, in which the most stable position takes place in the intersection channel. This observation is different from that reported theoretically for the light alkane molecules, which stated that they bind more strongly in the straight or sinusoidal than in the intersection channels.[18−23] Therefore, it is suggested by these results that the degree of hydrophobicity, typical character of the silicalite, of the intersection channel is less than those of the other channels. In addition, our value for the encapsulation energy of the water molecule in the silicalite pore of −3.9 kcal mol^{-1} is much higher than the expermental value of −9.6 kcal mol^{-1} and the calculated value of −12.5 kcal mol^{-1} reported by Vigne-Maeder et al.[12] However, it should be noted here, therefore, that the two values given in ref. (12) are too strong to represent the interaction energy between a polar molecule such as a water and the hydrophobic channels of the silicalite. This statement was supported by the simulation results published recently by Takabe et al.[24] The simulated results for the water−methanol mixture in the silicalite membrane show that no water molecule diffuses into the silicalite pore. Adsorption takes place only with the silanol groups on the external surface. Therefore, a strongly experimental heat of adsorption is a consequence of the adsorption on the surface but not in the hydrophobic micropore of the silicalite. However, preliminary result by Kärger[25] using PFG-NMR measurement indicates the diffusion of water molecule in the silicalite micropore at high temperatures.

References and Notes

(1) Breck, D. W. *Zeolite Molecular Sieve*s; Wiley: New York, 1974.
(2) Kärger, J.; Ruthven, D. M. *Diffusion in Zeolites and Other Microporous Solids*; Wiley: New York, 1992.
(3) Rao, C. N. R.; Natarajan, S.; Neeraj, S. *J. Am. Chem. Soc.* **2000**, *122*, 2810.
(4) Davis, M. E. *Microporous Mesoporous Mater.* **1998**, *21*, 173.
(5) Singh, A. P.; Kale, S. M. *Catal. Today* **1999**, *49*, 245.
(6) Demontis, P.; Suffritti, G. B.; Tilocca, A. *J. Phys. Chem. B*, **1999**, *103*, 8141.
(7) Vlugt, T. J. H.; Krishna R.; Smit, B. *J. Phys. Chem. B* **1999**, *103*, 1102.
(8) Haberlandt, R. *Thin Solid Films* **1998**, *330*, 34.
(9) Mikhailenko, S. D.; Kaliaguine, S.; Ghali, E. *Microporous Mater.* **1997**, *11*, 37.
(10) Komiyama, M.; Kobayashi, M. *J. Phys. Chem. B* **1999**, *103*, 10651.
(11) Flanigen, E. M.; Bennett, J. M.; Grose, R. W. *Nature* **1978**, *271*, 512.
(12) Vigné-Maeder F.; Auroux, A. *J. Phys. Chem.* **1990**, *94*, 314.

3414 *J. Phys. Chem. B, Vol. 105, No. 17, 2001*

Bussai et al.

(13) Olson, D. H.; Kokotailo, G. T.; Lawton, S. L.; Meier, W. M. *J. Phys. Chem.* **1981**, *85*, 2238.

(14) Hehre, W. J.; Random, L.; Schleyer, P. v. R.; Pople, J. A. *Ab Initio Molecular Orbital Theory*; Wiley: New York, 1987.

(15) Francl, M. M.; Petro, W. J.; Hehre, W. J.; Binkley, J. S.; Gordon, M. S.; Defrees, D. J.; Pople, J. A. *J. Chem. Phys.* **1982**, *77*, 3654.

(16) Benedict, W. S.; Gailar, N.; Plyler, E. K. *J. Chem. Phys.* **1956**, *24*, 1139.

(17) Frisch, M. J.; Trucks, G. W.; Head-Gordon, M.; Gill, P. M. W.; Wong, M. W.; Foresman, J. B.; Johnson, B. G.; Schlegel, H. B.; Robb, M. A.; Replogle, E. S.; Gomperts, R.; Andres, J. L.; Raghavachari, K.; Binkley, J. S.; Gonzalez, C.; Martin, R. L.; Fox, D. J.; Defrees, D. J.; Baker, J.; Stewart, J. J. P.; Pople, J. A. *Gaussian 98*, Revision A, Gaussian, Inc., Pittsburgh, PA, 1998.

(18) June, L. R.; Bell, A. T.; Theodorou, D. N. *J. Phys. Chem.* **1990**, *94*, 1508.

(19) June, L. R.; Bell, A. T.; Theodorou, D. N. *J. Phys. Chem.* **1992**, *96*, 1051.

(20) Nicholas, J. B.; Trouw, F. R.; Mertz, J. E.; Iton, L. E.; Hopfinger, A. J. *J. Phys. Chem.* **1993**, *97*, 4149.

(21) Zhu, W.; Van de Graaf, J. M.; Van den Broeke, L. P. J.; Kapteijn, F.; Moulijn, J. A. *Ind. Eng. Chem. Res.* **1998**, *37*, 1934.

(22) Gergidis, L. N.; Theodorou, D. N. *J. Phys. Chem.* **1999**, *103*, 3380.

(23) Vlugt, T. J. H.; Krishna, R.; Smit, B. *J. Phys. Chem. B* **1999**, *103*, 1102.

(24) Takaba, H.; Koyama, A.; Nakao, S. I. *J. Phys. Chem.* **2000**, *104*, 6353.

(25) Kärger, J. unpublished data.

APPENDIX II

On the Diffusion of Water in Silicalite-1: MD
Simulations Using *Ab Initio* Fitted Potential and PFG
NMR Measurements

Chuenchit Bussai, Sergey Vasenkov, Hui Liu, Winfried
Böhlmann, Siegfried Fritzsche, Supot Hannongbua,
Reinhold Haberlandt, Jörg Kärger

On the diffusion of water in silicalite-1: MD simulations using ab initio fitted potential and PFG NMR measurements

C. Bussai [a,b], S. Vasenkov [b], H. Liu [b], W. Böhlmann [b], S. Fritzsche [b,*],
S. Hannongbua [a], R. Haberlandt [b], J. Kärger [b]

[a] *Department of Chemistry, Faculty of Science, Chulalongkorn University, Bangkok 10330, Thailand*
[b] *Faculty of Physics and Geoscience, University of Leipzig, Linnéstreet 5, 04103 Leipzig, Germany*

Abstract

Molecular dynamics simulations of water diffusion in silicalite-1 are reported. The simulations are carried out using an ab initio fitted silicalite-1–water potential based on quantum chemical calculations. In addition, preliminary results of pulsed field gradient (PFG) NMR diffusion measurements of water and small alkane molecules in silicalite-1 samples are presented. Pre-adsorption of water in silicalite-1 samples was found to change the intra-crystalline diffusivities of small alkane molecules in silicalite-1. This is interpreted as an indirect evidence that under our experimental conditions water molecules occupy a significant part of the silicalite-1 channel system. The preliminary results of the PFG NMR diffusion measurements of water in silicalite-1 samples are discussed in terms of the contributions of extra- and intra-crystalline water to the measured signals. An-order-of magnitude agreement between the measured and the simulated intra-crystalline diffusivities of water in silicalite-1 is obtained. © 2002 Elsevier Science B.V. All rights reserved.

Keywords: Diffusion coefficient; Silicalite-1; Water; Ab initio fitted potential; Molecular dynamics; PFG NMR

1. Introduction

Zeolites have found applications in various fields of industry as catalysts and molecular sieves [1–3]. Unlike conventional, high-aluminum-content zeolites, silicalite-1 possesses a channel system, which can be regarded as cation-free. Silicalite-1 is widely used to separate paraffin or aromatics from water or other polar solvents as well as to sieve the molecules having different shapes [4–6]. Owing to low aluminum content, the affinity of this zeolite-to-water is weak. Earlier measurement of water diffusion in pentasil zeolites have been published [7], but there are experimental indications that water molecules can, at the best, occupy

only a part of the available pore volume of silicalite-1 crystals [8]. The presence of defect sites, such as hydroxyl groups on the surface of the silicalite-1 channels, may significantly affect the adsorption of water molecules [8].

In this paper, we report the results of molecular dynamics simulations of water diffusion in silicalite-1. We also present here the first, preliminary results of pulsed field gradient (PFG) NMR measurements of water diffusion in samples of silicalite-1. In addition, PFG NMR diffusion measurements of ethane, propane and *n*-butane in water-free samples of silicalite-1 and in silicalite-1 samples with pre-adsorbed water are reported and discussed. The latter measurements were performed in order to study the influence of pre-adsorbed water on the diffusion of alkane

---

* Corresponding author.

molecules in silicalite-1. An experimental detection of such an influence can be regarded as an indirect evidence that water molecules occupy a significant part of the silicalite-1 channel system.

2. Molecular dynamics simulations

2.1. Methodology and the used ab initio fitted potential

To obtain the self-diffusion coefficient by means of a theoretical approach, molecular dynamics simulations [9,10] have been performed at 298 and 393 K. Simulations have been carried out with a time step of 0.5 fs with a MD box consisting of two silicalite-1 unit cells. The system has been examined at a concentration of two water molecules per intersection corresponding to 16 water molecules per MD box and experimentally equivalent to water–silicalite-1 mass ratio (w/s) of 24 mg g^{-1}. Before starting evaluations each system was thermalized for 0.5 ps. Some trial calculations with longer thermalization showed no difference in the diffusion coefficients within the range of fluctuations. The evaluation part of the MD runs corresponded to trajectory lengths of 10 ns. There was no thermalization during the evaluation part of the run. Periodic boundary conditions have been applied. The silicalite-1 crystal structure used in this study is characterized by the two types of channels and belongs to the "Pnma" symmetry group. The crystallographic cell [11] ($Si_{96}O_{192}$) contains 288 atoms with lattice parameters $a = 20.07$ Å, $b = 19.92$ Å and $c = 13.42$ Å. The potential proposed by Bopp et al. [12] was employed to describe water–water interactions, with the stabilization energy of -6.1 kcal mol^{-1} at O–O distance of 2.86 Å. A recently developed potential:

$$\Delta E(\text{w}, \text{s}) = \sum_i^3 \sum_j^{288} \left\{ \frac{A_{ij}^{ab}}{r_{ij}^6} + \frac{B_{ij}^{ab}}{r_{ij}^{12}} + \frac{C_{ij}^{ab}}{r_{ij}^3} + \frac{q_i q_j}{r_{ij}} \right\},$$

(1)

was used to represent the silicalite-1–water interactions. A, B and C parameters are obtained from 1032 water-framework interaction energies calculated quantum mechanically. Here, the framework is represented by the three fragments taken from the sinusoidal, straight and intersection channels and water coordinates were generated inside those fragments. Eq. (1) contains 24 fitting parameters and six different atomic net charges, distinguishing interactions between Si and O atoms of silicalite in different channels and O and H atoms of water molecule. The optimal water-framework interaction energy is -7.0 kcal mol^{-1}. This energy is achieved when the water molecule resides at the center of the interaction channel [13]. A detailed description of the method used for the potential calculations from ab initio data is given in [13].

In the present simulations, the lattice was kept fixed while the water molecules are flexible. This approximation is in agreement with the findings observed for methane in silicalite-1 [14], where the effect of host–guest flexibility is already sufficiently accounted for if only the molecules are considered to be flexible while the lattice is kept rigid.

In [15,16], it has been shown that the use of Ewald summations for the Coulomb interactions can be avoided for the treatment of charged particles in zeolites [15] if the sum of all charges in the MD box is zero. Especially in the paper of Wolf et al. [16] it has been shown in detail that this approximation works surprisingly well. Taking into account that Ewald summation may produce the artifacts due to an artificial periodicity of long-range forces arising from distant water atoms, in the present paper we use the approximation proposed by Wolf et al. [16]. This approximation essentially means the use of shifted forces.

In this work, the silanol group free lattice was used. The elucidation of the potentially strong influence of these groups on water diffusion and adsorption in real silicalite-1 crystals remains to be the subject of future research.

2.2. Molecular dynamics results

The self-diffusion coefficients are calculated from the particle displacements. In [20–22], the process of self-diffusion was quite generally related to the moments of the propagator [20]. The propagator $P(\boldsymbol{r}, \boldsymbol{r}_0, t)$ represents the probability density to find a particle at position $\boldsymbol{r}$ at time t when it was at $\boldsymbol{r}_0$ at time $t = 0$.

The *n*th moment of the propagator is defined by the relation [20]:

$$\langle |\boldsymbol{r} - \boldsymbol{r}_0|^n \rangle = \int |\boldsymbol{r} - \boldsymbol{r}_0|^n \, P(\boldsymbol{r}, \boldsymbol{r}_0, t) \, \mathrm{d}\boldsymbol{r}, \tag{2}$$

$P(\boldsymbol{r}, \boldsymbol{r}_0, t)$ is the solution of the diffusion equation for the initial concentration $C(\boldsymbol{r}, t = 0) = \delta(\boldsymbol{r} - \boldsymbol{r}_0)$. In the case of isotropic diffusion and a homogeneous system the propagator results to be:

$$P(\boldsymbol{r}, \boldsymbol{r}_0, t) = (4\pi Dt)^{-3/2} \exp\left\{ \frac{-(\boldsymbol{r} - \boldsymbol{r}_0)^2}{4Dt} \right\}. \tag{3}$$

Although zeolites are not homogeneous the propagator can be represented in this way if the displacements exceed the size of the inhomogeneities [21]. Then $P(\boldsymbol{r}, \boldsymbol{r}_0, t)$ depends only on the difference $|\boldsymbol{r} - \boldsymbol{r}_0|$. For shorter times this is not true. As the transition time to the Gaussian behavior and the final D values were the quantities of main interest in the present paper an averaging over $\boldsymbol{r}_0$ has been carried out. The resulting propagator depends only upon $|\boldsymbol{r} - \boldsymbol{r}_0|$ for all times. But, it attains the shape shown in Eq. (3) (or its equivalents for the different components of the diffusion tensor in the anisotropic case, as shown below) only for sufficiently long times.

The first four moments can be calculated from Eqs. (2) and (3) in the case of normal diffusion as:

$$\langle |\boldsymbol{r} - \boldsymbol{r}_0| \rangle = 4\sqrt{\frac{Dt}{\pi}}, \tag{4}$$

$$\langle |\boldsymbol{r} - \boldsymbol{r}_0|^2 \rangle = 6Dt, \tag{5}$$

$$\langle |\boldsymbol{r} - \boldsymbol{r}_0|^3 \rangle = \frac{32}{\sqrt{\pi}} (Dt)^{3/2}, \tag{6}$$

$$\langle |\boldsymbol{r} - \boldsymbol{r}_0|^4 \rangle = 60(Dt)^2. \tag{7}$$

In the anisotropic system, the corresponding equations for each direction are [14]:

$$\langle |l - l_0| \rangle = 2\sqrt{\frac{D_l t}{\pi}}, \tag{8}$$

$$\langle |l - l_0|^2 \rangle = 2D_l t, \tag{9}$$

$$\langle |l - l_0|^3 \rangle = \frac{8}{\sqrt{\pi}} (D_l t)^{3/2}, \tag{10}$$

$$\langle |l - l_0|^4 \rangle = 12(D_l t)^2, \tag{11}$$

where l is x, y or z, respectively. The D values estimated from these four moments must synchronize each other in the case of normal diffusion for t values that are larger than the decay time of the velocity auto-correlation function. The elements of the diffusion tensor, corresponding to the x-, y- and z-axis are calculated from Eqs. (8)–(11). In this case, the diffusivity D is one-third of the trace of the diffusion tensor:

$$D = \tfrac{1}{3}(D_x + D_y + D_z). \tag{12}$$

The good agreement (within the range of fluctuations) of the final D values calculated for 298 K using the Eqs. (8)–(11) (as shown in Fig. 1), indicates that the diffusion time used in the evaluation procedure exceeds the correlation time. The self-diffusion coefficients calculated in this way at 298 and 393 K are summarized in Table 1.

It can be seen from these results that the largest component of the diffusion tensor is D_y. The D_y values are about two times larger than D_x at both temperatures and about seven times larger than D_z at 298 K and even larger at 393 K. This is consistent with the physical structure of the silicalite-1 crystal, which consists of zigzag channels lying in the xz-plane and the straight channels lying parallel to the y-axis. This causes the

Table 1

The diffusion coefficients D_x, D_y and D_z, of water molecules in x-, y- and z-directions as well as the average value D (one-third of the trace of the diffusion tensor) obtained from the simulations and comparison with the mean diffusivity obtained in the PFG NMR studies at 298 and 393 K

Temperature (K)	MD simulation				PFG NMR D (m^2 s^{-1})
	D_x (m^2 s^{-1})	D_y (m^2 s^{-1})	D_z (m^2 s^{-1})	D (m^2 s^{-1})	
298	2.6×10^{-9}	6.5×10^{-9}	7.9×10^{-10}	3.3×10^{-9}	1.7×10^{-9}
393	5.7×10^{-9}	1.3×10^{-8}	1.4×10^{-9}	6.7×10^{-9}	1.5×10^{-9}

Fig. 1. The diffusion coefficients in (a) *x*-axis; (b) *y*-axis; (c) *z*-axis vs. time window (0.4 ns) obtained from the simulations with two water molecules per intersection of silicalite-1 at 298 K.

significant difference of the elementary diffusion rates in different directions.

Considering the diffusion through silicalite-1 as a random walk of independent steps between the channel intersections, the main elements of the diffusion tensor may be shown to be correlated by the relation [23]:

$$\frac{c^2}{D_z} = \frac{a^2}{D_x} + \frac{b^2}{D_y}, \tag{13}$$

where *a*, *b* and *c* are the unit cell lengths. Eq. (13) implies that the correlation time of propagation is shorter than the mean time it takes a molecule to travel from intersection to intersection. Possible deviations from this case, i.e. correlated motion between the channel intersections, may be accounted for by introducing a parameter [24–26]:

$$\beta = \frac{c^2/D_z}{a^2/D_x + b^2/D_y} \tag{14}$$

The case $\beta = 1$, obviously represents the above considered case of completely random steps. The case $\beta > 1$ indicates preferential continuation of the diffusion path along one and the same channel, while $\beta < 1$ stands for molecular propagation with interchanges between the two channel types more probable than at random. The values of β calculated in this study are equal to 1.04 at 298 K and 1.25 at 393 K. In agreement with the behavior found for alkanes, e.g. [26], where $\beta = 1.2$ and 1.3, a tendency is observed that the xenon molecules and the methane molecules, respectively, in silicalite-1 prefer to remain in the same type rather than to change into a segment of the other channel type at a channel intersection.

The oxygen–oxygen radial distribution functions *g* for the water molecules at the two temperatures have been calculated and displayed in Fig. 2. In inhomogeneous systems, $g(\boldsymbol{r}_1, \boldsymbol{r}_2)$ depends upon $\boldsymbol{r}_1$, also, and is not simply $g(r)$ with $\boldsymbol{r} = |\boldsymbol{r}_1 - \boldsymbol{r}_2|$. But, as a first approximation, we have done the evaluation of $g(r)$ like in a homogeneous isotropic system. This is equivalent to an averaging over the sites $\boldsymbol{r}_1$ taking as a weight
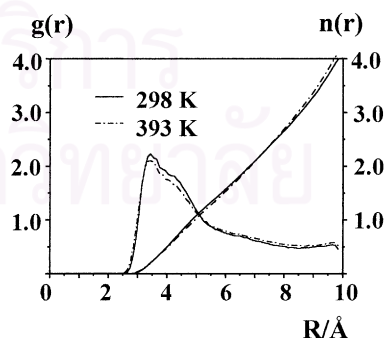
Fig. 2. Oxygen–oxygen radial distribution functions and corresponding running integration numbers for water molecules obtained from the simulations at 298 and 393 K.

function the relative number of events when the r_1 are found during the MD run. Note that due to the asymmetry of the silicalite-1 lattice the function $g(r)$, defined in this way, does not converge to 1.0 for distances of the order of 10 Å. The function $g(r) = 1$ would correspond to a homogeneous distribution in space that can be observed in systems with a structure on molecular level only at a length scale that is larger than the size of the inhomogenities, i.e. the channel structure in the present case. The radial density distributions show a first maximum at 3.5 Å followed by a pronounced shoulder centered at 4.4 Å. In order to see the number of neighbors the integral $n(r)$ of $g(r)$ is also displayed in Fig. 2. It can be seen that, e.g. within a distance of 7 Å around a given water molecule, there are in average only two other water molecules.

To decide whether the water molecules form clusters, the distribution of coordination numbers is examined. As the first minimum is not well-defined, the probability $P_r(i)$ to find 1, 2, 3,... water molecules within $r = 4$, 5 and 6 Å around a given one was examined for both temperatures and compared in Fig. 3. The highest probability is found for the number zero of water molecules in all cases. The average coordination numbers at 298 K integrated up to the three distances are 0.36, 0.94 and 1.44, respectively. The corresponding numbers at 393 K are 0.36, 0.90 and 1.40. It can be concluded that the simulations did not show any clustering of water molecules in the silicalite-1 channels for the examined temperatures and concentrations of guest molecules.

3. PFG NMR measurements

3.1. Experimental details

The measurements of self-diffusion of guest molecules in samples of silicalite-1 were carried out using the home-built PFG NMR spectrometer FE-GRIS 400 operating at a ^{1}H resonance frequency of 400 MHz [17]. For diffusion measurements, the standard stimulated echo and Hahn echo PFG NMR pulse sequences [18] were used. To obtain the diffusivity, the attenuation of the PFG NMR spin echo signal (Ψ) was measured as a function of the amplitude of the applied field gradient (g). For the PFG NMR diffusion measurements using both sequences the duration of the applied field gradient pulses (δ)
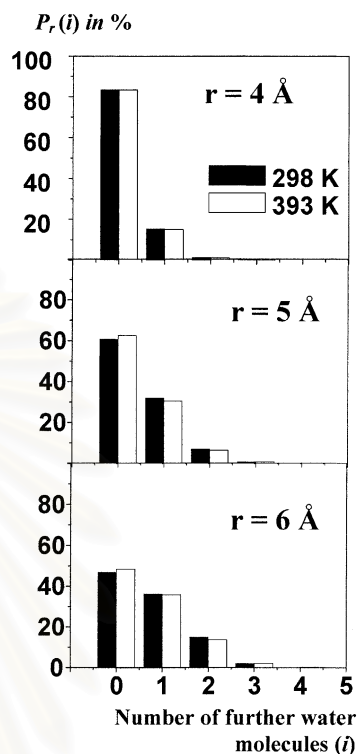
Fig. 3. Representation of nearest-neighbor probabilities: the heights of the columns represent the probability $P_r(i)$ to find i further water molecules within a distance of r (4, 5 and 6 Å) around a given water molecule. Distance means the distance between the oxygen atoms in the water molecules.

was set to 0.26 ms and the duration of the 'dephasing' and the 'read' intervals (τ) was set to 0.8 ms. For the PFG NMR measurements using the stimulated echo sequence the value of the time interval between the two gradient pulses (Δ) was in the range between 1.2 and 2 ms. The intensity of the applied gradients was varied between 0 and 24 T m^{-1}.

The average size of silicalite-1 crystals was 100 μm × 30 μm × 20 μm. The zeolite was used in the calcined form. The sample of silicalite-1, applied in the PFG NMR studies was synthesized as described in [19]. The investigations of this sample using H^1 MAS NMR revealed the presence of silanol groups (around one silanol group per two unit cells).

The samples for the PFG NMR measurements were prepared with the following method. Around 300 mg of silicalite-1 were introduced into the NMR tube. Then the tube was connected to the vacuum system

and the zeolite sample was activated by keeping the sample under high vacuum at 473 K for 20 h. Subsequently, the zeolite sample was loaded with water by freezing it from a fixed volume of the vacuum system. When preparing the samples with D_2O–alkane mixtures, upon loading with D_2O the samples were additionally loaded with alkane by freezing it from another fixed volume of the vacuum system. Upon loading, the NMR tube was sealed and separated from the vacuum system. The total amounts adsorbed corresponded to 24 mg g^{-1} of water in the alkane-free sample and to 28 mg g^{-1} of D_2O in the samples with the D_2O–alkane mixtures. These are exactly the concentrations considered in the MD simulations. The amounts of ethane, propane and n-butane adsorbed in the samples with the D_2O–alkane mixtures as well as in the samples loaded only with alkane were 42, 61 and 81 mg g^{-1}, respectively.

3.2. Results of the pulsed field gradient nuclear magnetic resonance measurements

Fig. 4 shows examples of the attenuation of the NMR signal $\left(\Psi(g, \Delta) \equiv \left(\frac{M(g,\Delta)}{M(0,\Delta)}\right)\right)$ of water molecules in the sample of silicalite-1 at 298 and 393 K. The attenuation curves were recorded using
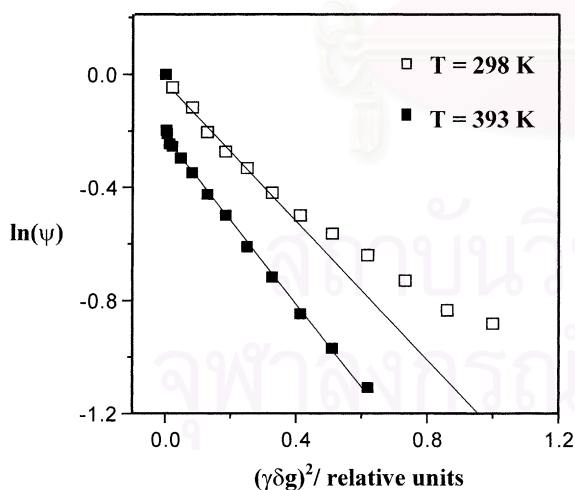
Fig. 4. ^{1}H PFG NMR spin echo attenuation curves for water in the sample of silicalite-1 recorded by using the stimulated echo PFG NMR sequence at 298 K ($\Delta = 2$ ms) and by using the Hahn echo PFG MR sequence at 393 K ($\Delta = 0.8$ ms). The lines show the fit curves used to calculate the diffusion coefficients.

the stimulated echo and the Hahn echo PFG NMR sequences. For both sequences the spin echo attenuation can be written as [21]:

$$\Psi(g, \Delta) = \exp\left(- \gamma^2 D \delta^2 g^2 \left(\Delta - \tfrac{1}{3}\delta\right)\right), \qquad (15)$$

where γ and D denote the gyromagnetic ratio and the diffusion coefficient. In deriving Eq. (15) it was assumed, that the diffusion can be described by a normal Gaussian propagator, given in Eq. (3), which represents the probability density for the diffusing molecules to be displaced over a distance $|r - r_0|$ during a time interval t. It was shown in [27] that for sufficiently small PFG NMR attenuations measured in powder samples, Eq. (15) is a good approximation even for anisotropic diffusion like diffusion in silicalite-1.

This diffusivity can be obtained from the initial slope of the $\ln(\Psi)$ versus g^2 representation using Eq. (15). For sufficiently large PFG NMR attenuations diffusion anisotropy leads to deviations from the linear dependence of $\ln(\Psi)$ on g^2 as predicted by Eq. (15).

It is seen in Fig. 4 that the attenuation curve measured at 298 K shows a pronounced non-linear behavior. At the same time, the curve measured at 393 K exhibits only minor deviations from a linear behavior except for the very rapid decay in the initial part of the curve. The deviations of the attenuation curves in Fig. 4 from straight lines can be attributed to the diffusion anisotropy of water molecules in silicalite-1 and/or to the existence of the distribution of the diffusivities of water molecules in silicalite-1 samples. Note that the root mean square displacements of water molecules were always sufficiently small in comparison to the size of the crystals so that the effect of diffusion restriction of water molecules in the crystals by the outer surface of the crystals was negligible. Hence, it is unlikely that the diffusion restriction is the reason of the deviations of the measured attenuation curves from the linear dependencies predicted by Eq. (15). An existence of a distribution of the diffusivities of the water molecules in the silicalite-1 samples, on the other hand, is feasible. It can be assumed that a part of the water molecules in the sample forms monolayers on the external surfaces of the zeolite crystals or even exists in the form of the liquid. The difference between the diffusion coefficient of this type of water and that of water molecules residing in silicalite-1 crystals can

lead to the non-linear attenuation curves at 298 K. The diffusivity obtained from the initial slope of the attenuation curve measured at 298 K (Fig. 4) is equal to $1.7 \times 10 \, m^2 \, s^{-1}$. This diffusivity can be attributed to the characteristic, mean diffusivity of all the types of water in the sample. A heating of the sample up to 393 K will reduce or completely eliminate the liquid phase and the monolayers of water in the sample. At this temperature the water molecules can be expected either to be primarily in the gas phase of the NMR sample or to reside in silicalite-1 crystals. This is in agreement with the experimental observation of the very fast initial signal decay followed by the almost linear signal decay at 393 K (Fig. 4). The fast initial decay can be attributed primarily to the water in the gas phase while the slower portion of the attenuation curve can be assigned to the water in silicalite-1 crystals. The diffusion coefficient of water obtained from the slower portion of the attenuation curve (Fig. 4) using Eq. (15) is equal to $1.5 \times 10^{-9} \, m^2 \, s^{-1}$. This diffusivity is significantly lower than the diffusivity of water in the liquid phase even at 373 K ($8.7 \times 10^{-9} \, m^2 \, s^{-1}$ from [28]). Hence, the diffusivity measured at 393 K may definitely not be assigned to the diffusion coefficient of water in a liquid or a quasi-liquid phase. We tentatively assign this diffusivity to the diffusion of water in silicalite-1 crystals. The small deviations of the slower part of the attenuation curve from a straight line (Fig. 4, at 393 K) may be attributed primarily to the diffusion anisotropy in silicalite-1 crystals.

The study of the diffusion of one component in zeolite under the influence of other diffusants was recently a point of interest for both theoreticians and experimentalists [26,29–31]. It was generally observed that the diffusivity of one component kept at a constant loading decreases as the loading level of another, usually less mobile component increases. Here, we report the preliminary results of the PFG NMR diffusion measurements of ethane, propane and n-butane in samples of silicalite-1 with and without pre-adsorbed D_2O. The loadings of alkanes in both types of the samples were kept at the same level. In all cases the initial part of the PFG NMR attenuation curves ($-1.0 < \ln(\Psi) < 0.0$) of alkane diffusion in silicalite-1 shows the linear behavior as predicted by Eq. (15). The diffusion coefficients of the alkanes in the samples with and without water are presented in Table 2. The diffusivities were obtained from the

Table 2
The diffusion coefficients D of ethane, propane and n-butane obtained from the PFG NMR measurements at 298 K in the samples of silicalite-1 with and without pre-adsorbed D_2O

Alkane	D without pre-adsorbed D_2O (m^2 s^{-1})	D with pre-adsorbed D_2O (m^2 s^{-1})
Ethane	1.3×10^{-9}	4.0×10^{-10}
Propane	4.4×10^{-10}	2.2×10^{-10}
n-Butane	1.9×10^{-10}	1.4×10^{-10}

initial slope of the attenuation curves. Diffusion studies of small alkanes in water-free MFI-type zeolites by the PFG NMR technique are reported in [29,32–34]. The comparison of the present data obtained for the water-free samples with those previously reported shows general agreement between the absolute values of the diffusion coefficients. The data presented in Table 2 show that the diffusivities of all three alkanes are lower in the samples with pre-adsorbed water than in the water-free samples. It can be seen in Table 2 that for smaller, more mobile alkanes the influence of water on the self-diffusion of alkane molecules is larger. This observation is in qualitative agreement with the results previously reported for other two-component systems [26,29–31]. The data presented in Table 2 provide, in our opinion, evidence that under our experimental conditions significant loadings of water molecules in silicalite-1 crystals are achieved.

4. Comparison and conclusions

MD simulations carried out at 298 and 393 K at a concentration of two water molecules per intersection using an ab initio fitted potential model that has been obtained from ab initio calculations do not show cluster formation of water in silicalite-1. So, diffusion coefficients that agree with experimental values could be expected.

The PFG NMR results reported in this paper indicate that under our experimental conditions not only extra-crystalline but also intra-crystalline water is present in the silicalite-1 samples. This conclusion is supported by the observation of the influence of pre-adsorbed water on the intra-crystalline diffusivities of alkane molecules in silicalite-1 as well as by the comparison of the measured diffusivity of water in silicalite-1 sample at 393 K with that of liquid water.

Although our PFG NMR results are preliminary in nature they allow us to estimate the intra-crystalline diffusivity of water at 393 K. This value differs by less than one order of magnitude from the results of MD simulations at the same temperature. In view of the fact that for other zeolitic adsorbate–adsorbent systems like, e.g. longer alkanes in MFT, there are still orders-of-magnitude differences between experimental results and MD simulations (see e.g. [35]), this first comparative study of MD simulation and measurement of water diffusion in zeolites appears to yield reasonable agreement.

Acknowledgements

References

[1] M. Anpo, S. Guo Zhang, S. Higashimoto, M. Matsuoka, H. Yamashita, Y. Ichihashi, Y. Matsumura, Y. Souma, J. Phys. Chem. B 103 (1999) 9295.

[2] K. Kageyama, S. Ogino, T. Aida, T. Tatsumi, Macromolecules 31 (1998) 4069.

[3] C.N.R. Rao, S. Natarajan, S. Neeraj, J. Am. Chem. Soc. 122 (2000) 2810.

[4] E. Jolimaitre, M. Tayakout-Fayolle, C. Jallut, K. Ragil, Ind. Eng. Chem. Res. 40 (2001) 914.

[5] T. Sano, S. Ejiri, K. Yamada, Y. Kawakami, H. Yanagishita, J. Membr. Sci. 123 (1997) 225.

[6] T. Sano, M. Hasegawa, Y. Kawakami, H. Yanagishita, J. Membr. Sci. 107 (1995) 193.

[7] J. Caro, S. Hocevar, J. Kärger, L. Riekert, Zeolites 6 (1986) 213.

[8] V.V. Turov, V.V. Brei, K.N. Khomenko, R. Leboda, Micropor. Mesopor. Mater. 23 (1998) 189;
P.H. Kasai, P.M. Jones, J. Mol. Cat. 27 (1983) 81.

[9] M.P. Allen, D.J. Tildesley, Computer Simu1ution of Liquids, Clarendon Press, Oxford, 1990.

[10] R. Haberlandt, S. Fritzsche, G. Peinel, K. Heinzinger, Molekulardynamik: Grundlagen und Anwendungen, Vieweg, Göttingen, 1995.

[11] D.H. Olson, G.T. Kokotailo, S.L. Lawton, W.M. Meier, J. Phys. Chem. 85 (1981) 2238.

[12] P. Bopp, G. Jancso, K. Heinzinger, Chem. Phys. Lett. 98 (1983) 129.

[13] C. Bussai, S. Hannongbua, S. Fritzsche, R. Haberlandt, Ab initio potential energy surface and MD simulations for the determination of the diffusion coefficient of water in silicalite, Chem. Phys. Lett. B 105 (2001) 3409.

[14] S. Fritzsche, M. Wolfsberg, R. Haberlandt, Chem. Phys., submitted for publication.

[15] H. Dufner, S.M. Kast, J. Brickmann, M. Schlenkrich, J. Comp. Chem. 18 (1997) 660.

[16] D. Wolf, P. Keblinski, S.R. Phillpot, J. Eggebrecht, J. Chem. Phys. 110 (1999) 17.

[17] J. Kärger, N.-K. Bär, W. Heink, H. Pfeifer, G. Seiffert, Z. Naturforsch Teil A 50 (1996) 186.

[18] J. Kärger, D.M. Ruthven, Diffusion in Zeolites and Other Microporous Solids, Wiley, New York, 1992.

[19] B. Staudte, A. Gutsze, W. Böhlmann, H. Pfeifer, B. Pietrewicz, Micropor. Mesopor. Mater. 40 (2000) 1.

[20] S. Fritzsche, R. Haberlandt, J. Kärger, H. Pfeifer, K. Heinzinger, Chem. Phys. Lett. 198 (1992) 283.

[21] J. Kärger, H. Pfeifer, W. Heink, Principles and application of self-diffusion measurements by nuclear magnetic resonance, in: Advances in Magnetic Resonance, Vol. 12, Academic Press, New York, 1988.

[22] R. Haberlandt, J. Kärger, Chem. Eng. J. 74 (1999) 15.

[23] J. Kärger, J. Phys. Chem. 98 (1991) 5558.

[24] E.J. Maginn, A.T. Bell, D.N. Theodoroou, J. Phys. Chem. 100 (1996) 7155.

[25] J. Kärger, P. Demontis, G.B. Suffritti, A. Tilocca, J. Chem. Phys. 110 (1999) 2.

[26] S. Jost, N.K. Bär, S. Fritzsche, R. Haberlandt, J. Kärger, J. Phys. Chem. B 102 (1998) 6375.

[27] U. Hong, J. Kärger, R. Kramer, H. Pfeifer, G. Seiffert, U. Mäller, K.K. Unger, H.-B. Lück, T. Ito, Zeolites 11 (1991) 816;
U. Hong, J. Kärger, H. Pfeifer, U. Muller, K.K. Unger, Z. Phys. Chem. (Leipzig) 173 (1991) 225.

[28] K. Holz, S.R. Heil, A. Sacco, Phys. Chem. Chem. Phys. 2 (2000) 4740.

[29] R.Q. Snurr, J. Kärger, J. Phys. Chem. B 101 (1997) 6469.

[30] S. Jost, N.K. Bär, S. Fritzsche, R. Haberlandt, Chem. Phys. Lett. 219 (1997) 385.

[31] L.N. Gergidis, D.N. Theodorou, H. Jobic, J. Phys. Chem. B 104 (2000) 5541.

[32] J. Caro, M. Bülow, W. Schirmer, J. Kärger, W. Heink, H. Pfeifer, J. Chem. Soc. Faraday Trans. I 81 (1985) 2541.

[33] W. Heink, J. Kärger, H. Pfeifer, K.P. Datema, A.K. Nowak, J. Chem. Soc. Faraday Trans. 88 (1992) 3505.

[34] W.D. Ylstra, H.P.C.E. Kuipers, M.F.M. Post, J. Kärger, J. Chem. Soc. Faraday Trans. 87 (1991) 1935.

[35] H. Jobic, Recent Advances in Gas Separation by Microporous Ceramic Membranes, Elsevier, Amsterdam, 2000.

APPENDIX III

Ab Initio Potential Energy Surface and Molecular Dynamics Simulations for the Determination of the Diffusion Coefficient of Water in Silicalite-1

Chuenchit Bussai, Siegfried Fritzsche, Reinhold Haberlandt, Supot Hannongbua

ELSEVIER

Ab initio potential energy surface and molecular dynamics simulations for the determination of the diffusion coefficient of water in silicalite-1

C. Bussai [a,b], S. Hannongbua [a,*], S. Fritzsche [b], R. Haberlandt [b]

[a] *Department of Chemistry, Faculty of Science, Chulalongkorn University, Bangkok 10330, Thailand*
[b] *Department of Molecular Dynamics/Computer Simulations, Faculty of Physics and Geoscience,*
Institute for Theoretical Physics (ITP), University of Leipzig, Augustusplatz 10-11, 04109 Leipzig, Germany

Received 6 November 2001; in final form 16 January 2002

Abstract

The silicalite-1/water potential function has been developed using quantum chemical calculations at the Hartree–Fock level using the 6-31G* basis sets. The silicalite-1 crystal structure is represented by three fragments, in which the chemical compositions are $O_{10}Si_{10}H_{20}$, $O_{30}Si_{22}H_{44}$ and $O_{35}Si_{29}H_{58}$. Ab initio calculations have been performed for 1032 fragment–water configurations where water coordinates are generated inside the fragments. The intermolecular silicalite-1/water potentials developed from those data points have been used in the molecular dynamics simulations. The obtained diffusion coefficients at 298 K of 3.3×10^{-9} m^2 s^{-1} and at 393 K of 6.7×10^{-9} m^2 s^{-1} are in agreement with those of the PFG-NMR measurements. © 2002 Elsevier Science B.V. All rights reserved.

1. Introduction

The interaction of water with zeolites is a subject of great scientific and technological interest, as water plays strong and essential roles for both absorption and catalytic properties of zeolites [1–3]. As coadsorbents, the presence of water has a large impact on the arrangement of the cations in the zeolite. Among non-cationic zeolites, interest is focused on silicalite-1, which due to its selectivity has been widely used in the separation of mixtures

between light hydrocarbons and water or dipole solvents [4–7]. Several attempts have been made to study the absorption and diffusion of hydrocarbons in silicalite-1 by means of both theoretical, [8–10] and experimental [11–14] investigations. However, very little information is available on the water/silicalite-1 interaction because one believes that water is not able to enter and diffuse in a hydrophobic zeolite such as silicalite-1.

Recently, we have investigated this issue intensively using quantum chemical calculations and found that water can enter the silicalite-1 channel [15]. An activation energy of approximately 1.9 kcal mol^{-1} is required to diffuse through the linked domain to or from the intersection channel. In

---
* Corresponding author. Fax: +66-2-254-1309.
E-mail address: supot.h@chula.ac.th (S. Hannongbua).

addition, preliminary results by Kärger et al. [16] using PFG-NMR measurements indicate that diffusion of water in silicalite-1 takes place even at room temperature.

As it is known that simulation results depend strongly on the quality of the potential function used, one of the best choices is to develop such a function by parameterizing directly from the data yielded from quantum mechanical calculations. However, in practice it is not possible, especially for large molecular systems, to generate such data even with a small basis set, because of the unreasonable computation time that would be required. Several attempts have been made with substantial success by Catlow et al. [17,18] and Sauer et al. [19–21]. The potential parameters were derived from the results of ab initio calculations. The molecular models, which represent typical structural elements of zeolites, consist of SiO_4 and protonated AlO_4 tetrahedra connected to chain rings and cages.

In this study, an alternative choice in deriving potential function parameters is proposed. Numerous silicalite-1/water energy points have been generated using quantum chemical calculations at the Hartree–Fock (HF) level. Molecular dynamics simulations have been performed using the newly developed ab initio potential and diffusion coefficients for water molecules in the silicalite-1 have been investigated.

2. Calculation details

2.1. Development of the intermolecular pair potential

To develop intermolecular potential functions representing the interaction between two molecules in all configurations, numerous coordinations of the second molecule around the first one have to be generated. The interaction energies of all configurations have to be calculated and the obtained data points must then be fitted to an analytical form.

Due to the size of the silicalite-1 lattice, in which a crystallographic cell [22] consists of 96 Si and 192 O atoms (Figs. 1a and e), it is not possible to take
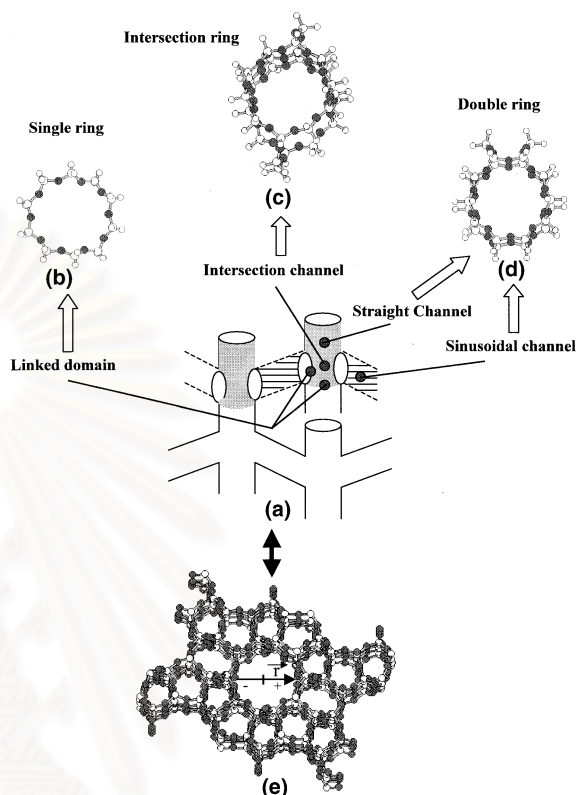
Fig. 1. Schematic representations of the (a) silicalite-1 crystal structure, (b) linked domain, (c) straight and sinusoidal channels, (d) intersection channel and (e) chemical structure of the silicalite-1 lattice.

into account the whole lattice in the quantum chemical calculations. Therefore, the silicalite-1 crystal structure was represented by three fragments (Figs. 1b–d), taken from different parts of the lattice, which contain different chemical compositions and structures. They were, for simplicity, named single, intersection and double rings. Their chemical compositions, after filling up the remaining valence orbitals of the silicon atoms with hydrogen atoms, are $O_{10}Si_{10}H_{20}$, $O_{30}Si_{22}H_{44}$ and $O_{35}Si_{29}H_{58}$, respectively. More details of the classification have been given elsewhere [15]. Numerous configurations of the water molecule have been generated inside the three fragments considered. Ab initio [23] calculations at the HF level with the extended 6-31G* basis sets have been performed for all water/silicalite-1 configurations.

Experimental geometries of water [24] and silicalite-1 [22] have been used and kept constant throughout. All calculations are performed using the G98 program [25].

More than 1000 ab initio data points were fitted to an analytical function of the form

$$\Delta E(\text{w}, \text{s}) = \sum_i^3 \sum_j^{288} \left\{ \frac{A_{ij}^{ab}}{r_{ij}^6} + \frac{B_{ij}^{ab}}{r_{ij}^{12}} + \frac{C_{ij}^{ab}}{r_{ij}^3} + \frac{q_i q_j}{r_{ij}} \right\},$$

(1)

where 3 and 288 denote the numbers of atoms in a water molecule (w) and the silicalite-1 (s) unit cell, respectively. The constants A_{ij}, B_{ij} and C_{ij} are fitting constants and r_{ij} is the distance between atom i of water and atom j of silicalite-1. Also, q_i and q_j are the atomic net charges of atoms i and j in atomic units, as obtained from the population analysis of the isolated molecules in the quantum chemical calculations. Superscripts a and b on the fitting parameters have been used to classify atoms of equal atomic number but different environmental conditions, for example, oxygen and silicon atoms of silicalite-1 in the different channels. The third polynomial term (C_{ij}/r_{ij}^3) was added in order to obtain better numerical fitting. The silicalite-1/water fitting parameters were summarized in Table 1.

Concerning an assignment of a negative or positive value to the fitting parameters, it is generally not possible in all cases to control A/r^6 to be negative and B/r^{12} to be positive, in order to rep-

resent attractive and repulsive interactions of the pair, respectively. A fit in which the A/r^6 terms were separately forced to the van der Waals interaction and the B/r^{12} terms to the real repulsion have led to worse agreement with the quantum mechanical results. In these cases, physical meaning of the atomic-based pair potentials, 864 pairs running over $i = 1$–3 and $j = 1$–288 for Eq. (1), is not achieved. However, physical meaning, as well as quality, of the molecular-based water/silicalite-1 function is its ability in representing ab initio data. An advantage of this approach is that it is a one-to-one correspondence between the predicted (by the potential function) and the observed (by the ab initio calculation) interaction energies. Analogously, as well as for better numerical fitting, the third polynomial term (C_{ij}/r_{ij}^3) was added and not considered separately. Some examples are those in Refs. [26–28].

2.2. Molecular dynamics simulations

The silicalite-1 crystal structure used in this study is characterized by two types of channels whose symmetry group is *Pnma*. The crystallographic cell [22] contains 288 atoms ($Si_{96}O_{192}$), with lattice parameters $a = 20.07$ Å, $b = 19.92$ Å and $c = 13.42$ Å. Simulations have been carried out at 298 and 393 K with the time step of 0.5 fs for the system consisting of two silicalite-1 unit cells. The box contains two water molecules per intersection of the silicalite-1 that means totally 16 in the MD

Table 1
Final optimization parameters for atom i of water interacting with atom j in each channel of the silicalite-1 lattice

i	j	q_i	q_j	A (Å^6 kcal mol^{-1})	B (Å^{12} kcal mol^{-1})	C (Å^3 kcal mol^{-1})
O	Si$_{sd}$	−0.87	1.57	− 9043.97	1161167.97	1418.92
O	Si$_{st}$	−0.87	1.67	− 4159.83	989963.68	617.02
O	O$_{sd}$	−0.87	−0.78	1371.19	−21045.58	−351.61
O	O$_{st}$	−0.87	−0.84	− 110.79	51208.44	−110.82
H	Si$_{sd}$	0.43	1.57	3724.97	−4314.90	−792.37
H	Si$_{st}$	0.43	1.67	2077.13	−8925.29	−415.82
H	O$_{sd}$	0.43	−0.78	−406.18	689.37	222.32
H	O$_{st}$	0.43	−0.87	34.87	32.84	102.59

Subscripts sd and st denote sinusoidal (zig-zag) and straight channels, respectively. Energies in kcal mol^{-1}, distances (r_{ij}) in Å and atomic net charges (q) in atomic units.

box. Periodic boundary conditions have been applied. The potential proposed by Bopp et al. [29] was employed to describe water–water interactions while the newly developed potential shown in Eq. (1), with the optimal parameters summarized in Table 1, was used to represent the silicalite-1/water interactions. According to [30,31] the use of Ewald summations can be avoided in systems with total charge zero if shifted force potentials are applied instead. The evaluation part each run corresponds to trajectory length of 10 ns after 0.5 ps thermalization.

3. Results and discussion

3.1. Quality of the silicalite-1/water potential

With the analytical potential shown in Eq. (1), the lattice–water interactions in the straight channel have been calculated and plotted in Fig. 2. Here, the oxygen atom of the water molecule moves from one surface to the opposite surface along the vector **r** (see Fig. 1e), its dipole moment points parallel to vector **r** and its molecular plane is parallel to the window of the lattice. The ab

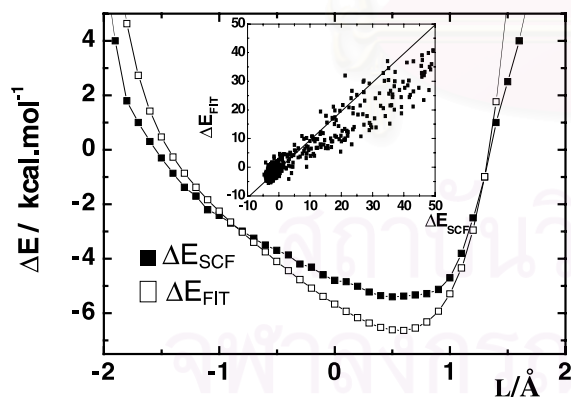initio interaction energies at the same lattice–water configurations have been calculated and given also for comparison. Good agreement between the two curves in Fig. 2 clearly illustrates the reliability and quality of the fit. This conclusion was, again, confirmed by the plot shown in the inset of this figure, where all 1050 ab initio and fitted energies have been compared.

Some comments could be made concerning the quality of the ab initio interaction energies given in this study. Discrepancies and reliabilities of the data points due to the size of the fragments, the calculated methods and the basis sets used as well as an error due to the unbalance of the basis set, basis set superposition error, have been intensively examined and discussed in a previous paper [15].

3.2. Characteristics of the silicalite-1/water potential

To visualize characteristics of the silicalite-1/water potential function, the interaction energies for different orientations of the water molecule in the straight channel have been computed according to Eq. (1). The changes of the energies as a function of the distances along **r** were plotted in Fig. 3.

Curves 1 and 4 in Fig. 3 show the minima at $L < 0$, and the interaction energies for $L > 0$ increase more slowly than those for $L < 0$. This occurrence can be clearly understood as water

Fig. 2. Silicalite-1/water interaction energies (ΔE) obtained from the ab initio calculations (ΔE_{SCF}) with the extended 6-31G* basis sets and from the potential function (ΔE_{FIT}) according to Eq. (1), where the oxygen atom of the water molecule lies along the vector **r** (see Fig. 1e), its dipole moment is parallel to **r** and its molecular plane is parallel to the window of the lattice. All ab initio and fitted data points are also compared in the inset.
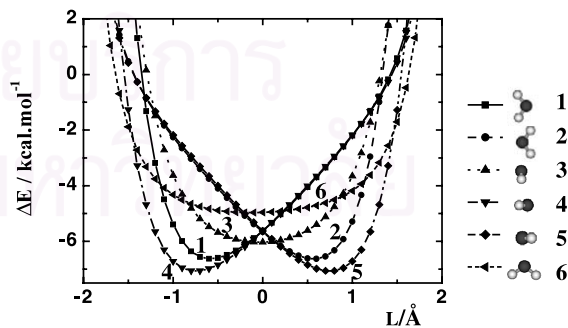

Fig. 3. Silicalite-1/water interaction energies (ΔE, kcal mol^{-1}) obtained from the potential function according to Eq. (1) for different orientations of a water molecule, where its oxygen atom lies along **r** (see Fig. 1e) in the straight channel.

molecules in these configurations (at the right of this figure) approach the surface at $L > 0$ by pointing hydrogen atoms toward the oxygen atoms of the lattice, i.e., attractive Coulomb interactions between the hydrogen atoms of water and the oxygen atoms of the surface compensate the water–surface repulsion. This leads to a slow increase of the interaction energy and hence an asymmetry of the lattice–water potential. The difference between the shapes of the two curves indicates how sensitive the obtained function is. That means it is able to classify the two orientations of the water molecule which differ only by rotating the molecule by 90° around its dipole vector. The situation is very similar for curves 2 and 5, in which the minima take place at $L > 0$ and the interaction energies for $L < 0$ increase faster than those for $L > 0$. For curves 3 and 6, the shapes are much more symmetric than the other curves. The reason is that the water molecule in these configurations approaches the lattice, both for $L > 0$ and $L < 0$, by pointing its dipole vector parallel to the surface. Curve 6 is broader than curve 3 because in curve 3 water moves toward the surface in configurations for which distances from the surface to the two hydrogen atoms are identical. For curve 6, at the same position of water as in curve 3, one hydrogen atom is closer to the surface than the other (see legend of Fig. 3). This fact confirms the ab initio interaction energies reported in [15].

As can be seen from Eq. (1) and Table 1, different fitting data sets have been used to represent the interaction between the lattice and a water molecule lying in the sinusoidal (zig-zag) or in the straight channel. To visualize this effect, the interaction energies have been calculated separately for a water molecule in the two channels. In this example, the water molecule was in the same configurations as those of Fig. 2. The results are displayed in Fig. 4. The sensitivity of the silicalite-1/water potential to different environments has been clearly monitored, in addition to that due to water orientation as shown in Fig. 3. The difference between the interactions in the straight and the zig-zag channels is consistent with the energy data analyzed intensively in our previous work [12].
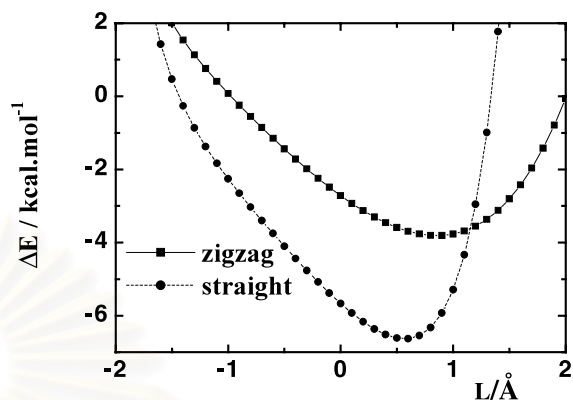
Fig. 4. Silicalite-1/water interaction energies obtained from the potential function according to Eq. (1), where water molecule lies in the same configurations as those of Fig. 2 in the sinusoidal and the straight channels.

3.3. Diffusion coefficients

To justify the quality of the model in representing a real system, MD simulations have been performed at 298 and 393 K for a loading of two water molecules per intersection of the silicalite-1. The diffusion coefficients have been calculated according to the method described in [32] from different moments of the particle displacements. The results obtained at 298 and 393 K are 3.3×10^{-9} and 6.7×10^{-9} m^2 s^{-1}, respectively. These values are in satisfactory agreement with those from PFG-NMR measurements [16] at the same loading and temperature.

References

[1] J. Kärger, D.M. Ruthven, Diffusion in Zeolites and Other Microporous Solids, Wiley, New York, 1992.

[2] D.M. Ruthven, Principles of Adsorption and Adsorption Processes, Wiley, New York, 1984.

[3] J.J. Van Dum, W.J. Mortier, J. Phys. Chem. 92 (1988) 6740.

[4] T. Matsufuji, K. Watanabe, N. Nishiyama, Y. Egashira, M. Matsukata, K. Ueyama, Ind. Eng. Chem. Res. 39 (2000) 2434.

[5] P. Ciaverella, H. Moueddeb, S. Miachon, K. Fiaty, J.A. Dalmon, Catal. Today 56 (2000) 253.

[6] A. Tavolaro, E. Drioli, Adv. Mater. 11 (1999) 975.

[7] X. Lin, J.L. Falconer, R.M. Noble, Chem. Mater. 10 (1998) 3716.

[8] D.N. Theodorou, R.Q. Snurr, A.T. Bell, Molecular Dynamics and Diffusion in Microporous Materials, vol. 7, Pergamon Press, Oxford, 1996.

[9] F. Keil, R. Krishna, M.-O. Coppens, Chem. Eng. 16 (2000) 71.

[10] P. Demontis, G.B. Suffritti, Chem. Rev. 97 (1997) 2845.

[11] J.M. Van de Graaf, F. Kapteijn, J.A. Moulijn, Microporous Mesoporous Mater. 35 (2000) 267.

[12] W. Zhu, F. Kapteijn, J.A. Moulijn, Phys. Chem. Chem. Phys. 2 (2000) 1989.

[13] B. Millot, A. Methivier, H. Jobic, J. Phys. Chem. B 102 (1998) 3210.

[14] M.S. Sun, D.B. Shah, H.H. Xu, O. Talu, J. Phys. Chem. 102 (1998) 1466.

[15] C. Bussai, S. Hannongbua, R. Haberlandt, J. Phys. Chem. B 105 (2001) 3409.

[16] C. Bussai, H. Liu, S. Vasenkov, S. Fritzsche, S. Hannongbua, R. Haberlandt, J. Kärger, Appl. Catal. A-Gen, in press.

[17] R.A. Jackson, C.R.A. Catlow, Mol. Simul. 1 (1988) 207.

[18] G. Aloisi, P. Barnes, C.R.A. Catlow, R.A. Jackson, A.J. Richards, J. Chem. Phys. 93 (1990) 3573.

[19] J.R. Hill, J. Sauer, J. Phys. Chem. 98 (1994) 1238.

[20] J.R. Hill, J. Sauer, J. Phys. Chem. 99 (1995) 9536.

[21] K.P. Schröder, J. Sauer, J. Phys. Chem. 100 (1996) 11043.

[22] D.H. Olson, G.T. Kokotailo, S.L. Lawton, W.M. Meier, J. Phys. Chem. 85 (1981) 2238.

[23] W.J. Hehre, L. Random, P.V.R. Schleyer, J.A. Pople, Ab Initio Molecular Orbital Theory, Wiley, New York, 1987.

[24] W.S. Benedict, N. Gailar, E.K. Plyler, J. Chem. Phys. 24 (1956) 1139.

[25] M.J. Frisch et al., GAUSSIAN 98, Revision A, Gaussian Inc., Pittsburgh, PA, 1998.

[26] W.L. Jorgensen, M.E. Cournoyer, J. Am. Chem. Soc. 101 (1978) 4942.

[27] G. Karlström, P. Linse, A. Wallqvist, B. Jönsson, J. Am. Chem. Soc. 105 (1983) 3777.

[28] S. Udonsub, S. Hannongbua, J. Chem. Soc., Faraday Trans. 93 (1997) 3045.

[29] P. Bopp, G. Jancso, K. Heinzinger, Chem. Phys. Lett. 98 (1983) 129.

[30] D. Wolf, P. Keblinski, S.R. Phillpot, J. Eggebrecht, J. Chem. Phys. 110 (1999) 17.

[31] H. Dufner, S.M. Kast, J. Brickmann, M. Schlenkrich, J. Comput. Chem. 18 (1997) 660.

[32] S. Fritzsche, R. Haberlandt, J. Kärger, H. Pfeiffer, M. Wolfsberg, K. Heinzinger, Chem. Phys. Lett. 198 (1992) 283.

APPENDIX IV

Diffusion of Water in Silicalite by Molecular Dynamics
Simulations: *Ab Initio* based interactions

Chuenchit Bussai, Siegfried Fritzsche, Reinhold
Haberlandt, Supot Hannongbua

Diffusion of Water in Silicalite by Molecular Dynamics Simulations: *Ab Initio* based interactions

C. Bussai[a,b], S. Hannongbua[a], S. Fritzsche[b], and R. Haberlandt[b]

[a]*Department of Chemistry, Faculty of Science, Chulalongkorn University, Bangkok 10330, Thailand.*[*]

[b]*Department of Molecular Dynamics/Computer Simulations, Institute for Theoretical Physics (ITP), Faculty of Physics and Geoscience, University of Leipzig, Augustusplatz 10 – 11, 04109, Leipzig, Germany.*

The silicalite-1/water potential function has been developed using quantum chemical calculations at the Hartree-Fock level using the 6-31G* basis sets. The silicalite-1 crystal structure is represented by three fragments, in which the chemical compositions are $O_{10}Si_{10}H_{20}$, $O_{30}Si_{22}H_{44}$ and $O_{35}Si_{29}H_{58}$. *Ab initio* calculations have been performed for 1,032 fragment-water configurations where water coordinates are generated inside the fragments. The intermolecular silicalite-1/water potentials developed from those data points have been used in the molecular dynamics simulations. The obtained diffusion coefficients at 298 K of 3.3×10^{-9} $m^2.s^{-1}$ and at 393 K of 6.7×10^{-9} $m^2.s^{-1}$ are in agreement with those of the PFG-NMR measurements.

1. INTRODUCTION

Zeolites are microporous crystalline solids with well-defined structures. Generally they contain silicon, aluminium and oxygen in their framework and cations, water and/or other molecules within their pores. Due to their unique porous properties, major uses are in petrochemical cracking, ion exchange (water softening and purification), and in the separation and removal of gases and solvents [1]. To study these, several experiment tools have been achievable on one hand, on the other hand, theoretical tools, e. g. Molecular Dynamics simulations, become more feasible [2]. Such theoretical methods require knowledge of the interaction potentials. A crucial method to obtain such potentials is the use of *ab initio* calculations. Several function modification attempts and great success have been made by Sauer et al., with e. g., the QMPot method [3].

In this study, an alternative choice in deriving potential function parameters is proposed. Numerous silicalite-1/water
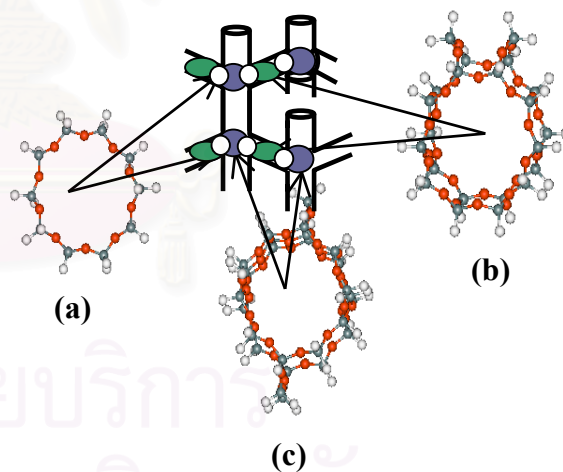
Figure 1. Schematic representations of the (a) linked domain, (b) straight and sinusoidal channels, (c) intersection.

energy points have been generated using quantum chemical calculations at the Hartree-Fock (HF) level using the 6-31G* basis sets. Molecular dynamics simulations have been performed using the newly developed *ab initio* potential and diffusion coefficients for water molecules in the silicalite-1 have been investigated.

2. CALCULATION DETAIL

2.1. Development of the intermolecular pair potential

To develop intermolecular potential functions representing the interaction between two molecules in all configurations, numerous coordinations of the second molecule around the first one have to be generated. The interaction energies of all configurations have to be calculated and the obtained data points must then be fitted to an analytical form.

Due to the size of the silicalite-1 lattice, in which a crystallographic cell [4] consists of 96 Si and 192 O atoms, it is rather difficult to take into account the whole lattice in the quantum chemical calculations. Therefore, the silicalite-1 crystal structure was represented by three fragments (Figures 1a-1c), for simplicity, named single, intersection and double rings with their chemical compositions $O_{10}Si_{10}H_{20}$, $O_{30}Si_{22}H_{44}$ and $O_{35}Si_{29}H_{58}$, respectively. More details of the classification have been given elsewhere [5]. *Ab initio* calculations at the HF level with the extended 6-31G* basis sets have been performed for all water configurations generated inside those silicalite-1 fragments. Experimental geometries of water [6] and silicalite-1 [4] have been used and kept constant throughout. All calculations are performed using the G98 program [7].

More than 1,000 *ab initio* data points were fitted to an analytical function of the form [8]:

$$\Delta E(\text{w},\text{s}) = \sum_{i}^{3}\sum_{j}^{288}\left\{\frac{A_{ij}^{ab}}{r_{ij}^{6}} + \frac{B_{ij}^{ab}}{r_{ij}^{12}} + \frac{C_{ij}^{ab}}{r_{ij}^{3}} + \frac{q_{i}q_{j}}{r_{ij}}\right\}, \quad (1)$$

where 3 and 288 denote the numbers of atoms in a water molecule (w) and the silicalite-1 (s) unit cell, respectively. The constants A_{ij}, B_{ij} and C_{ij} are fitting constants and r_{ij} is the distance between atom i of water and atom j of silicalite-1. Also, q_i and q_j are the atomic net charges of atoms i and j in atomic units, as obtained from the population analysis of the isolated molecules in the quantum chemical calculations. Superscripts a and b on the fitting parameters have been used to classify atoms of equal atomic number but different environmental conditions, for example, oxygen and silicon atoms of silicalite-1 in the different channels. The third polynomial term (C_{ij}/r^3_{ij}) was added in order to obtain better numerical fitting. The silicalite-1/water fitting parameters were summarized in Table 1. Concerning an assignment of a negative or positive value to the fitting parameters, physical meaning of the atomic-based pair potentials is not achieved. Instead, it is a one-to-one correspondence between the predicted (by the potential function) and the observed (by the *ab initio* calculation) interaction energies. An advantage of this approach is that it is a one-to-one correspondence between the predicted and the calculated interaction energies. Analogously, as well as for better numerical fitting, the third polynomial term (C_{ij}/r^3_{ij}) was added and not considered separately. Some examples are those in references [9-11].

Table 1

Optimization parameters for atom i of water interacting with atom j in each channel of the silicalite-1 lattice. Subscripts sd and st denote sinusoidal (zig-zag) and straight channels, respectively.

i	j	q_i	q_j	A ($\text{Å}^6\text{kcal.mol}^{-1}$)	B ($\text{Å}^{12}\text{kcal.mol}^{-1}$)	C ($\text{Å}^3\text{kcal.mol}^{-1}$)
O	Si_{sd}	-0.87	1.57	- 9043.97	1161167.97	1418.92
O	Si_{st}	-0.87	1.67	- 4159.83	989963.68	617.02
O	O_{sd}	-0.87	-0.78	1371.19	-21045.58	-351.61
O	O_{st}	-0.87	-0.84	- 110.79	51208.44	-110.82

i	j	q_i	q_j	A ($\text{Å}^6\text{kcal.mol}^{-1}$)	B ($\text{Å}^{12}\text{kcal.mol}^{-1}$)	C ($\text{Å}^3\text{kcal.mol}^{-1}$)
H	Si_{sd}	0.43	1.57	3724.97	-4314.90	-792.37
H	Si_{st}	0.43	1.67	2077.13	-8925.29	-415.82
H	O_{sd}	0.43	-0.78	-406.18	689.37	222.32
H	O_{st}	0.43	-0.87	34.87	32.84	102.59

2.2. Molecular Dynamics Simulations

The crystallographic cell [4] of Silicalite-1 contains 288 atoms ($Si_{96}O_{192}$), with lattice parameters $a = 20.07$ Å, $b = 19.92$ Å and $c = 13.42$ Å. Simulations have been carried out at 298 K and 393 K with the time step of 0.5 fs for the system consisting of 2 silicalite-1 unit cells. The box contains 2 water molecules per intersection of the silicalite-1. Periodic boundary conditions have been applied. The potential proposed by Bopp, Jancso and Heinzinger [12] was employed to describe water-water interactions while the newly developed potential shown in eq. (1), with the optimal parameters summarized in Table 1, was used to represent the silicalite-1/water interactions. According to [13.14] the use of Ewald summations can be avoided in systems with total charge zero if shifted force potentials are applied instead. The equations of motion are solved by means of the Velocity-Verlet algorithm. The evaluation part of each run corresponds to trajectory length of 10 ns after 0.5 ps thermalization during which the total

energy is adjusted to a value that leads to the wished average kinetic energy. Therefore, the evaluation part can be done in the microcanonical ensemble without perturbing the trajectories.

3. RESULT AND DISCUSSION

3.1. Quality of the Silicalite-1/Water Potential
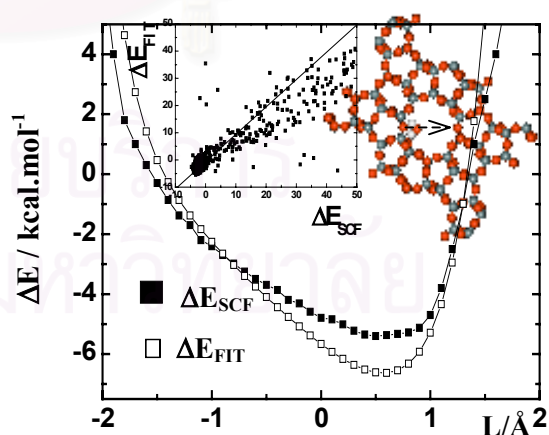

Figure 2. Silicalite-water interaction energies (ΔE) obtained from the *ab initio* calculations (ΔE_{SCF}) with the extended 6-31G* basis sets and from the potential function (ΔE_{FIT}) All *ab initio* and fitted data points were also compared in the insert.

With the analytical potential shown in eq. (1), the lattice-water interactions in the straight channel have been calculated and plotted in Figure 2. Here, the oxygen atom of the water molecule moves from one perpendicular surface to the opposite side along the vector **r** (see Figure 2), its dipole moment points parallel to vector **r** and its molecular plane is parallel to the window of the lattice. The *ab initio* interaction energies at the same lattice-water configurations have been calculated and given also for comparison. Good agreement between the two curves clearly illustrates the reliability and quality of the fit. This conclusion was, again, confirmed by the plot shown in the insert of this Figure, where all 1,050 *ab initio* and fitted energies have been compared.

Some comments could be made concerning the quality of the *ab initio* interaction energies given in this study. Discrepancies and reliabilities of the data points due to the size of the fragments, the calculated methods and the basis sets used as well as an error due to the unbalance of the basis set, basis set superposition error, have been intensively examined and discussed in some previous papers [5,8].

3.2. Characteristics of the Silicalite-1/Water Potential

To visualize characteristics of the silicalite-1/water potential function, the interaction energies for different orientations of the water molecule in the straight channel have been computed according to eq. (1). The changes of the energies as a function of the distances along **r** were plotted in Figure 3.

Curves 1 and 2 in Figure 3 show the minima at $L < 0$, and the interaction energies for $L > 0$ increase more slowly than those for $L < 0$. This occurrence can be clearly understood as water molecules in these configurations (at the right of this Figure) approach the surface at $L > 0$ by pointing hydrogen atoms toward the

oxygen atoms of the lattice, i.e., attractive Coulomb interactions between the hydrogen atoms of water and the oxygen atoms of the surface compensate the water-surface repulsion. This leads to a slow increase of the interaction energy and hence an asymmetry of the lattice-water potential. The difference between the shapes of the two curves indicates how sensitive the obtained function is. That means it is able to classify the two orientations of the water molecule which differ only by rotating the molecule by 90° around its dipole vector. The situation is very similar for curves 2 and 5, in which the minima take place at $L > 0$ and the interaction energies for $L < 0$ increase faster than those for $L > 0$. For curves 3 and 6, the shapes are much more symmetric than the other curves. The reason is that the water molecule in these configurations approaches the lattice, both for $L > 0$ and $L < 0$, by pointing its dipole vector parallel to the surface. Curve 6 is broader than curve 3 because in curve 3 water moves toward the surface in configurations for which distances from the surface to the   two hydrogen
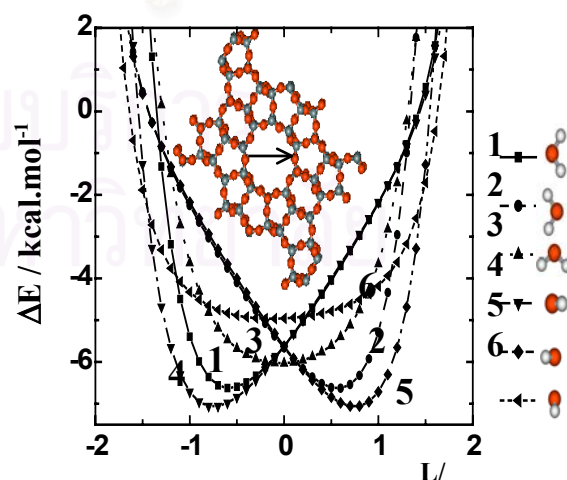

Figure 3. Silicalite-water interaction energies (ΔE) obtained from the potential function according to eq. (1) for different orientations of a water molecule

atoms are identical. For curve 6, at the same position of water as in curve 3, one hydrogen atom is closer to the surface than the other (see legend of Figure 3). This fact confirms the *ab initio* interaction energies reported [5].

The sensitivity of the silicalite-1/water potential to different environments has been clearly monitored, in addition to that due to water orientation as shown in Figure 3. The difference between the interactions in the straight and the zig-zag channels is consistant with the energy data analyzed intensively in our previous work [5,8].

3.3. Diffusion coefficients

The self-diffusion coefficients are calculated from the particle displacements. In [15-17] the process of self-diffusion was quite generally related to the moments of the propagator. The propagator $P(r, r_0, t)$ represents the probability density to find a particle at position r at time t when it was at r_0 at time $t = 0$. The nth moment of the propagator is defined by the relation [15]

$$\left\langle |r - r_0|^n \right\rangle = \int |r - r_0|^n \, P(r, r_0, t) \, dr, \qquad (2)$$

$P(r, r_0, t)$ is the solution of the diffusion equation for the initial concentration $C(r, t = 0) = \delta(r - r_0)$. In the case of isotropic diffusion and of a homogeneous system the propagator results to be

$$P(r, r_0, t) = (4\pi D t)^{-3/2} \exp\left\{ \frac{-(r - r_0)^2}{4Dt} \right\}. \qquad (3)$$

Although zeolites are not homogeneous the propagator can be represented in this way if the displacements exceed the size of the inhomogeneities [16]. Then $P(r, r_0, t)$

depends only on the difference $|r - r_0|$. For shorter times this is not true. As the transition time to the Gaussian behavior and the final D values were the quantities of main interest in the present paper an averaging over r_0 has been carried out. The resulting propagator depends only upon $|r - r_0|$ for all times. But, it attains the shape shown in eq. (3) (or its equivalents for the different components of the diffusion tensor in the anisotropic case, see below) only for sufficiently long times. The first four moments can be calculated from eqs. (2) and (3) in the case of isotropic diffusion [15] and of the anisotropic system, the corresponding equations for each direction, corresponding to the x-, y- and z-axes [18]. In this case, the diffusivity D is one third of the trace of the diffusion tensor:

$$D = \frac{1}{3}(D_x + D_y + D_z). \qquad (4)$$

The good agreement (within the range of fluctuations) of the final D values calculated for 298 K using different moments indicates that the diffusion time used in the evaluation procedure exceeds the correlation time. The self-diffusion coefficients calculated in this way at 298 and 393 K are summarized in Table 2.

It can be seen from these results that the largest component of the diffusion tensor is D_y. The D_y values are about two times larger than D_x at both temperatures and about seven times larger than D_z at 298 K and even larger at 393 K. This is consistent with the physical structure of the silicalite-1 crystal, which consists of zigzag channels lying in the xz-plane and the straight channels lying parallel to the y-axis. This causes the significant difference of the elementary diffusion rates in different directions.

Table 2

The self-diffusion coefficients calculated in this way at 298 and 393 K are summarized.

Temp (K)	MD Simulation			
	D_x (m^{2}s^{-1})	D_y (m^{2}s^{-1})	D_z (m^{2}s^{-1})	D(m^{2}s^{-1})
298	2.6×10^{-9}	6.5×10^{-9}	7.9×10^{-10}	3.3×10^{-9}
393	5.7×10^{-9}	1.3×10^{-8}	1.4×10^{-9}	6.7×10^{-9}

Considering the diffusion through silicalite-1 as a random walk of independent steps between the channel intersections, the main elements of the diffusion tensor may be shown to be correlated by the relation [19]

$$\frac{c^2}{D_z} = \frac{a^2}{D_x} + \frac{b^2}{D_y}, \tag{5}$$

where *a*, *b*, and *c* are the unit cell lengths. Eq. (5) implies that the correlation time of propagation is shorter than the mean time it takes a molecule to travel from intersection to intersection. Possible deviations from this case, i.e. correlated motion between the channel intersections, may be accounted for by introducing a parameter

$$\beta = \frac{c^2/D_z}{\left(a^2/D_x + b^2/D_y \right)} \tag{6}$$

The case $\beta = 1$, obviously represents the above considered case of completely random steps. $\beta > 1$ indicates preferential continuation of the diffusion path along one and the same channel, while $\beta < 1$ stands for molecular propagation with interchanges between the two channel types more probable than at random. The values of β calculated in this study are equal to 1.04 at 298 K and to 1.25 at 393

K. In agreement with the behavior found for alkanes, e.g. [20], where $\beta = 1.2$ and 1.3, a tendency is observed that the xenon molecules and the methane molecules, respectively, in silicalite-1 prefer to remain in the same type rather than to change into a segment of the other channel type at a channel intersection.

3.4. Radial distribution function

The oxygen-oxygen radial distribution functions *g* for the water molecules at the two temperatures have been calculated and displayed in Fig. 4. In inhomogeneous systems, $g(r_1, r_2)$ depends upon r_1 also and is not simply $g(r)$ with $r = |r_1 - r_2|$. But, as a first approximation, we have done the evaluation of $g(r)$ like in a homogeneous isotropic system. This is equivalent to an averaging over the sites r_1 taking as a weight function the relative number of events when the r_1 are found during the MD run. Note, that due to the asymmetry of the silicalite-1 lattice the function $g(r)$, defined in this way, does not converge to 1.0 for distances of the order of 10 Å. $g(r)=1$ would correspond to a homogeneous distribution in space that can be observed in systems with a structure on molecular level only at a length scale that is larger than the size of the inhomogenities i.e. the channel structure in the present case. The radial density

distributions show a first maximum at 3.5 Å followed by a pronounced shoulder centered at 4.4 Å. In order to see the number of neighbors the integral $n(r)$ of $g(r)$ is also displayed in Fig. 4. It can be seen that e.g. within a distance of 7 Å around a given water molecule there are in average only two other water molecules. Although, the first minimum is not well-defined, it can be concluded that the simulations did not show any clustering of water molecules in the silicalite-1 channels for the examined temperatures and concentrations of guest molecules.

4. CONCLUSION

To justify the quality of the model in representing a real system, MD simulations have been performed at 298 K and 393 K for a loading of 2 water molecules per intersection of the silicalite-1. The diffusion coefficients have been calculated according to the method described in [21] from different moments of the particle displacements. The results obtained at 298 K and 393 K are 3.3×10^{-9} and 6.7×10^{-9} $m^2.s^{-1}$, respectively. These values are in satisfactory agreement with those from PFG-NMR measurements [22] at the same loading and temperature.

REFERENCES

1. D. W. Breck, Zeolite Molecular Sieve, Wiley, New York, 1974; J. Kärger and D. M. Ruthven, Diffusion in Zeolites and Other Microporous Solids, Wiley-Interscience, New York, 1992.
2. M.P. Allen and D. J. Tildesley, Computer simulation of liquids, Clarendon Press, Oxford, 1990.
3. U. Eichler, M. Brandle and J. Sauer, J. Phys. Chem., 101 (1997) 10035.
4. D. H. Olson, G. T. Kokotailo, S. L. Lawton, W. M. Meier, J. Phys. Chem. 85 (1981) 2238.
5. C. Bussai, S. Hannongbua, R. Haberlandt, J. Phys. Chem. B 105 (2001) 3409
6. W. S. Benedict, N. Gailar, E. K. Plyler, J. Chem. Phys. 24 (1956) 1139.
7. M. J. Frisch, G. W. Trucks, M. Head-Gordon, P. M. W. Gill, M. W. Wong, J. B. Foresman, B. G. Johnson, H. B. Schlegel, M. A. Robb, E. S. Replogle, R. Gomperts, J. L. Andres, K. Raghavachari, J. S. Binkley, C. Gonzalez, R. L. Martin, D. J. Fox, D. J. Defrees, J. Baker, J. J. P. Stewart, J. A. Pople, *Gaussian 98*, Revision A, Gaussian, Inc., Pittsburgh, P A, 1998.
8. C. Bussai, S. Hannongbua, S. Fritzsche, and R. Haberlandt, Chem. Phys. Lett. in press.
9. W. L. Jorgensen, M. E. Cournoyer, J. Am. Chem. Soc. 101 (1978) 4942.
10. G. Karlström, P. Linse, A. Wallqvist, B. Jönsson, J. Am. Chem. Soc. 105 (1983) 3777.
11. S. Udonsub, S. Hannongbua, J. Chem. Soc. Faraday Trans. 93 (1997) 3045.
12. P. Bopp, G. Jancso, K. Heinzinger, Chem. Phys. Lett. 98 (1983) 129.

13. D. Wolf, P. Keblinski, S. R. Phillpot, J. Eggebrecht, J. Chem. Phys. 110 (1999) 17.

14. H. Dufner, S. M. Kast, J. Brickmann, M. Schlenkrich, J. Comput. Chem. 18 (1997)

15. S. Fritzsche, R. Haberlandt, J. Kärger, H. Pfeifer, K. Heinzinger, Chem. Phys. Lett. 198 (1992) 283.

16. J. Kärger, H. Pfeifer and W. Heink, "Principles and Application of Self-Diffusion Measurements by Nuclear Magnetic Resonance", in Advances in Magnetic Resonance, Vol. 12, Academic Press: New York, 1988.

17. R. Haberlandt, J. Kärger, Chem. Eng. J. 74 (1999) 15.

18. S. Fritzsche, M. Wolfsberg, R. Haberlandt, *submitted to Chem. Phys.*

19. J. Kärger, J. Phys. Chem. 98 (1991) 5558.

20. S. Jost, N. K. Bär, S. Fritzsche, R. Haberlandt, J. Kärger, J. Phys. Chem. B 102 (1998) 6375.

21. S. Fritzsche, R. Haberlandt, J. Kärger, H. Pfeiffer, M. Wolfsberg, K. Heinzinger, Chem. Phys. Lett. 198 (1992) 283.

22. C. Bussai, H. Liu, S. Vasenkov, S. Fritzsche, S. Hannongbua, R. Haberlandt, J. Kärger, *Appl. Catal. A-Gen, in press*.

APPENDIX V

Computer Simulations of Water in Zeolites

Chuenchit Bussai, Steffen Jost, Reinhold Haberlandt,
Supot Hannongbua

Computer Simulations of Water in Zeolites

C. Bussai[a,b], R. Haberlandt[b], S. Hannongbua[a], S. Jost[b]

[a]*University Leipzig, Institute for Theoretical Physics, Augustusplatz 10-11, D-04109 Leipzig, Germany*
[b]*Department of Chemistry, Faculty of Science, Chulalongkorn University, Bangkok 10330, Thailand*

The complex topic of water in zeolites is viewed from completely different points: On the one hand, quantum chemical calculations at the Hatree-Fock and MP2 levels have been performed to investigate water-silicalite interaction as well as the energy barrier and water orientations during diffusion into and in the silicalite. The silicalite-water pair potential has been developed using 1.000 ab initio data points. The results indicate how water molecules move and turn during movement through the center of the silicalite pore. The energy barriers for water molecules to enter the pore and to diffuse from one channel to the other channel have been examined. It was found that water molecules enter and leave the pores preferably by pointing its dipole vector towards the center of the cavity. Calculations have been performed using extended 6-31G and 6-31G* basis sets with BSSE (basis set superposition error) corrections. On the other hand we present molecular dynamics simulations with a well established empirical water model [1] in the natural zeolite chabazit. Both the water molecule and the zeolite lattice are modelled flexible. The diffusion and the configuration of the water molecules inside the zeolite are examined.

1. Introduction

As water plays a strong and essential role as well for absorption as for catalytic properties of zeolites [2,3], the water-zeolite interaction is of great interest. Water molecules facilitate the exchange of the charge-compensating cations, essential for the industrial catalysts. In addition, all naturally zeolites are hydrated. The only available data on the water-silicalite interactions are experimental measurements by Flanigen et al. [4] and Vigne-Maeder et al. [5] which reported the initial isostatic heat of adsorption of 6 kcal/mol and the mean heat of adsorption of the first four water molecules of 9.6 kcal/mol, respectively. Vigne-Maeder et al. has also reported that an average water-silicalite interaction at 300 K is -12.5 kcal/mol and the approximated energy barrier for diffusion through the intersection between the straight and the zig-zag channels of the silicalite is 8 kcal/mol. The aim of this study is to use

quantum chemical calculations at the Hartree-Fock(HF) and MP2 levels to determine the water-silicalite interactions in order to understand water orientation, preferable binding sites and energy barriers during the movement into and in the silicalite pores. In addition, 1,000 ab initio data points have been fitted to an analytical form. The obtained pair potential was, then, used in molecular dynamics simulation. The natural zeolite chabazit is of special interest for the research about
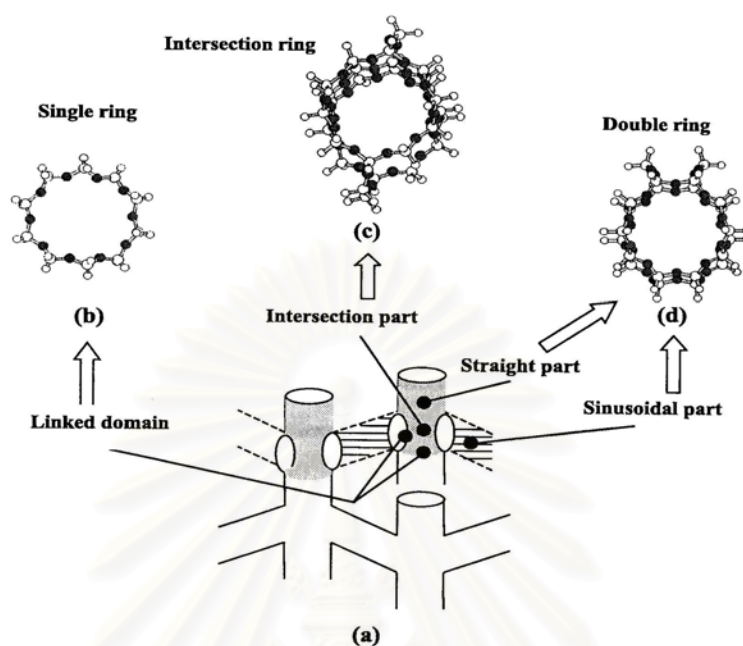
Figure 1. Schematic representations of the (a) silicalite crystal structure, (b) linked domain, (c) straight and sinusoidal channels and (d) intersection more details see text.

diffusion because of its anisotropic structure. The diffusion of water in chabazit was measured by Bär and Kärger [6] and they found an anisotropie of the diffusion, which does not fit to the crystal structure of chabazit. For this part of the study a well established empirical water model \cite{bjh83} is used. Vibrations are taken into account as well for the lattice as for the water molecule.

2. Computational details

2.1 Quantumchemical calculations

Ab initio calculations at the HF and the MP2 levels have been performed for the water-silicalite system using extended 6-31G and 6-31G* basis sets [7,8]. Experimental geometries of water [9] and silicalite [10] have been used and kept constant throughout the calculations. An error due to the unbalance of the basis set, BSSE, has been also examined and taken into consideration. All calculations are performed using the G98 program [11]. The silicalite crystal structure was represented by three fragments (Figures 1b-1d), called single, double and intersection rings. The sinusoidal channels and the main part of the straight channels of the crystal (Figure 1a), in which their inner surfaces are almost identical, were represented by the double 10-oxygen membered ring (Figure 1d). This fragment (mentioned later, for simplicity, as double ring) consists of 30 O and 22 Si atoms. The bigger fragment (35 O and 29 Si atoms) contains parts of the sinusoidal and the straight channel. It is used to represent the intersection and named intersection ring (Figure 1c). Note that, the remaining valence orbitals of the silicon atoms of both fragments are filled up by hydrogen atoms. To investigate the energy barrier via the diffusion from the intersection to the

straight or to the sinusoidal channels, the water-silicalite interaction in the linked domain has been also calculated. The selected fragment is the 10-oxygen membered ring (Figure 1b).

Numerous configurations of water molecules have been generated inside the three fragments shown in Figure 1. To search for the optimal binding site, interactions between water and silicalite for each fragment have been calculated outside and inside the windows.

2.2 MD-simulations

The molecular dynamics simulations use the BJH-model [1], a flexible valence force water model. The zeolite chosen for this work is chabazite, a natural zeolite, which is especially interesting for diffusion because of its anisotropic structure. The calculations are done with flexible framework. The interaction potentials are taken from the literature: For the lattice vibrations, the model of Suffritti and Demontis [12] is used. The missing interactions are taken from Probst et al. [13].

As a starting point for the zeolite lattice, data from the X-ray diffraction study of Smith and Rinaldi [14] is used. Before starting the simulation, the lattice is relaxed with respect to the model for lattice vibrations which is used.

Due to the very fast intramolecular vibrations of the water molecules, a very short time step, $\Delta t = 0.25$ fs had to be used. The simulation run was 2000000 steps long, simulating 0.5 ns. The MD-box is orthogonal, with x=26.4 Å, y=22.683 Å and z=30.2 Å, containing 6 rhombic unit cells with 39 water molecules. In the preceding thermalization period, the temperature is controlled to produce a well defined physical starting situation at T=300 K. During the evaluation period of the run, no additional thermalisation takes place.

The program is written in Fortran90 and the simulations were carried out on HP J5600.

3. Results and discussion

3.1 Optimal Method and Optimal Diffusion Path

The calculated results indicate clearly that the correlation (MP2) method and the BSSE correction do not play an essential role in predicting the geometry of the system. However, in order to increase the reliability of the interaction energies, all data points reported in this study are the results of the HF calculations with BSSE corrections. In addition, the effect of the small framework fragment on the interaction energy dominates at long distances (outside the channel) and is negligible in the region around the optimal distances (inside the channel). It is interesting to note here, therefore, that diffusion of water molecule through center of the window of the silicalite is a kind of rolling movement. The molecule must move and turn in order to find the optimal route. In addition, water enters and leaves the pores by pointing its dipole vector towards the center of the cavity.

Another energetically favourable pathway for a water molecule to move in the silicalite channel, is a kind of site hopping. It can attach to a specific binding site on the window first. Then it enters the pore, finds the next binding site and moves from one to the next site along the inner wall of the channel. Ab initio data show that

- the first binding site for a water molecule before entering the silicalite channel is to coordinate to the oxygen

atom of the linked domain to form a single hydrogen bond outside the pore

- it makes no significant difference for a water molecule to enter the pore along the inner wall of the sinusoidal or straight channels, or the intersection, and

- moving of water molecule along the inner wall of the channels is less preferable than that through center of the pore.

3.2 Energy Barrier to Enter and to Cross the Channels

To investigate the energy barriers for water molecules to enter the silicalite channels, the most stable water-silicalite interaction energies inside and outside the pores have been examined and compared. The energy data indicates clearly, that water molecules must bind to the oxygen membered ring on the window first, to enter the pore of the silicalite via the linked domain (represented by the single ring). The situation is different for the intersections. I.e., no difference has been found for water molecules between moving along the central line or starting binding to the window before entering into the silicalite via this channel. The energy difference between the two processes lies within the thermal fluctuations at room temperature. Similar investigation has been used to examine the energy barriers for water molecules to move from one channel to the other inside the silicalite. With the most stable interaction energy for encapsulation of a water molecule in the three channels, the diffusion process was schematically drawn in Figure 2. The barrier is placed at the linked domain which is represented by the single ring (Figures 1a and 1b). The amount of energy required to move from the straight or the sinusoidal channel to the intersection and back is 1.72 and 2.93 kcal/mol which is

Energy (ΔE)

Linked domain
(Single ring)

ΔE=0.59 kcal.mol^{-1}

ΔE=0.9 kcal.mol^{-1}

Straight and Sinusoidal channels
(Double ring)

Intersection channel
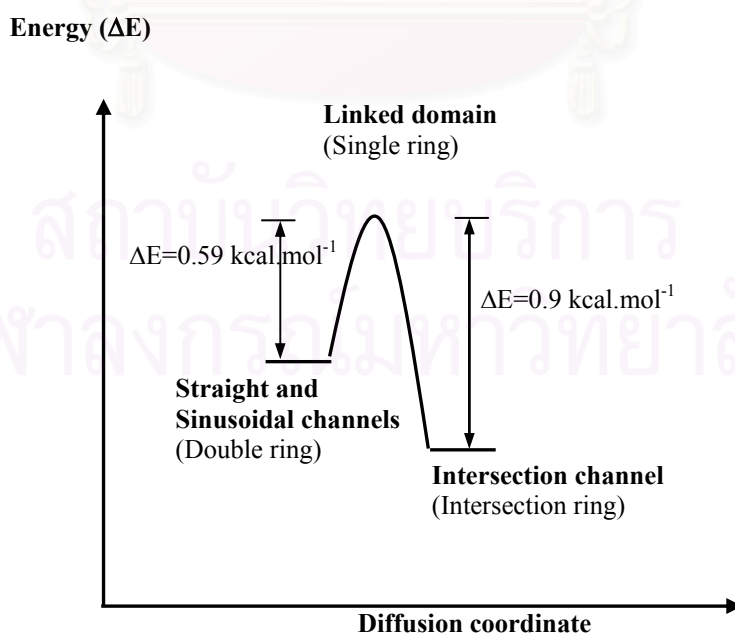(Intersection ring)

Diffusion coordinate

Figure 2. Changes of the water-silicalite interaction energy via the diffusion in the silicalite channels.

equivalent to the mean kinetic energy at temperature of about 800 K and 1440 K, respectively. These values are much smaller than that of 8 kcal/mol yielded from the development of the water-silicalite potential map using the empirical method [5].

3.3 Ab initio Silicalite-Water Pair Potential

To develop the silicalite-water pair potential, based on ab-initio SCF calculations, the experimental geometry of silicalite and the water molecules was treated as rigid throughout the calculations. The water molecule was placed at numerous positions inside the fragments. The obtained 1,000 SCF data points were fitted to an analytical function of the form:

$$\Delta E(W,S) \quad = \sum_{i}^{3}\sum_{j}^{288}\left\{\frac{A_{ij}^{ab}}{r_{ij}^{6}} + \frac{B_{ij}^{ab}}{r_{ij}^{12}} + \frac{C_{ij}^{ab}}{r_{ij}^{X}} + \frac{q_{i}q_{j}}{r_{ij}}\right\} \quad (1)$$

where 3 and 288 denote the numbers of atoms of water (W) and the silicalite (S) lattice, respectively. A_{ij}, B_{ij} and C_{ij} are fitting constants and r_{ij} is the distance between an atom i of water and an atom j of silicalite, q_i and q_j are the atomic net charges of the atoms i and j in atomic units, obtained from the population analysis of the isolated molecules. Superscripts a and b on the fitting parameters have been used to classify atoms of equal atomic number but different environment conditions, for example oxygen and silicon atoms of silicaite in the different channels. The third polynomial term C_{ij}/r^{8}_{ij} was added in order to obtain better numerical fitting. The silicalite-water fitting parameters were summarized in Table 1.

Table 1 Final optimization parameters for the *ith* atoms of water interacting with the *jth* atoms in different channels (subscripts *sd* andt *st* demote sinusoidal and straight channels, respectively) of the silicalite lattice (energy in Kcal.mol^{-1}, distance (r_{ij}) in Å and atomic net chagres (q) in atomic unit).

i	j	q_i	q_j	A(Å^6 kcal./mol)	B (Å^{12} kcal/mol)	C (Å^8 kcal/mol)
O	Si$_{sd}$	-0.86629	1.56986	-18023.70045	-2548026.49363	241557.06465
O	Si$_{st}$	-0.86629	1.67270	6035.98387	117801.34659	-21871.06318
O	O$_{sd}$	-0.86629	-0.78493	7592.37634	275412.63747	-50145.22438
O	O$_{st}$	-0.86629	-0.83653	-1605.57745	-26996.92676	8135.57650

i	j	q_i	q_j	A(Å^6 kcal./mol)	B (Å^{12} kcal/mol)	C (Å^8 kcal/mol)
H	Si$_{sd}$	0.43314	1.56986	-7525.63685	-192955.39323	2074.08326
H	Si$_{st}$	0.43314	1.67270	-8362.88299	-100800.83750	34694.38682
H	O$_{sd}$	0.43314	-0.78493	503.177431	-282.15505	-396.99593
H	O$_{st}$	0.43314	-0.83653	2074.08323	5641.19273	-5018.41068

3.4 MD-Simulations

The MD simulations which have been performed so far, turned out to be too short to determine the diffusion coefficient with a good reliability. For the elements of the diffusion tensor, this is valied even more. Up to now the diffusion coefficient can be only approximated $D \approx 3*10^{-11}\ m^2/s$
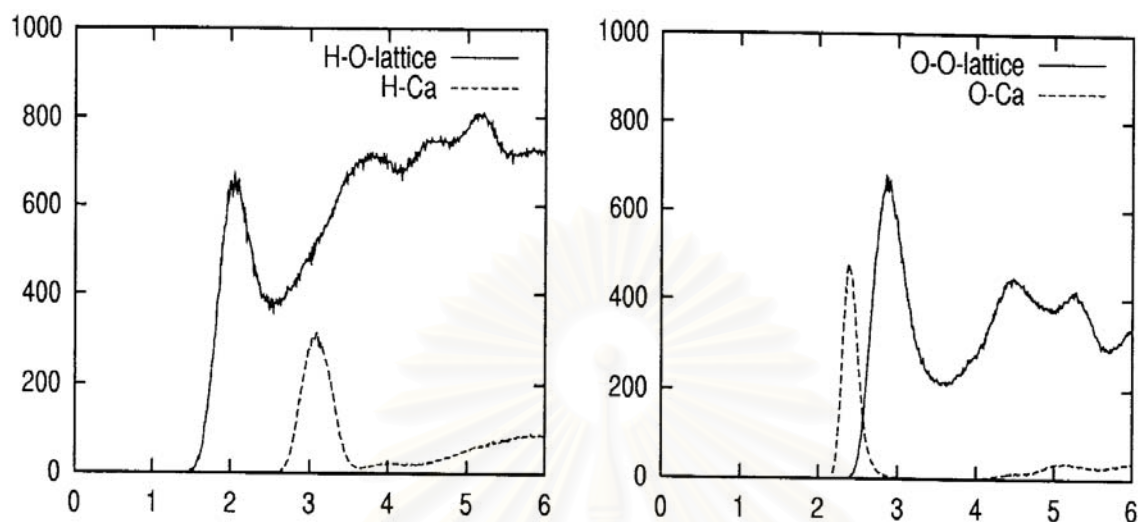
Figure 3. Radial distribution of the water atoms with the lattice oxygen and the calcium in arbitrary units over the distance in Å.

with an error of up to 100 %. Therefore longer simulations will be performed to

The structures of the radial distribution functions (rdf's) give some insight in the coordination of the guest molecules in the zeolite framework. The rdf $O(H_2O)$-Ca shows only one peak, indicating, that there

improve the reliability of the results and to analyse the anisotropy of the diffusion.
is only one hydration shell around the Ca-Ion. This can be seen in den H-Ca-rdf as well. The rdf of the water atoms with the framework oxygen show some more peaks, but those are probably caused by the next
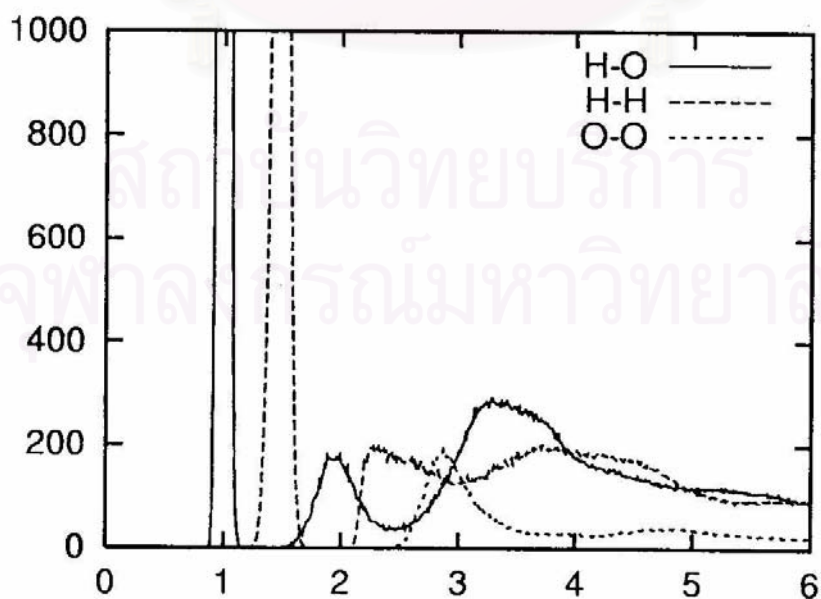

Figure 4. Radial distribution of the water atoms with each others in arbitrary units over the distance in Å.

oxygen atoms in the framework and by a second hydration shell. The fact, that the Ca-water rdfs show only one peak, means, that the water molecules are at this low loading in the middle of the two Ca-Ions in each cavity.

For the water-water rdfs the peaks can be easily identified for a coordination of just two atoms. Only the O-O-rdf shows a slight second peak, indicating a higher order of coordination.

4. Acknowledgements

REFERENCES

1. P. Bopp, G.Jancso, K. Heinzinger Chem. Phys. Lett., 98 (1983) 129.

2. Mikhailenko, S. D.; Kaliaguine, S.; Ghali, E. Microporous Mater. 11 (1997) 37.

3. Komiyama, M.; Kobayashi, M. J. Phys. Chem. B 103 (1999) 10651.

4. Flanigen, E. M.; Bennett, J. M.; Grose, R. W. Nature 271 (1978) 512.

5. Vigne-Maeder, F.; Auroux, A. J. Phys. Chem. 94 (1990) 314

6. Bär, N.-K.; Kärger, J.; Pfeifer, H.; Schäfer, H.; Schmitz, W. Mic. and Mes. Mat. 22 (1998) 289

7. Hehre, W. J.; Random, L.; Schleyer, P. V. R.; Pople, J. A. Ab Initio Molecular Orbital Theory; Wiley: New York, 1987.

8. Francl, M. M.; Petro, W. J.; Hehre, W. J.; Binkley, J. S.; Gordon, M. S.; Defrees, D. J.; Pople, J. A. J. Chem. Phys. 77 (1982) 3654.

9. Benedict, W. S.; Gailar, N.; Plyler, E. K. J. Chem. Phys. 24 (1956) 1139.

10. Olson, D. H.; Kokotailo, G. T.; Lawton, S. L.; Meier, W. M. J. Phys. Chem. 85 (1981) 2238

11. Frisch, M. J.; Trucks, G. W.; Head-Gordon, M.; Gill, P. M. W.; Wong, M. W.; Foresman, J. B.; Johnson, B. G.; Schlegel, H. B.; Robb, M. A.; Replogle, E. S.; Gomperts, R.; Andres, J. L.; Raghavachari, K.; Binkley, J. S.; Gonzalez, C.; Martin, R. L.; Fox, D. J.; Defrees, D. J.; Baker, J.; Stewart, J. J. P.; Pople, J. A. Gaussian 98, Revision A, Gaussian, Inc., Pittsburgh, P A, 1998.

12. Demontis ,P.; Suffritti, G.B.; Quartieri, S.; J. Fois , E.S.; Gamba, A. Phys. Chem 92 (1988) 867

13. Probst, M.M.; Radnai, T.; Heinzinger, K.; Bopp, p.; Rode, B.M. J. Phys. Chem. 89 (1985) 753

14. Smith, J.V.; Rinaldi, F. Acta Cryst. 16(1963) 45

APPENDIX VI

Formation of Low Density Water Cluster in the Silicalite-1 Cage as Studies by Molecular Dynamics Simulations

Chuenchit Bussai, Siegfried Fritzsche, Reinhold Haberlandt, Supot Hannongbua

Formation of Low Density Water Cluster in the Silicalite-1 Cage as Studies by Molecular Dynamics Simulations

Chuenchit Bussai[a,b], Siegfried Fritzsche[b], Reinhold Haberlandt[b],

Supot Hannongbua[a,*]

[a]Department of Chemistry, Faculty of Science, Chulalongkorn University, Bangkok 10330, Thailand.

[b]Department Molecule Dynamics/Computersimulations, Faculty of Physics and Geoscience, University of Leipzig, Linnéstr.5,04103,Leipzig,Germany.

TOTAL PAGE 28
TOTAL TABLES 2
TOTAL FIGURES 8

[*]To whom correspondence should be addressed. Email: supot.h@chula.ac.th

Abstract: Series of molecular dynamics simulations have been performed in order to examine changes of structural and dynamical properties of water molecules in silicalite-1 as a function of temperature and loading. The *ab initio* fitted silicalite-1/water potential which is newly developed [6] and the BJH flexible water/water potential [37] have been employed. The water loading was varied from 1 to 8 water molecules per intersection, equivalent to 8 to 64 molecules per simulation cube. The simulations have been carried out at 298 and 393 K. The results show that the water structure inside the silicalite-1 cages changes dramatically as a function of loading. We found that the probability of water molecules to reside in the straight channel is always higher than that to find them in the sinusoidal channels. The formation of water clusters has been detected for high loading. The observed clusters are found to display pure water like-structure. We name it "low density cluster" due to the following reasons: (*i*) The cluster consists of 5 water molecules (4 in the first hydration shell of the central one) which is consistent with that of pure water; (*ii*) Molecules in the cluster are not coordinated together via hydrogen bond. The radius of the first hydration shell of 3.35 Å is 0.5 Å longer than that of pure water; (*iii*) Molecules in the cluster are less flexible than those of pure water. In terms of dynamical properties, for low loadings a preferential diffusion path is observed along center of the channel tube. The water molecules were detected to diffuse closer to the surface when the concentration is higher than 6 molecules per intersection. The diffusion coefficient of water decreases when the concentration increases. The *D* values for all concentrations at 393 K are higher than those of 298 K. The temperature dependence almost disappears at a loading of 8 water molecules per intersection. In addition, the anisotropic diffusion is less pronounced for water in silicalite-1 in comparison to that of non-polar molecules.

1. Introduction

The dynamical behavior of molecules in zeolites and other microporous solids have become attractive subjects for both fundamental investigations and applied researches. The regular structure and numerous technical applications as catalysts, ion exchangers, adsorbents and host materials for advanced technologies have made zeolites to a particularly important candidate of research.[1,2,3] Water molecules in zeolites, even at small amount, can significantly influence properties of zeolite-like materials during some technological processes and water can also have an effect to the adsorption of other molecules.[4] Understanding of such phenomena cannot be obtained purely by experimental techniques due to the complex interplay between many physical and chemical processes taking place in the zeolites.[5] As a complementary technique in obtaining insight into the microscopic details, many MD studies on the interaction of water to various zeolites have been performed.[4-17]

To our best knowledge, most of the molecular dynamics simulations for water in zeolites have been reported by Demontis et al.,[18-20] and Leherte et al.[21-26] In the late 1990s, the sodium ions in hydrated zeolite A have been examined for the ranges of hydrations.[27-29] The self-diffusion coefficient at full hydration obtained from this simulation is 3 times higher than that obtained from experiments.[27] More recently, conformation of the triple helix of water in VPI-5, aluminophosphate-type material formation has been investigated by Fois et al.[10] through Car Perrinello molecular dynamics simulations. It was found that the helice lies close to the channel walls and avoids the channel center. Empirical potential functions including electronic-field-dependent terms have been developed and applied by Cicu et al.[13] to simulate classically water in natrolite. It was found that the electric-field-dependent terms in the intramolecular potential of water can improve the results in comparison to experimental one. Termath et al.[30] have performed *ab initio* molecular dynamics simulations (AIMD) for H_2O and H_3O^+ in HSAPO-34 and detected water cluster, $H_3O^+(H_2O)_2$, i.e., an acid-base reaction in HSAPO-34 requires at least three water molecules per two nearby acidic sites. More recently, the AIMD simulations of water-HSAPO-34, that have been studied by Jeanvoine et al.[31] in order to elucidate the water behavior to Bronsted acidic sites, stated the demand on a water dimer for the occurrence of proton transfer in the cage, hence the basicity of a hydrogen-bonded water dimer is required. However, such AIMD simulation is indeed still

computer time expensive. This requires the restriction on few 100 atoms system, and the typical run length of some picoseconds.

For the de-aluminated zeolite silicalite-1, the only available data is in terms of heat of adsorption. Vigné-Maeder and Auroux[32] had drawn the potential map in which the average energy is expressed as a sum of electrostatic, polarization, dispersion, and repulsion interactions between the atom pairs. The calculations yield heat of adsorption for water in silicalite-1 at 300 K of -12.5 kcal.mol^{-1}. Recently, Turov et al.[33-36] have measured water adsorption in silicalite-1 by H1 NMR and thermogravitric methods and observed a high chemical shift. This corresponds to the formation of more than three hydrogen bonds of the attributed water in the pores.

As a matter of fact, all previous classical simulations[11-13,15-29] of water in zeolites use the intermolecular potentials based on empirical force-field parameterizations. Some doubts arise when the potentials were used to represent the interaction between water and zeolites in which hydrogen bonding is very important as this is better represented by *ab initio* derived potentials. Such potentials are therefore used in the present paper. In addition, the water-water interaction is represented by an existing potential,[37] which is almost developed using *ab initio* data. It is known that unbalance of the pair potentials, water-zeolite and water-water, can easily lead to artificial results. To avoid this discrepancy, a fully *ab initio* fitted potential for water/silicalite-1 has been developed for the first time using fairly large fragments of 10T 20T, and 27T of silicalite-1, where T refers to silicon of corner sharing TO_4 tetrahedra in zeolite crystalline.[7] The function has been applied to study the diffusion coefficients of water in silicalite-1 which are in satisfactory agreement with those observed using PFG NMR measurements.[5]

In this paper, we present dynamical and structural properties of water molecules inside the siliceous ZSM-5 at various loadings with the aim of achieving their microscopic understanding. The *ab initio* fitted water/silicalite-1 model[6] based on quantum chemical methods have been employed.

2. Computational and Calculation Details

2.1. Structure of Silicalite-1

The silicalite-1 crystal structure used in the present investigation is characterized by a 3-dimensional channel system, whose symmetry group is *Pnma*. Its

framework structure incorporates two different channel systems, each defined by 10-oxygen-membered ring. A straight channel with an elliptical cross section of about 5.2-5.7 Å is parallel to the crystallographic axis *b*, and sinusoidal channels with almost circular cross section of 5.4 Å run along the crystallographic axis *a* (Figure 1). The resulting intersections are stretched out to cavities up to 9 Å of diameter. The crystallographic cell[38] contains 288 atoms ($Si_{96}O_{192}$), with lattice parameters *a* = 20.07 Å, *b* = 19.92 Å and *c* = 13.42 Å.

2.2. Potential Functions

The potential proposed by Bopp, Jancso and Heinzinger[37] was employed to describe water-water interactions. These functions are originally developed from the central force model by Lemberg and Stillinger.[39,40]

The silicalite-1/water pair potential was comprehensively developed by fitting almost 1,000 *ab initio* data points at the Hartree Fock 6-31G* level to the following functional form,[6,7]

$$\Delta E(\text{w,s}) \quad = \quad \sum_{i}^{3} \sum_{j}^{288} \left\{ \frac{A_{ij}^{ab}}{r_{ij}^{6}} + \frac{B_{ij}^{ab}}{r_{ij}^{12}} + \frac{C_{ij}^{ab}}{r_{ij}^{3}} + \frac{q_i q_j}{r_{ij}} \right\}, \tag{1}$$

where 3 and 288 denote the numbers of atoms in a water molecule (w) and the silicalite-1 (s) unit cell, respectively. The constants A_{ij}, B_{ij} and C_{ij} are fitting constants and r_{ij} is the distance between atom *i* of water and atom *j* of silicalite-1. Also, q_i and q_j are the atomic net charges of atoms *i* and *j* in atomic units, as obtained from the population analysis[41] of the isolated molecules in the quantum chemical calculations. Superscripts *a* and *b* on the fitting parameters have been used to classify atoms of equal atomic number but different environmental conditions, for example, oxygen and silicon atoms of silicalite-1 in the different channels. The third polynomial term (C_{ij}/r^3_{ij}) was added in order to obtain better numerical fitting. More detailed investigations as well as the silicalite-1/water fitting parameters are given elsewhere.[7]

2.3. Molecular Dynamics Simulations

The equations of motion were integrated using the Verlet algorithm[42] with time step of 0.5 fs at 298 and 393 K. Simulations[43,44] have been performed for

systems containing 1 - 8 water molecules per intersection, equivalent to 8 – 64 molecules per simulation cube, which contains 2 silicalite-1 unit cells. The NVT ensemble was employed after an aging of 0.5 ps where the velocities of the particles were rescaled to thermalize the system. Periodic boundary conditions were applied. The pair interactions were computed in the minimum image convention with a spherical cutoff of 10 Å. The length of each trajectory was 10 ns. The fluctuations of the total energy of the system were less than 0.005%. According to the long-range interactions, which are columbic forces, the shifted force strategy has been employed. Hence, Ewald summations can be avoided in this study in which the total charge of the system is zero.[45,46,12]

3. Results and Discussions

3.1. Structural Properties

3.1.1. Silicalite-Water Radial Distribution Function (RDF)

(1) Averaged RDF for All Channels

In order to investigate structural data of water molecules via diffusion in zeolite silicalite-1 at various loadings (n_{1d}), the radial distribution functions (RDFs) from surface oxygen atom (O_S) to oxygen (O_W) and hydrogen (H_W) atoms of water have been evaluated and plotted in Figure 2. The change of the water behavior has been exhibited by the O_S- O_W RDFs in which the transition takes place between the loadings of 6 and 7 water molecules per intersection.

The O_S-O_W RDFs for $n_{1d} \leq 6$ display first broad maxima around 4.2 Å, followed by a pronounced shoulder at around 5.8 Å and second broad peaks centered at 8.4 Å (Figure 2a). Due to the cylinder-like structure with the diameter of 8.2 Å (Figure 1) of silicalite-1 channels, water molecules lied under the first maximum and the established shoulder of the O_S-O_W RDFs can be assigned to molecules moving along the center of the tube. The distances from O_W to O_S of the nearest 10-oxygen membered-ring and their adjacent rings are between 4 to 6 Å. This is in good agreement with that predicted by *ab initio* calculations which state that central line is the optimal path for water molecule to travel along the silicalite-1 channels.[7]

A transition takes place for the $n_{1d} > 6$, in which the first broad O_S-O_W peak splits into two sharp peaks centered at 3.45 Å and 5.25 Å. This feature indicates dramatic changes of the water behavior in silicalite-1 channels. With concentrations

higher than 6 water molecules per intersection, the water molecules are forced by their repulsion to stay out of the central line region. This information cannot be obtained from *ab initio* calculations because only the interaction of a pair or only a few molecules can be taken into consideration. It is interesting to note here, therefore, that these two peaks are contributed from the same set of water because the sum of O_S-O_W distances for O_W centered at 3.45 Å far from O_S on one side and 5.25 Å from the opposite side of the 10-oxygen membered ring are, somehow, equivalent to the diameter of 8.2 Å of the tube.

Some comments could be made concerning an appearance of the O_S-O_W peak at 3.45 Å for $n_{1d} > 6$. The sharp, pronounced and discrete characters of the peaks are usually due to the tight binding between the two molecules. This is surely not true for the water/silicalite-1 system in which the interaction energies derived from *ab initio* calculations or the *ab initio* fitted potential for any configurations where the O_S-O_W distance = 3.45 Å of about -4.0 kcal.mol^{-1} is almost equal to that at the optimal configuration of the water dimer of -5.6 kcal.mol^{-1}, i.e., the water-water binding is superior to the surface-water one. Therefore, the formation of this peak can be assigned to a cluster formation of water molecules. Repulsion among molecules in the cluster in a limited space inside the silicalite-1 channels, leads not only to a shift of water positions out of the central line but also to a lower flexibility of their positions. As a consequence of the cluster formation and the repulsion of the water molecule in a limited space, the O_S-O_W RDF starts to be detected at shorter distance, when the concentration increases. The investigation and the discussion on the cluster formation are given in more details in the next section of water-water radial distribution functions.

Considering the O_S-H_W RDFs in Figure 2b, the plots for all loadings show corresponding RDFs with established shoulders around 3.2 Å, and first maxima around 5.2 Å. As a function of the water loading, the following conclusions can be made (*i*) An appearance of the first pronounced O_S-H_W shoulder at shorter distance than that of the O_S-O_W first peak implies that water molecules point their hydrogen atoms toward the inner surface of silicalite-1.; (*ii*) With the distances to the first peak of the O_S-O_W RDFs of 3.4 Å and the O_S-H_W shoulder of distances of both peaks mentioned earlier, it can be concluded that hydrogen bonding between water molecules and the inner surface of silicalite-1 cannot be formed. (*iii*) Broaden of these peaks and their shoulders indicate a flexibility of water molecules in terms of both

their positions and orientations. This finding confirms the *ab initio* results which suggest changes of water orientations via the diffusion in the silicalite-1 channels;[7] (*iv*) The same reasons as that of the O_S-O_W RDFs, the O_S-H_W RDF for low loadings start to be detected after those of high loadings. This is also true for the distance to the first shoulder of the O_S-H_W RDFs while their first peaks appear at the same position.

(2) Separated RDF for Each Channel

To understand more details of the water behavior in different channels, the O_S-O_W and O_S-H_W RDFs for each channel have been evaluated. The results are given as examples in Figures 3a and 3b for n_{ld} = 1 and 8, respectively. Here, the notation O_s representing oxygen atoms of the silicalite-1 surface were replaced by O_{It}, O_{St} and O_{Sd} for the intersection, straight and sinusoidal oxygens, respectively. An average O_S-O_W and O_s-H_w RDFs for both loadings are also given for comparison. The following conclusions can be extracted from the plots.

In terms of peak height, which give information on the probability of finding water molecules residence in the investigated channel, the detected order is intersection > straight > sinusoidal. This conclusion is valid for the RDFs from silicalite-1 surface to both oxygen and hydrogen atoms of water and both n_{ld} = 1 and 8. Note that, the averaged O_S-O_W and O_S-H_w RDFs are not able to compare with those of the separated channels because the number density, ρ (ρ = n/V where n is number of water molecules moving in each channel and V denotes the volume of the simulation cube), for each channel is not known. Therefore, the separated RDFs are not possible to be properly normalized and the total number of water molecules in the simulation cube, N, was used instead. In other words, the y-axis for the separated RDFs is in arbitrary unit. However, the peak position doesn't depend on the number density. What we learn from these facts is that the height of the O_{St}-O_W RDFs is similar to those of the O_{It}-O_W for n_{ld} = 1 (Figure 3a) and of O_{Sd}-O_W for n_{ld} = 8 (Figure 3b). At low loadings, the probabilities to detect water molecules in the intersection and the straight channels are considerably higher than that in the sinusoidal one, i.e., the diffusion along the straight channel is superior. The trajectory density plot for n_{ld} = 1 shown in Figure 4 confirms this statement. In contrary, no significant difference has been found for n_{ld} = 8 in the diffusion of water molecules along straight and sinusoidal channels.

Considering the RDFs in Figure 3 in terms of the peak positions and their shapes, all plots for separated RDFs are almost identical to those of averaged ones (for both concentrations and RDF to both oxygen and hydrogen atoms of water). The only separated RDF, the shape of which differs from the others, is the O_{Sd}-O_W one. In addition to the first peak at 4.2 Å of the averaged O_S-O_W RDF, the separated O_{Sd}-O_W RDF shows also a second peak at 5.6 Å. An appearance of this peak can be assigned to a contribution from the water molecules lying in the other channels. As it can be seen from the trajectory density plot (Figure 4), high density regions in the intersection and sinusoidal channels lay within a spherical shell with a radius of 5.3 Å with respect to the oxygen atoms of the sinusoidal channel. On the other hand, the contributions to the O_{It}-O_W and O_{St}-O_W RDFs are not visible because the water density in the sinusoidal channel is significantly lower than those in the other channels (Figure 3a).

3.1.2. Water-Water Radial Distribution Functions

In order to get insights how water molecules formulate inside the channels, the RDFs from oxygen atom (O_W) to oxygen (O_W) and to hydrogen (H_W) atoms of water at 8 loadings have been calculated and illustrated in Figures 5a and 5b respectively. The O_W-O_W RDF for pure water has been also given for comparison. Characteristics of the pronounced peaks of the RDFs are summarized in Table 2.

(1) The Oxygen-Oxygen Radial Distribution Function

Significant differences in the water structure can be observed, in comparison between that of pure water and water in the silicalite-1 cage. The O_W-O_W RDF for pure water shows a typical first peak at 2.80 Å, a second peak at 4.50 Å and a first shell coordination number (n) of 4.5 water molecules.[47]

Inside the cage, the O_W-O_W RDF changes dramatically as a function of loading. With the concentration of 8 water molecules per intersection, the plot shows a first sharp peak at 3.35 Å, a clear minimum at 5.25 Å and n = 3.9 water molecules. The distances to the first maxima (R_{M1}) and the first minima (r_{m1}) increase steadily if the concentration decreases. In addition, peak splitting starts to be detected at n_{ld} = 4 and separates at n_{ld} = 1. This indicates the changes of water structure in the cage of silicalite-1. An appearance of the first sharp peak for high loading is assigned to the formation of water clusters in the cage of silicalite-1 (details in the next paragraph)

while the splitted peak for low loading, especially for $n_{ld} = 1$, at 4.5 Å is interpreted as the water molecules lying separately in different channels.

In terms of first shell coordination numbers, a linear relation with the water concentrations has been detected and plotted in Figure 6. The coordination number of 3.9 for the loading of 8 water molecules per intersection is close to that of 4.5 for pure water.[47]

Some comments could be made concerning the O_W-O_W RDFs of pure water and of the high concentration of water in the silicalite-1 cage, especially for n_{ld} = 8, in which the shapes of the RDFs are totally similar and their first shell coordination numbers are about the same. It is known that bulk water forms a hydrogen bond network with the O-O distance, indicated by the first peak of the O_W-O_W RDF, of 2.80 Å. Therefore, it is evident from the O_W-O_W RDF of water molecules in the cage of silicalite-1, at least for n_{ld} = 8, that clusters are formed. Characteristics of the cluster can be figured out from the RDFs and summarized as the following: (*i*) Water molecules in the cluster in the cage of silicalite-1 don't bind together via hydrogen bond because the O-O distance of 3.35 Å (R_{M1} of the O_W-O_W RDF for n_{ld} = 8) which is about 0.5 Å longer than the typical hydrogen bond distance in bulk water, doesn't fit to the geometrical and the energetic criteria[48-50] of the hydrogen bond formation; (*ii*) The height of the O_W-O_W RDF indicates that the water clusters in the cage of silicalite-1 are less flexible than that of pure water. This observation can be understood in terms of their interactions with water molecules in the second solvation shell and with the silicalite-1 wall. Due to the limited space in the channel, the second solvation shell of water doesn't allow to be formed (the second peak at about 6.5 Å of the O_W-O_W RDF shown in Figure 5a for other loadings is due, surely, to the water molecules lying in different channels). This fact leads to a destruction of the hydrogen bond networks and, hence, a lower stability of the water clusters in the cage of silicaite-1 in comparison to those of pure water. Destructive contributions can be compensated by the interaction with the silicalite-1 wall in which the first shell molecules can be weakly held in place by the water/silicalite-1 potential. A conclusion is that, in spite of interactions among water molecules in the cluster, its stability which leads consequently to the sharp and pronounced O_W-O_W first peak at 3.35 Å, can be described in terms of destructive and constructive contributions from the second solvation shell and the silicalite-1 wall, respectively.; (*iii*) Based on the detailed description given in (*ii*), the size of the "low density water clusters", in terms

of spherical radius, r_{sphere}, (equivalent to R_{M1} of the O_W-O_W RDF), is expected to depend strongly on Δr, the difference between the radius of the pure water cluster and of the silicalite-1 channels, i.e., r_{sphere} increases as a function of Δr. In contrary, "high density water clusters" (R_{M1} of the O_W-O_W RDF > 2.80 Å) would be also possible to be formed for the high loading of water molecules in small-channel zeolite.

(2) Oxygen-Hydrogen Radial Distribution Function

Additional characteristics of the low density cluster of water molecules in the silicalite-1 cage can be extracted from the O_W-H_W RDFs, shown in Figure 5b. In good agreement with those of O_W-O_W RDF, the plots for high loadings show a pronounced shoulder centered at about 2.8 Å. This shoulder is less pronounced when the concentration decreases and disappears for $n_{ld} = 1$. An appearance of the clear shoulder at shorter distances than that of the first O_W-H_W main peak implies that $H_2O….H-OH$ is superior. This hydrogen-bond like configuration confirms the formation of low density clusters of water. Note, as already mentioned, that, the distances to the established shoulder of about 2.8 Å and to the first main peak of the O_W-H_W RDFs ranging from 3.75 Å to 4.05 Å for $n_{ld} = 1-8$, are surely not fit to any criteria of hydrogen bond formation,[48-50] i.e., it is too far to form hydrogen bond.

3.2. Dynamical Properties
3.2.1. Self-diffusion Coefficients

The self-diffusion coefficients are calculated from the particle displacements. The process of self-diffusion was quite generally related to the moments of the propagator.[51-53] The propagator $P(r,r_0,t)$ represents the probability density to find a particle at position r at time t if it was at r_0 at time $t = 0$. The nth moment of the propagator is defined by the relation[52]

$$\left\langle |r-r_0|^n \right\rangle = \int |r-r_0|^n P(r,r_0,t)\, dr. \tag{2}$$

Here, $P(r,r_0,t)$ is the solution of the diffusion equation for the initial concentration $C(r,t=0) = \delta(r-r_0)$. The elements of the diffusion tensor, corresponding to the x-, y-

and *z*-axes, are calculated. The overall diffusivity *D* is assumed to be one third of the trace of the diffusion tensor.

The self-diffusion coefficients of the water molecules as a function of the loading, varying from 1 to 8 water molecules per intersection, at 298 and 323 K are shown in Figure 7. Experimental values by PFG NMR measurements at the loading of 2 are also given for comparison. It can be seen that the simulation values overestimate the experimentally observed self-diffusivities of water by PFG NMR by approximately a factor of 2 at 298 K and of 4 at 393 K. Possibly experimental explanations for these discrepancies are discussed in terms of the contributions of extra-crystalline and intra-crystalline water to the measured signals by PFG NMR.[5] Note that the model employed in this study yields practically a one-to-one correspondence between the predicted (by the potential function) and the observed (by the ab initio calculation) interaction energies.

Changes of the water self-diffusion coefficients as a function of the loading can be seen from the plot (Figure 7). Similar to other small guest molecules such as, CH_4, CF_4, He, Ne, Ar, Xe and SF_6 in silicalite-1,[54] the diffusion of water decreases if the concentration increases. As expected, the diffusivities for all concentrations at 393 K are higher than those of 298 K. The temperature dependence is stronger at low concentrations, i.e., the difference of the diffusion coefficients obtained from the two temperatures is almost disappeared at the loading of 8 water molecules per interaction.

3.2.2. Anisotropic Diffusion

It has been observed experimentally and theoretically that the diffusion of alkanes and light gases in silicalite-1 is anisotropic.[54-58] To visualize this effect, a formula for the relation between the components of the diffusivity tensor (*D*) proposed by Kärger[58] has been applied,

$$\frac{c^2}{D_z} = \frac{a^2}{D_x} + \frac{b^2}{D_y}, \tag{3}$$

where *a*, *b* and *c* are the unit cell lengths. The deviation from Eqn. (3) can be accounted by introducing a parameter,[56,57,60]

$$\beta = \frac{c^2/D_z}{\left(a^2/D_x + b^2/D_y\right)}, \qquad (4)$$

where, $\beta = 1$ denotes random processing, e.g., a water molecule passing an intersection continues the diffusion path independent of how it gets to the intersection. A hint on preferentially continuative diffusion path either along in one or the same channel type is when $\beta > 1$. Vice versa, a higher diffusivity in z-direction, that is only possible by changes between straight and sinusoidal channels, occurs if $\beta < 1$. The interchange between the two channel types is more probable in this case.

Figure 8 visualizes the computed β as a function of the loading at the two temperatures. As expected, the βs for almost all concentrations and temperatures are higher than 1, indicating preferential continuation-diffusivity of the water molecule in the same silicalite-1 channels. This is in good agreement with examinations for xenon and alkane molecules in silicalite-1 in which $\beta = 1.2$ and 1.3 have been detected.[56] However, as the changes of the βs as functions of loading and temperature observed in the present paper are within the fluctuation limit, relations between these variables cannot be concluded.

The fact, that the continuation-diffusivity preferred by non-polar molecules in comparison to polar molecules in silicalite-1, can be due to the reason that the diffusion of a polar molecule is stronger influenced by its interaction with the silicalite-1 inner surface. Polar molecules are expected to approach closer to the channel wall than non-polar ones. Therefore, when a polar molecule gets into an intersection from a channel of type A, it expects to take the closest pore - which belongs to the channel of type B (while pores to the same type of channel are almost on the opposite side of the intersection) for discontinuation diffusion. This leads directly to decrease probability of taking the same channel type for the polar molecule, i.e., β for polar molecules is lower than that of non-polar molecules.

Acknowledgements

References:

1. Kärger, J.; Ruthven, D. M. *Diffusion in Zeolites and Other Microporous Solids*; Wiley: New York, 1992.

2. Ruthven, D. M. *Principles of Adsorption and adsorption Processes*; Wiley: New York, 1984.

3. Breck, D. W. *Zeolite Molecular Sieve*; Wiley: New York, 1974.

4. Turov, V. V.; Brei, V. V.; Khomenko, K. N.; Leboda, R. *Micropor. Mesopor. Mater.* **1998**, *23*, 189.

5. Bussai, C.; Vasenkov, S.; Liu, H.; Böhlmann, W.; Fritzsche, S.; Hannongbua, S.; Haberlandt, R.; Kärger, J. *Appl. Catal. A-Gen* **2002**, *232*, 59.

6. Bussai, C.; Fritzsche, S.; Hannongbua, S.; Haberlandt, R. *Chem. Phys. Lett.* **2002**, *354*, 310.

7. Bussai, C.; Hannongbua, S.; Haberlandt, R. *J. Phys. Chem. B* **2001**, *105*, 3409.

8. Bussai, C.; Haberlandt, R.; Hannongbua, S.; Jost, S. *Studies in Surf. Sci. Catal.* **2001**, *135*, 263.

9. Bussai, C.; Fritzsche, S.; Haberlandt, R.; Hannongbua, S. *Studies in Surf. Sci. Catal.* **2002**, *142B*, 1979.

10. Fois, E.; Gamba, A; Tilocca, A *J. Phys. Chem. B* **2002**, *106*, 4806.

11. Demontis, P.; Gulín González, J.; Suffritti, G. B.; Tilocca, A. *J. Amer. Chem. Soc.* **2001**, *123*, 5069.

12. Demontis, P.; Spanu, S.; Suffritti, G. B. *J. Chem. Phys.* **2001**, *114*, 7980.

13. Cicu, P.; Demontis, P.; Spanu, S.; Suffritti, G. B. ; Tilocca, A. *J. Chem. Phys.* **2000**, *112*, 8267.

14. Demuth, T. H.; Benco, L., Hafner, J.; Toulhoat, H. *Int. J. Quantum Chem.* **2001**, *84*, 110.

15. Pereira, J. C. G.; Catlow, C. R. A.; Price, G. D. *J Phys. Chem. A* **2001**, *105*, 1909.

16. Hill, J. R.; Minihan, A. R.; Wimmer, E.; Adams, C. J. *Phys. Chem. Chem. Phys.* **2000**, *2*, 4255.

17. Takaba, H.; Koyama, A.; Nakao, S. *J. Phys. Chem. B* **2000**, *104*, 6353.

18. Demontis, P.; Suffritti, G. B.; Quartieri, S.; Fois, E. S.; Gamba. A.; Morosi, G. *Mater. Chem. Phys.* **1991**, *29*, 357.

19. Demontis, P.; Suffritti, G. B. ; Quartieri, S.; Fois, E. S.; Gamba. A. *Zeolites* **1987**, *7*, 522.

20. Demontis, P.; Suffritti, G. B.; Alberti, A.; Quartieri, S.; Fois, E. S.; Gamba. A. *Gazz. Chim. Ital.* **1986**, *116*, 459.

21. Leherte. L.; André, J. M.; Derouane, E. G. ; Vercauteren, D. P. *Int. J. Quantum Chem.* **1992**, *42*, 1291.

22. Leherte. L.; André, J. M.; Derouane, E. G. ; Vercauteren, D. P. *Comput. Chem.* **1991**, *15*, 273.

23. Leherte. L.; André, J. M.; Derouane, E. G. ; Vercauteren, D. P. *Catal. Today* **1991**, *10*, 177.

24. Leherte. L.; André, J. M.; Derouane, E. G. ; Vercauteren, D. P. *J. Chem. Soc. Faraday Trans* **1991**, *87*, 1959.

25. Leherte, L.; André, J. M.; Vercauteren, D. P.; Derouane, E. G. *J. Mol. Catal.* **1989**, *54*, 426.

26. Leherte, L.; Lie, G. C.; Swamy, K. N.; Clementi, E.; Derouane, E. G.; Andre, J. M. *Chem. Phys. Lett.* **1988**, *145*, 237.

27. Faux, D. A. *J. Phys. Chem. B* **1999**, *103*, 7803.

28. Faux, D. A. *J. Phys. Chem. B* **1998**, *102*, 10658.

29. Faux, D. A.; Smith, W.; Forester, T. R.; *J. Phys. Chem. B* **1997**, *101*, 1762.

30. Termath, V.; Haase, F.; Sauer, J.; Hutter, J.; Parrinello, M. *J. Amer. Chem. Soc.* **1998**, *120*, 8512.

31. Jeanvoine, Y.; Angyan, J. G.; Kresse, G.; Hafner, J. *J. Phys. Chem. B* **1998**, *102*, 7307.

32. Vignemaaeder, F.; Auroux, A. *J. Phys. Chem.* **1990**, *94*, 316.

33. Turov, V. V.; Mironyuk, I. F. *Colloid Surf. A* **1998**, *134*, 257.

34. Turov, V. V.; Brei, V. V.; Khomenko, K. N.; Leboda, R. *Micropor. Mesopor. Mater.* **1998**, *23*, 189.

35. Turov, V. V.; Leboda, R. *Advan. Colloid Interface Sci.* **1999**, *79*, 173.

36. Turov, V. V.; Chodorowski, S.; Leboda, R.; Skubiszewska-Zieba, J.; Brei, V. V. *Colloid Surf. A* **1999**, *158*, 363.

37. Bopp, P.; Jancso, G.; Heinzinger, K. *Chem. Phys. Lett.* **1983**, *98*, 129.

38. Olson, D. H.; Kokotailo, G. T.; Lawton, S. L.; Meier, W. M. *J. Phys. Chem.* **1981**, *85*, 2238.

39. Lemberg, H. L. ; Stillinger, F. H. *J. Chem. Phys.* **1975**, *62*, 1677.

40. Stillinger, F. H.; Rahman, K. *J. Chem. Phys.* **1978**, *68*, 666.

41. Mulliken, R. S. *J. Phys. Chem.* **1962**, *36*, 3428.

42. Verlet, L. *Phys. Rev.* **1967**, *169*, 201.

43. Allen, M. P.; Tildesley, D. J. *Computer Simulation of Liquids*; Clarendon Press: Oxford, 1990.

44. Demontis, P.; Suffritti, G. B. *Chem. Rev.* **1997**, *97*, 2845.

45. Dufner, H.; Kast, S. M.; Brickmann, J.; Schlenkrich, M. *J. Comput. Chem.* **1997**, *18*, 660.

46. Wolf, D.; Keblinki, P.; Phillpot, S. R.; Eggebrecht, J. *J. Chem. Phys.* **1999**, *110*, 8254.

47. Rahman, A.; Stillinger, F. H.; Lemberg, H. L. *J. Chem. Phys.* **1975**, *63*, 5223.

48. Marti, J. *J. Chem. Phys.* **1999**, *110*, 6876.

49. Yoshii, N.; Yoshie, S.; Mira, S.; Okazaki, S. *J. Chem. Phys.* **1998**, *109*, 4873.

50. Kalinichev, A. G.; Bass, J. D. *J. Phys. Chem.* **1997**, *101*, 9720.

51. Kärger, J.; Pfeifer, H.; Heink, W. *Principles and Applications of Self-diffusion Measurements by Nuclear Magnetic Resonance, in*: Advances in Magnetic Resonance, Vol. 12; Academic Press: New York, 1988.

52. Haberlandt, R.; Kärger, J. *Chem. Eng. J.* **1999**, *74*, 15.

53. Fritzsche, S.; Haberlandt, R.; Kärger, J.; Pfeifer, H.; Heinzinger, K. *Chem. Phys. Lett.* **1992**, *198*, 283.

54. Skoulidas, A. I.; Sholl, D. S. *J. Phys. Chem. B.* **2002**, *106*, 5058.

55. Jost, S.; Bär, N. K.; Fritzsche, S.; Haberlandt, R.; Kärger, J. *J. Phys. Chem. B* **1998**, *102*, 6375.

56. Runnebaum, R. C.; Maginn, E. J. *J. Phys. Chem. B* **1997**, *101*, 6374.

57. Maginn, E. J.; Bell, A. T.; Theodorou, D. *J. Phys. Chem.* **1996**, *100*, 7155.

58. June, R. L.; Bell, A. T.; Theodorou, D. *J. Phys. Chem.* **1990**, *94*, 1508.

59. Kärger, J. *J. Phys. Chem.* **1991**, *98*, 5558.

60. Kärger, J.; Demontis, P.; Suffritti, G. B.; Tilocca, A. *J. Chem. Phys.* **1999**, *110*, 2.

Figure Captions

Figure 1. Schematic representation of silicalite-1 channels.

Figure 2. Radial distribution functions, $g(r)$, from oxygen atoms of silicalite-1 surface to (**a**) oxygen and (b) hydrogen atoms of water molecule at various loadings ($n_{ld} = 1 - 8$).

Figure 3. Radial distribution functions, $g(r)$, from the oxygen atoms in the intersection (O_{It}), straight (O_{St}), and sinusoidal (O_{Sd}) channels of silicalite-1 to oxygen (O_W, filled symbols) and hydrogen (H_W, unfilled symbols) atoms of water molecule for the loadings of (**a**) 1 and (b) 8 water molecules per intersection.

Figure 4. Projection on the xy plane of the 10 ns trajectory of a water molecule traveling along silicalite-1 channels at $n_{ld} = 1$ and 298 K where its enlargement has been given in the insert.

Figure 5. Oxygen-oxygen (a) and oxygen-hydrogen (b) radial distribution functions (RDF), $g(r)$ for water molecules in silicalite-1 at $n_{ld} = 1 - 8$ (Oxygen-oxygen RDF for bulk water taken from Ref. 47 has been also given).

Figure 6. First shell coordination number, n, as a function of loadings, n_{ld} (* stands for that of bulk water taken from Ref. 47).

Figure 7. Self-diffusion coefficients (D) as a function of loadings (n_{ld}) at 298 and 393 K.

Figure 8. Changes of β (detailed in Eqn. (4)) as a function of loadings (n_{ld}) at 298 and 393 K.

Table Captions

Table 1. Optimal fitting parameters for atom *i* of water interacting with atom *j* in each channel of the silicalite-1 lattice; Subscripts sd and st denote sinusoidal (zig-zag) and straight channels, respectively; Energies in kcal.mol^{-1}, distances (r_{ij}) in Å and atomic net charges (*q*) in atomic units.

i	*j*	q_i	q_j	A ($\text{Å}^{6}\text{kcal.mol}^{-1}$)	B ($\text{Å}^{12}\text{kcal.mol}^{-1}$)	C ($\text{Å}^{3}\text{kcal.mol}^{-1}$)
O	Si$_{sd}$	-0.87	1.57	- 9043.97	1161167.97	1418.92
O	Si$_{st}$	-0.87	1.67	- 4159.83	989963.68	617.02
O	O$_{sd}$	-0.87	-0.78	1371.19	-21045.58	-351.61
O	O$_{st}$	-0.87	-0.84	- 110.79	51208.44	-110.82
H	Si$_{sd}$	0.43	1.57	3724.97	-4314.90	-792.37
H	Si$_{st}$	0.43	1.67	2077.13	-8925.29	-415.82
H	O$_{sd}$	0.43	-0.78	-406.18	689.37	222.32
H	O$_{st}$	0.43	-0.87	34.87	32.84	102.59

Table 2. Characteristics of the radial distribution functions for water loadings (n_{1d}) of 1 to 8 molecules per intersection in silicalite-1 where R_{M1} and r_{m1} are the distances in Å for the first maxima and minima of RDFs, respectively, and n is the average coordination number integrated up to r_{m1}.

RDF $O_W O_W$	n_{1d}								Bulk[a]
	1	2	3	4	5	6	7	8	
R_{M1}	3.65, 4.3[b]	3.55, 4.3[b]	3.45, 4.2[b]	3.45, 4.2[b]	3.35	3.35	3.35	3.35	2.80
r_{m1}	8.05	6.45	5.95	5.85	5.65	5.45	5.35	5.25	3.2
n	0.1	0.7	1.2	1.9	2.5	2.9	3.4	3.9	4.5
RDF $O_W H_W$	n_{1d}								Bulk[a]
	1	2	3	4	5	6	7	8	
R_{M1}	4.05	4.05	3.95	3.95	3.85	3.85	3.75	3.75	1.85
r_{m1}	8.45[c]	9.05[c]	8.95[c]	8.75[c]	8.55[c]	5.65	5.45	5.35	2.4
n	1.3	5.7	9.6	11.9	15.8	7.5	8.3	9.2	4.4

[a]The values taken from Ref. 47. [b]The RDFs show broad splitting peak. [c]The RDFs show flat minima.

Intersection

Straight Channel

8.2 Å

Sinusoidal channel
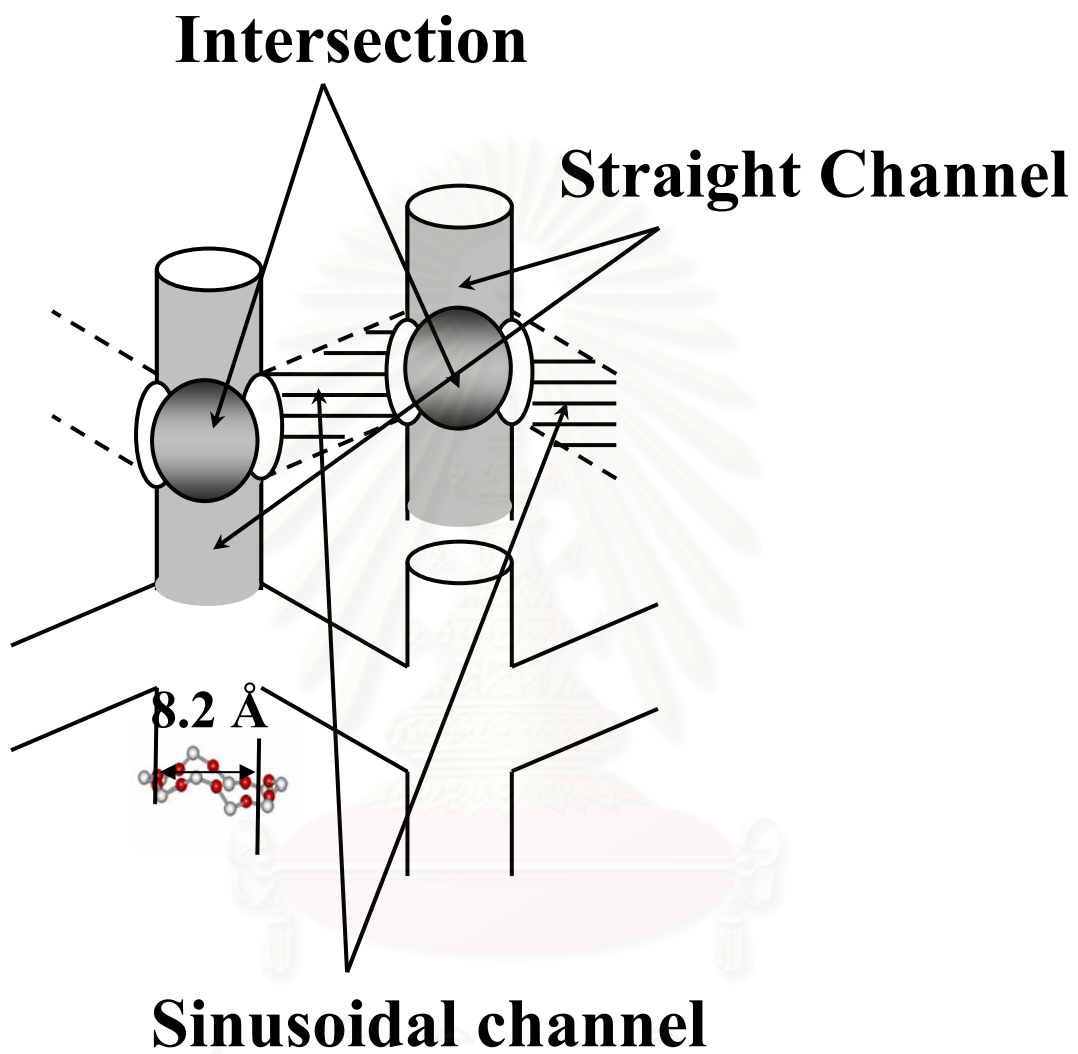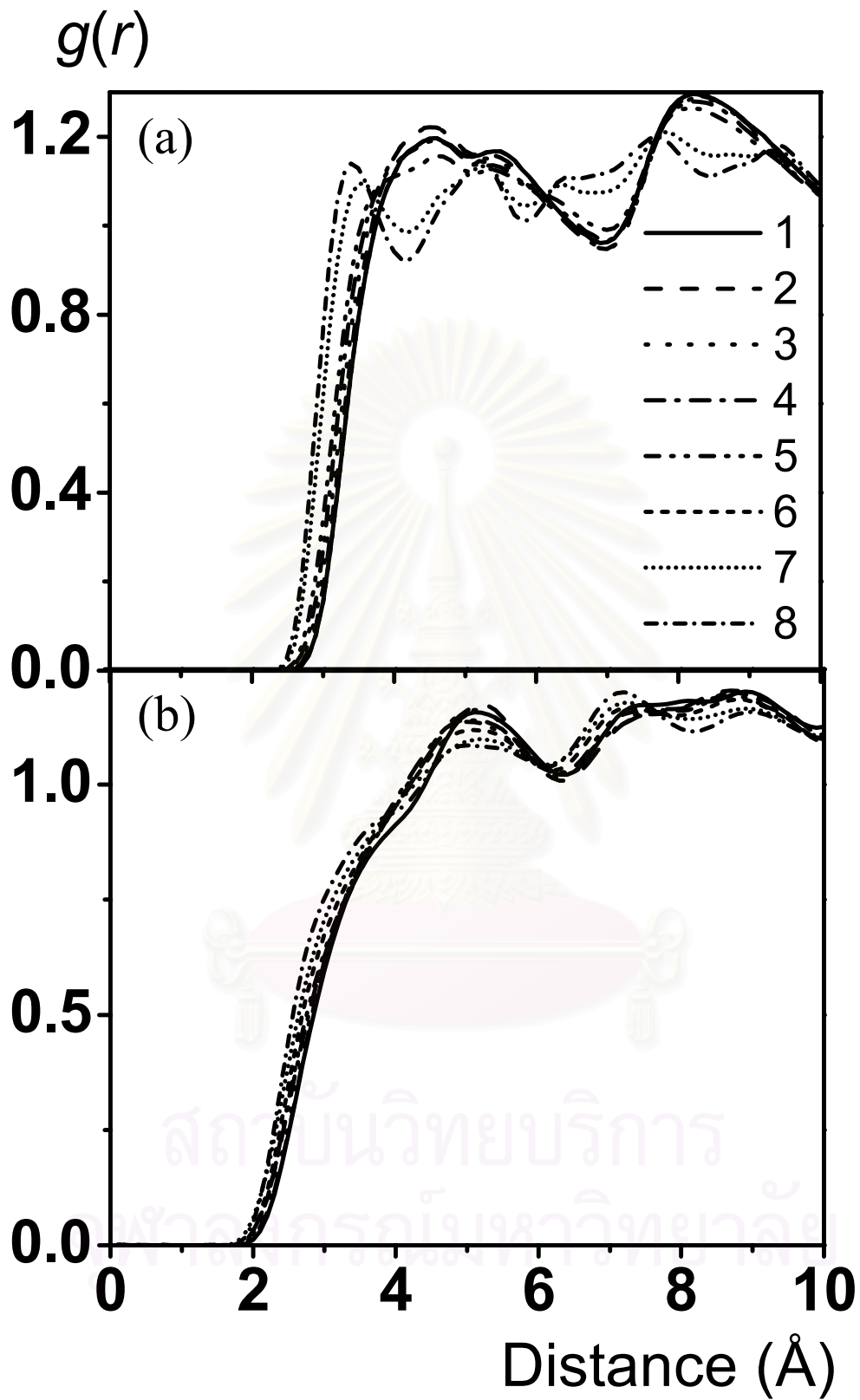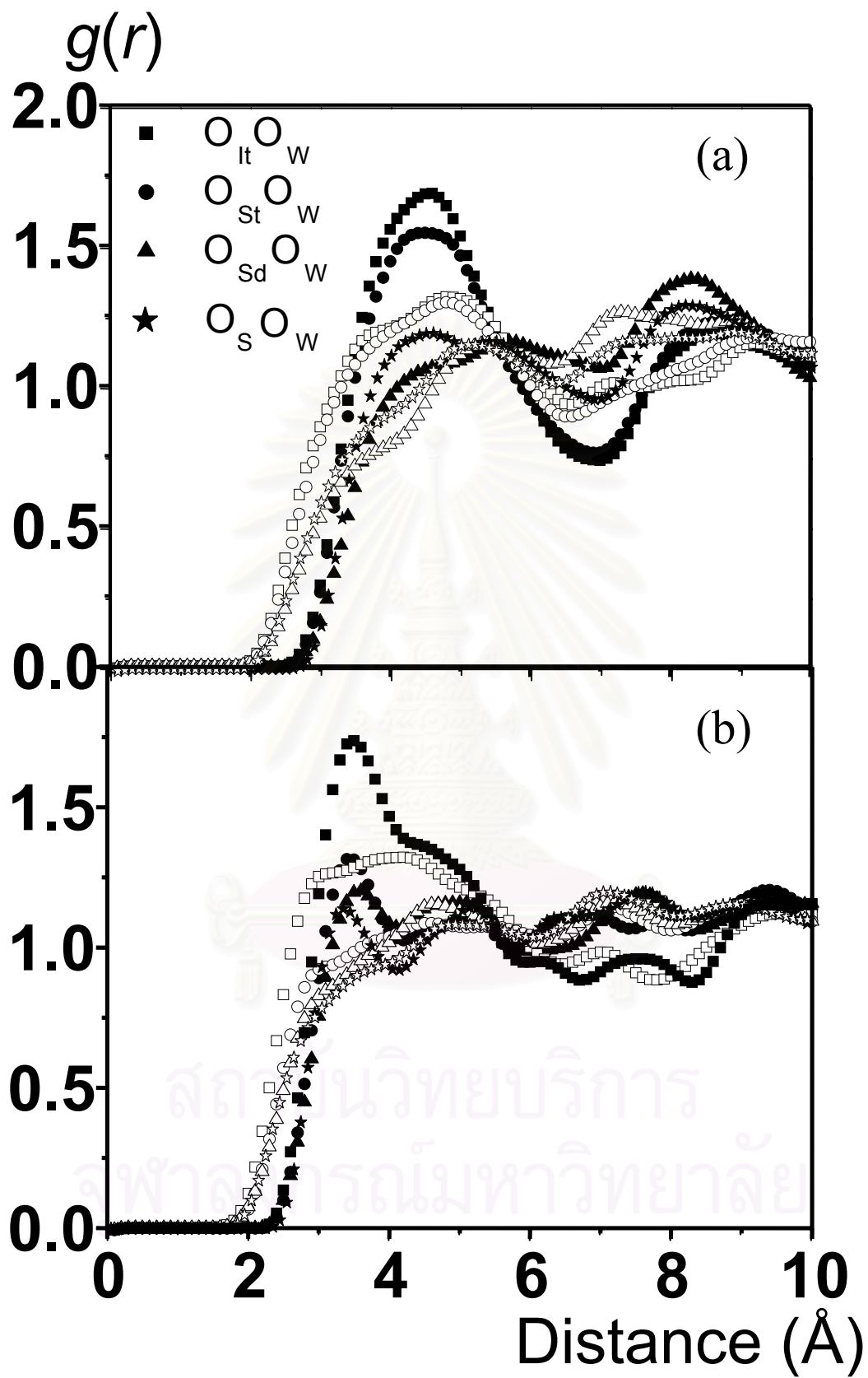
Figure 1

Figure 2

Figure 3
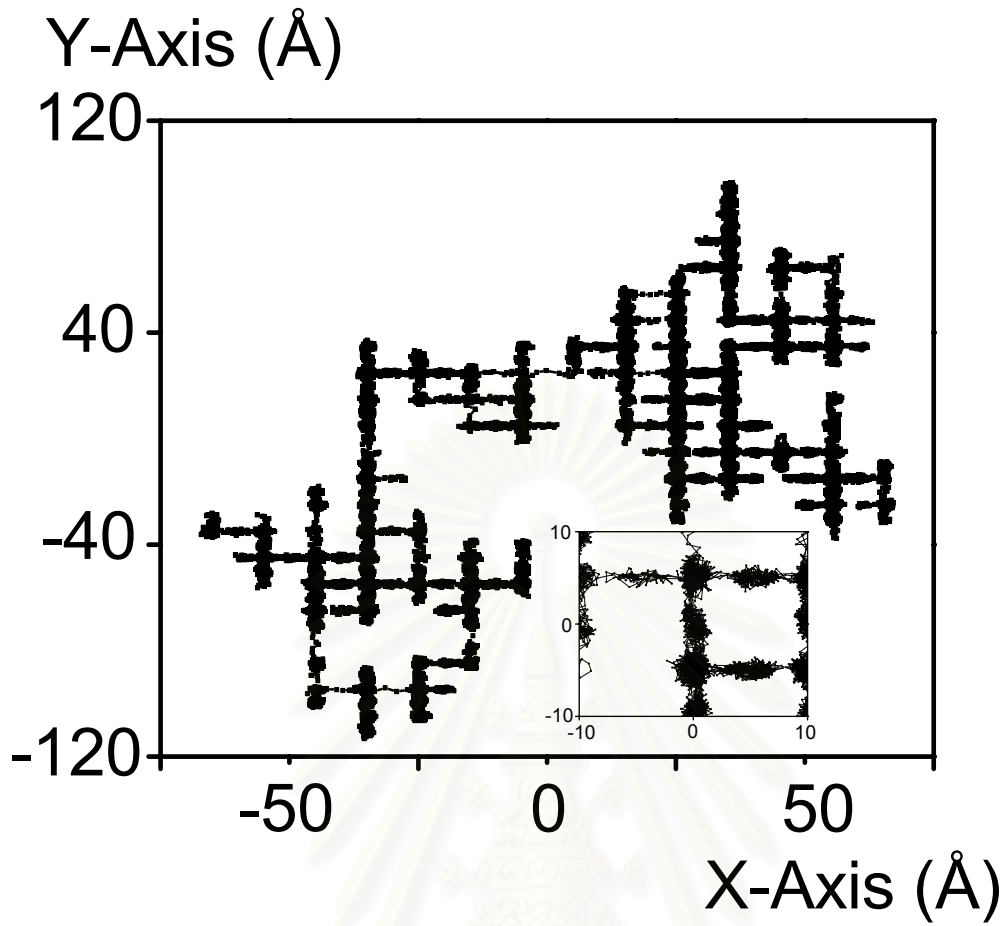
Figure 4
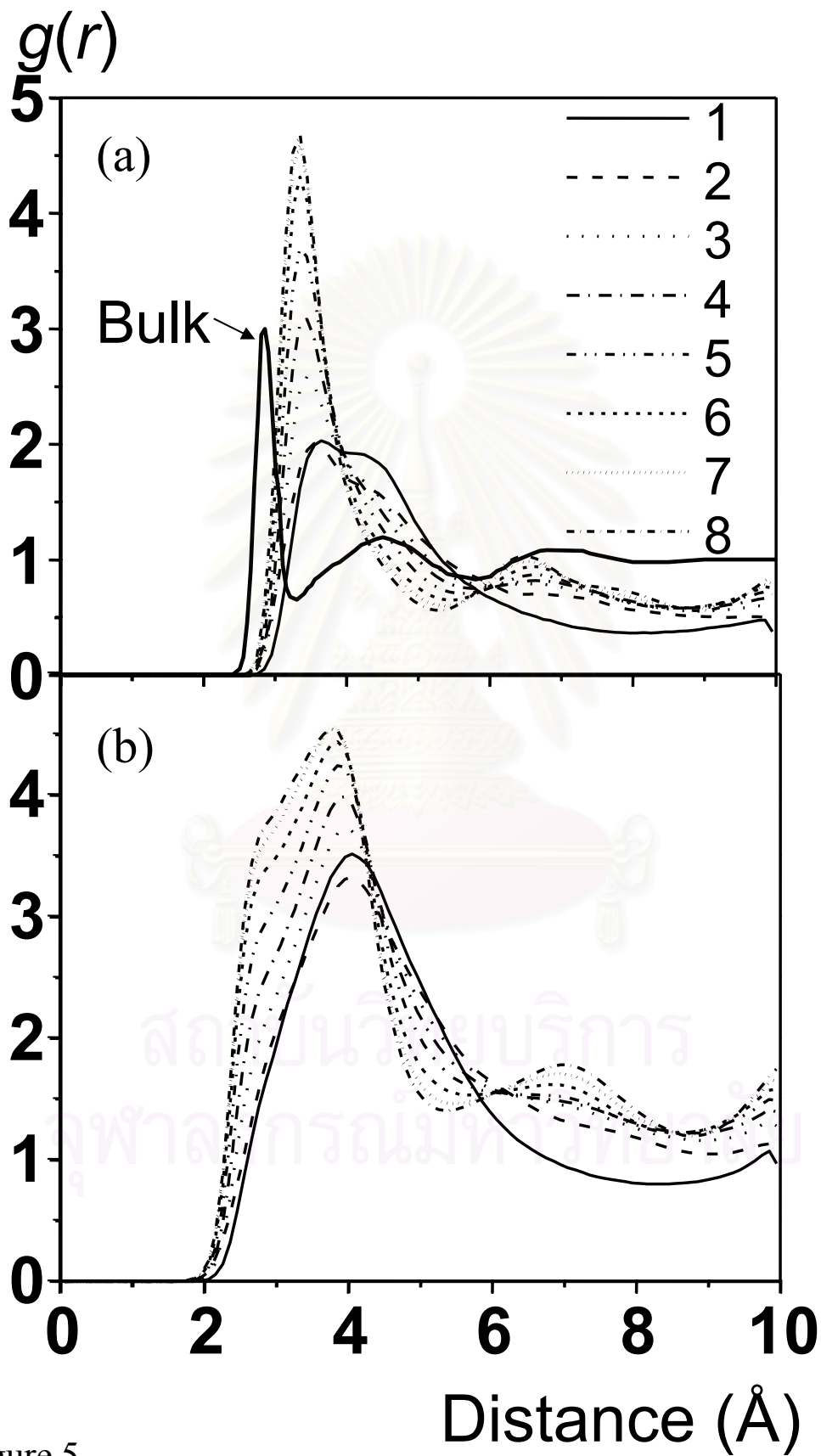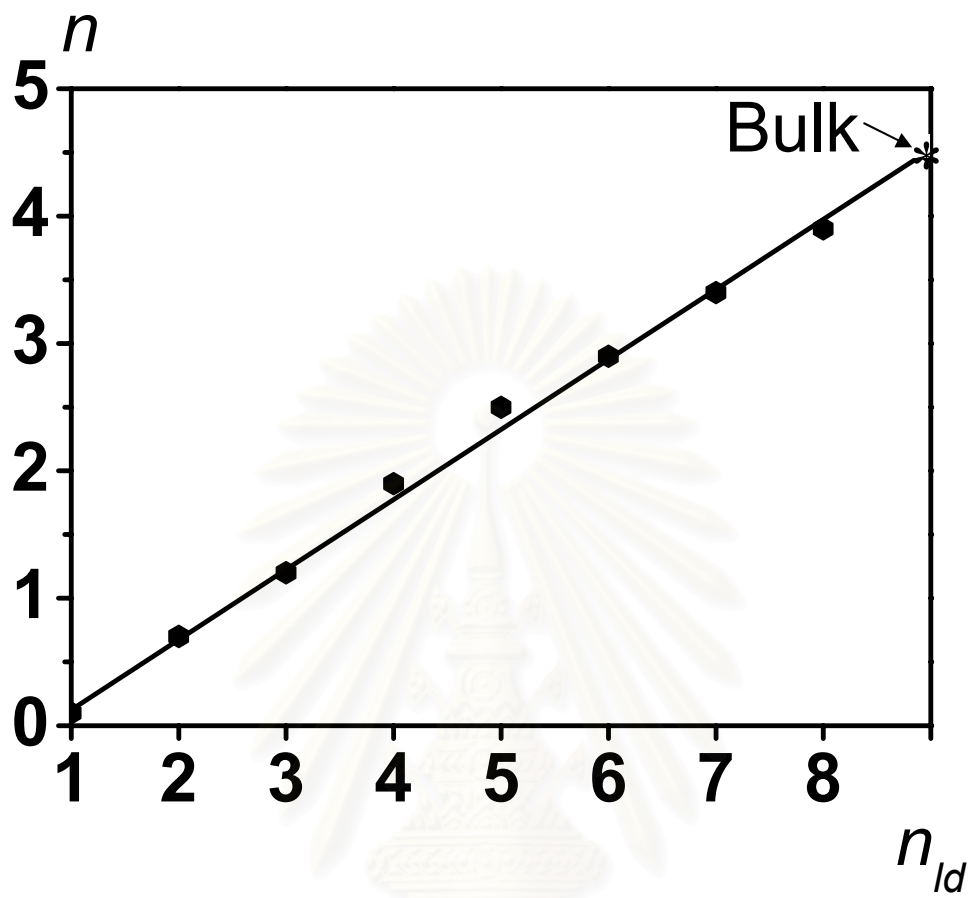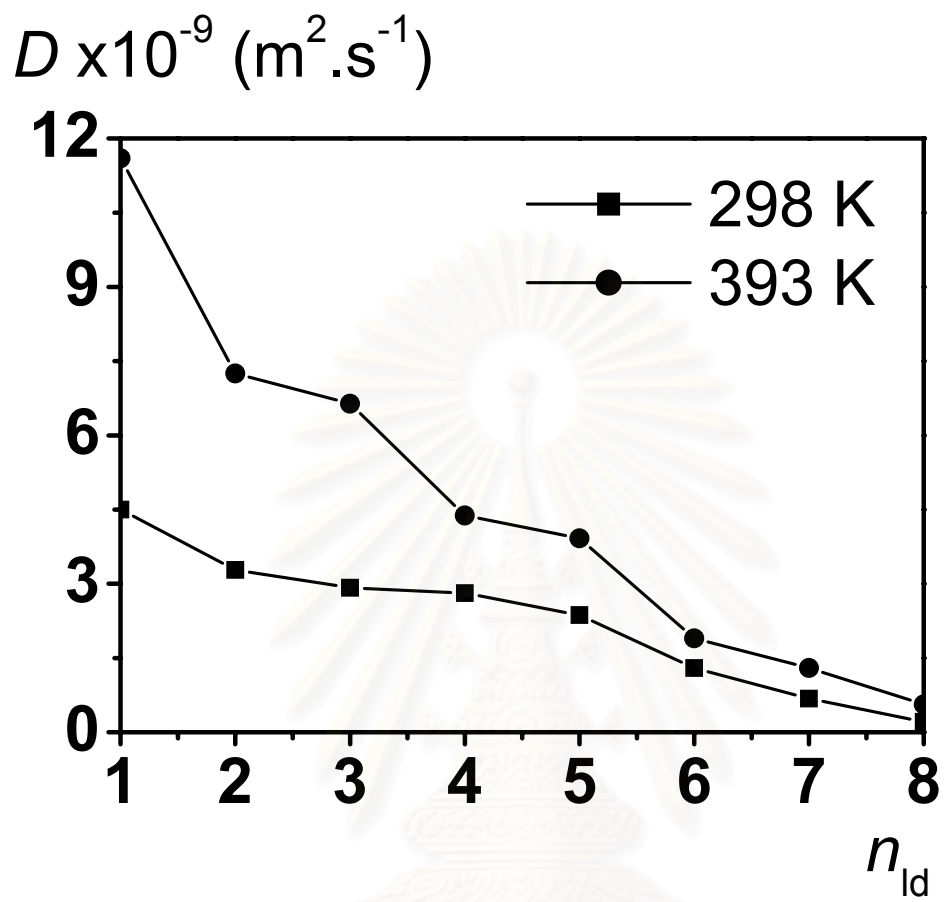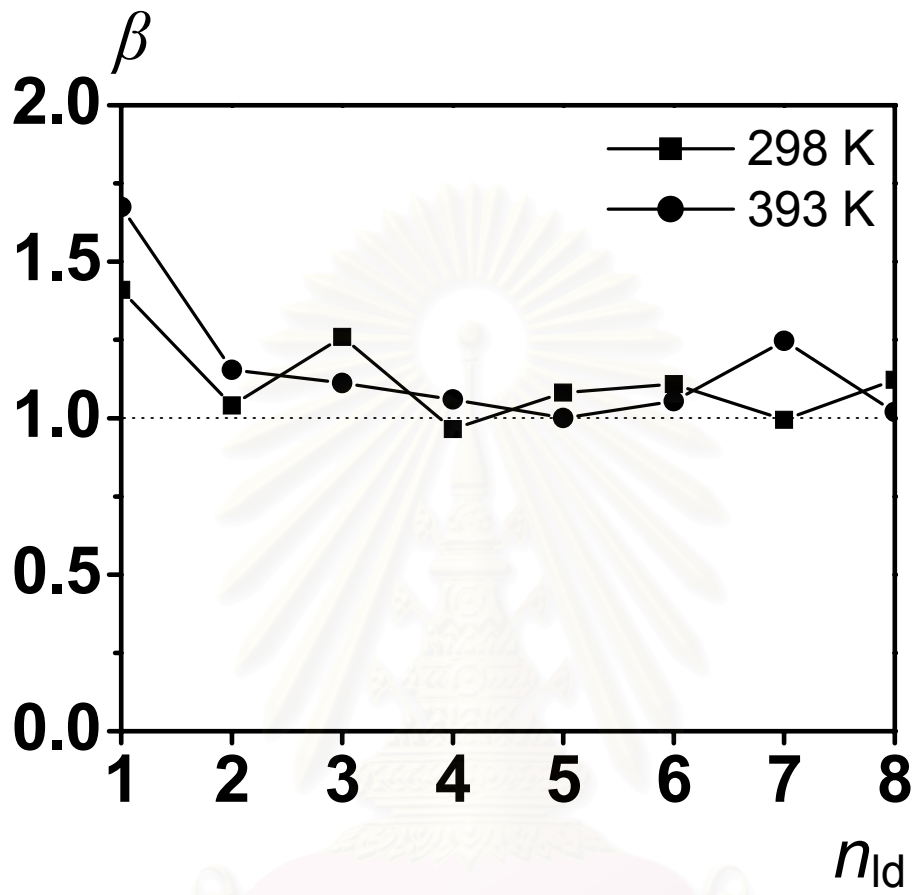
Figure 5

Figure 6

Figure 7

Figure 8

VITAE

Name   Miss Chuenchit Bussai

Birth   March 4th, 1977

EDUCATION

1997   B. Sc. Chemistry, Chulalongkorn University, Bangkok, THAILAND

2002   Ph. D. Chemistry, Chulalongkorn University, Bangkok, THAILAND

HONORS AND AWARDS

1998   Promotion 'Royal Golden Jubilee' Grant

1999   Short Term DAAD-Royal Golden Jubilee research grant.

2002   'Outstanding Oral Presentation' on *The 3rd Royal Golden Jubilee – Ph. D. Congress, 'Binding, Energy Barrier and Diffusion of Water in Silicalite-1: Ab initio, Molecular Dynamics and PFG NMR Studies'* Pataya, THAILAND, 25-27 April.

2002   'Applause Oral Presentation' on *The 10th Conference on Science and Technology of Chulalongkorn University, 'The Energy Barrier and the movement of Water Molecule through the Silicalite-1 Lattice: Ab Initio and Molecular Dynamics Studies'* Bangkok, THAILAND, 20-22 March.

PUBLICATIONS

1.   **Bussai C**.; Hannongbua S.; Haberlandt R. *Understanding the Movement, Encapsulation and Energy Barrier of Water Molecule via Diffusion in Silicalite using Ab initio Calculations*. J. Phys. Chem. B **2001**; 105 (17): 3409-3412.

2.   **Bussai C**.; Haberlandt R.; Hannongbua S.; Jost S. *Computer Simulations of Water molecules in Zeolites*. Studies in Surf. Sci. Catal. **2001**; 135: 263-269.

3.   **Bussai C**.; Hannongbua S.; Fritzsche S.; Haberlandt R. *Ab initio Intermolecular Potential and Molecular Dynamics Simulations for the Determination of Diffusion Coefficient of Water in Silicalite*. Chem. Phys. Lett. **2002**; 354 (3-4): 310-315.

4.   **Bussai C**.; Vasenkov S.; Liu H.; Böhlmann W.; Hannongbua S.; Fritzsche S.; Haberlandt R.; Kärger J. *On the Diffusion of Water in Silicalite: PFG-NMR Measurements and MD Simulations using Fully Ab initio Potential*. Appl. Catal. A- Gen. **2002**; 232 (1-2): 59-66.

5.   **Bussai C**.; Fritzsche S.; Haberlandt R.; Hannongbua S. *Diffusion of Water in Silicalite by Molecular Dynamics Simulations: Ab Initio based Interactions*. Studies in Surf. Sci. Catal. **2002**; 142B: 1979-1986.

6.   **Bussai C**.; Fritzsche S.; Haberlandt R.; Hannongbua S. *Formation of Low Density Water Cluster in the Silicalite-1 Cage as Studies by Molecular Dynamics Simulations*. Submitted for publication.

* 7 oral and 9 poster presentations in national and international conferences